1997
Technical
Digest Series
Volume 7

Applicati
High Field and Short Wavelength Sources VII

Technical Digest

March 19–22, 1997

Eldorado Hotel
Santa Fe, New Mexico

Conference Edition

OSA
Optical Society of America

Applications of High Field and Short Wavelength Sources VII

March 19–22, 1997
Eldorado Hotel
Santa Fe, New Mexico

1997 OSA Technical Digest Series
Volume 7

CONFERENCE EDITION

Sponsored and managed by
Optical Society of America

OSA
Optical Society of America
2010 Massachusetts Avenue NW
Washington DC 20036-1023

Articles in this publication may be cited in other publications. To facilitate access to the original publication source, the following form for the citation is suggested:

Name of Author(s), "Title of Paper," in *Applications of High Field and Short Wavelength Sources VII*, Vol. 7, 1997 OSA Technical Digest Series (Optical Society of America, Washington DC, 1997), pp. xx-xx.

Optical Society of America

ISBN

Conference Edition	1-55752-488-2
Postconference Edition	1-55752-489-0
(Note: Postconference Edition includes postdeadline papers.)	
1997 Technical Digest Series	1-55752-485-8

Library of Congress Catalog Card Number

Conference Edition	97-65494
Postconference Edition	97-65496

Printed in the U.S.A.

Contents

1997 APPLICATIONS OF HIGH FIELD AND SHORT WAVELENGTH SOURCES VII
TECHNICAL PROGRAM COMMITTEE

Chairs

Louis DiMauro, *Brookhaven National Laboratory, U.S.A.*
Margaret Murnane, *University of Michigan, U.S.A.*
Anne L'Huillier (European Cochair), *Lund Institute of Technology, Sweden*

Committee Members

Pierre Agostini, *Centre d'Etudes de Saclay, France*
Jean-Patrick Connerade, *Imperial College of Science and Technology, U.K.*
Paul Corkum, *National Research Council, Canada*
L. DaSilva, *Lawrence Livermore National Laboratory, U.S.A.*
David Ederer, *Tulane University, U.S.A.*
Eckhart Foerster, *Max-Planck-Gellschaft, Germany*
Richard Freeman, *Lawrence Livermore National Laboratory, U.S.A.*
George Gibson, *University of Connecticut, U.S.A.*
Chris Jacobson, *SUNY Stony Brook, U.S.A.*
Henry Kapteyn, *University of Michigan, U.S.A.*
Yoshiaki Kato, *Osaka University, Japan*
Vladimir Krainov, *Moscow Institute of Physics and Technology, Russia*
Kenneth Kulander, *Lawrence Livermore National Laboratory, U.S.A.*
Peter Lambropoulos, *Max Planck Institute for Quantenoptik, Germany*
James Long, *Naval Research Laboratory, U.S.A.*
Thomas McIlrath, *University of Maryland, U.S.A.*
Howard Milchberg, *University of Maryland, U.S.A.*
Gerard Mourou, *University of Michigan, U.S.A.*
Harm Muller, *FOM Institute for Atomic and Molecular Physics, The Netherlands*
Wolfgang Sandner, *Max Born Institute, Germany*
Sune Svanberg, *Lund Institute for Technology, Sweden*
Gregory Tallents, *University of Essex, U.K.*
Michael White, *Brookhaven National Laboratory, U.S.A.*

WEDNESDAY
MARCH 19, 1997

All sessions and events will be held in the Eldorado Hotel.

ZIA CONCOURSE

6:00pm–8:00pm
Conference Registration

THURSDAY
MARCH 20, 1997

ZIA CONCOURSE

7:30am–12:00m
Conference Registration and Speaker/Presider Check-in

ZIA A

8:15am–8:30am
Opening Remarks

8:30am–10:15am
ThA • Applications of Short Wavelength Light I
Pierre Agostini, *Centre d'Etudes de Saclay, France, Presider*

8:30am
ThA1 (Keynote) • Extreme ultraviolet lithography, Jeffrey Bokor, *Univ. California–Berkeley.* Some of the highlights of the recent dramatic progress in the development of extreme ultraviolet lithography technology will be reviewed, with emphasis on the challenge of fabricating and testing a diffraction-limited optical imaging system at 13 nm wavelength. **(p. 2)**

9:15am
ThA2 (Invited) • X-ray microscopy: New capabilities and short pulse possibilities, C. Jacobsen, J. Kirz, J. Maser, A. Osanna, S. Spector, S. Wang, B. Winn, S. Wirick, *SUNY Stony Brook;* B. Calef, M. Howells, S. Lindaas, D. Pinkus, *Lawrence Berkeley Laboratory;* D. Tennant, *Lucent Technologies Bell Laboratories.* New capabilities in soft x-ray microscopy are described, with an emphasis on biological applications. Desirable short wavelength source characteristics are considered. **(p. 3)**

9:45am
ThA3 • Laser-driven hard x-ray sources for angiography, Z. Jiang, A. Ikhlef, J. C. Kieffer, *INRS-Énergie et Matériaux, Canada;* A. Krol, C. C. Chamberlain, D. A. Bassano, S. C. Prasad, *SUNY Health Science Center.* A laser-driven X-ray source for mammography and angiography has been developed to overcome the limits of current technology used in medical imaging. **(p. 6)**

10:00am
ThA4 • Radiological applications of hard x-ray emission from a laser-produced plasma, M. Grätz, C. Tillman, A. Nykänen, L. Kiernan, C.-G. Wahlström, S. Svanberg, *Lund Institute of Technology, Sweden;* K. Herrlin, *University Hospital, Sweden.* Advances in various x-ray imaging techniques and the corresponding requirements on the x-ray source are presented, including a comparison to existing competitive x-ray techniques. **(p. 9)**

ZIA CONCOURSE

10:15am–10:45am
Coffee Break

ZIA A

10:45am–12:15pm
ThB • Laser-Produced Plasmas
George Kyrala, *Los Alamos National Laboratory, Presider*

10:45am
ThB1 (Invited) • Experimental studies of the propagation of ultrashort, intense laser pulses in underdense plasmas, B. D. Thompson, A. McPherson, A. B. Borisov, K. Boyer, C. K. Rhodes, *Univ. Illinois–Chicago.* Measurements of the spatial and spectral properties of ultrashort, intense laser pulses propagating in underdense plasmas demonstrate nonlinear propagation and ionization-induced self-phase-modulation. **(p. 14)**

11:15am
ThB2 (Invited) • High energy explosion of super-heated atomic clusters, T. Ditmire, J. W. G. Tisch, E. Springate, M. B. Mason, N. Hay, R. A. Smith, J. P. Marangos, M. H. R. Hutchinson, *Imperial College of Science, Technology, and Medicine, U.K.* We have examined the explosion of atomic clusters heated by intense femtosecond pulses. We observe electrons with energy up to 3 keV and ions with energy up to 1 MeV. **(p. 17)**

11:45am
ThB3 • Hard x-ray emission from femtosecond laser interaction in overdense plasmas, A. A. Andreev, V. N. Novikov, K. Yu. Platonov, *S. I. Vavilov State Optical Institute, Russia;* J.-C. Gauthier, *Ecole Polytechnique, France.* Calculations of the electron energy distribution, the absorption coefficient, and the hard x-ray emission in high-intensity femtosecond laser-produced plasmas is presented. **(p. 20)**

12:00m
ThB4 • Continuum lowering in 100-fs laser-produced plasmas, M. Nantel, T. Buma, J. Workman, A. Maksimchuk, D. Umstadter, *Univ. Michigan.* Through time- and space-resolved emission and absorption XUV spectroscopy, we observe and measure continuum lowering in high-density plasmas created by 100-fs laser pulses. **(p. 23)**

12:15pm–2:00pm
Lunch on Own

ZIA CONCOURSE

2:00pm–6:00pm
Conference Registration and Speaker/Presider Check-in

ZIA A

2:00pm–3:30pm
ThC • X-ray Lasers
L. DaSilva, *Lawrence Livermore National Laboratory, Presider*

2:00pm
ThC1 (Keynote) • Saturated table-top soft x-ray lasers by discharge excitation, J. J. Rocca, F. G. Tomasel, J. L. A. Chilla, M. C. Marconi, V. N. Shlyaptsev, C. H. Moreno, B. R. Benware, J. J. Gonzalez, *Colorado State Univ.* We discuss the realization of compact soft x-ray lasers directly excited by fast discharges. Saturated operation of a 46.9 nm table-top amplifier has been achieved. **(p. 28)**

2:45pm
ThC2 (Invited) • Low energy pumped x-ray lasers with saturated transient gain, P. V. Nickles, M. P. Kalachnikov, M. Schnürer, W. Sandner, *Max-Born-Institut, Germany;* V. N. Shlyaptsev, *Colorado State Univ.;* C. Danson, D. Neely, E. Wolfrum, M. Key, *Rutherford Appleton Laboratory, U.K.;* A. Behjat, A. Demir, G. Tallents, *Univ. Essex, U.K.;* G. J. Pert, *Univ. York, U.K.;* J. Warwick, C. Lewis, *Queens Univ. Belfast, U.K.* A short-long pulse excitation of [Ne]-like Ti and Ge has succeeded in saturated short pulse lasing at 32.6 nm and 19.6 nm with low pump energy level. **(p. 31)**

3:15pm
ThC3 • Generation of intense x-ray laser radiation at 8 nm in Ni-like Nd ions, H. Daido, Y. Kato, T. Imani, S. Sezaki, S. Hirose, G. Y. Yoon, T. Jitsuno, Y. Takagi, K. Mima, *Osaka Univ., Japan:* S. Wang, Z. Lin, Y. Gu, G. Huang, H. Tang, D. Ximing, *National Laboratory for High Power Lasers and Physics, China;* G. Zhang, *Institute for Applied Physics and Computational Mathematics, China;* K. Murai, *Osaka National Research Institute, Japan;* H. Takenaka, *NTT Advanced Technology, Japan.* Very intense radiation at 8 nm has been generated by amplification in Ni-like Nd ions using double curved targets, which were irradiated with laser pulses tightly line-focused with new optical configurations. **(p. 34)**

ZIA CONCOURSE

3:30pm–4:00pm
Coffee Break

ZIA A

4:00pm–5:45pm
ThD • Applications of Short Wavelength Light II
Michael White, *Brookhaven National Laboratory, Presider*

4:00pm
ThD1 (Keynote) • Synchrotron radiation and applications, Irène Nenner, *CEA-Centre de Saclay, France.* The performances of synchrotron radiation are presented by comparison with selected laser based sources. Some applications in radiation-matter interaction and material science are described. **(p. 38)**

4:45pm
ThD2 • Time-resolved x-ray diffraction from laser excited crystals, J. Larsson, E. Judd, P. J. Schuck, R. W. Falcone, *Univ. California–Berkeley;* P. A. Heimann, H. A. Padmore, *Lawrence Berkeley National Laboratory;* Z. Chang, H. C. Kapteyn, M. M. Murnane, *Univ. Michigan;* R. W. Lee, *Lawrence Livermore National Laboratory;* A. Machacek, J. S. Wark, *Univ. Oxford, U.K.* We have developed an apparatus for x-ray probing of laser-matter interaction in solids. Our detection system has demonstrated a temporal response of 1.5 ps. **(p. 41)**

5:00pm
ThD3 • Ultrafast X-ray diffraction: Theory, M. Ben-Nun, Kent R. Wilson, *Univ. California–San Diego;* T. J. Martínez, *Univ. Illinois;* P. M. Weber, *Brown Univ.* Theoretical calculations of optical pump, diffraction probe measurements of electronic structures of excited state atoms and molecules and the nuclear dynamics during chemical reactions are discussed. **(p. 44)**

5:15pm
ThD4 • The optimization of soft X-ray laser output, G. J. Tallents, A. Behjat, A. Demir, J. Y. Lin, R. Smith, *Univ. Essex, U.K.;* C. L. S. Lewis, A. MacPhee, S. P. McCabe, P. J. Warwick, *Queen's Univ. Belfast, U.K.;* D. Neely, E. Wolfrum, *Rutherford Appleton Laboratory, U.K.;* J. Zhang, *Univ. Oxford, U.K.;* G. J. Pert, *Univ. York, U.K.;* P. V. Nickles, M. Kalashnikov, M. Schnürer, *Max-Born-Institut, Germany.* Short duration (2–100 ps) multi-pulse pumping of x-ray laser media is shown to significantly enhance the x-ray laser output from neon-like ions. **(p. 47)**

5:30pm
ThD5 • Biological x-ray microscopy with a compact laser system, M. Richardson, M. Kado, D. Torres, K. Nekula, *Univ. Central Florida;* Y. Yamamoto, H. Friedman, *Univ. South Florida–Tampa;* J. Rajyaguru, M. J. Muszynski, *Arnold Palmer Hospital for Children & Women.* Nanosecond flash x-ray microscopy of living biological specimens is demonstrated with subcellular spatial resolution of ~10 nm. Single shot images, produced by a compact laser-plasma x-ray source, optimized for maximum image contrast, are captured before radiation processes can affect the specimen. **(p. 50)**

ANASAZI SOUTH

6:00pm–8:00pm
ThE • Poster Session

ThE1 • Moved to ThD4

ThE2 • Tunable, ultrashort, high-intensity kilohertz mid-infrared laser system, B. Sheehy, M. Widmer, R. Lafon, A. Gambhir, L. F. DiMauro, *Brookhaven National Laboratory.* An ultrashort pulse kilohertz laser system operating between 3 and 4.5 microns has been developed. Initial MPI studies and applications to coherent control are discussed. **(p. 55)**

ThE3 • Characterization of a flatfield spectrometer for the VUV and XUV spectral range, K. Sokolowski-Tinten, G. Jenke, A. Orisch, D. von der Linde, *Univ. GHS-Essen, Germany.* A flatfield spectrometer in conjunction with a thinned, back-illuminated CCD camera is characterized in the XUV spectral range to study high-order harmonic generation from solid surfaces. **(p. 58)**

ThE4 • Demonstration of a 0.54 ps x-ray streak camera, Z. Chang, A. Rundquist, H. Wang, H. C. Kapteyn, M. M. Murnane, *Univ. Michigan;* X. Liu, B. Shan, J. Liu, L. Niu, M. Gong. X. Zhang, *Xi'an Institute of Optics and Precision Mechanics, China;* R. W. Lee, *Lawrence Livermore National Laboratory.* We have demonstrated the fastest x-ray detector to date. The instrument response was calibrated with use of femtosecond x-ray pulses produced by high-harmonic generation. **(p. 60)**

ThE5 • Multiterawatt ultraviolet laser system, F. G. Omenetto, K. Boyer, J. W. Longworth, A. McPherson, T. Nelson, W. A. Schroeder, C. K. Rhodes, *Univ. Illinois–Chicago.* New improvements on our Ti:Sapphire/KrF* laser system have opened the road to stable multiterawatt pulse generation in the UV region at $\lambda = 248$ nm. **(p. 63)**

ThE6 • 0.125 terawatt kilohertz laser system, Sterling Backus, Charles Durfee, Margaret Murnane, Henry Kapteyn, *Univ. Michigan.* We describe a high-average-power terawatt laser system that generates 20-fs pulses with 2.5 mJ of energy. **(p. 66)**

ThE7 • X-ray magneto-optical Kerr effect and its applications, Chi-Chang Kao, *Brookhaven National Laboratory.* Dramatic enhancement of the magneto-optical Kerr effect is observed in x-ray range because of large spin-orbit coupling of core-electrons. Examples and applications will be given. **(p. 69)**

ThE8 • Barrier-suppression ionization of complex atoms and diatomic molecules, V. P. Krainov, *Moscow Institute of Physics and Technology, Russia.* Analytical expressions are obtained for energy and angular distributions of ejected electrons at the barrier-suppression ionization of complex atoms, atomic ions, and diatomic molecules by strong low-frequency laser radiation. New effect of resonance tunneling in molecules is suggested. **(p. 72)**

ThE9 • Precision tests of laser-tunneling ionization models, B. Buerka, J. P. Knauer, S. J. McNaught, D. D. Meyerhofer, *Univ. Rochester.* Electron spectrometers are used for precision tests of tunneling ionization rates and electron initial conditions in an intense 1.5 ps, 1 μm laser field. **(p. 75)**

ThE10 • Tunneling ionization of molecules, B. A. Zon, *Voronezh State Univ., Russia.* A generalization of Ammosov-Delone-Krainov theory is presented for ionization of molecules in laser field. **(p. 77)**

ThE11 • Spectral structure in high harmonic emission, Hai-Wen Wang, Zenghu Chang, Andy Rundquist, Henry Kapteyn, Margaret Murnane, *Univ. Michigan;* Ivan P. Christov, *Sofia Univ., Bulgaria.* We demonstrated experimentally, for the first time, we believe, the existence of spectral structure in the mid-plateau region of high harmonic emission in gases. **(p. 78)**

ThE12 • Enhanced harmonic generation using pulse shaping, Andy Rundquist, Erik Zeek, Haiwen Wang, Zenghu Chang, Margaret Murnane, Henry Kapteyn, *Univ. Michigan;* Ivan Christov, *Sofia Univ., Bulgaria.* We present theory and experiments on the use of pulse shaping techniques to enhance the output from high harmonic generation in atoms. **(p. 81)**

ThE13 • Time-dependent Schrödinger equation for the interaction between a laser pulse and a one-dimensional metal, P. Martin, G. Petite, *CEN Saclay, France.* Electron and harmonic spectra resulting from the interaction between a short laser pulse and a linear chain of atoms are calculated and discussed. The case of a nearly free electron metal is taken as an example. **(p. 84)**

ThE14 • Determination of the duration of UV femtosecond pulses, J.-F. Ripoche, B. S. Prade, M. A. Franco, G. Grillon, R. Lange, A. Mysyrowicz, *ENSTA-École Polytechnique, France.* Using cross-phase modulation and spectral analysis, one determines the duration of femtosecond pulses at wavelengths ranging from the near infrared to the near ultraviolet. **(p. 87)**

ThE15 • Increased coherence length in high order harmonic generation by a self-guided beam, H. R. Lange, A. Bouhal, J.-F. Ripoche, A. Mysyrowicz, *ENSTA-Ecole Polytechnique, France;* P. Breger, P. Agostini, *Centre d'Etudes de Saclay, France.* We report on the generation of harmonics in xenon up to the 15th order by an optical filament with 120-fs and 0.9-mJ laser pulses. **(p. 90)**

ThE16 • Spectral-spatial measurements of fundamental and third harmonic light scattered from ionizing gas in the focus of a 25-fs laser pulse, J. Peatross, *Brigham Young Univ.;* S. Backus, J. Zhou, M. M. Murnane, H. C. Kapteyn, *Univ. Michigan.* An intense 25-fs laser pulse undergoes severe distortions as it ionizes gas near the focus in a backfilled chamber. The spectral content of the scattered light is measured verses angle. **(p. 93)**

ThE17 • Coherence properties of ultrashort high-order harmonics, P. Salières, B. Carré, M. Lewenstein, *Centre d'Etudes de Saclay, France;* Ph. Antoine, *Univ. Catholique de Louvain, Belgium;* A. L'Huillier, *Lund Institute of Technology, Sweden.* We discuss the coherence properties of high-order harmonics and the related possibilities of generating ultrashort pulses. **(p. 96)**

ThE18 • Spatial coherence measurement of high order harmonic radiation, T. Ditmire, E. T. Gumbrell, R. A. Smith, J. W. G. Tisch, M. H. R. Hutchinson, *Imperial College of Science, Technology, and Medicine, U.K.;* D. D. Meyerhofer, *Univ. Rochester.* With a Young's two-slit experiment, we have measured the spatial coherence of soft x-rays produced by high order harmonic generation in the 270 Å to 480 Å range. **(p. 98)**

ThE19 • Application of MeV x rays from femtosecond laser-produced plasmas to the study of photonuclear effects, H. Schillinger, Ch. Ziener, R. Sauerbrey, *Friedrich-Schiller-Univ. Jena, Germany;* H. Langhoff, *Univ. Würzburg, Germany.* We measured X-ray spectra from femtosecond laser-produced plasmas in the energy range 200 keV–7 MeV to determine the feasibility of triggering and observing laser-driven photonuclear reactions. **(p. 101)**

ThE20 • Ultra-intense lasers for fast ignition in inertial confinement fusion at Ile, Osaka, T. Yamanaka, Y. Kato, Y. Kitagawa, R. Kodama, H. Takabe, H. Fujita, T. Kanabe, M. Nakatsuka, K. Mima, *Osaka Univ., Japan.* A 1 ps-30 TW laser and a 100 TW laser as thirteenth beam of the GEKKO XII laser system are constructed to experimentally verify the fast ignition concept in inertial confinement fusion. **(p. 103)**

ThE21 • Conical emission of a femtosecond pulse undergoing self-focusing and ionization in air, O. G. Kosareva, V. P. Kandidov, *Moscow State University, Russia;* A. Brodeur, S. L. Chin, *Univ. Laval, Canada.* Conical emission from the long (≈100 m) filament created by a femtosecond pulse in air is shown to be the consequence of spatiotemporal pulse transformation in the conditions of ionization. Numerical and experimental studies of conical emission are presented. **(p. 106)**

ThE22 • A three-dimensional ponderomotive trap for high energy electrons, J. L. Chaloupka, T. J. Kessler, D. D. Meyerhofer, *Univ. Rochester.* A three-dimensional ponderomotive-optical trap for high energy electrons is generated by placing a phase mask in the near-field of an intense laser. **(p. 109)**

ThE23 • X-laser induced nuclear decay: Resonance internal conversion, B. A. Zon, V. E. Chernov, *Voronezh State University, Russia.* Induced discrete conversion involving a nuclear transition in keV-region is considered. The numerical results are presented for ^{99}Tc; some other nuclei (^{105}Ag, ^{189}Os, ^{191}Os, ^{191}Au, ^{193}Ir, ^{205}Pb, ^{229}Th, ^{235}U) are discussed. **(p. 110)**

ThE24 • Laser wakefield acceleration experiments, H. Kotaki, K. Nakajima, H. Ahn, K. Tani, *Japan Atomic Energy Research Institute;* H. Nakanishi, A. Ogata, *National Laboratory for High Energy Physics, Japan;* T. Watanabe, T. Ueda, M. Uesaka, K. Kinoshita, *The Univ. Tokyo, Japan;* M. Kando, *Kyoto Univ., Japan.* Laser wakefield acceleration of electrons was demonstrated using the 100 fs, 2 TW laser system and 17 MeV RF linac electron injector. Accelerated electrons up to 100 MeV were observed. **(p. 112)**

ThE25 • Influence of relativistic structure and retardation in two-photon transitions in hydrogenic systems, C. Szymanowski, V. Véniard, R. Taïeb, A. Maquet, *Univ. Pierre et Marie Curie Paris VI, France.* Two-photon probability amplitudes for bound-bound transitions including retardation are calculated by use of a Sturmian-like expansion of the Dirac Coulomb Green's function. **(p. 115)**

ThE26 • Self-guiding without focusing nonlinearity: Leaking mode self-effect resulting from field-induced saturable ionization, A. M. Sergeev, A. V. Kim, *Russian Academy of Sciences;* M. Lontano, *EURATOM-ENEA-CNR Association, Italy.* We demonstrate that ultrashort pulse self-guiding over distances of many Rayleigh lengths can be achieved in the absence of any focusing nonlinearity as a result of trapping of a slowly leaking wave in a plasma channel produced by field-induced ionization in the saturation regime. **(p. 118)**

ThE27 • All-optical femtosecond electron accelerator, J.-K. Kim, E. Dodd, D. Umstadter, *Univ. Michigan.* Electrons are optically injected into a laser wakefield without the need for either a photocathode or an RF gun injector. Femtosecond bunches of multi-MeV electrons with small energy spread are produced. **(p. 121)**

ThE28 • High-intensity subfemtosecond sub-cycle pulses, solitons, and shock waves via cascade SRS and "EM-bubbles" generation, A. E. Kaplan, P. L. Shkolnikov, *The Johns Hopkins Univ.* High-intensity (10^{14}–10^{16} W/cm^2), sub-cycle, near- or sub-femtosecond (~10^{-16} s) pulses, solitons, and shock optical waves can be achieved via multifrequency modelocking in the cascade stimulated Raman scattering or half-cycle solitons ("EM-bubbles") resulting from quantum or classical ionization potentials. We discuss related physics and possible applications. **(p. 124)**

ThE29 • Backward and multi-echo field ionization by intense non-envelope "superpulses," P. L. Shkolnikov, A. E. Kaplan, *The Johns Hopkins Univ.* We demonstrate the feasibility of a qualitatively new quantum effect, backward and multi-echo field ionization, in the interaction of ultrashort nonoscillating pulses ("superpulses") with atoms and quantum wells. **(p. 127)**

ThE30 • Absorption of high intensity femtosecond laser pulses in solids and the production of suprathermal electrons, T. Feurer, W. Theobald, R. Sauerbrey, I. Uschmann, D. Altenbernd, U. Teubner, P. Gibbon, E. Förster, *Friedrich-Schiller-Univ., Germany;* G. Malka, J. L. Miquel, *Centre d'Etudes de Limeil-Valenton, France.* Using a femtosecond frequency-doubled Nd:Glass laser system with a contrast ratio of 10^{12} and an intensity of up to 2×10^{19} W/cm^2 the absorption in solid targets and the production of hot electrons has been investigated. **(p. 130)**

ThE31 • Absolute measurement of the spectral brilliance of a subpicosecond UV-laser-induced soft x-ray source, R. Häßner, W. Theobald, R. Sauerbrey, D. Altenbernd, U. Teubner, E. Förster, *Friedrich-Schiller-Univ. Jena, Germany;* T. Wilhein, B. Niemann, G. Schmahl, *Georg-August-Univ. Göttingen, Germany.* Absolute measurements of the spectral brilliance of subpicosecond laser-plasmas are obtained with a novel soft x-ray spectrograph. More than 10^{11} photons/shot are emitted by the strongest lines in the water window. **(p. 133)**

ThE32 • Control of the x-ray emission from high-intensity ultrashort laser-produced plasmas, Y. Teubner, D. Altenbernd, E. Förster, *Friedrich-Schiller-Univ. Jena, Germany.* Results of a detailed investigation to understand, control, and optimize the x-ray emission from high-intensity picosecond and femtosecond laser plasmas at various experimental conditions are presented. **(p. 136)**

ThE33 • Solid to plasma transition in femtosecond-laser-irradiated Fe: Collapse of the spin-orbit gap, M. K. Grimes, Y.-S. Lee, M. C. Downer, *The Univ. Texas–Austin.* Self-reflectivity of high contrast 100-fs pulses up to 10^{15} W/cm^2 from Fe targets determines the dielectric constant and the length of the expanding density gradient. **(p. 139)**

ThE34 • Anomalous short wavelength emission by optical field ionization of a preformed boron plasma, Katsumi Midorikawa, Yutaka Nagata, Cornelius Wülker, Koichi Toyoda, *The Institute of Physical and Chemical Research, Japan.* We report reduction of the pump laser intensity required for an optical-field ionized x-ray laser operating below 10 nm. **(p. 142)**

ThE35 • Overheating of femtosecond plasma in freely suspended superthin films, V. G. Babaev, M. S. Dzhidzhoev, V. M. Gordienko, M. A. Joukov, A. B. Savel'ev, A. A. Shashkov, A. P. Tarasevitch, R. V. Volkov, *Moscow State Univ., Russia.* A threefold increase in plasma temperature up to 450 eV has been obtained when heating a 30 nm carbon film by 10^{15} W/cm^2, 200 fsec laser pulse. Promising the advantages of the superthin targets under relativistic intensities are discussed. **(p. 145)**

ThE36 • The role of wavebreaking in second harmonic generation from femtosecond laser-produced plasmas, D. von der Linde, T. Engers, *Univ. Essen, Germany.* Time-resolved measurements suggest that the reflected second harmonic is strongly affected by wavebreaking in an early stage of the expansion at a scale length of a few percent of the wavelength. **(p. 148)**

ThE37 • 100-fs laser absorption in solid density targets, Dwight F. Price, R. M. More, R. S. Walling, R. E. Stewart, *Lawrence Livermore National Laboratory.* Experimental and numerical results are presented for the variation of solid target absorption over a range of intensities, incidence angles, polarizations, and target materials. **(p. 151)**

ThE38 • Propagation of subpicosecond laser pulses through a fully ionized plasma, P. E. Young, P. R. Bolton, *Lawrence Livermore National Laboratory.* Measurements of transmitted light, 90° sidescattered light, and FROG traces have demonstrated relativistic filamentation of 600-fs laser pulses in a preformed, fully ionized plasma. **(p. 154)**

ThE39 • Hot electron distribution from short pulse laser plasma, M. Schnürer, M. P. Kalachnikov, P. V. Nickles, Th. Schlegel, W. Sandner, *Max-Born-Institut, Germany;* P. Ambrosi, R. Nolte, *Physikalisch-Technische Bundesanstalt, Germany.* Energy resolved absolute hard x-ray dose values from sub-ps laser plasmas, compared with a Monte Carlo Bremsstrahlung code, show a non-Boltzmann hot electron distribution. **(p. 157)**

ThE40 • Strong-field ionization of molecules at 35 fs, G. N. Gibson, M. Li, C. Guo, *Univ. Connecticut.* We describe a novel aberration-free multipass kilohertz Ti:Sapphire amplifier suitable for ultrashort laser pulses, which we have used to study the strong-field ionization of molecules. **(p. 160)**

ThE41 • Intensity-dependent probabilities for strong field ionization of xenon, M. A. Walker, P. Hansch, L. D. Van Woerkom, *The Ohio State Univ.* We present ionization probability versus intensity measurements for xenon, extracted directly from time-of-flight mass spectra taken using ISS. **(p. 163)**

ThE42 • Eight- and nine-photon resonances in above threshold ionization of xenon, P. Hansch, M. A. Walker, L. D. Van Woerkom, *The Ohio State Univ.* We report the first observation of higher order multiphoton resonances in xenon using 800 nm light near the saturation intensity. **(p. 166)**

ThE43 • Simulation of ionization ignition and inner atom shell ionization in ultrafast laser-driven clusters, C. Rose-Petruck, K. R. Wilson, C. P. J. Barty, *Univ. California–San Diego;* K. J. Schafer, *Louisiana State Univ.* The ionization dynamics of rare gas clusters in intense, ultrafast laser fields is simulated revealing "ionization ignition." Approximate atomic inner shell ionization probabilities are calculated. **(p. 168)**

ThE44 • Rare gas clusters in intense laser fields, M. Lezius, S. Dobosz, P. d'Olivera, P. Meynadier, M. Schmidt, *CEA-Saclay, France;* J.-P. Rozet, D. Vernet, *Univ. Paris VI, France.* A quantitative study on x-ray photon yield, ion temperature, and ion charge states depending on clustering conditions, intensity and wavelength of laser irradiation. **(p. 171)**

ThE45 • Femtosecond stimulation of atomic and nuclear processes in high intensity laser plasmas, V. S. Rozanov, N. Demchenko, S. Gus'kov, *P. N. Lebedev Physical Institute, Russia;* M. Richardson, *Univ. Central Florida;* D. Salzmann, *Soreq Nuclear Research Center, Israel.* The dynamics of the interaction of intense femtosecond laser pulses with dense plasmas is examined. In particular we consider the effect of the high fields generated in plasmas created from heavy isotopes of hydrogen on the ion kinetics and neutron generation. **(p. 173)**

ThE46 • A debris-less laser-plasma source for EUV and XUV generation, David S. Torres, Christopher M. DePriest, Martin Richardson, *Univ. Central Florida.* The development of compact, high repetition rate (>1 kHz), EUV-XUV laser-plasma source, which uses mass-limited, debris-less, droplet targets is described. **(p. 175)**

ThE47 • Guiding of sub-100 femtosecond pulses in preformed plasma channels, S. P. Nikitin, T. R. Clark, H. M. Milchberg, *Univ. Maryland.* Sub-100-fs pulses from a Ti:sapphire laser system were synchronously injected and guided in preformed plasma channels. Synchronization issues, the guided pulse profile and FROG measurements of guided pulses are presented. **(p. 178)**

ZIA CONCOURSE

8:00am–12:00m
Conference Registration and Speaker/Presider Check-in

ZIA A

8:30am–10:15am
FA • Harmonics I
P. Salieres, *Centre d'Etudes de Saclay, France, Presider*

8:30am
FA1 (Keynote) • Photoelectron spectroscopy with broadly tunable femtosecond harmonics: Applications in physics and chemistry, Richard Haight, *IBM T. J. Watson Research Center.* Photoelectron spectroscopy carried out with high harmonics of femtosecond lasers provides a unique means of investigating the physics and chemistry of a wide variety of materials. Method and experiment will be described. **(p. 182)**

9:15am
FA2 • Temporal coherence of high-order harmonics, C.-G. Wahlström, C. Altucci, M. B. Gaarde, A. L'Huillier, C. Lyngå, R. Zerne, *Lund Institute of Technology, Sweden;* M. Bellini, *L.E.N.S., Italy;* T. W. Hänsch, *Max-Planck-Institut für Quantenoptik, Germany.* We present results from an investigation where we study the interference of two different sources of high-order harmonic radiation produced by the same laser beam. **(p. 185)**

9:30am
FA3 • Coherent, tunable, x-ray emission at 5 nm using high-harmonic generation, Zenghu Chang, Andy Rundquist, Haiwen Wang, Henry Kapteyn, Margaret Murnane, *Univ. Michigan;* Xiuqin Liu, Bing Shan, *Xi'an Institute of Optics and Precision Mechanics, China.* High-harmonics of a 25-fs Ti:sapphire laser, up to the 155th order or 5.2 nm, have been generated in helium. **(p. 187)**

9:45am
FA4 • Ultrafast diffraction from Rydberg wave packets using high harmonics, Kenneth J. Schafer, *Louisiana State Univ.;* Jeffrey L. Krause, *Univ. Florida.* We present calculations that demonstrate that high harmonics can be used to image the time-dependent spatial distribution of a Rydberg wave packet. **(p. 190)**

10:00am
FA5 • Ultrashort high harmonic pulse generated in a highly ionized gas, A. Bouhal, G. Grillon, A. Mysyrowicz, A. Antonetti, *ENSTA-École-Polytechnique, France;* P. Breger, P. Salières, P. Agostini, *Centre d'Etudes de Saclay, France;* R. Constantinescu, H. G. Muller, *FOM-AMOLF, The Netherlands.* Using a cross-correlation technique, we study the effect of the ionization rate on the duration of high-order harmonics generated in a rare gas. **(p. 193)**

ZIA CONCOURSE

10:15am–10:45am
Coffee Break

ZIA A

10:45am–12:15pm
FB • Harmonics II
Justin Peatross, *Brigham Young University, Presider*

10:45am
FB1 (Invited) • Intense laser interactions: Hot electrons and high harmonic ionization, L. D. Van Woerkom, S. Evans, P. Hansch, M. A. Walker, *Ohio State Univ.* We report new high resolution photoelectron and ion yield studies of strong optical field ionization using intense 800 nm fundamental light and its high harmonics. **(p. 196)**

11:15am
FB2 (Invited) • High harmonics as a probe for femtosecond laser-produced plasmas, W. Theobald, R. Häßner, R. Sauerbrey, *Friedrich-Schiller-Univ. Jena, Germany.* High harmonics produced by intensive terawatt lasers can be used to measure the evolution of laser-produced plasmas on a femtosecond time scale. **(p. 199)**

11:45am
FB3 • Short pulse laser drive of a supersonic radiation front into solid matter, E. T. Gumbrell, T. Ditmire, R. A. Smith, M. H. R. Hutchinson, *Imperial College of Science, Technology and Medicine, U.K.* Using picosecond, time-resolved optical probing of high intensity laser-heated fused silica, we have observed radiation-driven ionization fronts with velocities up to 10^9 cm/s. **(p. 202)**

12:00m
FB4 • Developments in XUV laser radiography of laser driven targets, M. H. Key, D. H. Kalantar, J. Nilson, B. A. Remington, S. V. Weber, *Lawrence Livermore National Laboratory;* E. Wolfrum, D. Neely, S. J. Rose, *Rutherford Appleton Laboratory, U.K.;* J. Zhang, N. S. Kim, J. S. Wark, *Oxford Univ., U.K.;* C. L. S. Lewis, A. G. Mac Phee, J. Warwick, *Queens Univ. Belfast, U.K.;* A. Demir, J. Lin, R. Smith, G. J. Tallents, *Essex Univ., U.K.* We report new radiography results with a Ge XUV laser, characterization of the speckle pattern of the laser and development of shorter wavelength Ni-like lasers for radiography. **(p. 205)**

12:15pm–1:45pm
Lunch on Own

FRIDAY
MARCH 21, 1997

ZIA CONCOURSE

1:45pm–5:00pm
Conference Registration and Speaker/Presider Check-in

ZIA A

1:45pm–3:45pm
FC • High Field Laser-Electron Interaction
Richard R. Freeman, *Lawrence Livermore National Laboratory, Presider*

1:45pm
FC1 (Keynote) • Accelerator based source development: Higher, wider and shorter, Erik D. Johnson, *Brookhaven National Laboratory.* A host of new sources are currently being pursued throughout the world which push the performance boundaries higher, wider and shorter than thought possible only a few years ago for accelerator based technologies. Various free electron laser configurations open the window to high power, sub-picosecond synchrotron radiation sources over a wide range of wavelengths. Storage ring sources still have some room for improvement within reason, and intense pulsed x-ray sources by Compton scattering are now being experimentally investigated. This talk will outline the scope of these developments as they relate to the production, and possible utilization, of novel sources of radiation based on accelerator technology. **(p. 208)**

2:30pm
FC2 (Invited) • Observation of nonlinear laser-electron and laser-photon scattering, C. Bamber, S. Boege, T. Koffas, T. Kotseroglou, A. C. Melissinos, D. D. Meyerhofer, D. Reis, *Univ. Rochester;* C. Bula, K. T. McDonald, E. Prebys, *Princeton Univ.;* D. L. Burke, R. C. Field, G. Horton-Smith, A. C. Odian, J. C. Spencer, D. Walz, *Stanford Linear Accelerator Center;* S. Berridge, W. Bugg, K. Shmakov, A. Weidemann, *Univ. Tennessee.* Nonlinear laser-electron and laser-photon scattering (positron production by laser light) were observed during the interaction of an intense laser with 46.6 GeV electrons. **(p. 209)**

3:00pm
FC3 (Invited) • High energy photon generation in colliding laser pulses, F. V. Hartemann, A. L. Troha, J. R. Van Meter, N. C. Luhmann, Jr., *Univ. California–Davis;* A. K. Kerman, *Massachusetts Institute of Technology.* An ultrahigh intensity drive laser boosts the energy of relativistic electrons; a counterpropagating probe pulse then stimulates Compton backscattering at the peak energy to produce TeV photons. The critical probe laser injection angle and the wavelength scaling of this process are derived. **(p. 211)**

3:30pm
FC4 • Single pass free electron lasers as sources of short wavelength coherent radiation, Li Hua Yu, *Brookhaven National Laboratory.* We discuss the properties of single pass free electron lasers starting from a sub-harmonic seed or from self amplified spontaneous radiation. **(p. 214)**

ZIA CONCOURSE

3:45pm–4:15pm
Coffee Break

ZIA A

4:15pm–6:00pm
FD • Strong Field Atomic Physics
Wolfgang Sandner, *Max Born Institute, Germany, Presider*

4:15pm
FD1 (Invited) • Nonperturbative time-dependent theory of two-electron atoms in strong fields, Jian Zhang, P. Lambropoulos, *Max-Planck-Institut, Germany.* A method for the nonperturbative solution of the time-dependent Schrödinger equation in the presence of several open channels and double ionization is presented. **(p. 216)**

4:45pm
FD2 • Photoelectron spectrometry of XUV multiphoton processes in helium, A. Bouhal, G. Hamoniaux, A. Mysyrowicz, A. Antonetti, *ENSTA-Ecole-Polytechnique, France;* P. Breger, P. Agostini, *Centre d'Etudes de Saclay, France;* R. Constantinescu, H. G. Muller, *FOM-AMOLF, The Netherlands;* L. F. DiMauro, *Brookhaven National Laboratory.* By focusing with a wide-band W-Re spherical mirror an XUV beam of harmonics 3–15 of 800 nm (266-61 nm) in helium, we observe two-photon ionization processes. **(p. 219)**

5:00pm
FD3 • Laser-assisted multicolor photoionization of atoms with higher harmonics, Alfred Maquet, Richard Taïeb, Valérie Véniard, *Univ. Pierre et Marie Curie, France.* We simulate photoelectron spectra as they would be obtained by using a radiation pulse containing higher harmonics together with the laser used to generate them. **(p. 221)**

5:15pm
FD4 • Generation and stimulated amplification of high energy photon bursts at gas ionization by few-optical-cycle laser pulses, A. V. Kim, M. D. Chernobrovtseva, D. V. Kartashov, A. M. Sergeev, *Russian Academy of Sciences.* We present an investigation of high energy photon production in subfemtosecond time scale that is driven by few-optical-cycle laser pulses. It is shown that coherent ultrashort x-ray pulses may be exponentially amplified. **(p. 223)**

5:30pm
FD5 • Electron dynamics in the strong field limit of photoionization, B. Sheehy, B. Walker, R. Lafon, M. Widmer, A. Gambhir, L. F. DiMauro, *Brookhaven National Laboratory;* P. Agostini, *Centre d'Etudes de Saclay, France;* K. C. Kulander, *Lawrence Livermore National Laboratory.* Strong field tunnel ionization has been examined over a large dynamic range using kilohertz lasers, making quantitative comparison to rescattering calculation possible. **(p. 226)**

5:45pm
FD6 • Molecular hydrogen in an intense light field, J. Ludwig, H. Rottke, W. Sandner, *Max-Born-Institut, Germany.* We investigate the interaction of $X^1\Sigma_g^+$ ground state H_2 and D_2 molecules with intense subpicosecond laser pulses at 1053 nm and 527 nm and for the first time the interaction of selectively prepared $B^1\Sigma_u^+$ state H_2 molecules with intense near IR light pulses. **(p. 229)**

ANASAZI NORTH

6:00pm–8:00pm
Conference Reception

SATURDAY
MARCH 22, 1997

ZIA CONCOURSE

8:00am–12:00m
Conference Registration and Speaker/Presider Check-in

ZIA A

8:30am–10:15am
SaA • Wakefields
Henry Kapteyn, *University of Michigan, Presider*

8:30am
SaA1 (Invited) • Time and space resolved density development of a laser produced plasma waveguide, T. R. Clark, H. M. Milchberg, S. P. Nikitin, *Univ. Maryland.* Interferometer measurements are presented for a laser-produced plasma waveguide suitable for the guiding of high intensity laser pulses over many Rayleigh lengths. **(p. 234)**

9:00am
SaA2 (Invited) • Relativistically self-guided laser-wakefield acceleration, R. Wagner, S.-Y. Chen, A. Maksimchuk, D. Umstadter, *Univ. Michigan.* The effect of the relativistic self-guiding on the energy and divergence of an electron beam accelerated by a laser wakefield is presented. **(p. 237)**

9:30am
SaA3 (Invited) • Temporal characterization of plasma wakefields driven by intense femtosecond laser pulses, S. P. Le Blanc, M. C. Downer, T. Tajima, *The Univ. Texas–Austin;* C. W. Siders, *Los Alamos National Laboratory;* R. Wagner, S.-Y. Chen, A. Maksimchuk, G. Mourou, D. Umstadter, *Univ. Michigan.* Femtosecond pump-probe techniques based on frequency domain interferometry and forward, collective Thomson scattering are used to characterize resonant and self-modulated laser wakefield accelerators. **(p. 240)**

10:00am
SaA4 • Research in laser acceleration at LLNL, C. A. Back, H. A. Baldis, T. E. Cowan, R. R. Freeman, A. Friedman, D. P. Grote, C. A. Hagmann, W. L. Kruer, A. B. Langdon, N. C. Luhmann, M. J. Mugge, M. D. Perry, T. W. Phillips, W. M. Sharp, K. van Bibber, W. E. White, S. C. Wilks, J. G. Woodworth, *Lawrence Livermore National Laboratory;* F. Hartemann, J. P. Heritage, C. J. Jackson, B. Kolner, G. Le Sage, A. L. Troha, *Univ. California–Davis;* A. K. Kerman, *Massachusetts Institute of Technology.* A research effort is beginning on laser acceleration, emphasizing scalable concepts. Tools include: X-band photoinjector, 100-TW and 1.25-PW lasers, 100-MeV linac, theory and modeling. **(p. 243)**

ZIA CONCOURSE

10:15am–10:45am
Coffee Break

ZIA A

10:45am–12:15pm
SaB • Lasers I
Catherine LeBlanc, *ENSTA, France, Presider*

10:45am
SaB1 (Invited) • Ultrahigh peak power lasers in the 10-fs regime, C. P. J. Barty, T. Guo, F. Raksi, C. Rose-Petruck, J. Squier, B. Walker, K. R. Wilson, V. V. Yakovlev, *Univ. California–San Diego;* C. LeBlanc, *ENSTA-LOA, France;* K. Yamakawa, *Japan Atomic Energy Research Institute, Japan.* Techniques for high-fidelity, high-repetition-rate amplification of 10-fs-range pulses to ultrahigh peak powers are presented. A 70 TW-level Ti:sapphire system incorporating these ideas is described and requirements for the extension to petawatt power levels are outlined. **(p. 246)**

11:15am
SaB2 • Scaling of Nd:glass pumped Ti:sapphire chirped pulse amplification (CPA) systems to 100 TW and beyond, W. E. White, D. F. Price, J. Bonlie, F. G. Patterson, R. E. Stewart, *Lawrence Livermore National Laboratory.* We report on progress in production of >10 J, <100 fs pulses from a Ti:sapphire CPA system. Data is presented demonstrating energies of >1J, focussed intensities of >5 $\times 10^{19}$ W/cm^2. **(p. 249)**

11:30am
SaB3 • Amplitude and phase characterization of 10-fs pulses generated by hollow-core fiber pulse compression, Charles G. Durfee III, Sterling Backus, Henry C. Kapteyn, Margaret Murnane, *Univ. Michigan.* We use frequency-resolved optical gating to optimize and characterize compression of amplified pulses. These are the shortest high-power pulses characterized to date. **(p. 251)**

11:45am
SaB4 • Multi-pulse interferometric frequency resolved optical gating: Real-time phase-sensitive imaging of ultrafast dynamics, C. W. Siders, A. J. Taylor, *Los Alamos National Laboratory;* M. C. Downer, *Univ. Texas–Austin.* We demonstrate a powerful new tool for real-time imaging of ultrafast phase shifts and recovering the intensity and phase of three pulses in a single shot. **(p. 254)**

12:00m
SaB5 • Generation of tunable femtosecond VUV pulses around 100 nm by resonant and near-resonant four-wave difference frequency mixing, G. Korn, O. Kittelmann, J. Ringling, A. Nazarkin, I. V. Hertel, *Max-Born-Institut, Germany.* Using a 0.1 TW Ti:sapphire "master laser," tunable femtosecond VUV radiation has been generated in the region 100–124 nm by two-photon resonant and near-resonant four-wave difference-frequency mixing ($\omega_D = 2\omega_P - \omega_1$) in krypton and argon using intense femtosecond ArF laser pulses (ω_P) and tunable femtosecond pulses (ω_1) generated by an optical parametric generator. **(p. 257)**

12:15pm–2:00pm
Lunch on Own

ZIA CONCOURSE

2:00pm–5:00pm
Conference Registration and Speaker/Presider Check-in

ZIA A

2:00pm–3:30pm
SaC • Lasers II
A. Taylor, *Los Alamos National Laboratory, Presider*

2:00pm
SaC1 (Keynote) • Design and performance of the petawatt laser system, M. D. Perry, D. M. Pennington, B. C. Stuart, R. Boyd, J. A. Britten, C. G Brown, S. Herman, J. L. Miller, H. Hguyen, B. Shore, G. Tietbohl, V. Yanovsky, *Lawrence Livermore National Laboratory.* We recently demonstrated the production of 1.25 PW of peak power in the Nova/Petawatt Laser Facility, generating >500 J in 430 fs. Recent experiments on active beam control and targeting system producing $>10^{21}$ W/cm^2 will be described. **(p. 264)**

2:45pm
SaC2 (Invited) • Ultrahigh peak power lasers present and future, Gerard Mourou, *Univ. Michigan.* We have seen over the past few years an explosion in laser peak power. Today the lasers have peak power of TW and average power of few watts with focused intensity well in the exawatt/cm^2 range. We will describe the next generation of CPA lasers that will take us into the yottawatt/cm^2 range with kW average power. **(p. 267)**

3:15pm
SaC3 • Generation of 30 TW femtosecond pulses at 10 Hz in a Ti:Sapphire laser chain, A. Antonetti, F. Blasco, J. P. Chambaret, G. Chériaux, G. Darpentigny, G. Hamoniaux, C. Le Blanc, P. Rousseau, F. Salin, *ENSTA-Ecole Polytechnique, France.* We describe a femtosecond laser chain capable of reaching 30 TW at 10 Hz in 27 fs with focused intensities higher than 6 10^{19} W/cm^2. **(p. 268)**

ZIA CONCOURSE

3:30pm–4:00pm
Coffee Break

ZIA A

4:00pm–5:30pm
PdP • Postdeadline Paper Session
Anne L'Huillier, *Lund Institute of Technology, Sweden, Presider*

5:30pm–5:45pm
Closing Remarks

Thursday, March 20, 1997

Applications of Short Wavelength Light I

ThA 8:30am – 10:15am
Zia A

Pierre Agostini, *Presider*
Centre d'Etudes de Saclay, France

Extreme Ultraviolet Lithography

Jeffrey Bokor
University of California–Berkeley

Some of the highlights of the recent dramatic progress in the development of extreme ultraviolet lithography technology will be reviewed, with emphasis on the challenge of fabricating and testing a diffraction-limited optical imaging system at 13 nm wavelength.

X-ray microscopy: new capabilities and short pulse possibilities

C. Jacobsen, J. Kirz, J. Maser, A. Osanna, S. Spector, S. Wang, and S. Wirick
Department of Physics, SUNY Stony Brook
Stony Brook NY 11794-3800
B. Calef, M. Howells, S. Lindaas, and D. Pinkus
Advanced Light Source
Lawrence Berkeley Laboratory
Berkeley CA 94720
D. Tennant
Lucent Technologies Bell Laboratories
Crawford Corners Rd
Holmdel NJ 07733-1988

Discussions of x-ray holography as a demanding application for high intensity sources date back at least two decades [1, 2], and x-ray lasers have been used in demonstrations of x-ray microscopy [3, 4, 5]. At the same time, synchrotron-based x-ray microscopes have been developed for imaging of hydrated, unsectioned biological specimens at 30–50 nm resolution, and these microscopes are in regular operation at Göttingen/Berlin, Berkeley, Århus, Stony Brook/Brookhaven, and elsewhere.

This paper discusses new developments in x-ray microscopy, and considers the roles which high intensity sources might play in light of these developments. The new developments include:

- More complete characterizations of radiation damage effects, which clarify the limits imposed by the long exposure times (seconds to minutes) required at synchrotron radiation sources.
- The introduction of cryo methods, whereby a hydrated specimen is rapidly frozen in a manner which can lead to an amorphous form of ice with no apparent ice crystal damage. In electron microscopy, this has been shown to give well-preserved specimens with greatly increased radiation tolerance. First results in x-ray microscopy have shown similar promise [6, 7, 8, 9].
- The development of zone plates with outer zone widths of 30 nm and below, both with specialized systems [10] and with commercially-available equipment in microfabrication labs [11].
- The development of atomic force microscopy readout and computer reconstruction for high resolution x-ray holography [12].
- The use of x-ray absorption near-edge resonances for chemical-state imaging [13]. An example application has been the quantitative mapping of protein and DNA concentrations in sperm at 100 nm resolution so as to rule out certain models of chromosome packing [14].

- The use of dark field methods for visualizing gold labels with antibodies to tag specific biochemical sites [15], and the possibilities for luminescent labeling [16, 17].

- Detailed simulations of contact microscopy, pointing out the difficulties of interpretation of high resolution structure in the images [18, 19].

Activities in these areas at the X-1A beamline at the NSLS will be described.

What are the pulsed source characteristics that would be most useful for x-ray microscopy? The requirements include:

- The right x-ray wavelengths, or (better yet) tunability. Penetration and contrast considerations lead to a desire for wavelengths in the range of 4.5 nm (the carbon edge) down to perhaps 0.4 nm for phase contrast microscopy, or 0.1 nm for x-ray diffraction applications. Both Fresnel zone plates and holography require monochromaticity, either from the intrinsic linewidth of the source or through the use of a monochromator.

- Sufficient number of photons. All high resolution experiments presently use either Fresnel zone plates with 5–10% efficiency, or photoresist detectors which also have about 10% efficiency. The unique capabilities of x-ray microscopy center on samples with water thickness 1–10 μm rather than 0.1 μm, and support membranes and monochromator systems lead to additional flux loss. Total exposures of at least 10^{10} photons on the sample and 10^{12} photons from the source are typical, and for scanning microscopy and holography these photons must have a high degree of mutual coherence.

- Either single-pulse exposure in a timescale of $\lesssim 10^{-9}$ seconds, or a compact system for multiple-pulse integration.

  Short pulse exposure would make possible flash imaging of initially living specimens. This would be especially useful if the pulse could be split to acquire data from multiple angles simultaneously (see e.g., [20]). Hydrodynamic blurring is likely to degrade exposures made over longer times [21, 22], unless the exposure were to be made over timescales of a millisecond or longer so as to allow for efficient heat transport [22, 23].

  With cryo specimens, cheap, convenient, and compact systems could be used for longer exposure times or multiple-pulse integration, and microscope systems with such sources are under development.

The unique types of experiments which would be made possible with short pulse sources will be described.

References

[1] G. Chapline and L. Wood, *Physics Today* **28**, 40–48, June 1975.

[2] J. C. Solem and G. C. Baldwin, *Science* **218**, 229–235 (1982).

[3] J. E. Trebes *et al.*, *Science* **238**, 517–519 (1987).

[4] C. H. Skinner *et al.*, *J. Microscopy* **159**, 51–60 (1990).

[5] L. B. DaSilva *et al.*, *Optics Letters* **17**, 754–756 (1992).

[6] G. Schneider *et al.*, *Synchrotron Radiation News* **8**(3), 19–28 (1995).

[7] G. Schneider and B. Niemann, in [24].

[8] J. Maser *et al.*, in [24].

[9] S. Lindaas *et al.*, in [24].

[10] C. David *et al.*, *Journal of Optics (Paris)* **23**, 255–258 (1992).

[11] S. Spector, C. Jacobsen, and D. Tennant, in [24].

[12] S. Lindaas *et al.*, *J. Opt. Soc. Am. A* **13**, 1788–1800 (1996).

[13] H. Ade *et al.*, *Science* **258**, 972–975 (1992).

[14] X. Zhang *et al.*, *J. Structural Biology* **116**, 335–344 (1996).

[15] H. N. Chapman *et al.*, *J. Microscopy Society of America* **2**, 53–62 (1996).

[16] C. Jacobsen *et al.*, *J. Microscopy* **172**, 121–129 (1993).

[17] M. M. Moronne *et al.*, in G. W. Bailey and A. J. Garratt-Reed, eds., *Proceedings of the 52nd Annual Meeting of the Microscopy Society of America* (San Francisco Press, 1994), pp. 48–49.

[18] A. R. Hare and G. R. Morrison, *J. Modern Optics* **41**, 31–48 (1994).

[19] S. Wang and C. Jacobsen, in [24].

[20] M. R. Howells, C. J. Jacobsen, and S. Lindaas, in J. Arthur, G. Materlik, and H. Winick, eds., *Proceedings of the Workshop on Scientific Applications of Coherent X-rays* (National Technical Information Service CONF-940250, 1994).

[21] J. C. Solem, *J. Optical Society of America B* **3**, 1551–1565 (1986).

[22] R. A. London, J. E. Trebes, and C. J. Jacobsen, *Proc. SPIE* **1741**, 333-340 (1992).

[23] C. Jacobsen and S. Williams, *Proc. SPIE* **1740**, 108–116 (1992).

[24] J. Thieme, G. Schmahl, E. Umbach, and D. Rudolph, eds., **X-ray Microscopy and Spectromicroscopy** (Springer, Berlin, to be published in 1997).

Laser Driven Hard X-ray Sources for Angiography

Z.Jiang [1], A.Ikhlef [1], J.C.Kieffer [1], A. Krol [2], D.A. Bassano [3], C.C.Chamberlain [2], S.C.Prasad [3]

[1)] INRS-énergie et matériaux, 1650 Boul.Lionel-Boulet, C.P.1020, Varennes, Québec, Canada J3X 1S2; Tel: (514) 929 8205; Fax: (514) 929 8102; e-mail: zjiang@inrs-ener.uquebec.ca
[2)] SUNY Health Science Center, Department of Radiology, 750 E. Adams St., Syracuse, NY 13210; [3)] SUNY Health Science Center, Department of Radiation Therapy, 750 E. Adams St., Syracuse, NY 13210

The electron-impact x-ray tube has reached its technological limit, and after many years of improvements it is clear that some of the inherent deficiencies of this x-ray source for radiology cannot be overcome. These deficiencies are the heat-dissipation problem which limits the density of the power that can be delivered by the electron beam, and the related problem of the limit on the minimum focal spot size. The relatively large focal spot size prevents effective work in a high magnification regime and limits the ability to image morphology of the coronary artries, after intravenous injection of the iodine contrast agent, with a spacial resolution of $0.5mm^{-1}$.

A laser- driven, photon-impact X-ray source for mammography and angiography may be able to overcome these limitations. The x-ray source is created upon the collision of visible or infrad photon beam with the surfaces of solids. Presently, modern high power lasers can deliver easily in excess of $10^{19}W/cm^2$ to a target area as small as 5μm in diameter. This should be contrast with the power density delivered by traditional electron-impact X-ray tubes which typically does not exceed $10^{9}W/cm^2$. An extremely short X-ray pulse duration, determined by the laser pulse temporal structrue and target structrure, typically of the order of $10^{-12}s$ and a very small focal spot diameter, determined by the laser beam diameter on the target and the laser-target interaction, are the inherent features of this new-X-ray source.[1]

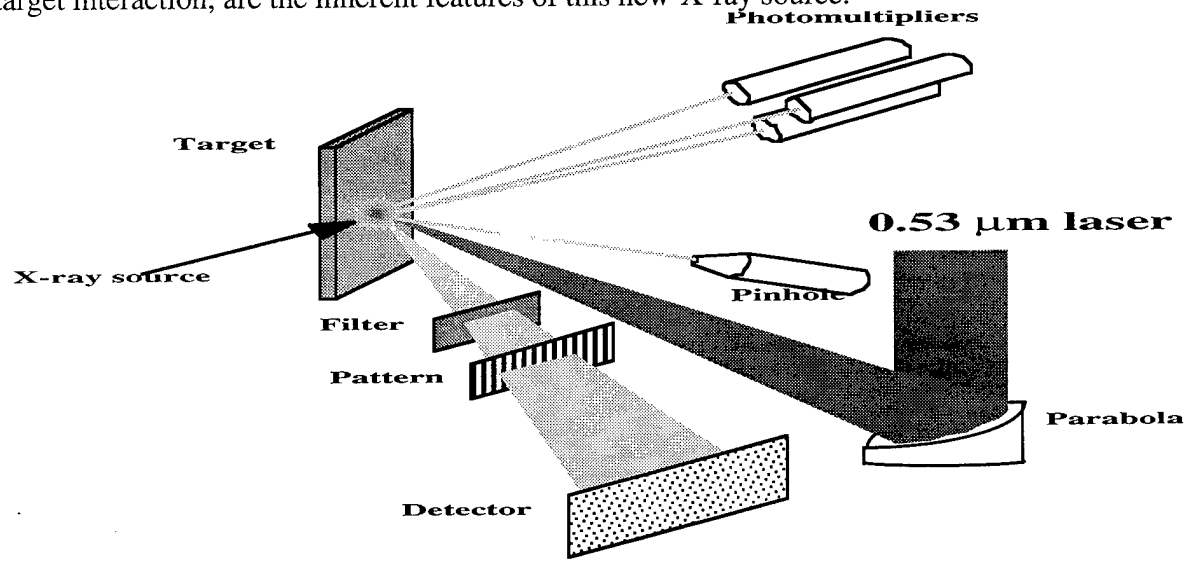

Fig.1 Experimental setup. Infrad laser pulse was not shown.

A laser-driven hard X-ray source is characterized at INRS laser facility. INRS laser system consists of a T^3 laser opearting at 1J, 0.03Hz repetition rate, infrad coherent radiation with 1.05μm wavelength in 550fs pulses. The initial laser beam is split by a KDP crystal into two pulses: a low intensity, infrad pulse (1.053μm, 550fs and 400mJ) and a high intensity, green pulse (0.53μm, 400fs, 400mJ). The time delay between the two pulses can be varied from 0 to 200ps. The infrad pulse is focused by a f/6 lens on a Mo target forming a controlled preplasma about 100μm in diameter, while the delayed green pulse is focused by a f/3 off-axis parabolic mirror to about 10μm in diameter. The radiation intensities are $10^{16}W/cm^2$ and $10^{18}W/cm^2$ for the infrad and green pulses. The target is kept in a vacuum chamber. An experimental setup is shown in Fig.1.

The X-ray yield was measured with a multichannel spectrometer which consisted of several photomultipliers-NaI(Tl) scintillator detectors with suitable K-edge filters and a crystal spectrometer. Background signals were eliminated by the use of very thick lead shielding and electron sweeping magnets in the front of the dectors. The spectrometers were carefully calibrated to investigated the conversion efficiency from laser light to X-rays photons in the 10-100keV range. The image of the focal spot were obtained using a pinhole camera and photographic film. The images of test objects were obtained using suitable filters and films.

The high energic electrons, or suprathermal electrons are created in the laser-target interaction. The suprathermal electrons then penetrate the solid target to conver their energy into hard x-ray by Bremsstrahlung and characteristic X-ray emission. The temperature of suprathermal electrons created in the present experiment was estimated from the slope of the hard X-ray spectra (10-100keV) to be at 25keV. The conversion efficiency of laser energy to X-ray photons is varied with the time delay between the infrad and green pulses. The maximum conversion efficiency of about $2x10^{-4}$ was reached. This is comparable to the conversion efficiency of an X-ray tube with a Mo target at $25kV_p$ which is estimated as $9x10^{-4}$. The duration of the X-ray pulse was estimated by our time-resolved spectroscopy to be about 8ps. The emitted X-ray flux at 20keV within a 1keV bandwidth can be estimated as $6x10^8$ photons in 2 π srd. per laser shot, which is around 0.2MW.

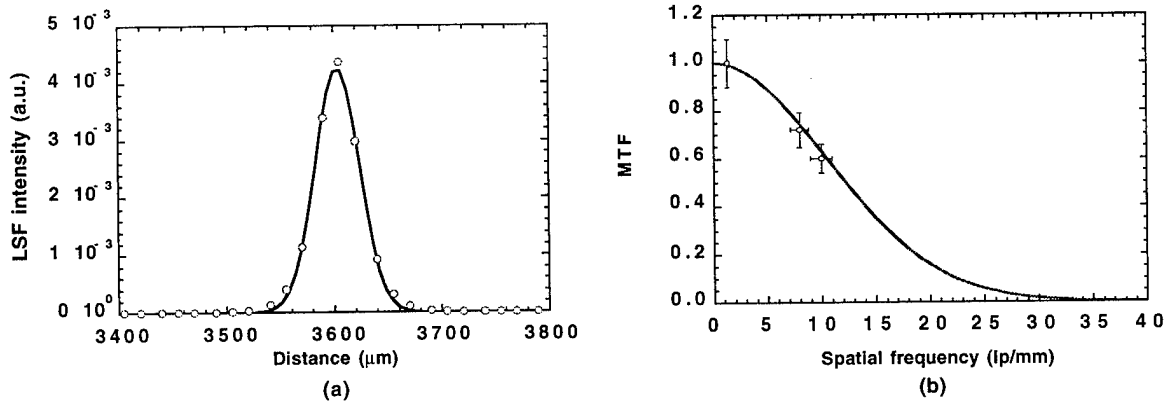

Fig.2 (a)Line-spread function inferred from resolution pattern image and (b) Predicted modulation function with 48μm FWHM for objective magnification of 2.

The X-ray focal spot was evluated from the images taken with resolution test patten set at different objective magnification, as well as from pinhole camera images. We observed that the characteristic dimention of laser driven X-ray source is reduced by an order of magnitudeas

compared with the micro focal spot produced by an X-ray tube. We found the brightness distibution of a X-ray focal spot of a laser driven source could be best described by a two-dimensional Gaussian distribution from the analysis of an image of a resolution pattern taken in the experiment. The line spread function (LSF) inferred from the microdensitometer trace of the image of resolution test pattern is shown in Fig.2a. The FWHM of fitted Gaussian LSF is equal to 48μm. It is well known that the modulation transfer function (MTF) of a focal spot with Gaussian intensity distribution is also a Gaussian function[2]. Therefore, we can easily predict MTF due to the focal spot for different object magnification (M). Results obtained for a FWHM equal to 48μm and M equal to 2 is shown in Fig.2b.

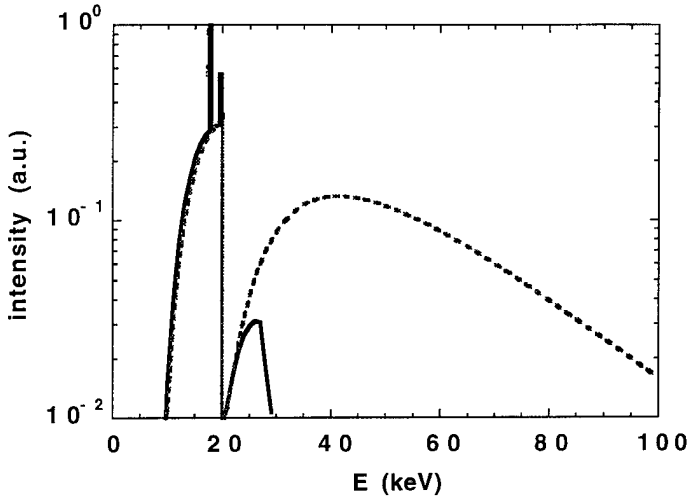

Fig.3 Bremsstrahlung spectra from filtered X-ray tube (solid line) and laser driven X-ray source (dashed line)

The disadvantage of a laser based X-ray source is the high energy component of its emission spectrum, which may reduce the subject contrast, another concern of the imaging system. Fig.3 shows the comparison Bremsstrahlung spectra delivered by calculated 30keV X-ray tube and laser driven X-ray source filtered by 50μm of molybdenum filter. We found that X-ray tube provides a more suitable spectrum for contrast ratio at 20keV because it shows a low number of high energy (greater than 20keV) photons compared to laser based X-ray source.

Due to high spatial resolution performance using laser X-ray source, it would be interesting to use Ross filter imaging technique where the transmission window will be centered at desired wavelength range or digital subtraction to improve the contrast effect from the emission spectrum.

Reference

1. K.Herrlin, G.Svahn, C.Olsson, H.Petterson, C.Tillman, A.Persson, Wahlstrom and S.Svanberg, Radiology **189**, 65-68, 1993
2. A.P.Tzannes and J.M.Mooney, Optical Eng.**34**, 1808-1817, 1995

Radiological applications of hard X-ray emission from a laser-produced plasma

M. Grätz[1], C. Tillman[1], A. Nykänen[1], L. Kiernan[1], C.-G. Wahlström[1], S. Svanberg[1], K. Herrlin[2]
[1]Department of Physics, Lund Institute of Technology, P.O. Box 118, S-221 00 Lund, Sweden
[2]Department of Radiology, University Hospital, S-221 85 Lund, Sweden
Phone: + 46 46 2227654, Fax: + 46 46 2224250, E-Mail: Matthias.Graetz@fysik.lth.se

INTRODUCTION

The use of laser-produced plasmas as soft x-ray sources has been investigated for a long time. Laser pulse durations were normally of the order of nanoseconds, and high peak powers were consequently only available at very large laser facilities. This situation changed with the development of terawatt laser systems based on the chirped-pulse amplification technique. With these laser systems, peak powers in the terawatt range became available in ultra-short pulses, leading to focused intensities well above 10^{17} W·cm^{-2}.

It was soon found, that focusing of such intense pulses onto solid targets resulted in the generation of intense, energetic bursts of x-ray radiation [1]. The unique properties of this x-ray emission have lead to an increasing interest in possible radiological applications which cannot be implemented with conventional x-ray tube technology. Key-points for advanced applications are the very short x-ray pulse duration and the small source size, corresponding to a high brightness of the source, and the spectral composition of the x-ray emission. The conversion efficiency from laser light into x-rays, above 25 keV, can be as high as 0.16 % [2].

A laser-produced plasma source has the advantage of being relatively compact and less expensive than for example a synchrotron, which is another x-ray source that can be used for novel medical applications. More recently introduced x-ray generation schemes, which might become relevant for radiological application (e.g. free-electron lasers), are still hampered by the relatively low achievable photon energy and flux.

Apart from radiological applications discussed in this paper, x-ray radiation from laser-produced plasmas is also used in a large number of more research-orientated applications, e.g. ultrafast diffraction experiments and x-ray pump-and-probe schemes.

SETUP AND SOURCE CHARACTERISTICS

The Lund Laser Centre terawatt laser system [3] was used in the presented work. In its present setup, it typically delivers pulses of 110 fs duration, at 794 nm and 10 Hz repetition rate, with about 150 mJ of energy on target. In the target chamber, the laser pulses are focused with a parabolic mirror onto a rotating tantalum target [4]. Focused intensities on the target surface are of the order of 10^{17} W·cm^{-2}. X-ray radiation is emitted in a broad spectral range, extending from below 1 keV up to several 100 keV or even MeV [5]. The x-ray pulse duration in the region below 10 keV is of the order of a few picoseconds [6]. At higher photon energies, it becomes increasingly difficult to measure the pulse duration. We measured an apparatus-limited pulse duration, at effective detection energies of > 50 keV, to be less than 10 ps. The X-ray intensity after filtering with 0.15 mm of copper (in order to suppress the low-energy part of the emission) is of the order of 100 MW/sr (assuming a pulse length of 2 ps), as determined with TLD dosimeters. The x-ray

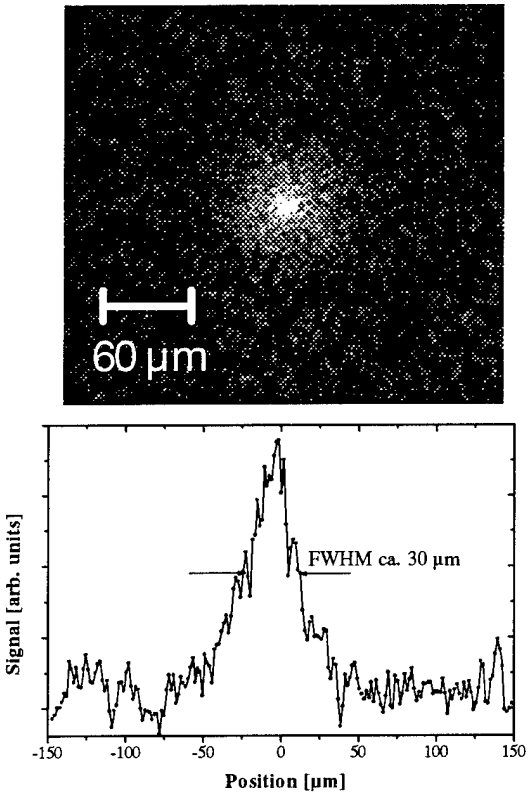

Figure 1: X-ray source pinhole image and corresponding intensity profile.

source size was measured to be about 30 µm (FWHM), using a 5 µm diameter platinum pinhole. A typical pinhole image is shown in Figure 1. Source size measurements at different energy ranges will be presented.

At the present stage, the *average* x-ray intensity is still much lower than for conventional x-ray devices. An intensity increase can be achieved by both increasing laser intensity and repetition rate. However, dosimetric considerations have to be taken into account for radiological applications, because an increase in laser intensity will change the x-ray emission spectrum.

MAGNIFICATION AND SHORT-PULSE IMAGING

The small source size allows for the sharp x-ray imaging of very small objects, which will be shown for some test patterns. The ability to detect such small objects is of importance both in medical (e.g. breast tissue micro-calcifications or bone-microstructures) and technical imaging (e.g. detection of microcracks). Another advantage of using x-ray magnification imaging is the reduction of scattered radiation due to the air gap (scattered radiation is less directional than unscattered radiation, therefore decreasing relatively faster with increasing path length to the detector). The x-ray intensity is sufficiently high to obtain images in a single x-ray pulse [5]. This opens new possibilities for the x-ray imaging of short-lived processes, as for example solid-state phase transitions or fast rupture processes. However, fast processes of radiological interest on such short time scales are quite rare.

When aiming towards medical applications, dosimetry becomes an important aspect and was therefore addressed in a study on cell survival, where living cells were exposed to various doses of laser-generated x-rays [7]. Results from this study will be presented.

SCATTER-REDUCED IMAGING

Scattered radiation has always been a major concern in medical radiology, because it reduces the contrast and the detectability of structures of interest. The potential of scatter-reduced imaging is not only an improved image quality (with unchanged absorbed dose for the patient), but also a possible reduction in the absorbed dose received by the patient (while preserving the image quality).

As demonstrated earlier, scattered radiation can be partly suppressed by time-gated detection of short x-ray pulses [8]. This concept of time-gated imaging has been succesfully applied in the optical domain [9]. We have studied in more detail the potential image improvements through time-gated x-ray imaging, investigating the influence of photon energy, time resolution and tissue composition [10]. As shown in Figure 2 for the example of soft tissue, significant image im-

provements (up to a factor of 5 at 20 cm tissue thickness) can be obtained, when choosing an appropriate photon energy.

Results will be presented, showing the influence of the x-ray pulse shape on the performance of time-gated imaging. For example, a fast rising edge of the x-ray pulse can result in an increased image improvement, allowing the trailing edge to have a longer temporal decay without loss of image quality. These results might guide x-ray pulse-shaping considerations in more application-orientated setups. Comparisons with already established scatter-reduction techniques, i.e. anti-scatter grids, will be given. The intrinsic advantage of time-gated imaging is that all photons exiting the patient reach the detector. This is in contrast to grid techniques where some part of the radiation is attenuated by the collimating structures. Therefore, at comparable detector sensitivities, time-gated imaging would be superior. However, at present times the limitations in x-ray sensitivity of time-gated image detectors result in inferior performance compared to anti-scatter grids. Fortunately, the rapid technical development of detection techniques might soon overcome this problem.

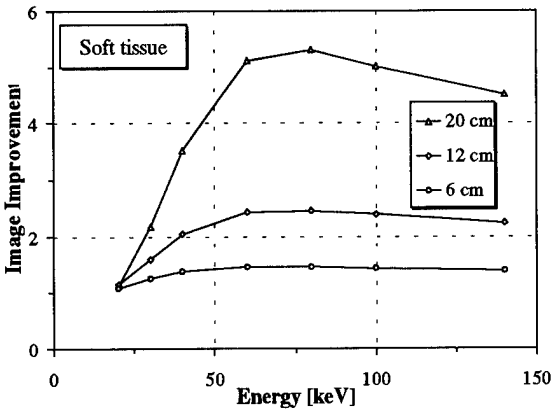

Figure 2: Simulated image improvement relative to non-gated imaging for soft tissue as a function of photon energy (gate width: 20 ps).

REFERENCES

[1] J.D. Kmetec, C.L. Gordon III, J.J. Macklin, B.E. Lemoff, G.S. Brown and S.E. Harris, *MeV X-ray generation with a femtosecond laser*, Phys. Rev. Lett. **68**, pp. 1527-1530, 1992

[2] M. Schnürer, P.V. Nickles, M.P. Kalachnikov, W. Sandner, R. Nolte, P. Ambrosi, J.L. Miquel, A. Dulieu and A. Jolas, *Characteristics of hard X-ray emission from subpicosecond laser-produced plasmas*, to be published in J. Appl. Phys.

[3] S. Svanberg, J. Larsson, A. Persson and C.-G. Wahlström, *Lund High-Power Laser Facility - Systems and first results*, Phys. Scr. **49**, pp. 187-197, 1994

[4] C. Tillman, A. Persson, C.-G. Wahlström, S. Svanberg and K. Herrlin, *Imaging using hard X-rays from a laser-produced plasma*, Appl. Phys. B **61**, pp. 333-338, 1995

[5] K. Herrlin, G. Svahn, C. Olsson, H. Pettersson, C. Tillman, A. Persson, C.-G. Wahlström and S. Svanberg, *Generation of X-rays for medical imaging by high-power lasers: Preliminary results*, Radiology **189**, pp. 65-68, 1993

[6] J.C. Kieffer, M. Chaker, C.Y. Côté, Y. Beaudoin, H. Pépin, C.Y. Chien, S. Coe and G. Mourou, *Time-resolved kiloelectron-volt spectroscopy of ultrashort plasmas*, Appl. Opt. **32**, pp. 4247-4252, 1993

[7] C. Tillman, G. Grafström, A.-C. Jonsson, I. Mercer, S. Svanberg, B.-A. Jönsson, S.-E. Strand and S. Mattson, *Survival of V76-CH cells studied* in vitro *after extremely high absorbed dose irradiation by X-rays from a lalser-produced plasma*, submitted to Phys. Med. Biol

[8] C.L. Gordon III, G.Y. Yin, B.E. Lemoff, P.B. Bell and C.P.J. Barty, *Time-gated imaging with an ultrashort-pulse laser-produced-plasma X-ray source*, Opt. Lett. **20**, pp. 1056-1058, 1995

[9] S. Andersson-Engels, R. Berg, O. Jarlman and S. Svanberg, *Time-gated transillumination for medical diagnostics*, Opt. Lett. **15**, pp. 1179-1181, 1990
L.-H. Wang, P.P. Ho, C. Liu, G. Zhang and R.R. Alfano, *Ballistic 2D-imaging through scattering walls using an ultrafast optical Kerr gate*, Science **253**, pp. 769-771, 1991

[10] M. Grätz, A. Pifferi, C.-G. Wahlström and S. Svanberg, *Time-gated imaging in radiology: Theoretical and experimental studies*, submitted to J. Selec. Topics Quantum Electron. on Lasers in Medicine and Biology

Thursday, March 20, 1997

Laser-Produced Plasmas

ThB 10:45am – 12:15pm
Zia A

George Kyrala, *Presider*
Los Alamos National Laboratory

Experimental Studies of the Propagation of Ultrashort, Intense Laser Pulses in Underdense Plasmas

B.D. Thompson, A. McPherson, A.B. Borisov, K. Boyer and C.K. Rhodes
Laboratory for Atomic, Molecular and Radiation Physics
Department of Physics (M/C 273)
University of Illinois at Chicago
845 W. Taylor St.
Chicago, IL 60607-7059
Telephone: (312) 996-5443; Telefax: (312) 996-8824; E-mail: thompson@uic.edu

Many practical applications of ultrashort, high power laser pulses require the laser pulse to be focused to a high intensity and remain relatively collimated over large distances in plasmas. Such applications include x-ray lasers [1], laser-plasma-based electron accelerators [2] and laser-induced nuclear fusion schemes [3]. Self-focusing and self-channeling of laser pulses by relativistic and ponderomotive mechanisms [4] are laser-plasma processes which can accomplish this feat.

This summary describes experimental measurements of the spatial and spectral properties of high power laser pulses propagating in underdense plasmas. The laser pulses were generated using a Ti:Al_2O_3/KrF^* laser system [5] which produces 200 mJ laser pulses at 248 nm with a 270 fs pulse duration. The laser pulses were focused with an f/3 off-axis parabolic mirror to a spot size of 3 μm which corresponds to a peak intensity of about 10^{19} W/cm^2. The target was a xenon gas jet produced by a sonic nozzle with a 1.5 mm orifice. A stainless steel gas block was attached to the nozzle on the incoming side of the orifice in order to block the expansion of the gas jet in the direction of the incoming laser pulse and minimize the amount of ionization-induced defocusing that can occur before the laser pulse reaches the focal plane. The plasma is formed when the xenon atoms undergo optical-field and collisional ionization. The propagation of the laser pulse was imaged by focusing the Thomson-scattered radiation emitted in the transverse direction from the plasma onto a CCD.

Fig. 1 shows magnified images of the laser pulse propagation in the xenon gas jet for two different gas densities. The laser pulse propagates from left to right in the figure and the spatial resolution of each image is 6 μm. The gap in the signal on the left side of each image is due to the presence of the gas block attached to the nozzle and indicates where the edge of the nozzle orifice is located in the image. The laser propagation observed when the atom density of the target was 5.0×10^{18} cm^{-3} is shown in Fig. 1(a). The propagation shows the "bow tie" structure that is characteristic of a linearly propagating laser pulse which can be explained by the low atom density in this case for which the presence of the plasma will have a weak effect on the laser pulse. Fig. 1(b) shows the laser pulse propagation when the target density was 1.6×10^{19} cm^{-3}. When the laser pulse reaches a diameter of about 70 μm the laser pulse self-focuses. After the pulse self-focuses it appears to propagate in a filament for a distance of about 200 μm. The measured diameter of the filament is resolution-limited at 6 μm. After this filament the pulse is seen to diverge with a divergence angle less than that expected due to diffraction. The filament itself is very difficult to observe due to the weak level of Thomson-scattered radiation emitted from it. This is possibly due to the

ponderomotive effect which expels free electrons from the high intensity core of the laser pulse. Evidence for the ponderomotive effect is also shown by the weak Thomson emission from the central portion of the laser pulse immediately before and after the filament.

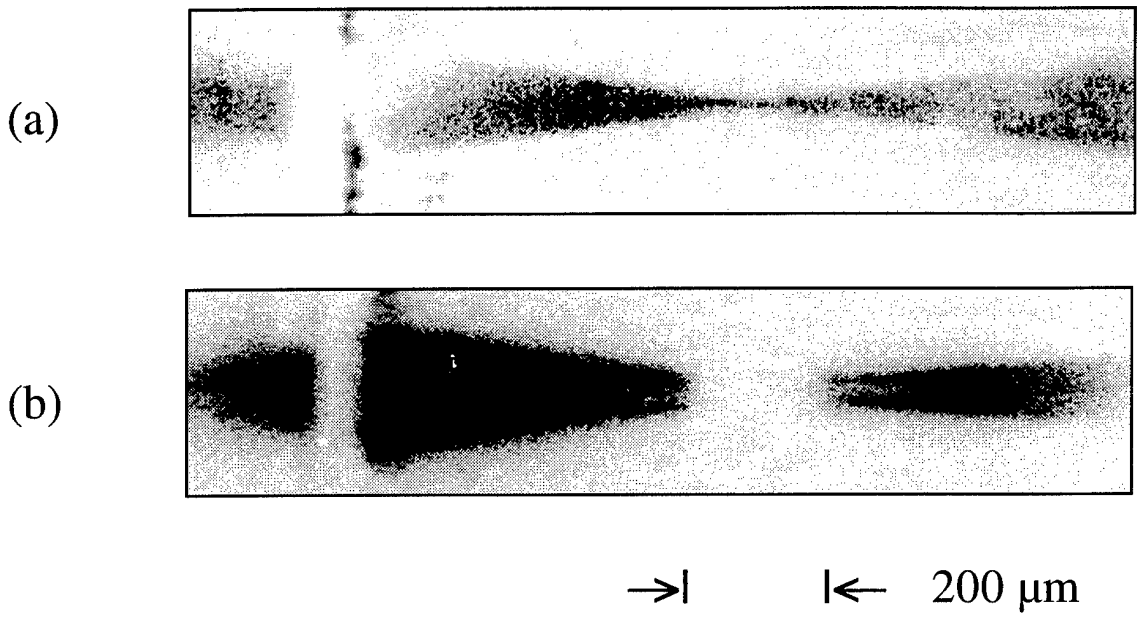

Figure 1. Spatially-resolved Thomson-scattered radiation from a laser-irradiated xenon gas jet when the target density was a) 5.0×10^{18} cm^{-3} and b) 1.6×10^{19} cm^{-3}. The laser pulse propagates from left to right.

Measurements of the laser pulse energy transmitted through the gas jet as a function of the target density show that virtually all of the laser energy is absorbed when the target density exceeds about 10^{19} cm^{-3}. Above this density only ASE from the KrF^* amplifiers in the laser system was transmitted and its transmittance was observed to fall off very slowly with increasing gas density. The ASE in the laser pulse will focus to a much lower intensity than the amplified seed pulse because of its lower energy (5 mJ), longer duration (20 ns) and greater divergence. Hence, it will not be absorbed as strongly due to the lower rate for multiphoton processes. The high degree of absorption in the gas jet is also evidenced by the termination of the Thomson-scattered signal before the end of the gas jet in Fig. 1(b). The strong coupling of the laser to the target gas is attributed to the generation of clusters in the gas jet which have been shown to enhance the absorption of laser energy [6].

Fig. 2 shows the transmitted pulse spectra for three different target densities including the unmodulated laser pulse. The blueshifting of the laser pulse spectrum observed for the nonzero gas densities is due to ionization-induced self-phase-modulation [7]. No evidence of stimulated Raman scattering (SRS) was observed in the spectra of the forward or transverse scattered light. The presence of SRS was investigated for several gases (Ne, Ar, Kr and Xe) spanning a large range of atomic number and for a large range in target density, $(2.0\text{-}30) \times 10^{18}$ cm^{-3}. The absence of stimulated

Raman scattering is attributed to the low electron density for the lighter gases and to the large amounts of laser energy depletion for the heavier gases. In agreement with the energy transmission measurements, only the spectrum of the ASE in the laser pulse was observed when the gas density exceeded 10^{19} cm^{-3}.

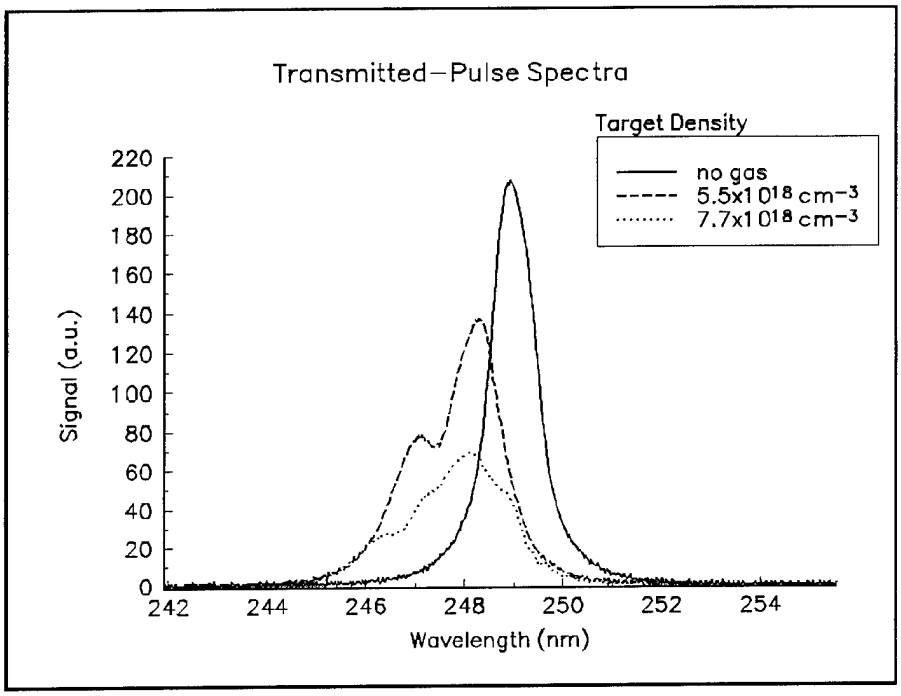

Figure 2. Spectra of the transmitted pulse for three different target densities.

[1] N.H. Burnett and P.B. Corkum, J. Opt. Soc. Am. B **6**, 1195 (1989); D.C. Eder *et al.*, Phys. Rev. A **45**, 6761 (1992).
[2] E. Esarey *et al.*, Phys. Fluids B **5**, 2690 (1993).
[3] M. Tabak *et al.*, Phys. Plasmas **1**, 1626 (1994).
[4] A.B. Borisov *et al.*, Phys. Rev. Lett. **68**, 2309 (1992); A.B. Borisov *et al.*, Phys. Rev. A **45**, 5830 (1992).
[5] B. Bouma *et al.*, J. Opt. Soc. Am. B **10**, 1180 (1993).
[6] A. McPherson *et al.*, Phys. Rev. Lett. **72**, 1810 (1994).
[7] Wm. M. Wood *et al.*, Phys. Rev. Lett. **67**, 3523 (1991).

HIGH ENERGY EXPLOSION OF SUPER-HEATED ATOMIC CLUSTERS

T. DITMIRE, J. W. G. TISCH, E. SPRINGATE, M. B. MASON, N. HAY, R. A. SMITH, J. P. MARANGOS AND M. H. R. HUTCHINSON

Blackett Laboratory, Prince Consort Road,
Imperial College of Science, Technology, and Medicine
London, SW7 2BZ, United Kingdom
t.ditmire@ic.ac.uk
phone: 0171 243 2655

Though the nature of intense, short pulse laser interactions with single atoms and solid targets has been the subject of extensive experimental and theoretical investigation over the last 15 years, only recently has the nature of intense laser interactions with van der Waals bonded atomic clusters of 20 - 100 Å been addressed in experiments. These experiments have suggested that the laser-cluster interaction is much more energetic than that of isolated atoms, producing bright x-ray emission (100 - 5000 eV photons) when a low density gas containing clusters is illuminated [1,2]. While experiments have indicated indirect evidence for keV electron production in the cluster through time resolved x-ray spectroscopic data [2], until recently no direct data on the exact nature of the kinetic energies produced by the intense irradiation of clusters existed. In this paper we present the first energy distribution measurements of both electrons and ions resulting from the interaction of a femtosecond laser pulse with van der Waals bonded clusters. We find that the cluster is rapidly heated by collisional inverse bremsstrahlung. This heats a sizable fraction of the electrons in the cluster to a temperature above 1 keV. The super-heated cluster then explodes, ejecting ions with substantial kinetic energy. In fact, ions with energy up to 1 MeV are produced in Xe clusters.

Our experiment used a chirped pulse amplification Ti:sapphire laser capable of delivering 40 mJ, 150 fs pulses at a wavelength of 780 nm. The linearly polarized laser pulse was focused into a time-of-flight (TOF) chamber, yielding a peak intensity of about 2.0×10^{16} W/cm^2. The Xe-clusters were produced with a solenoid valve pulsed sonic gas-jet. With sufficiently high backing pressure, clusters form in the gas jet flow due to the cooling associated with the adiabatic expansion of the gas into vacuum [3]. The jet was operated with a backing pressure range from 0 - 6 bar. A skimmer served to produce a low density cluster beam which intercepted the laser beam at the laser focus. The presence of Xe clusters in the flow from our gas jet has been confirmed through a series of Rayleigh scattering measurements in the gas jet. These measurements indicated that the clusters formed reach an average diameter of 65Å ± 5Å with a jet backing pressure of 6 bar. Three closely spaced grids were placed behind the entrance aperture to the TOF drift tube. These grids allowed us to retard electrons produced at the laser focus and determine the electron energy. The ion energy spectra were determined from the TOF spectrum.

The energy spectrum of the electrons produced during the irradiation of 50 Å Xe clusters (4.5 bar backing pressure) with an intensity of 1.5×10^{16} W/cm^2 is shown in figure 1a. This spectrum was found by measuring the electron yield in the direction of the laser polarization as a function of retarding voltage and then differentiating the

result. The most remarkable aspect of this energy distribution is the presence of a large fraction of the electrons with between 2 and 3 keV of kinetic energy. Previous measurements of ATI spectra from single atoms at this intensity and pulse duration has indicated that the vast majority of the electrons produced exhibit energy below 100 eV [4]. The spectrum observed from the Xe clusters clearly exhibits a much greater coupling of laser energy to hot electrons than is present during the irradiation of single atoms. Another striking aspect of the shape of the electron energy spectrum is the presence of a sharply defined peak at 2.5 keV.

To further illuminate the physics of the laser cluster interaction and explain the presence of the sharp peak in the electron spectrum we have conducted numerical modeling of the dynamics. In brief, the model treats the cluster as a spherical microplasma, subject to the standard processes of a laser heated plasma including tunnel and collisional ionization, collisional heating, expansion, and electron free streaming. The electric field in the spherical cluster is given as

$$E = 3E_0/|\varepsilon + 2|, \qquad (1)$$

where E_0 is the laser electric field in vacuum and ε is the dielectric constant of the free electron cluster plasma. Eq. 1 has a sharp maximum when $\varepsilon = -2$. At this point the cluster undergoes rapid collisional heating because of an enhancement of the field in the cluster. This resonance is similar to the giant resonance in light absorption observed in metallic clusters [5]. The calculated electron distribution for a 50 Å Xe cluster subject to a 150 fs Gaussian, 780 nm pulse with a peak intensity of 10^{16} W/cm^2 is shown in figure 1b. The calculated distribution exhibits a close similarity to the measured electron distribution, having a two lobed structure. The sharp peak near 2 keV is clearly consistent with the observed data, both in position and its narrow width. The modeling indicates that this peak is the result of the plasmon resonance predicted by eq. (1).

Charge separation of these hot electrons inevitably leads to a very fast expansion of the cluster ions. The ambipolar potential created by the hot electrons radially accelerate the ions of the cluster. In figure 2, the energy spectrum, derived from the TOF trace in the inset, of Xe ions produced from the irradiation of 65 Å (~ 2500 atom) Xe clusters is illustrated. This energy spectrum is radically different than previously observed ion energy spectra from the intense field fragmentation of molecules or small clusters. Most surprising is the production of significant numbers of very hot ions with energies out to 1 MeV. This energy is four orders of magnitude higher than has previously been observed in the Coulomb explosion of molecules [6] and about 1000

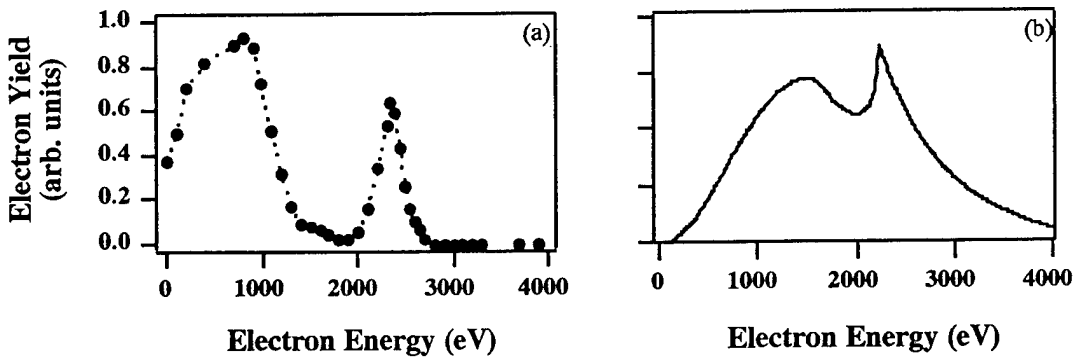

Figure 1: (a) Measured electron kinetic energy distribution from Xe clusters for a peak intensity of 1 x 10^{16} W/cm^2 (cluster size = 50 Å). (b) Calculated electron energy distribution for a peak intensity of 1 x 10^{16} W/cm^2 and a cluster size of 50 Å.

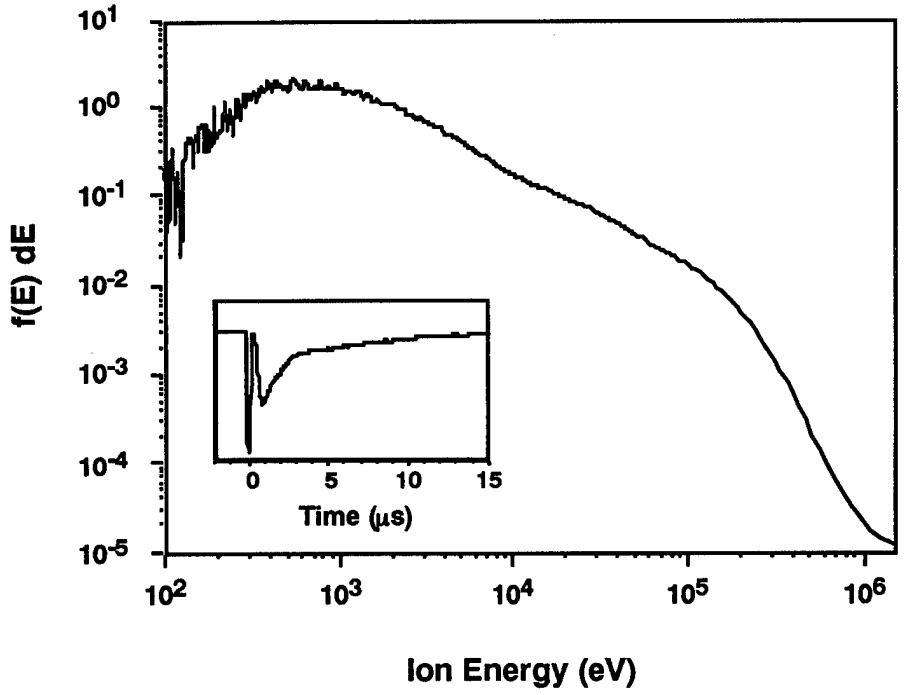

Figure 2: Measured ion kinetic energy distribution from Xe clusters for a peak intensity of 2 x 10^{16} W/cm^2 (cluster size = 65 Å). The inset shows the time-of-flight spectrum.

times higher than the energy of Ar ions ejected in the Coulomb explosion of small clusters irradiated at lower intensity [7]. The average ion energy of the distribution shown in figure 2, defined as $\langle E \rangle = \int Ef(E)dE / \int f(E)dE$, is 45±5 keV. Thus the average laser energy deposited in the cluster per ion is substantial. Furthermore, we find that the ions are ejected with equal energy in all directions with respect to the laser polarization, an artifact of the spherical geometry of the exploding cluster. Again, this is in stark contrast to the Coulomb explosion of small linear molecules.

In conclusion, we have measured the energies of electrons and ions produced during the interaction of intense, 150 fs laser pulses with atomic clusters. We find that rapid collisional heating of the electrons in the cluster prior to significant expansion yields an electron distribution that exhibits two distinct peaks with energies ranging up to 3 keV. The explosion of this hot micro-plasma results in the ejection of ions with energy up to 1 MeV.

References

1. A. McPherson, B.D. Thompson, A.B. Borisov, K. Boyer, and C.K. Rhodes, Nature **370**, 631 (1994).
2. T. Ditmire, T. Donnelly, R.W. Falcone, and M.D. Perry, Phys. Rev. Lett. **75**, 3122 (1995).
3. O.F. Hagena and W. Obert, J. Chem. Phys. **56**, 1793 (1972).
4. U. Mohideen, M.H. Sher, H.W.K. Tom, G.D. Aumiller, O.R.Wood II, R.R. Freeman, J. Bokor, and P.H. Bucksbaum, Phys. Rev. Lett. **71**, 509 (1993).
5. C. Bréchignac and J.P. Connerade, J. Phys. B: At. Mol. Opt. Phys. **27**, 3795 (1994).
6. C. Cornaggia, M. Schmidt, and D. Normand, *J. Phys. B: At. Mol. Opt. Phys.* **27**, L123 (1994).
7. J. Purnell, E.M. Snyder, S. Wei, and A.W.C. Jr., *Chem. Phys. Lett.* **229**, 333 (1994).

Hard X-ray Emission from Femtosecond Laser Interaction in Overdense Plasmas

A.A. Andreev, V.N. Novikov*, K.Yu. Platonov*, J.-C. Gauthier†*
** ILPh, SC "S.I.Vavilov State Optical Institute",*
12, Birzhevaya line, St. Petersburg, Russia
†LULI, Ecole Polytechnique, 91128 Palaiseau Cedex, France
Tel: 0169333260, Fax: 0169333009, e-mail: gauthier@greco2.polytechnique.fr

1 Introduction

The recent development of ultra-short pulse lasers has made possible the investigation of laser matter interaction at ultra-high intensities. For sub-picosecond pulses, a hot and overdense plasma is produced very rapidly during the rise of the pulse and further laser interaction occurs with this plasma. One of the results of the interaction is the generation of fast electrons and of intense hard x-ray emission. The x-ray pulse duration is determined by the mean free path of the fast electrons in the target material. It can be very short ($< 1ps$) and its intensity sufficient to be registered by the usual methods. With high laser pulse repetition rates, it has been demonstrated [1] that one can obtain an instantaneous signature of fast-x-ray dense-matter interaction processes. The high energy of the x-ray photons (up to $\approx 1MeV$) makes it possible to study small size objects and even to excite nuclear levels. Numerous papers [2-7] have been devoted to the study of femtosecond laser pulse interaction with plasmas. In this paper, we calculate the electron energy distribution function in the presence of the laser field, the absorption coefficient, and the parameters of the fast electron flux in the plasma. Our absorption results are in agreement with previously published [3-5] papers. A new feature of our calculations is the determination of the energy and spectrum characteristics of the hard x-ray pulse produced by the interaction of an intense laser with a solid-state target.

2 Basic set of equations and numerical solution

We consider a plane linearly polarized electromagnetic wave with oblique incidence on a semi-infinite plasma. The plasma temperature is T_e and the electron density n_e is higher than the critical density n_c. The wave with amplitude E_0 and frequency ω_0 is chosen in such a way that the electron quiver velocity v_e is larger than the thermal velocity v_T. The scale length of the electron density gradient is very much smaller than the depth of the skin layer l_s. This is justified by the fact that during the laser pulse ($< 100fs$) the movement of the ions is negligible and the plasma edge preserves its sharpness. The dynamics of the plasma electron component is described by a self consistent set of equations involving the collisionless kinetic Boltzmann equation ($0 < x < l_s$), the Maxwell equations for electromagnetic fields (in covariant form), and the kinetic Fokker-Plank equation for $x > l_s$. Oblique incidence is "boosted" into normal incidence by using the method of Gibbon [5]. The ambipolar field E_a is determined from the constraint of zero current along the x laser axis. We use the requirement of mirror-like reflection of the electrons by the edge of the plasma. This model was implemented in our code KINET1D2V. In Fig. 1a, we show the distribution function f_e calculated at time $180\omega_0 t$ and position $x = 3l_s$. The calculation was

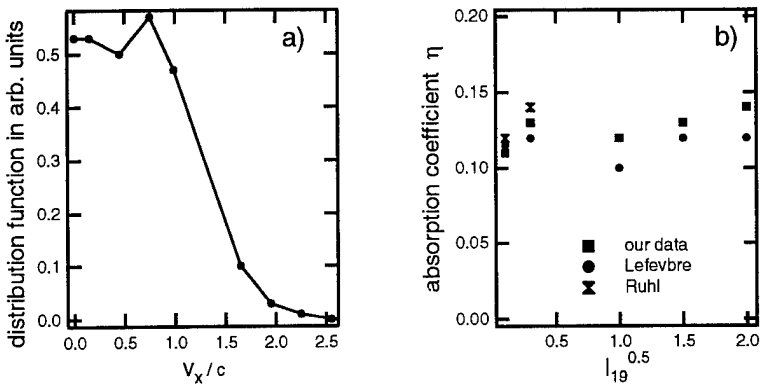

Figure 1: a) distribution function for normal incidence. $x/l_s = 3$, $\omega_0 t = 180$. b) absorption coefficient η as a function of the square-root of laser intensity in units of $10^{19} W/cm^2$.

carried out with a laser intensity of $I = 10^{18} W/cm^2$, a plasma temperature of $T_e = 20keV$, and a density of $n_e = 15 n_c$. One can see that f_e is significantly distorted in comparison with the starting Maxwellian distribution. It means that the laser ponderomotive force expel the electrons from the interaction region into the plasma. So, twice during the period of laser oscillation, a flux of fast electrons is produced which propagates inside the plasma and generates intense x-rays.

In Fig. 1a, the fast electron flux reveals itself as a "tail" in the distribution function. The average hot electron energy is $\sim 0.5 MeV$. The characteristic lifetime of the fast electron $t_h = 1/n_i v_h \sigma \approx 0.1 ps$ (here σ is the cross-section for inelastic scattering of the fast electron with velocity v_h in the matter with ion concentration n_i) can exceed the duration of the laser pulse. These fast electrons can leave the ionized region and penetrate into the solid target. However, the ion density is almost the same in the plasma and the solid matter, so that bremsstrahlung and x-ray line emission have the same behavior in the plasma and the solid target. Analysis of the calculated distribution function at oblique incidence angle θ shows that the constant magnetic field which builds up in the normal incidence frame ("boosted frame") results in an acceleration of the fast electrons in the longitudinal x direction during one half of the laser oscillation period and in a deceleration during the other half of the period. In Fig. 1b we show the calculated absorption coefficient η as a function of laser intensity. We note that the change in the absorption coefficient is small with laser intensity as in previous works [4-6]. Noteworthy, for low intensities the absorption depends on the incidence angle with a characteristic maximum for $\theta \approx \pi/2$; for higher intensities ($> 10^{18} W/cm^2$) such a dependence with the incidence angle is absent. In this case, the absorption coefficient reaches the same value as for normal incidence, similarly to what was found by Ruhl [4]. The reason is that high harmonics generation and strong magnetic field production perturb the plasma modes. The mode frequencies becoming very different from the laser frequency ω_0, this decreases the efficiency of conversion in the plasma waves — the source of the resonant character of the absorption.

3 Evaluation of the x-ray pulse parameters

Spectral intensity of the hard bremsstrahlung x-ray emission from a unit volume of the hot plasma is determined in our work for an optically thin plasma. This requirement is fulfilled for high energy photons ($> 10keV$), the case that we consider in this paper. If the intensity of laser radiation is high ($> 10^{18} W/cm^2$) the velocity v_h of the hot electrons approaches the speed of light c. In this case the

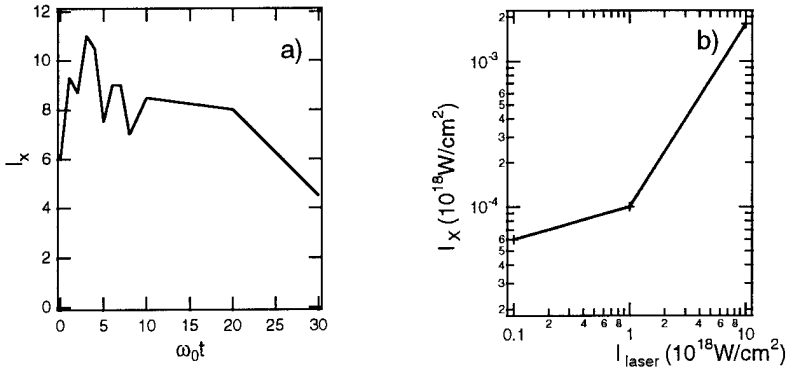

Figure 2: a) Spatially averaged $[0, 10l_s]$ intensity of X-ray radiation as a function of time $\omega_0 t$. b) Intensity of X-ray radiation as a function of laser intensity in units of $10^{18} W/cm^2$.

dependence of the bremsstrahlung emission on the electron velocity and, hence, on the specific distribution function, is rather weak (logarithmic). The x-ray pulse shape of photons with a frequency of $\hbar w_x = 30T_e$ is shown in Fig. 2a as a function of time for a thick target. In our numerical calculations, we have used the distribution function f_e that was found before. Pulse duration ($\approx 0.1ps$) is determined by the hot electrons lifetime t_h. The intensity of the X-ray emission from the plasma I_x can be evaluated from the parameters of the incident wave:

$$I_x \approx (Z\epsilon^7 n_e^2 E_0 l_x)/(m^2 c^3 \hbar \omega_{x0}) \tag{1}$$

where Z is the plasma ion charge, ω_{x0} the x-ray frequency and l_x the photon mean free path length. Spectral intensity depends, to a low extent, on the photon frequencies for the whole spectral range of generated photons from T_e ($20keV$) to $e^2 E_0^2/m\omega_0^2$ ($\sim 500keV$). Laser radiation to x-ray emission conversion efficiency can be as high as 10^{-4}. In Fig. 2b, we show the hard x-ray conversion efficiency as a function of laser intensity. We can see an increase of the conversion efficiency, roughly as $I_0^{1.25}$. This dependence is in good agreement with the experimental results of Kmetec [7]. Approximately $0.1ps$ (lifetime of hot electrons corresponding to their mean free path) after switching off the laser radiation, x-ray emission does not disappear completely, but is replaced by the equilibrium, comparatively long ($\sim 1ps$), thermal X-ray emission of the residual plasma.

This work was partly supported by the INTAS grant 94-934 and by the Centre National de la Recherche Scientifique.

[1] F. Ráksi, *et al.*, J. Chem. Phys. **104**, 6066 (1996).

[2] A. Rousse *et al.*, Phys. Rev. E **50**, 2200 (1994).

[3] S.C. Wilks, Phys. Fluids **5**, 2603 (1993).

[4] H. Ruhl, Proceedings of Conference LIRPP, (Osaka, Japan, 1995), p.65.

[5] P. Gibbon, Phys. Rev. Lett. **68**, 1535, (1992); *ibid* **73**, 664 (1994).

[6] E. Lefevbre, Ph. D. Thesis, Paris (1996).

[7] J.D. Kmetec, Phys. Rev. Lett. **68**, 343 (1992).

Continuum lowering in 100-fs laser produced plasmas

M. Nantel, T. Buma, J. Workman, A. Maksimchuk, D. Umstadter
Center for Ultrafast Optical Science, University of Michigan
1006 I.S.T. Building, 2200 Bonisteel Blvd.
Ann Arbor, MI 48109-2099
(313) 763-4875 (tel), (313) 763-4876 (fax)

We present what we believe to be the first measurements of continuum lowering in high-density plasmas produced by 100-fs laser pulses. Continuum lowering arises in dense plasmas when the excited states of an ion are perturbed by the close proximity of the neighboring ions, and can be a useful density diagnostic. It is a fundamental atomic physics concept in high-density plasmas important to work in X-ray lasers, ICF plasma diagnostics, astrophysics and plasma simulations. In our experiments, a 10-Hz, 100 mJ 100-fs laser system is used to create the plasmas studied, essentially providing a delta-function heat pump which terminates before significant hydrodynamic motion occurs. Continuum lowering was observed both in the high-density, high-temperature expanding plasma plume and in the solid, low-temperature shocked material of the target. In the expanding plasma, we used XUV emission spectroscopy to observe the suppression of high-lying excited levels of He-like and H-like boron. In the compressed plasma behind the shock wave, we used XUV absorption spectroscopy to measure the shifts in inner-shell absorption edges in boron (*K*-edge) and in aluminium (*L*-edge).

For emission spectroscopy of plasma plumes, we focus 5 to 25 mJ on a boron wire target near the entrance of an imaging XUV spectrometer. Temporal resolution is obtained with a streak camera coupled to the end of the spectrometer. Time-resolved spectra are taken of regions near (high-density) and far from (low density) the wire. As shown in Fig. 1, the emission from high-lying He-like states are present in the plasma far from the target (Fig. 1a) but greatly reduced near the target (Fig. 1b), giving evidence supporting continuum lowering suppression of the n = 4, 5 and 6 levels in the high-density part of the plume. This data is preliminary and analysis is ongoing.

The laser can also be used to create a quasi-continuum of XUV radiation ($30\ \text{Å} < \lambda < 300\ \text{Å}$) from a gold plasmas to act as an absorption probe source. The temporal duration of the probe is typically on the order of 20 ps but can be made shorter or longer by varying the laser parameters.[1] Part of the 100-fs laser beam heats a sample onto which the XUV probe source is focused by a novel XUV imaging optics. Time resolution is obtained by varying the delay between the pump laser and the probe XUV source to collect spatially-resolved spectra

of the sample's absorption at different times after the laser heating. The samples are thin films (1000-4000 Å) of aluminum or boron. The dynamics of the shocked material is inferred from shifts in the inner-shell absorption edges during the compression. Fig. 2 shows an example of two aluminum absorption spectra. The solid line is from the undisturbed material, and the dashed line is the spectrum from the compressed material showing a red shift. This resultant shift is due to a combination of ionization blue shift, a continuum lowering red shift and chemical potential contributions. From the value of the edge-shift, one can obtain the pressure in the solid due to the shock, the relaxation time of the shocked material, as well as the changes in density.[2] Collecting spectral images for different values of the delay between the pump and probe beams permits the reconstruction of the edge-shift as a function of time, as shown in Fig. 3. Before time 0 ps, the XUV source probes unshocked sample; at time 0 ps, the edge's largest red-shift indicates that the probe sees the maximum compression in the sample; at later times, the *L*-edge returns to its original position as the material relaxes. The 20 ps duration of the XUV probe pulse insures a very good time resolution for the determination of the shock parameters.

This research is supported by NSF under Grant STC PHY 8920108, LLNL DOE Contract W-7405-ENG-48, the Torrey Foundation and the FCAR fund.

References

[1] J. Workman, A. Maksimchuk, X. Liu, U. Ellenberger, J.S. Coe, C.-Y. Chien, and D. Umstadter, Phys. Rev. Lett. **75**, 2324 (1995).

[2] L. Da Silva, A. Ng, B.K. Godwal, G. Chiu, F. Cottet, M.C. Richardson, P.A. Jaanimagi, and Y.T. Lee, Phys. Rev. Lett. **62**, 1623 (1989).

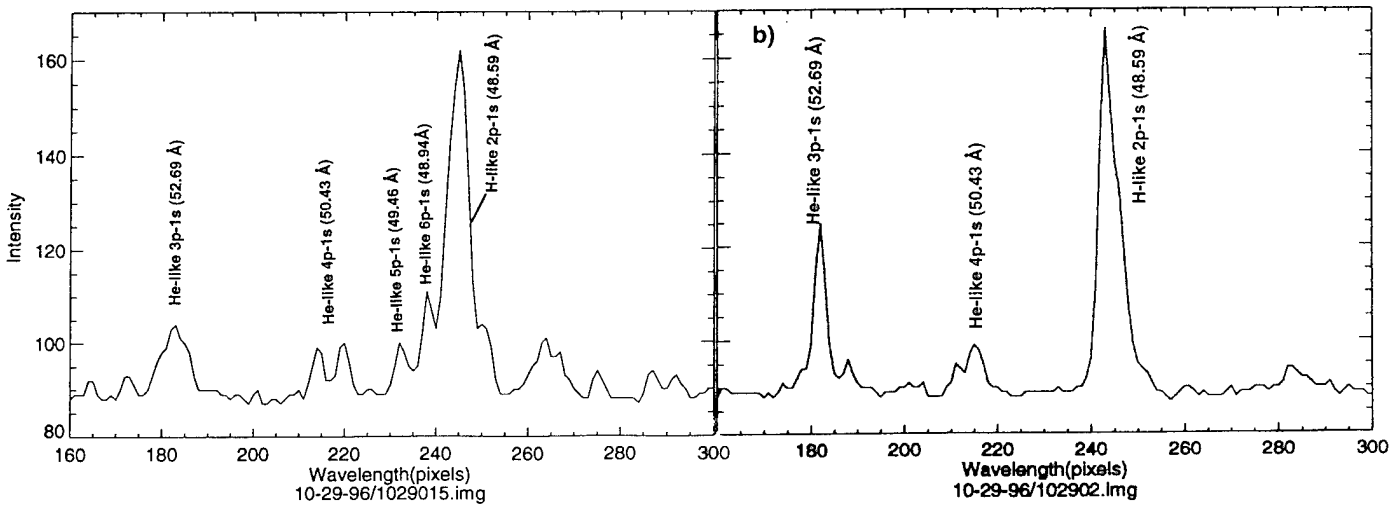

Figure 1. Spectra of He-like and H-like boron emission: a) 200 μm from the target, b) near the surface of the target.

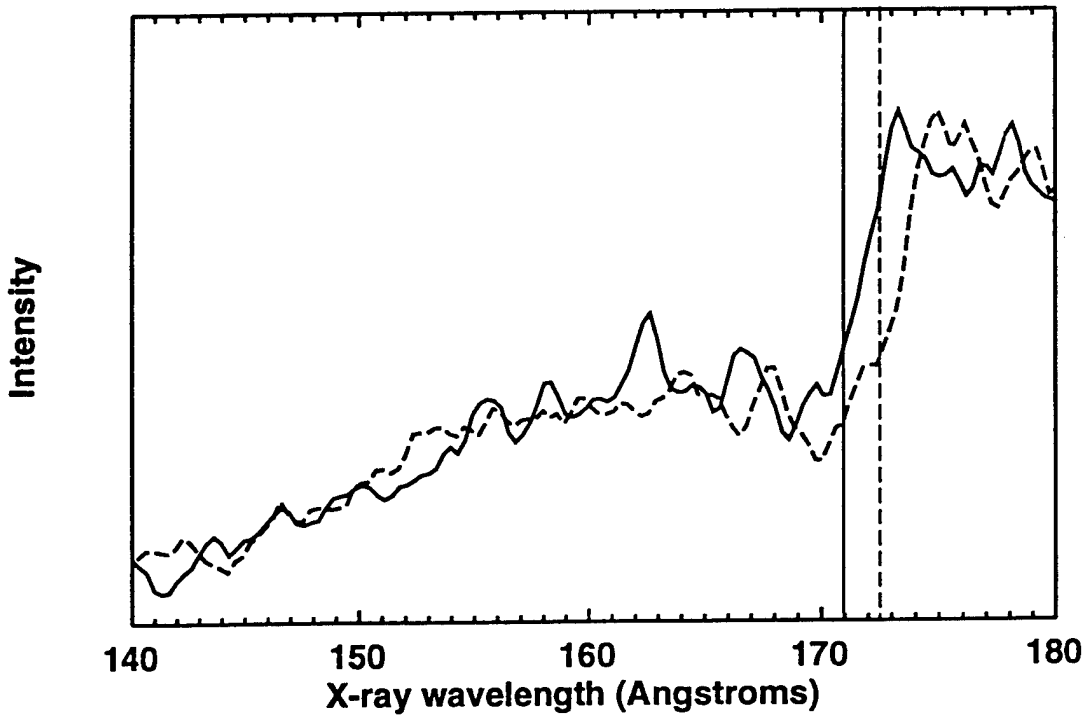

Figure 2. Spectra of the backlighter source through normal (solid line) and shocked (dashed line) 1000 Å aluminum films.

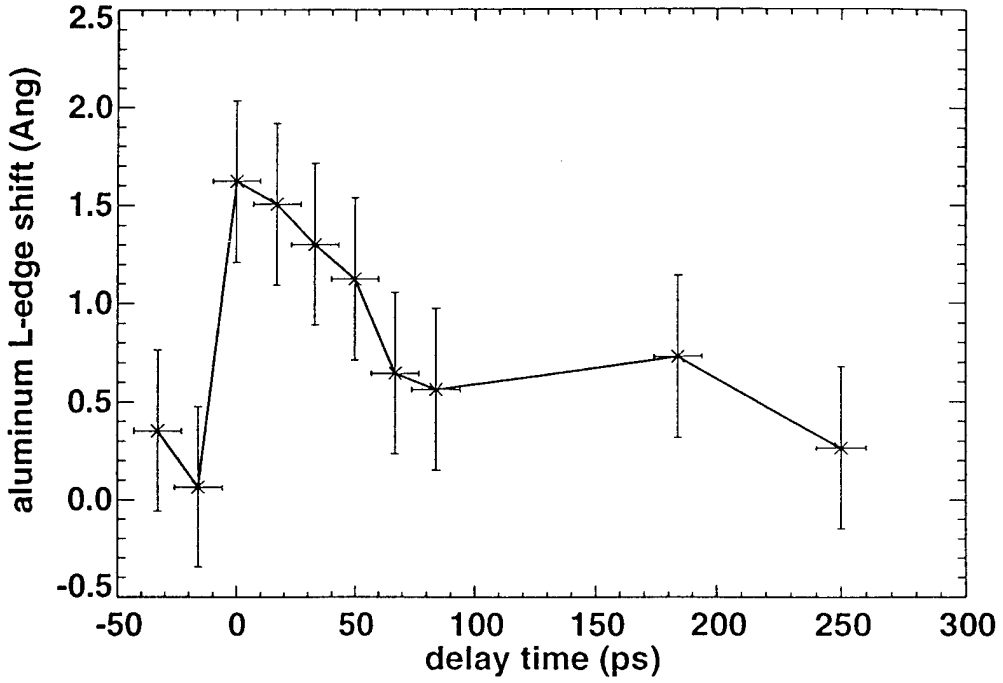

Figure 3. Dynamics of the aluminum *L*-edge red-shift in shocked 1000 Å films.

Thursday, March 20, 1997

X-Ray Lasers

ThC 2:00pm – 3:30pm
Zia A

L. DaSilva, *Presider*
Lawrence Livermore National Laboratory

Saturated Table-top Soft X-Ray Lasers by Discharge Excitation

J.J. Rocca , F.G.Tomasel, J.L.A. Chilla, M.C. Marconi, V.N.Shlyaptsev, C.H.Moreno, B.R.Benware, and J.J.Gonzalez.
Department of Electrical Engineering
Colorado State University
Fort Collins, CO 8052
Tel: (970)-491-8514.Fax: (970)-491-8671

Introduction

The development of practical "table-top" sources of soft x-ray laser radiation will have a very important impact in many disciplines of science and technology. In the decade that followed the first successful soft x-ray amplification experiments [1,2], large soft x-ray amplification and significant laser output energy could only be obtained using large optical lasers as the energy source. Much progress was accomplished using as pump the same type of lasers utilized in fusion research. However, the widespread use of these sources is limited by their very large size, high cost and low accessibility. These limitations motivates the development of compact soft x-ray laser sources that can impact applications.

Of particular interest are "table-top" lasers capable of producing substantial energy output. Such development requires the demonstration of gain media generated by compact devices that can be successfully scaled in length to reach the large gain-length products necessary to saturate the amplifier. For example, saturated operation of collisionally excited soft x-ray laser systems requires a gain- length product of g*l=14-20. Significant progress has been made in the last few years in the demonstration of soft x-ray amplification employing table-top laser drivers . To date, three experiments using relatively compact ultrashort pulse laser pumps have yielded gain-length products greater than 5. These include the demonstration of 11-13 gain-lengths at 41.8nm in Pd-like Xe [3], of about 9 gain-lengths at 32.6nm in Ne-like Ti [4], and the recent report of a gain-length product of 5.5 at 13nm in H-like Li [5].

Herein we discuss the successful development of table-top soft x-ray amplifiers directly excited by fast discharges. In this excitation scheme amplification occurs in a hot and dense plasma column generated by a fast compressional discharge in a capillary channel [6,7]. To demonstrate lasing by collisional excitation of Ne-like ions we have generated axially uniform plasma columns of about 200-300um diameter with lengths up to 20 cm. Below we discuss the achievement of up to 27 gain-lengths in the 46.9nm line of Ne-like Ar. Single pass amplification experiments resulted in laser pulses with an energy of 6uJ. Laser output energies up to 30uJ were obtained by double pass of the beam through the plasma column using an iridium mirror. These experiments resulted in the first demonstration of saturated operation of a table-top soft x-ray amplifier [7]. We also report the demonstration of large amplification at 60.8nm in Ne-like S ions in vapor produced by discharge induced ablation of a solid target [8]. These results open a new road for the development of very compact and efficient soft x-ray lasers.

Demonstration of Saturated Operation of a Ne-like Ar soft x-ray amplifier.

The experiments were conducted exciting capillaries 4mm in diameter filled with 700 mtorr

of pure argon gas with current pulses of approximately 39kA peak current having a half cycle duration of about 70ns. The current pulses were generated by rapidly discharging a 3nF liquid dielectric capacitor. The capacitor was pulse-charged by a Marx generator and its discharge was controlled with a spark-gap switch filled with SF6. A detection system consisting of a 2.2m grazing incidence spectrograph with an MCP intensified CCD array detector was used to measure the relative variation of the laser energy as a function of plasma column length. Absolute measurements of the laser output pulse energy were performed using a fast vacuum photodiode having an Al photocathode.

The result of single-pass amplification measurements for capillary plasma columns up to 15.8cm in length are shown as open circles in Figure 1. The energy of the laser pulse is observed to increase exponentially for lengths up to 12cm, where it begins to saturate. A fit of the data corresponding to plasma columns up to 11.5cm with the Linford formula yields a gain coefficient of 1.16 cm^{-1}. Saturation of the intensity is observed at gain-length products of about 14. A laser pulse energy of 6uJ was measured to exit the 15.8 cm plasma column. As discussed below, double-pass amplification experiments allowed us to substantially increase the laser pulse energy and to study the saturation behavior for effective plasma column lengths significantly longer than the maximum capillary length of 16 cm used in these experiments.

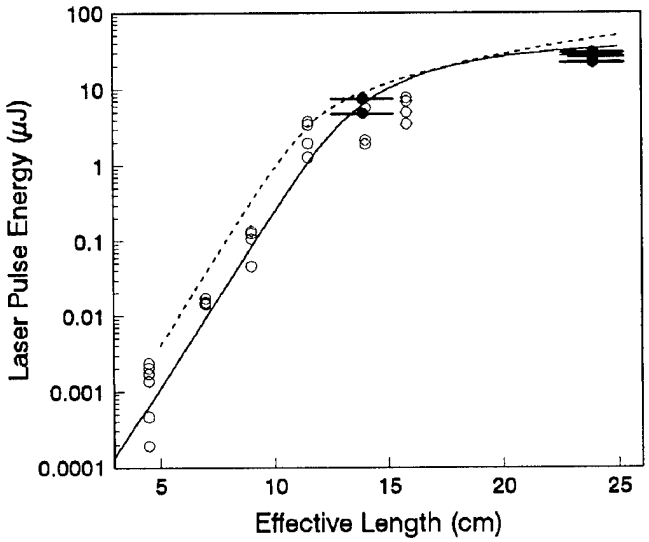

Figure 1. Measured and computed 46.9nm laser output energy as a function of capillary discharge plasma length. The single and double- pass measurements are indicated by open and full circles respectively. The solid line is the result of a simple radiation transport calculation assuming parabolic gain and density profiles. The dashed line was computed with a self-consistent hydrodymic/atomic physics radiation transport code.

The double-pass amplification measurements were performed using flat iridium mirrors for two different plasma column lengths: 9cm and 14 cm. In the 9cm capillaries the laser intensity enhancement due to the mirror was measured to be 63 x. In contrast, the enhancement observed in the 14 cm long capillaries was in the average only 8x. This behavior is indicative of saturation of the amplification in the second pass.

The increase in the laser energy measured in the double- pass experiments in the 14 cm long capillaries corresponds to laser pulse energies up to 30uJ and to beam intensities larger than the computed saturation intensity of 56-78 MW/cm^2. The saturation intensity was calculated considering an ion temperature of 100eV, and an effective-to-radiative lifetime ratio for the laser upper level between 20 and 30 for plasma densities of 5-8x 10^{18}cm^{-3}, as computed by our magneto-hydrodynamic calculations for these discharge conditions. Such laser pulse energy is a significant fraction of the maximum energy that can be extracted in a 0.8ns pulse from a 46.9nm Ne-like Ar amplifier column 14 cm in length and 300um diameter. Assuming a gain of 1.2 cm^{-1}, this energy is estimated to be about 100uJ. The results of two independent radiation transport models confirm the saturated operation of the amplifier.

Lasing in Ne-like sulfur.

In our most recent experiment we have succeeded in demonstrating lasing in Ne-like sulfur ions at 60.8nm in vapor produced by discharge ablation of a solid target. This result is of interest, because it demonstrates the feasibility of also obtaining ultrashort wavelength amplification by discharge excitation in materials that are solid at room temperature. The sulfur vapor was produced by ablating with a slow current pulse the wall of a secondary capillary channel drilled in a sulfur rod. The vapor generated by this secondary discharge was injected into the main capillary channel and was subsequently excited by a fast current pulse of 35-37 kA peak amplitude to generate a narrow plasma column with the necessary conditions for amplification.

Measurements of the integrated intensity of the laser line as a function of the plasma column length yielded a gain coefficient of 0.45cm^{-1}, corresponding to a gain-length product of 7.55 for 16.8 cm long capillaries. At the time of lasing the electron density and temperature in the gain region are computed to be about 2-3 10^{18} cm^{-3} and 60-80eV, respectively. This electron temperature corresponds to a plasma which is overheated respect to the conditions for maximum Ne-like sulfur abundance in a steady state regime .Our computations show substantial differences respect to a steady-state scenario and indicate that plasma overheating and transient population effects make an important contributions to the measured gain.

In summary using discharge excitation we have achieved the first demonstration of saturated operation of a table-top soft x-ray amplifier. Laser output energies up to 30uJ have been measured for the 46.9nm line of Ne-like Ar. Large amplification has also been observed in the 60.8nm line of Ne-like S in vapor produced by discharge ablation of a solid target. These results can be expected to lead to the use of very compact and practical discharge pumped table-top ultrashort wavelength lasers in applications. This work was supported by the NSF.

1. D.L. Matthews et al. Phys. Rev. Lett. 54, 110,(1985).
2. S. Suckewer et al. Phys. Rev. Lett. 55, 1753, (1985)
3. B. Lemoff et al. Phys. Rev. Lett. 74, 1574 (1995)
4. P.V. Nickles et al. SPIE J. 2520, 373,(1995)
5. S. Suckewer, private communication.
6. J.J.Rocca et al. Phys.Rev.Lett, 73, 2192, (1995).
7. J.J.Rocca et al. Phys. Rev. E. 47, 1299,(1993).
8. J.J.Rocca et al. Phys Rev. Lett., 77, 1476,(1996)
9. F.G. Tomasel et al. Phys. Rev. E. (In press).

Low energy pumped X-ray lasers with saturated transient gain

P.V. Nickles[1], M.P. Kalachnikov[1], M. Schnürer[1], W.Sandner[1], V.N. Shlyaptsev[2], C. Danson[3], D. Neely[3], E. Wolfrum[3], M. Key[3], A.Behjat[4], A. Demir[4], G. Tallents[4], G.J. Pert[5], J. Warwick[6] and C. Lewis[6]

[1] *Max-Born-Institut, Rudower Chaussee 6, D-12489 Berlin, Germany*
Tel.: 0049-30-63921310, Fax: 0049-30-63921329, e-mail: nickles@mbi.fta-berlin.de
[2] *Colorado State University, Fort Collins, Colorado, USA*
[3] *Rutherford Appleton Laboratory, Chilton, U.K.*
[4] *University of Essex, Colchester, UK*
[5]. *University of York, York, UK*
[6] *U.K. Queens University Belfast, Belfast, U.K*

Collisionally excited X-ray lasing in [Ne]-like Ti with a gain value of 19 cm^{-1} at a drastic reduced pump level of only a few Joules was demonstrated recently [1]. This achievement is based on a novel two step excitation scheme, which was proposed some years ago [2]. The scheme comprises at first a long (ns) heating pulse to establish a [Ne]-like ionic stage of desired target atoms in a plasma and second a short (ps) excitation pulse to produce efficiently a transient population inversion in the [Ne]-like ions. Due to the short pulse produced fast heating of the preformed plasma, a transient inversion [2] occurs, which is related to the different population rates of the levels via collision and not determined by the slower relaxation rates of the excited levels relevant in the quasi-steady state (QSS) regime. The transient inversion yields favourably much higher gain values (several tens of cm^{-1}) as well shorter X-pulse output as obtained in the QSS regime (several cm^{-1}) with long pulse pumping.

In this work the amplification characteristic of the 3p-3s (J=0-1) transition at λ= 32.6 nm and the 3d-3p (J=1-1) transition at λ= 30 nm in Ti as well as the 3p-3s (J=0-1) transition at λ=19.6 nm in Ge has been studied with plasma column length up to 10 mm. Also the dependence of the X-ray lasing signal on the optical laser pump energy was investigated. The duration of the Ti X- ray laser pulse as well as the X-ray beam divergency was measured and the output energy was estimated.

Experimental Setup

The experiments have been carried out with both the two beam MBI CPA- Glass laser system described in [3] and the RAL-Vulcan Nd:glass laser using a CPA-laser beam [4] of up to 24 J laser energy (E_L) with a pulse width of several ps (2-3 ps at low E_L and 6-8 ps at high E_L) and a second synchronized ns-laser beam. The short pulse was timed at the falling edge of the long flat toped 1 ns pulse. The line foci of the two pulses with a length of 10 mm and a width of 100 μm have been super-imposed on the target. Titanium and Germanium stripes on glass with a thickness between 0.6 and 1.0 μm and a width of about 200-300 μm as well as massive slab targets were used. The amplification length was varied with the target length. The targets were centered in the line focus. The primary diagnostic along the target axis was a flat field grazing incidence XUV-spectrometer with a 1200 line/mm aperiodically ruled grating. Focussing perpendicular to the dispersion direction was provided by a cylindrical mirror. The time integrated spectrum was recorded with a back-thinned cooled 16 bit CCD-camera.

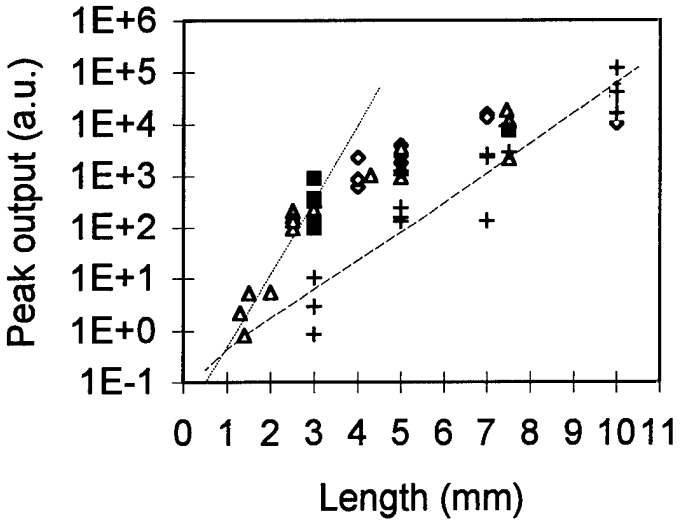

Fig.1 Peak output signals at 32.6 nm and 30 nm (crosses only) as a function of target length with pump intensities of $1*10^{12}$ W/cm^2 in the long and $2*10^{14}$ W/cm^2 in the short pulse

Results and Discussion

The XUV-signals at λ=32.6 nm and λ=30 nm as a function of the length variation of the Ti-plasma column are plotted in fig.1. For the plot we have taken the peak values from the line signals and have substracted the recorded plasma background emission near the wings of the two lasing lines. This amplification series was carried out at a pump energy level in the long pulse of 20 J and in the short pulse of 18 J . As visible from the obtained data the output signals can be fitted (Linford et al. [5]) with a gain g=35 cm^{-1} up to target lengths L=3 mm. With further increasing target length the increase rate of the output signals drops, which is a clear sign of the X-ray laser output saturation.

Lower gain values of g=15 were measured for the 3d-3p line at about 30nm. No saturation effect is visible, and even at a target length of 10 mm higher output signals at this line compared to the 32.6 nm line were measured. Careful theoretical analysis of the whole system will include the transient gain behaviour, the X-ray beam propagation in the plasma and saturation effects.

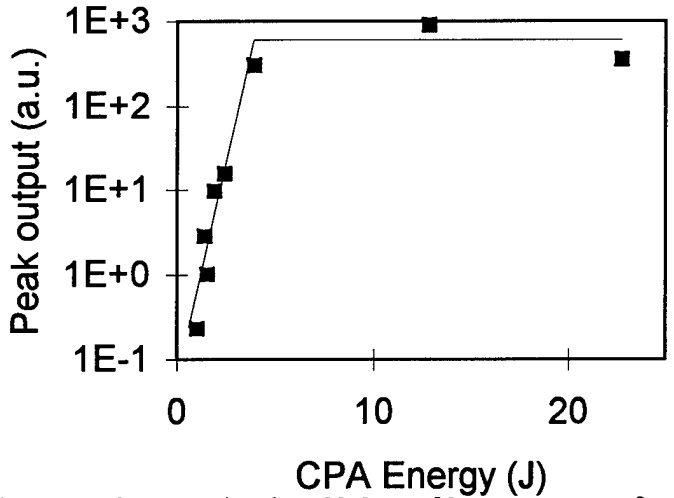

Fig.2 Peak output signals at 32.6 nm of 3mm targets as a function of pump energy in the short pulse with pump intensities of about$1*10^{11}$ W/cm^2 in the long pulse

In a second series of experiments depicted in fig.2 we have determined the threshold pump values for lasing at 32.6 nm. As it was visible pump energies as low as E_L = 1 J for the long 1 ns pulse and E_L = 1.5 J for the short 3 ps pulse yield amplified emission. The target length was 3 mm. The corresponding pump intensities are I_L= $7*10^{10}$ W/cm^2 in the long pulse and I_L= $5*10^{13}$ W/cm^2 in the short pulse. So we could really verify, that X-ray lasing in the [Ne]-like Ti system is possible with table top class pump lasers.

Divergency measurements of the X-ray laser beam at 32.6 nm from 9 mm long Ti-stripe targets have yield 2 to 3 mrad if the long pulse was 600 ps and 6 to 8 mrad for an 1 ns long pulse. Tests with a travelling wave focus have not given an increased output of the Ti-system concerning the pump pulse conditions used here.

Investigation of the Ti X-ray laser pulse duration carried out with the MBI CPA- laser system using a Kentech X-ray streak camera with a CCD -camera read out have revealed that the pulse length is of 15-20ps. This very short duration corresponds pretty good to the calculated life time of the transient high gain regime.

Neonlike Ge- XRL experiments done at the Rutherford CPA laser facility in the same configuration as for the Ti X-ray laser have also demonstrated a saturated amplification at the 3p-3s (J=0-1) transition at 19.6 nm characterized by a gain value of $\sim 25\ cm^{-1}$.

Summarizing we can state, that with evaporated Ti- as well as Ge- stripes on to glass a reliable X-ray lasing was achieved. In case of Ti the lasing signal at 32.6 nm shows saturation due to high gain values of $g=35\ cm^{-1}$ if the plasma column is longer than 4 mm. The second laser line at 30 nm having a lower gain of $g=15\ cm^{-1}$ shows no saturation up to target length of 10 mm. Low pump intensities for that novel two step excitation scheme and high output energies in the μJ range as well short pulse duration are attractive characteristics of this [Ne]-like Ti X-ray laser.

This work was supported by the European Communities Large Facilities Programme. The authors gratefully acknowledge the support of C. Edwards as well as the help of laser operations, target preparation, and engineering support groups of the CLF of the Rutherford Appleton Laboratory.

References

[1] P.V. Nickles, V.N. Shlyaptsev, M.P. Kalachnikov, M. Schnürer, I. Will, W. Sandner SPIE **2520**, (1995)

[2] Y.V. Afanasiev, V.N. Shlyaptsev Sov. J. Quant. Electr. **19**, 1606 (1989); L.B. Da Silva et al., SPIE 1229, **128** (1990); S. Maxon et al., Phys Rev. Lett. **70**, 1335 (1993)

[3] M.P. Kalachnikov et al., Laser and Part. Beams **12**, 463 (1994)

[4] C.N. Danson et al. Opt. Comm. **103**, 392 (1993)

[5] G.J.Linford et al. Appl.Opt. **13**, 379 (1974)

Generation of Intense X-Ray Laser Radiation at 8 nm in Ni-like Nd Ions

H. Daido, Y. Kato, T. Imani, S. Sezaki, S. Hirose, G. Y. Yoon, T. Jitsuno, Y. Takagi and K. Mima
Institute of Laser Engineering, Osaka University, Suita Osaka 565 Japan
Phone: 81-6-879-8766
Fax: 81-6-877-4799
e-mail: kato@ile.osaka-u.ac.jp

S. Wang, Z. Lin, Y. Gu, G. Huang, H. Tang and D. Ximing
National Laboratory for High Power Lasers and Physics
P.O.Box 800-211 Shanghai China

G. Zhang
Institute for Applied Physics and Computational Mathematics, P.O.Box 8009
Beijing 100088, China

K. Murai
Osaka National Research Institute Ikeda Osaka 563 Japan

H. Takenaka
NTT Advanced Technology, Midorimachi, Musashino 180 Japan

Lasing in various Ni-like ions at the wavelengths below 10 nm has been demonstrated [1,2]. Achieving saturated amplification with the Ni-like ions is considered to be difficult compared with the Ne-like ions at longer wavelengths, since the plasma parameter space for amplification is narrower with the Ni-like ions [3]. In this paper we report generation of very intense x-ray laser radiation at 8 nm in Ni-like Nd ions by amplification using double curved targets. This result shows that it will be possible to achieve saturated amplification in Ni-like ions by properly optimizing the irradiation conditions and target configurations.

In comparison to our previous experiments where a single curved slab target was irradiated with a train of short pulses[2], we have improved the experimental conditions in the following aspects.

Two new line-focusing optics configurations were introduced to increase the irradiation intensity and to improve the intensity distribution. The first configuration consists of a cylindrical lens array composed of 4 cylindrical lenses and an aspheric focusing lens. Each cylindrical lens forms a line focus on a target, thus producing a line focus with uniform energy distribution along the line. Another configuration is composed of a deformable mirror, a single cylindrical lens and a focusing lens. The deformable mirror compensates for the aberration of the cylindrical lens, forming a straight line focus at the target plane. In both of these configurations, the width of the focus pattern on target was uniform over the length with a width of 30-50 μm and a length of approximately 28 mm. In our previous experiments using a single cylindrical lens, the focusing pattern had a "bowtie" shape with the width of 160 μm at the widest region. Using these new focusing optics the average intensity on target has increased by 2 times, reaching to 10^{14} W/cm^2 and the width of the gain region is more uniform.

Two curved targets were placed in series to double the gain length. Two opposing laser beams irradiated the double targets in an arrangement shown in Fig. 1. The performance of the curved target was compared with that of the double plane target, developed at NLHPLP, which has proven to be successful in Ge. Also double pass amplification using a soft x-ray mirror was tested.

The desirable condition for efficient x-ray lasing is to create a plasma with a long density scale length and a broad gain region, if radiation trapping is not serious. Among a few pulse shapes tested to control the plasma profiles, the best result was obtained with 4 pulses of 100 ps pulse widths with the separations of 1 ns, 400 ps and 400 ps. One of the laser beams was delayed by 100 ps relative to another for traveling wave excitation of the double target.

The on-axis spectra of the x-ray laser emission were measured with 2 grazing-incidence spectrometers placed on opposite sides with a soft x-ray CCD on one side and a streak camera on another side for time-integrated and time-resolved measurements, respectively. The results reported herein are preliminary since calibrations for various components are necessary for quantitative evaluation.

In the first stage of the experiment, the performance of the single curved slab and the 2-planer-slab targets was tested with the new line-focus optics configurations. With both of the irradiation configurations, the observed x-ray laser intensity was at least one order of magnitude stronger than our previous experiments, where the x-ray laser energy was estimated to be approximately 1 μJ. This remarkable enhancement of x-ray lasing obtained with the same pumping energy is ascribed to the improved irradiation where the higher intensity leads to higher electron temperature resulting in an increased collisional excitation rate.

In the second stage of the experiment, double target amplification was tested with two beam irradiation. The separation between the 2 curved slabs transverse to the on-axis was varied from 210 to 320 μm. The maximum x-ray laser output was observed at 320 μm separation. The x-ray laser intensity with the double target amplified along the traveling wave has increased over 10 times in comparison to that against the traveling wave as shown in Fig.2. With a single curved slab target, x-ray lasing occurred at the latter 3 pumping pulses with approximately equal intensities, whereas with the double curved targets, the last pulse gave the strongest lasing. These results indicate the better condition for coupling of the x-ray laser beam between the 2 targets at the last part of the pulse.

Horizontal beam divergence was within a few mrad with a single curved target, whereas it has increased to over 5 mrad with double targets. There are indications that the beam divergence can be reduced by optimizing the double target configurations. The x-ray laser energy obtained in this experiment is estimated to be over 100 μJ, based on comparison with our previous experiments. We believe that it is not difficult to achieve saturated amplification in Ni-like ions by further optimizing the experimental conditions.

References

1. B. J. MacGowan et al., Phys. Fluids B4, 2326 (1992).
2. H. Daido et al. Phys. Rev. Lett. 75, 1074 (1995).
3. B. J. MacGowan et al., Phys. Rev. Lett. 65, 420 (1990).

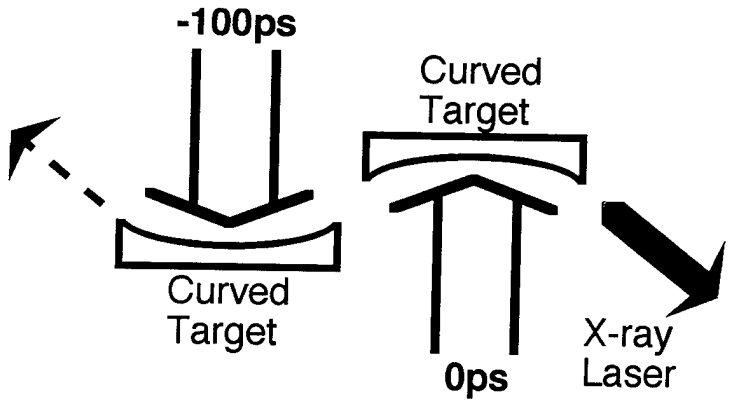

Fig. 1 Schematic diagram of the double target

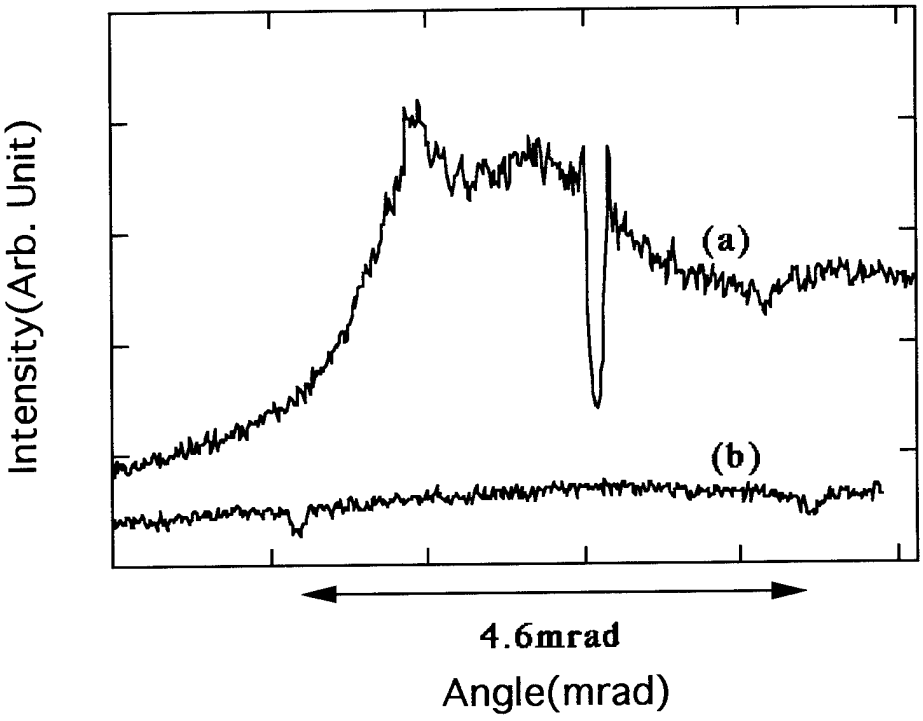

Fig. 2 Intensity profiles of the x-ray laser at 8 nm detected with a filtered soft x-ray CCD. The attenuation ratio of the filter is 1/1500. Intensities along and against the traveling wave are shown in (a) and (b), respectively.

Thursday, March 20, 1997

Applications of Short Wavelength Light II

ThD 4:00pm – 5:45pm
Zia A

Michael White, *Presider*
Brookhaven National Laboratory

Synchrotron Radiation and Applications

Irène Nenner

Service des Photons, Atomes et Molécules
Bâtiment 522
CEA- Centre de Saclay
91191 Gif sur Yvette cedex FRANCE

Telephone : +33-(0)1 69 08 24 73
Fax : +33-(0)1 69 08 87 07
e-mail : nenner@drecam.cea.fr

General trends

The use of synchrotron radiation has reached a quite mature stage all over the world with dedicated electron storage rings equipped with a large number of beam lines to accommodate an even larger number of simultaneous experiments. The spectrum of the light which depends upon the energy of the accelerated particles covers continuously the electromagnetic spectrum from the infra-red to the ultra-violet up to the soft X-ray and hard X-ray range. The main characteristics are the high flux or mean power, the high brillance, the small divergence, an access to linear and circular polarization, the high spatial and temporal stability and a usable time structure. The interest and the complementarity of these sources with respect to conventional laboratory sources (X-ray tubes, discharge lamps and lasers) is now recognized and explains the growing demand in fundamental and finalized research.

In recent machines in which undulators are installed on long straight sections, the light emitted along the undulator axis shows exceptional qualities in flux and brillance. If this radiation is stored in an optical cavity in order to interact transversally with the electron bunches at each pass in the undulator field, the optical pulse can be amplified at the cost of the particle kinetic energy leading to a laser oscillation. This is the principle of the free electron laser. Such lasers are operating with low energy particles (linear accelerators) for infra-red radiation and high energy particles (storage rings) for UV radiation. Both are now in routine use. It is possible to obtain coherent radiation in a single pass, without an optical cavity. Such lasers known as SASE (self amplified spontaneous emission) are free electron lasers working in the super-radiant mode have been found feasable in the millimeter and infra-red but not yet in the UV and soft X-ray range.

Comparison between synchrotron radiation [1] from the most advanced machines and lasers such as free electron lasers [2], harmonic generation [3], laser-plasma sources [4], X-ray lasers [5], shows the superiority in terms of mean flux (number of photons/second/0.1% bandwidth) of synchrotron sources over lasers because of their high repetition rate and full tunability. This is demonstrated in Figure 1, on the basis of a typical third generation synchrotron radiation machine, i.e. the SOLEIL project. In contrast, the comparison in terms of intensity (Watts/cm^2) favors strongly lasers over synchrotron radiation, at least for specific wavelengths, because of their short pulses and high peak power. This is shown in Figure 2

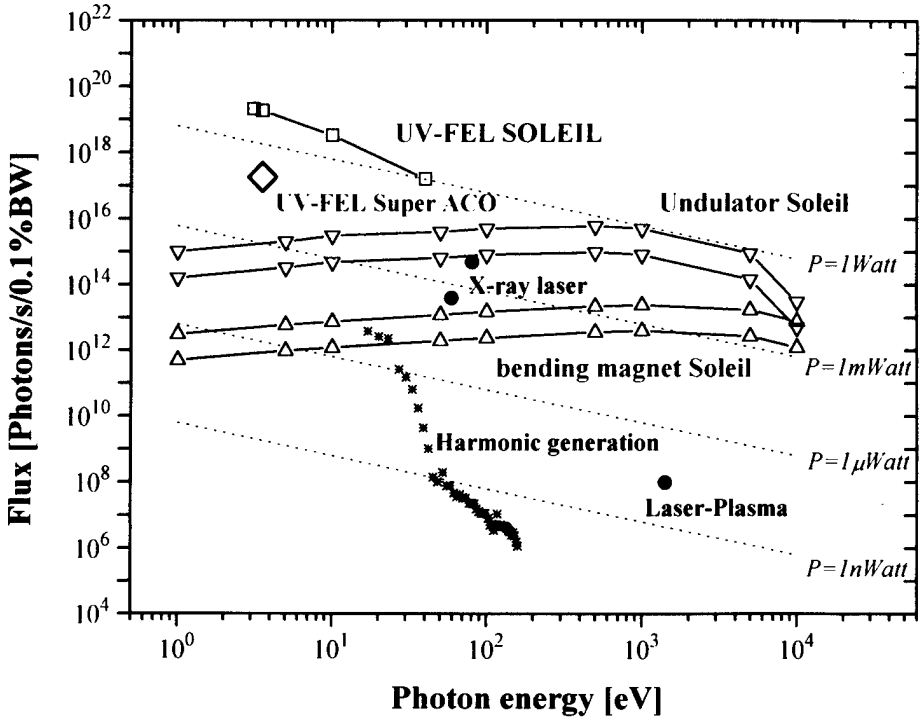

Figure 1 : Comparison of the mean flux of synchrotron radiation (bending magnet and undulators) of a third generation machines, such as the SOLEIL project. (both operating modes "high brillance" and "time structure" are considered) with the UV-free electron laser at SuperACO and SOLEIL, some laser based sources such as harmonic generation, X-ray lasers and laser-Plasma.

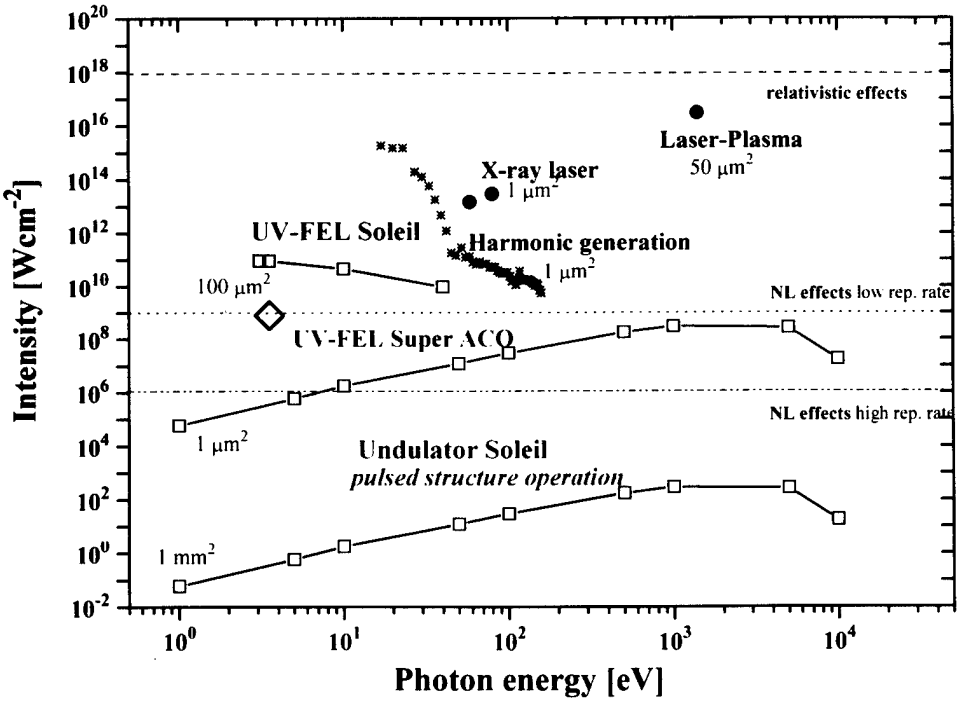

Figure 2 : Comparison of the intensity of synchrotron radiation (undulator sources) of a third generation machines, such as the SOLEIL project (case of the "time structure" operating mode) with the UV-free electron laser at SuperACO and SOLEIL, some laser based sources such as harmonic generation, X-ray lasers and laser-Plasma. The surface of the focal point obtained with an appropriate optics is indicated for each source. The approximated detection thresholds of non linear effects (NL) are indicated for sources with a low and high repetition rates are indicated as well as the threshold for detection of relativistic effects.

taking the SOLEIL project as the reference for synchrotron radiation. The position of the free electron laser in the UV is exceptionnally attractive in both flux and intensity

Combination of synchrotron radiation and lasers are developing. The most common way is to combine SR with cw lasers, as done since fifteen years with visible and infra-red lasers. The combination with pulsed lasers with synchronisation is more recent : mode locked argon ion and solid state lasers as well as free electron lasers who have the same or a multiple value of the repetition rate of synchrotron radiation are the most convenient to obtain a reasonable signal to noise ratio.

Applications

Applications can be classified in four categories : radiation-matter interaction, optical, structural, electronic and magnetic properties of matter, calibration of optics and detectors, deep lithography for making micro-objects. These topics interest a large variety of fundamental scientific fields : atomic and molecular physics, surface and condensed matter physics, chemistry and material sciences, life sciences, earth sciences and astrophysics. Finalized research is also strongly concerned in fine chemistry, oil chemistry, electrochemistry, electronics, plastics, automobile, packaging, glasses, pharmacy, cosmetics, agriculture and food, medical diagnostics, environnement (air and ground pollution), nuclear wastes etc.....The main problems raised in industry concerns mainly material science, i.e. the correlation between structure, at the atomic or mesoscopic level, and properties (or functionality) of materials, elaboration processes under vaccuum, development of processes, quality control, aging effects, materials under external constraints such as chemistry, temperature, pressure, electric field, radiations.

Selected examples in various fields of fundamental and finalized research will be presented, emphasizing the tunability from UV to the X-ray range, the mean power, polarization, coherence and pulsed structure of synchrotron radiation as well as the coupling with laboratory lasers and free electron lasers for pump-probe experiments.

Photoionization of hollow states of lithium
Dynamics of photodissociation of polyatomic molecules
Time-resolved studies in semi-conductors surface
Imaging of magnetic domains by photoelectron spectromicroscopy
Structural properties of minerals under high pressure and temperature
Structure of a polymer-metal interface
Imaging by phase contrast
Biocristallography
Caracterisation of cosmetics

References

[1] I. Nenner, *Colloque UVX96*, Annales de Physique, in press
[2] M.E. Couprie, *Colloque UVX94*, Annales de Physique, C1 Suppl. **5**, 19 (1994)
[3] A. L'Huillier et al. Int. J. Non Linear optical Physics and Mat. **4**, 7467 (1995)
[4] J.C. Gauthier, P. Audebert, S. Bastiani, J.P. Geindre, A. Dos Santos, G. Grillon, A. Mysyrowicz, A. Antonetti, *Colloque UVX96*, Annales de Physique, in press
[5] Ph. Zeitoun, F. Albert, A. Carillon, P. Jaeglé, G. Jamelot, A. Klisnick, S. Sebban, D. Ros et B. Rus, *Colloque UVX96*, Annales de Physique, in press

Time-resolved x-ray diffraction from laser excited crystals

J. Larsson, E. Judd, P. J. Schuck, R. W. Falcone
Department of Physics, 366 LeConte Hall, University of California Berkeley, Berkeley CA 94720-7300, USA, E-mail: jorgen@physics.berkeley.edu

P. A. Heimann, H. A. Padmore
Advanced Light Source, Accelerator and Fusion Research Division, Lawrence Berkeley National Laboratory, Berkeley, California 94720, USA

Z. Chang, H. C. Kapteyn, M. M. Murnane.
Center for Ultrafast Optical Science, University of Michigan, Ann Arbor, MI 48109, USA

R. W. Lee
L-399, Lawrence Livermore National Laboratory,P.O. Box 808, Livermore, CA 94551, USA

A. Machacek, J. S. Wark
Department of Physics, Clarendon Laboratory, University of Oxford, Parks Road, Oxford, OX1 3PU, U.K.

We have constructed an ultra-fast time-dependant x-ray diffraction experiment in order to probe laser-induced phase transitions in solids. Such studies have previously been performed using laser probes in the infra-red, visible or ultraviolet spectral range. However, in order to directly probe structures in solids, it is necessary to use x-ray radiation. A laser system producing pulses with a duration of 100 fs has been set-up adjacent to a bending magnet at the Advanced Light Source (ALS). In addition an averaging streak camera with a temporal jitter smaller than 1.5 ps has been incorporated [1]. This diagnostic will permit us to study lattice disordering in materials such as Si. Single-shot measurements were also made using a Kentech streak camera.

The ALS bending magnets emit a broad spectrum of x-rays with a critical energy of 3.7 keV when the electron energy is 1.9 GeV. These initial experiments were performed with the ALS operating in double-bunch mode for which the repetition frequency is 3 MHz.

Our laser system consists of a non-commercial Ti:Sapphire oscillator pumped by a Millenium Nd:Yag laser and a Positive Light Spitfire regenerative amplifier operating at a frequency of 1 kHz. The pulse duration is about 100 fs and the pulse energy is about 0.5 mJ.

Using a Kentech streak camera we detect a single pulse from the synchrotron and measure the duration of the ALS pulse to be about 80 ps. In order to achieve a better signal-to noise ratio and thereby obtain higher temporal resolution we average multiple pulses using a streak camera [1] triggered by a photo-conductive switch [2]. This streak camera has demonstrated 550 fs single-shot time resolution [3].

The jitter of the camera was studied using UV pulses obtained by frequency mixing in KDP crystals. Since single shot data was not obtained, an accurate value for the trigger jitter can not be given separately. Instead, the temporal multiple shot response is specified as 1.5 ps when averaging 5000 laser pulses. As a test case for studying events on a picosecond time scale in the x-ray spectral region, we measured the pulse duration of the ALS operating at an electron energy of 1.9 GeV and a beam current of 30 mA in 2-bunch mode. The results of the measurements are shown in

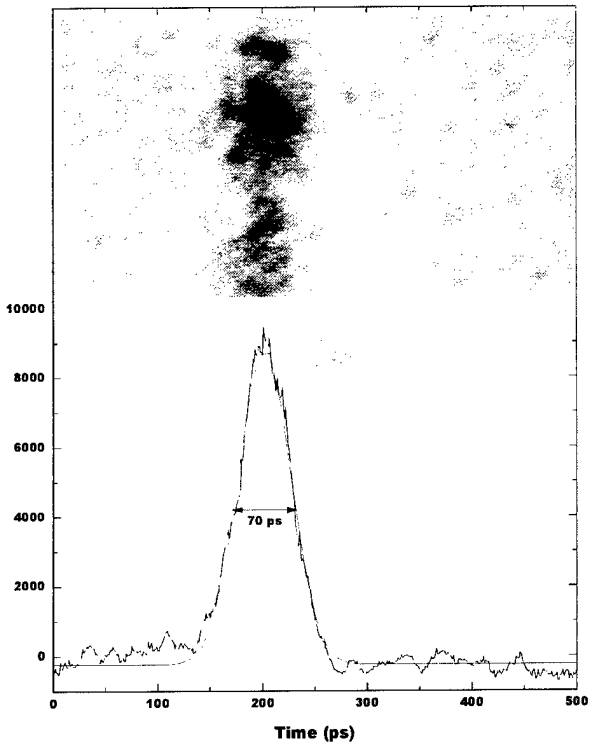

Fig. 1 The pulse duration of the ALS was measured to 70 ps with a streak camera operating an averaging mode.

Fig.1. The data was obtained by averaging 2000 pulses. The 70 ps pulse duration is in good agreement with previous measurements of the ALS pulse duration obtained using a fast photo diode and a streak camera sensitive to visible light [4].

In conclusion, we have demonstrated detection of x-ray radiation using an averaging streak camera with a temporal resolution of 1.5 ps. Work is now in progress in order to perform laser pump/x-ray probe experiments to study structural changes in solid state materials.

References

1. Z. Chang, A. Rundquist, J. Zhou, M. M Murnane, H. C. Kapteyn, X. Liu, B. Shan, J. Liu, L. Niu, M. Gong and X. Zhang: Appl. Phys. Lett. 69, 133 (1996)
2. A. Maksimchuk, M. Kim, J. Workman, G. Korn, D. Du, D. Umstadter and G. Mourou: Rev. Sci. Instr. 67, 697 (1996)
3. Z. Chang,, H. C. Kapteyn, M. M.. Murnane: Private communication
4. R. Keller, T. Renner and D. J. Massiletti: Proceedings of the 7th Beam Instrumentation Workshop, Argonne, IL, May 6-7, 1996

Ultrafast X-Ray Diffraction: Theory

M. Ben-Nun[a] , T. J. Martínez[b],
P. M. Weber[c] and Kent R. Wilson[a]

(a) Department of Chemistry and Biochemistry
University of California, San Diego
La Jolla, CA 92093-0339

(b) Depertment of Chemistry
University of Illinois,
Urbana, IL 61801

(c) Department of Chemistry
Brown University
Providence, Rhode Island 02912

Ever since their discovery by Röntgen (more than 100 years ago), x-rays have made the unseen visible. In particular, much of our experimental knowledge about the structure and electronic densities of atoms and molecules is due to x-ray and electron diffraction measurements. X-ray and electron diffraction have been used to measure the structures of almost all small molecules and x-ray diffraction has been the basis (along with nmr) of most of our structural knowledge about biomolecules. Recent advances in the production of ultrashort x-ray and electron pulses[1-3] suggest that diffraction (and absorption) techniques may be used to observe evolving, non-equilibrium structures of systems that are undergoing chemical (or biochemical) reactions or physical changes such as a phase transition or annealing. In such an ultrafast diffraction (or absorption) experiment, an ultrashort optical pulse can be used to initiate a chemical reaction and a second delayed x-ray (or electron pulse) can interrogate the reacting system. By varying the time delay between the two pulses, the motions of atoms during a chemical reaction may be reconstructed.[4-6] In addition to watching the nuclear motion, at least in principle, x-ray diffraction could be used to follow the dynamics of the electron density involved in chemical bonding and electron flow, and x-ray absorption in the form of chemical shifts of atomic absorption edges could be used to follow the charge or oxidation state of chosen types of atoms. Hence, time resolved x-ray absorption and diffraction may serve as direct ways to watch the evolution of chemical reactions en route from reactants to products, to observe the microscopic processes by which biomolecules perform their tasks and to observe ultrafast process in solid state materials.

A time resolved x-ray (or electron) experiment should ideally have sufficient temporal and spatial resolution to resolve the quantum dynamics of fast chemical processes. To follow the vibrational motions by which molecules evolve and the making and breaking of chemical bonds, one needs temporal resolution of better than 100 fs. The range of internuclear distances in molecules requires spatial resolution of ~0.1 nm, which for diffraction requires hard x-ray wavelengths of comparable size. (In order to be able to follow the time evolution of the electron density itself, even shorter pulses with better spatial resolution will be needed.) This prospect has led us to a series of theoretical and experimental studies[4-7] beginning in 1982, aimed at realizing this potential of ultrafast x-ray diffraction and absorption with second to subpicosecond time resolution.

It is convenient to divide the time dependent measurement of electronic densities into two parts. In the first part one attempts to measure stationary excited electronic state densities. As the

lifetime of many, but not all, excited electronic states of atoms and molecules is in the nanosecond time regime, such experiments do not require ultrafast x-ray pulses. The purpose of this type of study is to see if one can actually observe the change in electron density upon a "single electron" electronic excitation by an optical laser pulse. Such a study attempts to resolve the shell structure of atoms and the molecular orbitals of molecules. The second part addresses the nuclear time evolution. Here one ignores the fine details of the electronic density (i.e., the valence electrons in molecules) and asks what are the expected changes in diffraction or absorption due to the nuclear dynamics and whether these "frames" can be inverted to produce the position of the atoms as a function of time. Eventually one hopes to be able to combine these two studies and actually measure the time evolution of matter simultaneously on the level of time evolving electronic density and nuclear dynamics.

As an example of changes in an x-ray diffraction pattern upon electronic excitation, we show in Fig. 1 the x-ray scattering intensity of the ground and excited ^{2}P(2p←2s) electronic states of the Li atom and the differences between them.[8] The new features in the diffraction pattern can be interpreted in terms of the extended and non-spherical structure of the excited electronic state (the closed shell ground state atom has spherical symmetry). Our computation showed that even though the changes in the total electronic densities are small in real space, they are significant in the inverse k space which is the domain of diffraction experiments. In particular, the difference in the scattering intensity (right panel of Fig. 1) is of the same order as the scattering intensity itself. These results suggest that electronic structures of excited electronic states may be directly observed using optical pump-diffraction probe techniques.

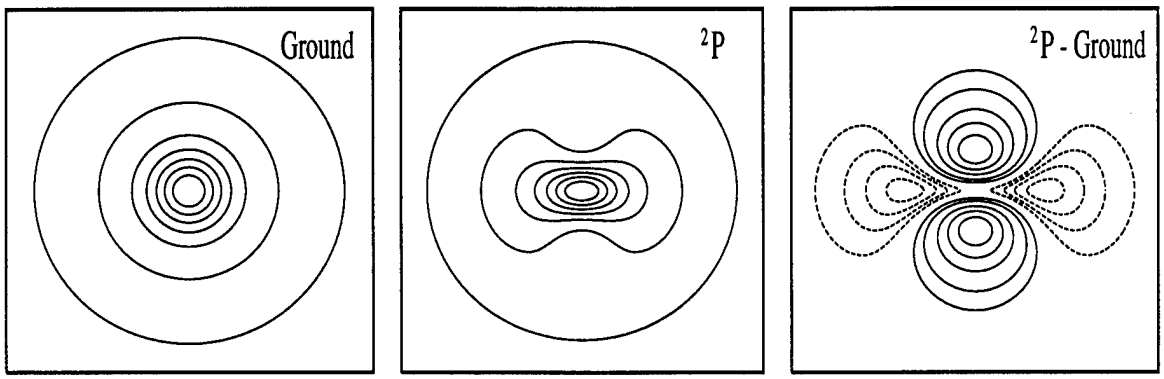

Fig 1: Two dimensional polar contour plots of x-ray scattering intensities from the ground (left panel) and excited ^{2}P (middle panel) states of the Li atom. The distance from the origin to any point on the graph is the scattering angle (a circle inscribed within the bounding box would be at scattering angle of 60°) and the angle between this line and the x axis is the azimuthal angle φ ($0 \le \varphi \le 2\pi$). The contours are equally spaced between 8 and 2. The difference between these two plots is shown in the right panel. Dashed contours are plotted at negative values of -2, -1.5, -1, -0.5 and -0.25, whereas the solid ones are equally spaced between 0.4, innermost contour, and 0.1 outermost one.

We also studied nuclear (i.e., atomic) dynamics in molecules.[9] The simplest chemical reaction that can be studied is the photodissociation of a diatomic molecule, and we take bromine as our example. An optical pulse pumps the ground state molecule into a dissociative excited state and a diffraction pulse probes the system at various (increasing) delay times. In Fig. 2 the diffraction pattern for this two electronic state system is computed as a function of the delay time between the optical pump pulse and the x-ray probe pulse. For the initially isotropically distributed molecules,

the pattern is cylindrically symmetric. Once the molecule interacts with the optical pump field, the diffraction pattern changes, with the most prominent features being the breaking of symmetry, due to the interaction with linearly polarized light, and the collapse of the scattering intensity toward smaller diffraction angles, as the Br atoms separate due to the excited state dissociative dynamics. In this specific example, no interference between the two well separated electronic states is observed, yet, whenever two electronic states approach each other (and even cross) and given a coherent x-ray probe pulse, one should actually be able to observe the effect of electronic interference on the diffraction pattern.

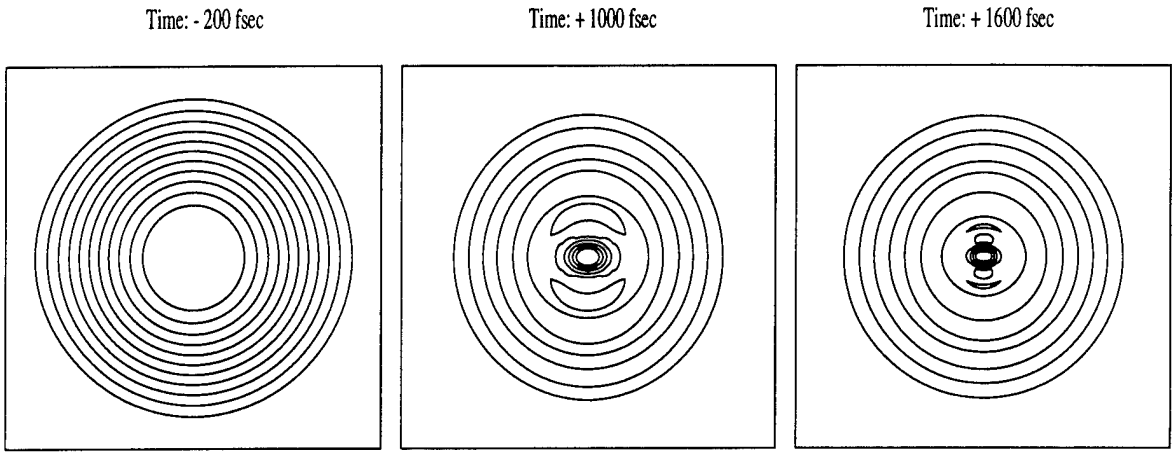

Fig. 2: As in Fig. 1 but for molecular bromine at a series of increasing pump-probe time delays measured between the centers of a 100 fs optical pump and a 200 fs x-ray probe pulses. Only small diffraction angles are shown ($0 \leq \theta \leq 24°$). The changes in intensity as a function of time are mainly due to the time evolution of the excited state. (The ground state is almost stationary.)

Finally, we wish to emphasize that other time resolved x-ray spectroscopic tools may be used to study chemical reactions. As demonstrated recently in a plasma generated x-ray absorption experiment,[6] the photofragmantation of a molecule (SF_6 in this study) could be followed using absorption shape resonances that are known to be sensitive to the chemical structure of the molecule.

References

1.*Time-Resolved Electron and X-Ray Diffraction*, Vol. 2521, edited by P. M. Rentzepis (SPIE, Bellingham, 1995).
2. R. W. Schoenlein, W. P. Leemans, A. H. Chin, P. Volbeyn, T. E. Golver, P. Balling, M. Zolotorev, K.-J. Kim, S. Chattopadhyay, and C. V. Shank, *Science* **274**, 236-238 (1996).
3. *Time Resolved Electron and X-Ray Diffraction*, edited by P. M. Rentzepis and J. Helliwell (Oxford University Press, New York, in press).
4. P. Bado, P. H. Berens, J. P. Bergsma, M. H. Coladonato, C. G. Dupuy, P. M. Edelsten, J. D. Kahn, K. R. Wilson, and D. R. Fredkin, *Laser Chem.* **3**, 231 (1983).
5. J. P. Bergsma, M. H. Coladonato, P. M. Edelsten, K. R. Wilson, and D. R. Fredkin, *J. Chem. Phys.* **84**, 6151 (1986).
6. F. Ráksi, K. R. Wilson, Z. Jiang, A. Ikhlef, C. Y. Côté, and J.-C. Kieffer, *J. Chem. Phys.* **104**, 15 (1996).
7. C. P. J. Barty, F. Ráksi, C. Rose-Petruck, K. J. Schafer, K. R. Wilson, V. V. Yakovlev, K. Yamakawa, Z. Jiang, A. Ikhlef, C. Y. Côté, and J.-C. Kieffer, in *Time-Resolved Electron and X-Ray Diffraction*, Vol. 2521, edited by P. M. Rentzepis (SPIE, San Diego, 1995), pp. 246.
8. M. Ben-Nun, T. J. Martinez, P. M. Weber, and K. R. Wilson, *Chem. Phys. Lett.* **262**, 405 (1996).
9. C. P. J. Barty, M. Ben-Nun, T. Guo, F. Ráksi, C. Rose-Petruck, J. Squier, K. R. Wilson, V. V. Yakovlev, P. M. Weber, Z. Jiang, A. Ikhlef, and J.-C. Kieffer, in *Time Resolved Electron and X-Ray Diffraction*, edited by P. M. Rentzepis and J. Helliwell (Oxford University Press, New York, in press).

The optimisation of soft X-ray laser output

G J Tallents*, A Behjat, A Demir, J Y Lin, R Smith
Department of Physics, University of Essex, Colchester CO4 3SQ, England.
C L S Lewis, A MacPhee, S P McCabe, P J Warwick
Department of Pure and Applied Physics, Queen's University Belfast, Belfast BT7 1NN, Northern Ireland.
D Neely and E Wolfrum
Central Laser Facility, Rutherford Appleton Laboratory, Chilton, Didcot, OX11 0QX, England.
J Zhang
Clarendon Laboratory, University of Oxford, Oxford OX1 3 PU, England.
G J Pert
Department of Physics, University of York, York YO1 5DD, England.
P V Nickles, M Kalashnikov and M Schnürer
Max-Born-Institut, Rudower Chaussee 6, 12489 Berlin, Germany.

*Presented by Greg Tallents, Department of Physics, University of Essex, Colchester Co4 3SQ, England.
Tel. + 44 1206 87 2847 Fax. + 44 1206 873598 Email. tallg@essex.ac.uk

The efficiency of producing soft X-ray laser output from nanosecond duration optical pumping pulses has been found to be low ($\approx 10^{-6}$). This means that moderately large optical pumping lasers are required (typically producing 100 - 1000 joules in nanosecond pulses) and that because of the rapid scaling of efficiency with X-ray laser wavelength, the X-ray wavelengths able to be pumped with such medium-sized laser facilites are limited to typically > 15 nm.

Recent experiments and simulations have shown that soft X-ray laser output can be increased by orders-of-magnitude by pumping with multiple-pulse, short duration (< 150 ps) pulses. Experiments undertaken at the Central Laser Facility, Rutherford Appleton Laboratory will be reviewed in this paper.

Multipulse irradiation with 100 ps pulses of stripe Germanium targets has been shown to enhance by up to several orders-of-magnitude the output of Ne-like Ge lasing on the

J = 0-1 line at 19.6 nm compared to single pulse pumping [1]. The VULCAN glass laser at the Rutherford Appleton Laboratory was modified to produce pairs of 100 ps pulses separated by 400 or 800 ps with an optional double pre-pulse 2 ns earlier. Three beams from the laser were overlapped to produce a line focus of 100 μm width and 18 mm length with an average irradiance of ~$4X10^{13}$ Wcm^{-2}. The total number of X-ray laser photons recorded by a grazing incidence flat field spectrometer is plotted as a function of the ratio of the irradiance of the two driving laser pulses in figure 1.

Figure 1 show a large scatter on the data points as would be expected of a highly non-linear phenomena such as unsaturated mirrorless laser output. However, the X-ray laser output can be seen to increase with irradiance ratio (first pulse/second pulse) of the main driving pulses up to a maximum at ≈ 1. The X-ray laser output was simulated using the EHYBRID fluid code [2] and a post-processor ray tracing code [3]. Figure 1 show superimposed on the experimental data points the simulated output of the 19.6 nm lasing line integrated over all angles and in time from the post-processor ray trace far-field image as a function of the ratio of the two main pulses. It can be seen that the output intensity increases as the pulse ratio increases and that the predicted optimum output is with the two main pulses of irradiance ratio ~ 1 with 400 ps separation and two prepulses heating the target 2 ns earlier in agreement with the experimental results. The simulations show that the increase in output with increasing pulse ratio is due to an increase in the gain zone spatial size and reduced refraction of the X-ray laser beam resulting from reduced average density gradients. The position of the gain peak and the outer edge of the gain region move away from the target surface to regions of reduced electron density gradient. The peak gain coefficients remain approximately constant (at ~ 30 cm^{-1}) with varying pulse ratio.

Enhanced efficiency of neon-like X-ray lasing has been obtained by transient pumping using a short pulse (~ 2 - 8 ps) laser impinging onto the plasma produced by a long pulse, low intensity laser. The VULCAN laser at the Rutherford Appleton Laboratory was employed with one of the six beamlines producing the long pulse of irradiance $5X10^{12}$ Wcm^{-2} and pulse duration 700 ps and another beamline producing the short pulse (2-8 ps) with an irradiance of ~ 10^{15} Wcm^{-2} over a line focus of length 10 mm. Lasing with Ne-like Ge and Fe has been observed with very large gain coefficients and evidence for gain saturation at lengths of ~ 5 mm.

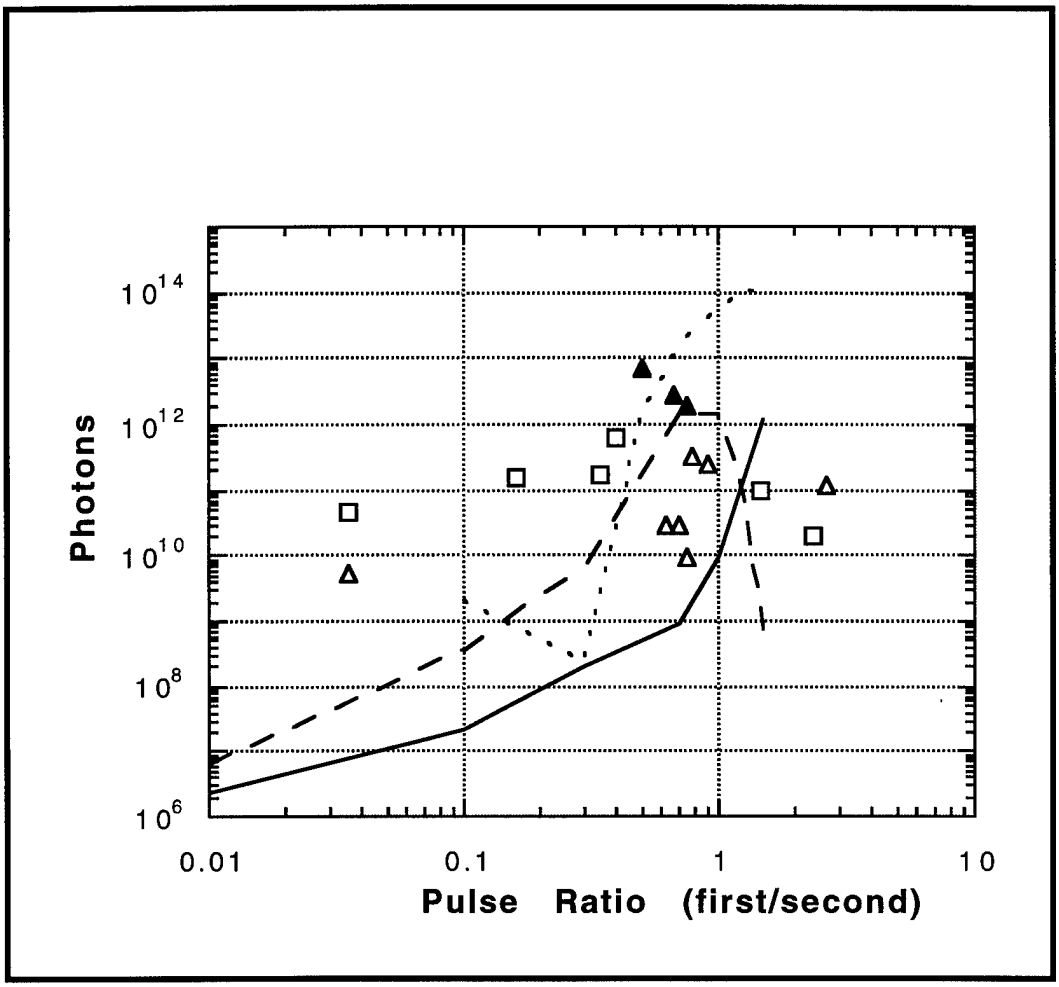

Figure 1. X-ray laser output as a function of the irradiance ratio of the two main drive pulses (first/second). Δ Double pulse with 400 ps separation. ☐ Double pulse with 800 ps separation. ▲ Double pulse with 400 ps separation and two prepulses. The variations of the x-ray laser output for the 196Å line calculated using EHYBRID and the ray tracing code normalised to the experimental data are also shown as continuous curves. The solid line is for double pulse irradiation with 400 ps separation. The broken line is for double pulse irradiation with 800 ps separation. The dotted line is for double pulse irradiation with 400 ps separation and two prepulses.

These experiments will be discussed in detail along with modelling studies of the X-ray laser output with multipulse experiments using the EHYBRID and ray tracing codes. Such modelling is important as there are a range of experimental parameters which can be varied with muti-pulse pumping (the pulse durations, pulse separations, relative intensities of the pulses) which it is difficult to investigate experimentally.

[1] A Behjat, J Lin, G J Tallents, A Demir, M Kurkcuoglu, C L S Lewis, A G MacPhee, S P McCabe, P J Warwick, D Neely, E Wolfrum, S B Healy and G J Pert 1996 Optics Communication *in press.*

[2] G J Pert 1983 J Fluid Mech. **131**, 401.

[3] P B Holden, S B Healy, M T M Lightbody, G J Pert, J A Plowes, A E Kingston, E Robertson, C L S Lewis and D Neely 1994 J Phys B**27**, 341.

Biological x-ray microscopy with a compact laser system

M. Richardson[1], M. Kado[1], Y. Yamamoto[2], J. Rajyaguru[3], D. Torres[1], K. Nekula[1], H. Friedman[2], and M. J. Muszynski[3]

1 Laser Plasma Laboratory, CREOL, University of Central Florida
4000 Central Florida Blvd., P.O. Box 162700, Orlando, FL 32816-2700
Tel: 407-823-6819, Fax: 407-823-3570, Email: mcr@mail.creol.ucf.edu

2 College of Medicine, Dept. of Medical Microbiology and Immunology,
University of South Florida Tampa, FL.
12901 Bruce B. Downs Blvd., Tampa, FL 33612
Tel: 813-974-2332, Fax: 813-974-4151

3 Department of Pediatric Infection Disease Research
Arnold Palmer Hospital for Children & Women, Orlando FL.
85 West Miller Street, Suite 303, Orlando, FL 32806-2036
Tel: 407-841-5111 Ext 5691, Fax: 407-426-7553

The development of x-ray microscopy for the biological and medical sciences offers several inherent advantages over other high resolution microscopy techniques, such as confocal optical microscopy and electron microscopy [1]. Short wavelength radiation allows for much higher spatial resolution than optical techniques, while at the same time possessing sufficient depth of field to image whole-cell structures of several microns size. High image-contrast, and even elemental mapping, can be obtained by selection of the appropriate x-ray wavelength. Moreover in avoiding the need for the sample preparation procedures inherent to electron microscopy (staining, drying, sectioning etc.) x-ray imaging permits the visualization of biological specimens in their natural state. Previous developments in x-ray microscopy have mostly used synchrotron radiation sources [2]. These offer precision variability in x-ray emission but are restricted to major facilities, and require long exposure times to record an image. This latter limitation prevents the high resolution analysis of mobile living organisms [3]. Early work with laser plasma x-ray sources also required the use of major facilities (dedicated to laser fusion) [4].

In this paper we present the first demonstration of single frame x-ray imaging of biological specimens in their natural state, made with a compact solid-state laser plasma source. In these experiments live mouse macrophages [5] and lipopolysaccharide (LPS) [6] from *Burkholderia cepacia* were used as specimens. The ultrashort duration of laser plasma x-rays permits single-shot framed images to be recorded in times much shorter than any kinetic response of biological organisms, including those produced by the x-ray radiation[7]. Thus the images obtained by this method portray the organism in its natural state, unaltered by preparation or radiation.

An x-ray image of lipopolysaccharide (LPS) in (dH_2O) from *Burkholderia cepacia* is shown in Fig.1. The images of the aggregated LPS molecules are similar to the space-filling models that are constructed using data from chemical degradation. Thus, visualization of the LPS

allows for the study of the role of LPS in conferring antibiotic resistance in gram-negative bacteria such as *Burkholderia cepacia*.

The image shown in Fig.2 are of thioglycollate-elicited macrophages obtained from a BALB/c mouse peritoneal cavity. Macrophages are professional phagocytic cells capable of ingesting and destroying antigens. They also cooperate with lymphocytes in the production of variety of cytokines which regulate inflammatory responses. The figure shows an x-ray image of live, un-fixed, macrophage cells suspended in tissue culture medium.

In summary, we have demonstrated single frame x-ray imaging with 5 ns time resolution. The data obtained with LPS shows that the spatial resolution of our system is better than 50nm. The x-ray image of the fixed macrophage is comparable to an image taken by a scanning electron microscope. The short exposure time made it possible to take an x-ray image without fixation. We have observed two types of unfixed macrophage images. One that appears rigid and steady, much like those from an SEM, the other appears fragile, and dissimilar to those taken with an SEM. These fragile images are reported for the first time. It is possible that the fixation process, used to view these fragile samples, destroys these features, and that only by imaging live, unfixed organisms, can features like this be examined.

REFERENCES

1. E. Spiller, R. Feder, D. Sayre, J. Topalian, D. Eastman, W. Gudat & D. Sayre Science 191, pgs 1172-1174 (1976).
2. S.S. Rothman, K.K. Goncz, and B.W. Loo, Jr., in "X-ray Microscopy III", A.G. Michette, G. R. Morrison & C. J. Buckley eds. (Springer-Verlag, New York, 1992), pp. 373-383; J.R. Gilbert, J. Pine, J. Kirz, C. Jacobsen, S. Williams, C.J. Buckley and H. Rarback, ibid.; D. Rudolph, G. Schneider, P. Guttmann, G. Schmahl, B. Niemann, and J. Thieme, ibid.
3. M. Richardson, K. Shinohara, K. A. Tanaka, Y. Kinjo, N. Ikeda, and M. Kado Proc. SPIE 1741 pgs. 97-104 (1992).
4. P.C. Cheng, S. P. Newberry, H.G. Kim & I.S. Hwang, in "Modern X-ray Microscopies" ed. P. Duke & A. Michette, Publ. Penum Press 1990, p 87-118
5. T.W. Klein, Y. Yoshimasa, H. K. Brown, and H. Friedman, Journal of Leukocyte Biology, 49, 98 (1991).
6. "Biology of micro-organisms", ed: T.D. Brock, M.T. Madigan, J. M. Martinko & J. Parker, Prentice Hall, NJ , pg 60-112 (1988).
7. J. C. Solem J. Opt. Soc. Am B3 1551-1565 (1986): R. A. London, M.D. Rosen & J. E. Trebes Appl. Opt. 28, pgs 3397-3404 (1989).

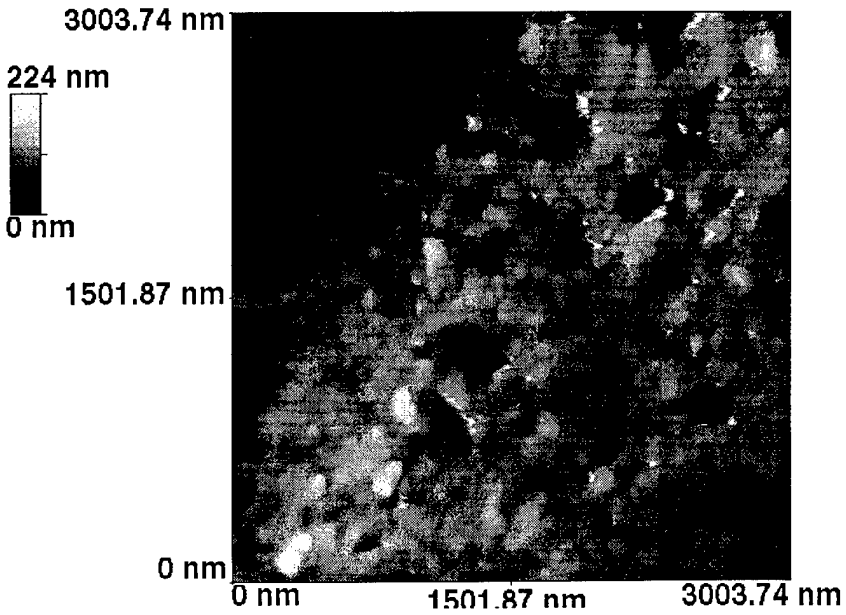

Fig. 1. An x-ray image of *lipopolysaccharide* (LPS) from *Burkholderia cepacia.* The smallest feature size resolved is ~ 50 nm.

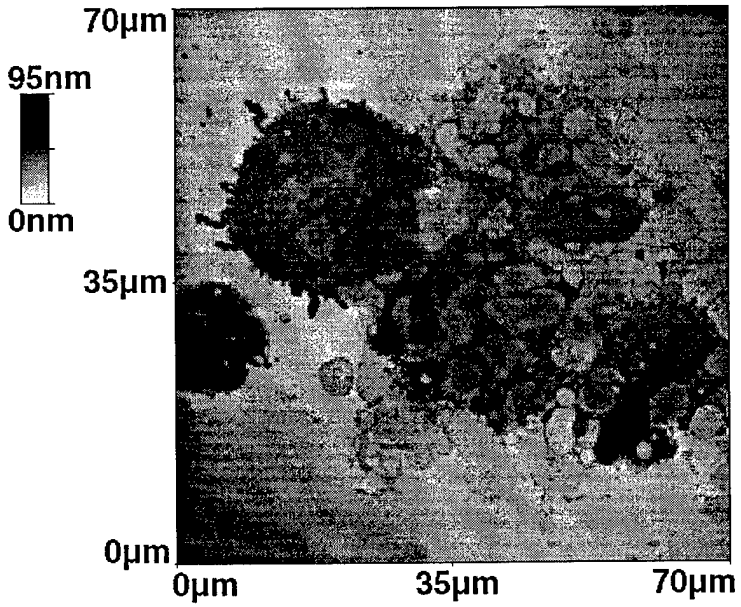

Fig. 2. An x-ray image of mouse macrophage obtained in its natural state.

Thursday, March 20, 1997

Poster Session

ThE 6:00pm – 8:00pm
Anasazi South

ThE1 • Moved to ThD4

Tunable, Ultrashort, High-Intensity Kilohertz Mid-Infrared Laser System

B. Sheehy, M. Widmer, R. Lafon, A. Gambhir, L. F. DiMauro
Brookhaven National Laboratory, Chemistry Department, Upton, NY 11973

We have developed a high intensity, ultra-short kilohertz laser system operating in the mid-infrared, between 3 and 4.5 μm. The output of an ultrashort pulse oscillator (sync-pumped dye laser or mode-locked Ti:Sapphire laser), which is tunable about 800 nm, is amplified in a Ti:Sapphire regenerative amplifier, using chirped pulse amplification . Another pulse at λ=1053 nm, synchronized with the tunable pulse, is amplified in a cw pumped Nd:YLF regenerative amplifier. Mixing the two pulses in a nonlinear crystal, we obtain the difference frequency in the mid-infrared. A schematic of one configuration is shown in the figure below. The 800 nm oscillator in this case is a dye laser synchronously pumped by a mode-locked Nd:YLF laser, which also acts as the seed source for the 1053 nm light, thus providing optical synchronization between the two pulses at the mixing crystal. This configuration yields 1 psec pulses in the mid-infrared with an energy of 70 microjoules, which may be focussed, using f/4 optics, to peak intensities above 10^{12} W/cm^2. The 1053 nm seed source may also be electronically synchronized with a mode-locked Ti:Sapphire oscillator in place of the dye laser, reducing the pulsewidth and increasing the peak intensity by an order of magnitude.

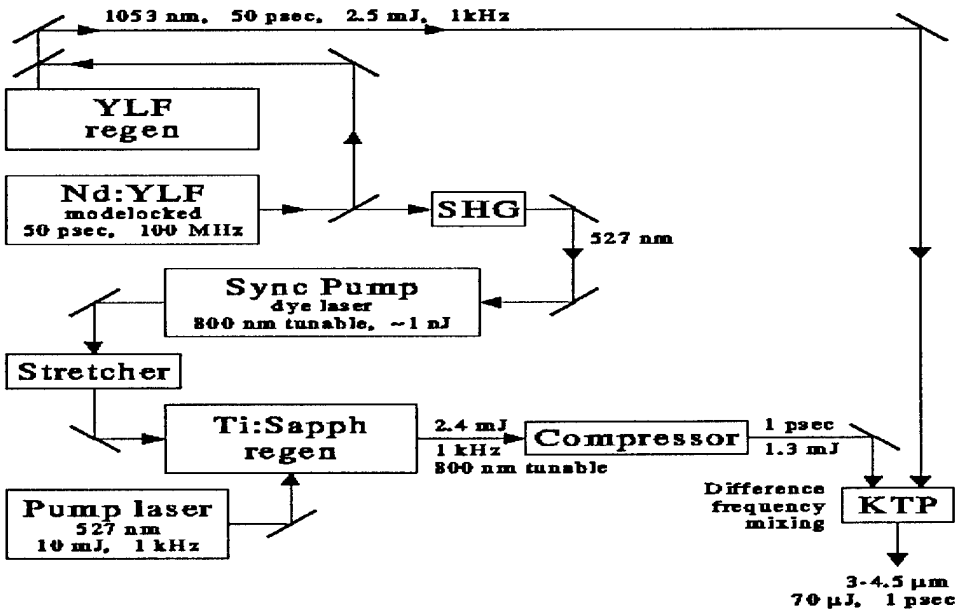

Figure 1 Schematic diagram of the 1 psec configuration of the mid-infrared laser system

The physics of nonlinear phenomena in this wavelength range is relatively unexplored due to a lack of sources. The dynamics of multiphoton ionization (MPI) may be quite different in this regime, as the ponderomotive potential, which scales as λ^2, is over an order of magnitude larger than at visible wavelengths. The onset of the tunneling regime of MPI ($\gamma < 1$) then occurs at intensities well below the point where the Coulomb barrier is suppressed below the ground state. An electron which is ionized by tunneling and oscillating in the optical field near the core will also have an oscillation amplitude larger by a factor of λ^2. An anomalous enhancement of the photodetachment cross-section of Cl^- at longer wavelengths (1.9 vs 1.0 μm) has already been observed [1]

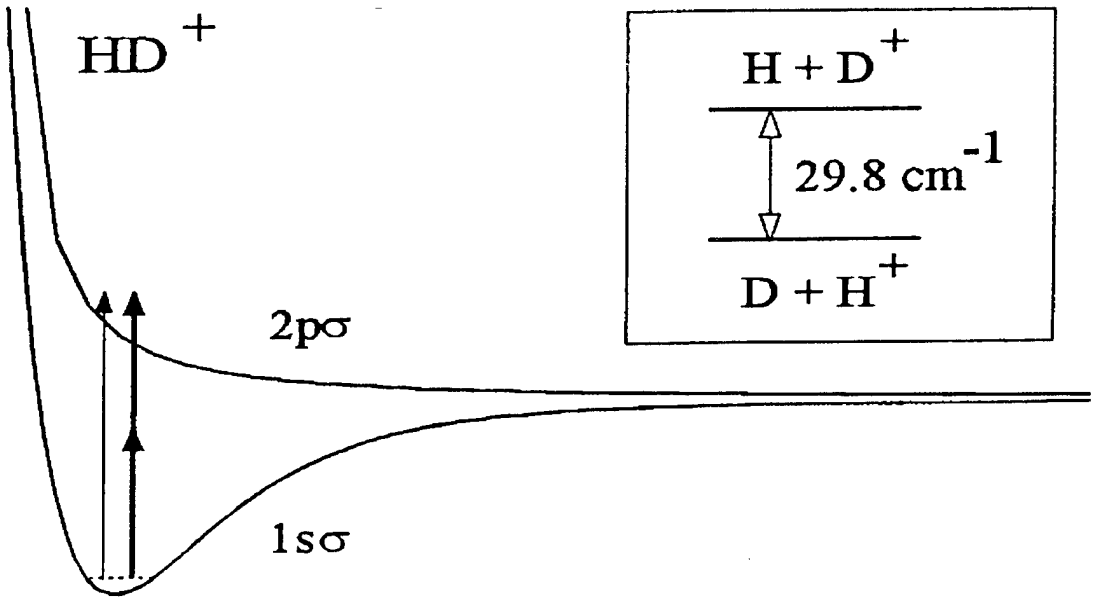

Figure 2 Potential curves for the 1sσ and 2pσ states of HD^+

Applications of coherent control should also prove more interesting at longer wavelengths. For example, in the coherent control of the multiphoton dissociation of HD^+, going to longer wavelengths allows one to manipulate interferences involving closely spaced levels near the dissociation threshold, and leads to a more precise control of the dissociation process. Figure 2 shows the potential curves of the $1s\sigma_g$ ground state and the $2p\sigma_u$ repulsive state of the HD^+ ion. The arrows shown correspond to the photon energies at 1μm and its second harmonic. The two dissociation channels become degenerate at large internuclear separation in H_2^+ and D_2^+, but this is lifted in the heteronucluear case, due to the nuclear mass difference. Because of the mixing of states of opposite symmetry, both electronic states acquire permanent dipole moments, opposite in sign, which distinguish the two asymptotic dissociation channels ($H + D^+$) and ($D + H^+$). Coherent control of the photodissociation fragment angular distribution through the manipulation of the relative phase between the fundamental and second harmonic has already been demonstrated at 1μm [2]. This occurs through a phase-dependent interference between different

multiphoton pathways in a transition between the two electronic states. At longer wavelengths, rovibrational transitions within an electronic state become important, sampling the potential at large internuclear separations, where the dipole moment is large. It is then possible to spatially separate the products from the two dissociation channels [3]. This effect is predicted to peak near $\lambda = 10$ μm, but should already be clearly visible at 4 μm.

References

1. Davidson et al. *Physical Review Letters* **69,** 3459 (1992).
2. Sheehy et al. *Physical Review Letters* **74** 4799 (1995).
3. Charron et al *Physical Review Letters* **75** 2815 (1995)

Characterization of a flatfield spectrometer for the VUV- and XUV-spectral range

K. Sokolowski-Tinten, G. Jenke, A. Orisch, and D. von der Linde

Institut für Laser- und Plasmaphysik, Universität-GHS-Essen,
D-45117 Essen, Fed. Rep. of Germany,
Phone: +49 201 183 2570 / Fax: +49 201 183 2120
e-mail: kst@agvdl.ilp.physik.uni-essen.de

High order harmonic generation of intense femtosecond laser pulses has attracted much interest during the last years. These harmonics cover a rather broad spectral range and especially in the VUV and XUV (corresponding to wavelengths from approximately 10 - 100 nm) the spectral analysis and the efficient detection of the laser generated radiation is not a trivial task. For our own studies on harmonic generation from femtosecond laser plasmas on solid surfaces we have build a XUV-spectrometer consisting of a flatfield grating in conjunction with a thinned, back-illuminated CCD-camera.

The experimental setup for the characterization of our detection scheme consists of a hollow-cathode discharge lamp as a calibrated VUV-source coupled to a VUV-grating monochromator. For part of the experiments we also used a silicon photodiode (UDT XUV-100). All measurements are necessarily conducted in vacuum. Although the spectrographs and the detectors are differentially pumped the vacuum conditions are rather poor (base pressure $\approx 10^{-4}$ mbar) because of the direct coupling to the (windowless) hollow cathode discharge lamp.

In a first step we determined the diffraction efficiency of the flatfield-grating. The monochromator is used to select a specific wavelength and the diffraction efficiency of the flatfield grating is determined simply by comparing the signals from the CCD or the photodiode before and after the grating. Because in this experiment only relative signals are compared we do not need the absolute characteristic of our source and of the detector. Typical diffraction efficiencies lie in the range from 2% up to 15% with a relative uncertainity of 10 - 20%. Due to the rather bad vacuum conditions and the problems which may arise from a contamination of the gratings or the detectors with hydrocarbons we repeated the measurements several times for different vacuum conditions and with the CCD cooled (Peltier) or at room temperature. We usually found *no* dependence of our results on the different enviromental conditions.

After the calibration of our spectrometer we measured the XUV-sensitivity of two thinned, back-illuminated CCD-cameras. Both cameras are commecially available systems (Spectroscopy Instruments Inc.) and use CCD´s from SiTe (TK1024T and TK512CB). It is well known that such CCD´s are directly sensitive to electromagnetic radiation from the visible/ near-infrared up to the keV-X-ray-range. The sensitivity is limited to this range because for photon energies below 1eV and above a few keV the propability for absorption becomes so low that the light passes through the (thinned) device without creating an electron-hole pair. On the other hand the sensitivity in the VUV- and XUV-range is decreased due to the fact that here the absorption is too strong. The incident photons

are absorbed in the oxide layer or in the first few nanometers of the silicon. Near the surface the potential gradient becomes inverted due to surface- and interface states and the photogenerated electrons drift towards the surface and recombine there without being detected. This effect can be reduced by ion-implantation coupled with laser-annealing of the near surface region. However it is not trivial to achieve homogenous implantation *and* annealing on larger CCD´s and it should be noted that such special design devices are not yet commercially available. That was the main reason for us to investigate the VUV-perfomance of commercially available CDD-cameras.

We will report here on measurements of the spectral sensitivity of the two cameras from 10 - 50 eV, discuss the reproducibilty of our devices especially under the aspect of surface contamination of the CCD and compare their performance to that of a phosphor based detection scheme. Beside that we will discuss the occurance of some type of radiation damage in the CCD caused by VUV-radiation from a rather narrow spectral range around 80 nm. Due to this damage the VUV-sensitivity of the CCD is significantly reduced and the dark current is increased. We found that the damage is not permanent and describe a procedere to anneal the CCD.

Demonstration of a 0.54 Picosecond X-Ray Streak Camera

Z. Chang, A. Rundquist, H. Wang, H. C. Kapteyn, M. M. Murnane
Center for Ultrafast Optical Science, The University of Michigan, Ann Arbor, MI 48109-2099
Phone:(313) 763-0573; Fax: (313) 763-4876; E-mail: kapteyn@eecs.umich.edu

X. Liu, B.Shan, J. Liu, L. Niu, M. Gong, X. Zhang
State Key Laboratory of Transient Optics Technology,
Xi'an Institute of Optics and Precision Mechanics, Xi'an, 710000, P. R. China

R.W. Lee
Lawrence Livermore National Laboratory, Livermore, CA 94551

X-ray streak camera detectors are important as diagnostics for monitoring fast x-ray processes such as the emission from laser-produced plasmas, and also for obtaining high time-resolution in x-ray studies done using quasi-CW x-ray sources such as synchrotrons. In work in 1990, an x-ray streak camera was demonstrated to have 2 ps time resolution;[1] however, in subsequent years, progress in obtaining faster resolution has been slow. Progress has been limited by two factors: the intrinsic time response of the streak camera itself, and the time duration of the x-ray source itself (usually a laser-produced plasma with x-ray pulse duration of ~1-2 ps).

In this work, we describe a significant improvement in streak-camera performance, resulting from a complete rethinking of the streak camera design, to reduce the limitations on the temporal resolution as much as possible.[2] Our camera uses a pair of meander-type deflection plates, located before a magnetic focusing lens. This configuration has several advantages over past electrostatic focusing designs. First the electron transit time dispersion from the anode to the deflection plates is minimized. Second, the fast time response and high deflection sensitivity (8 cm/kV) of the meander type deflection plates allows high sweep speeds on the phosphor screen. Third, the short transit time also reduces space charge effects. Fourth, using a pulsed extraction field makes it possible to use high acceleration fields without electrical breakdown. And finally, the use of a GaAs photoconductive switch makes possible a fast sweep speed well-synchronized to the source.

The x-ray streak camera uses a KBr photocathode, followed by an acceleration region driven by a -5kV pulse superimposed on a -5kV DC voltage. The beam then passes through a pair of sweep plates driven by a GaAs photoconductive switch. After the magnetic lens, the photoelectrons strike an intensifier consisting of a double microchannel plate and a phosphor-coated fiber-optic faceplate. The output phosphor screen is then fiber-optically coupled to a CCD camera. The measured width of the slit image is ~80μm. The obtained sweep speed is $2x10^8$ m/s, so that the camera time resolution is limited at 400 fs by the spatial resolution and sweep speed. Taking into account the time dispersion also, the total estimated time resolution for our camera is ~0.5ps.

To test the time resolution of the camera, we used the fastest x-ray pulses available to date, which are higher harmonics generated by a 25 fs Ti:Sapphire laser.[3] A single high harmonic peak centered at 170Å was selected by an X-ray spectrometer to use for the streak camera calibration. The pulse duration of the high harmonics is expected to be shorter than the laser pulse of 26 fs, while the dispersion of the x-ray spectrometer was calculated to broaden the time duration by at most 300 fs. We obtained a time resolution of 880 fs in the x-ray region using our streak camera, as shown in Fig.1. This is, to our knowledge, the first demonstration of a sub-picosecond response x-ray streak camera.

In this preliminary measurement, we found that the sweep speed of the camera could not be increased beyond a certain point, because the electron path became obstructed by the plates. This happens when the speed of the electron bunch through the deflection region does not perfectly match the speed of the voltage pulse in the deflection plates.

Tests were also performed using the third harmonic of a Ti:Sapphire laser, generated by focusing an 800 nm, 26 fs, 3 mJ laser pulse in air with an f-30 lens. The uv beam was collimated using a second lens, and separated from the infrared light by a pair of prisms. Finally, the uv light was focused onto the photocathode of the streak camera. Using this setup, we observed a time-response of 0.8 ps using the original setup, and very recently we demonstrated a time response of 540 fs using a set of redesigned deflection plates. The sweep speed was calibrated by inserting a known thickness glass plate into part of the beam to delay that part. The theoretical time resolution of the camera at this wavelength is not clear, since the photoelectron energy distribution of the photocathode at this wavelength is not available. From our uv tests, we found that the dynamic spatial resolution in the scanning direction deteriorates with increasing sweep speed. However, this could be corrected by readjusting the focusing current.

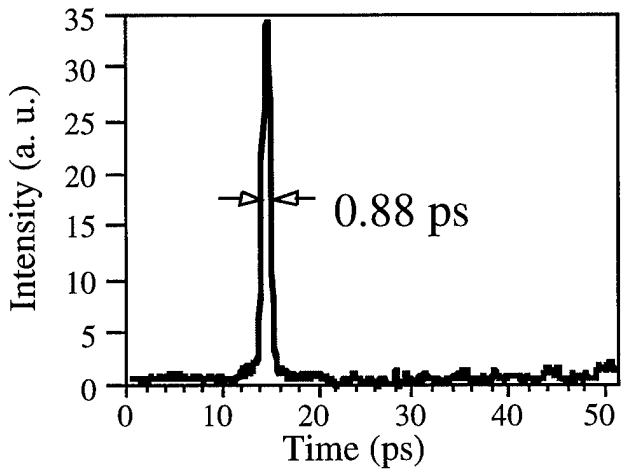

Figure 1: The 0.88 ps time-response of our streak camera using femtosecond x-rays at 17 nm produced by high-harmonic generation.

References

1. M. M. Murnane, H. C. Kapteyn, R. W. Falcone, Appl. Phys. Lett. **56**, 1948 (1990).
2. Z. Chang, A. Rundquist, J. P. Zhou, H. C. Kapteyn, M. M. Murnane, Applied Physics Letters **69**, 133 (1996).
3. J. Zhou, J. Peatross, M. M. Murnane, H. C. Kapteyn, I. P. Christov, Physical Review Letters **76**, 752 (1996); I. Christov, J. Zhou, J. Peatross, A. Rundquist, M. M. Murnane, H. C. Kapteyn, I. P. Christov, Physical Review Letters **77**, 1743 (1996).

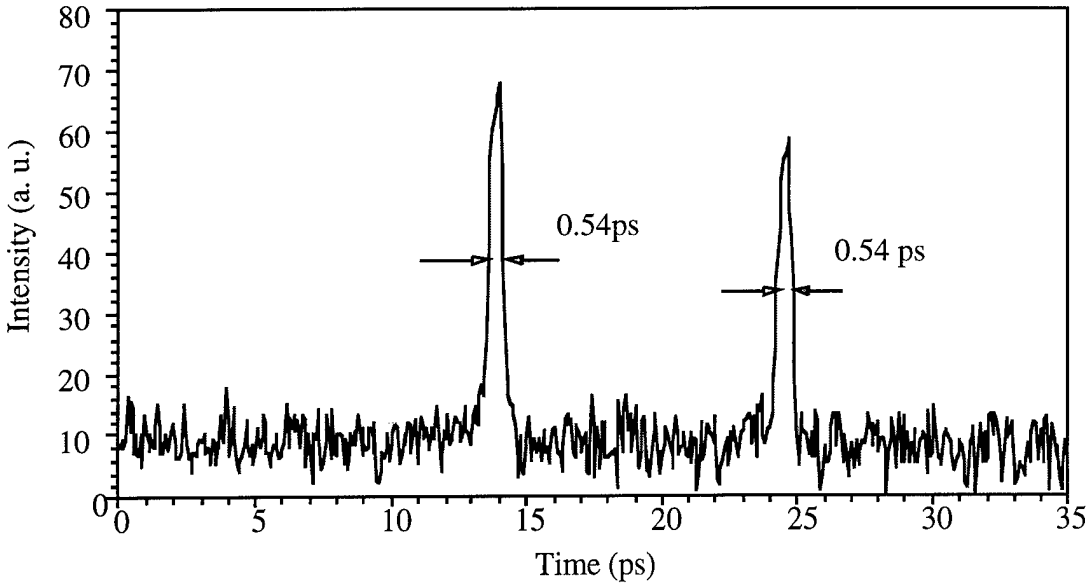

Fig.2: UV time response of the streak camera using redesigned sweep plates.

Multiterawatt Ultraviolet Laser System

F. G. Omenetto, K. Boyer, J. W. Longworth,
A. McPherson, T. Nelson, W. A. Schroeder,
and C. K. Rhodes

Laboratory for Atomic, Molecular and Radiation Physics, rm.2136, University of Illinois at Chicago, 845 W. Taylor Street,
Chicago, Illinois 60607-7059. e-mail: rhodes@uic.edu

The combination of ultrashort pulse generation and chirped pulse amplification (CPA) techniques has been the driving force in the development of laser systems with peak powers at the terawatt level [1-6]. Most high power systems developed to date, work in a spectral region between 0.8 and 1.1 microns, and TW-class lasers have been demonstrated in Ti:Sapphire, Nd:glass and Cr:LISAF based systems. A known alternative is offered by excimer lasers. Efforts in this direction have been undertaken by a number of groups [7-9].

We report on the performance of a Ti:Sapphire/KrF* laser system leading to the generation of what could prove to be the first multi-terawatt pulses reported in this spectral region. The initial pulses are obtained with a Ar-ion pumped KLM Ti:Sapphire oscillator optimized for stable operation at λ=745 nm with a single-plate birefringent filter. The average mode-locked power is 350 mW (P_{pump}=6.7 W) for a pulse of duration τ=85 fs. After the initial stretching, amplification in the red is performed. Gold-replica gratings (groove density of 1200 lines/mm) are used in a single grating stretcher/single grating compressor combination (stretch factor=1000). The previous dye preamplifier/triple pass Ti:Sapphire combination [12] has been substituted by a home built regenerative amplifier illustrated in Fig. 1. Pumping is achieved by means of a Continuum Q-switched Nd:YAG, furnishing ~30 mJ of energy to the amplifier crystal. The combination of the prism stage and curved end mirror allows *spectral tunability* of the regen cavity: for our purposes it is tuned for operation at 745 nm. The SF10 prisms are set to approximately compensate the other optical elements in the regen cavity. Typical energy outputs are of 1.8 mJ, with fluctuations of ±5% caused by instabilities in the pump energy. This gives us, as expected, considerable improvement over the previous dye-cell arrangement. The repetition rate of the amplified pulses is 2 Hz. Frequency conversion takes place at this point. Two KDP crystals of thickness 3 mm and 1 mm, respectively, for

doubling and mixing of the 372 nm radiation with the residual 745 nm fundamental. Seeding energies of at least 10 μJ from the tripler are desirable, to guarantee a good contrast ratio between the signal and the amplified spontaneous emission (ASE) in the KrF* amplifier.

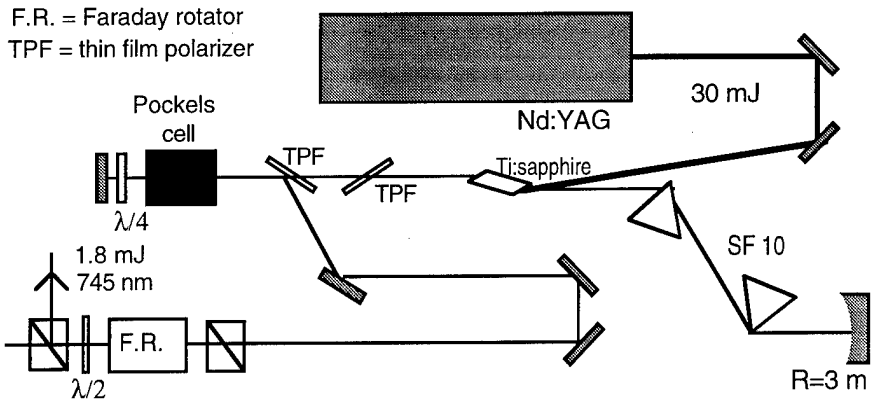

Fig. 1 Schematic of the tuneable regenerative amplifier

Average output energies from the tripler are of 18 μJ at 248 nm for a 1 mJ 745 nm input, which are sent to seed the excimer preamplifier. To ensure good beam quality, the beam is spatially filtered in vacuum after the tripler by focusing it into a 35 μm pinhole which reduces the seed energy to 15 μJ. The first UV amplification stage is performed in a KrF* excimer (Lambda Physik 201 MSC EMG) arranged in a double-pass off-axis geometry [11]. The device is operated with a 22 kV discharge voltage and a pressure of 2000 mbar (100 mbar F_2, 120 mbar Kr, 1800 mbar Ne). The off-axis angles in the two paths are designed to achieve optimum amplification over the whole beam dimension. The output energies are measured to be an average of 3.5 mJ. The duration of the 248 nm pulse, after the double-pass excimer, is obtained through a two-photon fluorescence (TPF) measurement giving a duration of 200 fs. The beam is focused and sent through a second pinhole in order to filter out any ASE leaking from the first excimer. The contrast ratio signal to ASE is measured to be in excess of 1000. The final amplification is obtained by means of a large aperture (10 cm) excimer amplifier [12]. The beam is then directed through a telescope beam expander before entering the final amplification stage. This power amplifier is operated at relatively low pressure and low gain in order to reduce wave-front distorsions and ASE. The pulses, produced at a repetition rate of 0.4 Hz exhibit a 10-

shot average energy above 0.5 J, with peak recorded shots, for a fresh gas fill, of 0.75 J. Characterization of the spectral and temporal features of the final pulse are presently underway. From the previous performance of the system , there is reason to believe that there will not be considerable broadening of the pulse through the final amplification stage.

In conclusion, evidence for a femtosecond laser system that can operate in the 2-3 Terawatt power level in the UV region of the spectrum (248 nm), is presented. Preliminary observations indicate improved experimental conditions, which provide a more efficient tool for ultraintense physics experiments.

References

[1] T. Ditmire and M. Perry, Optics Letters, **18** (6), 426 (1993)
[2] C. P. J. Barty *et al.*, Optics Letters, **21** (9), 668 (1996)
[3] J. Zhou *et al.*, Optics Letters, **19** (2), 126 (1994)
[4] A. Sullivan *et al.*, Optics Letters, **21** (8), 603 (1996)
[5] P. Beaud *et al.*, Optics Letters, **18** (18), 1550 (1993)
[5a] A. Antonetti *et al.*: *Ultrafast Phenomena 8*, , (OSA, Washington D.C. 1996) p.160
[6] Y. Nabekawa *et al.*, Optics Letters, **18** (22), 1922 (1993)
[7] I. N. Ross *et al.* , Optics Comm., **109**, 288 (1994)
[8] S. Szatmári *et al.* , Optics Comm., 63, 305 (1987)
[9] B. Bouma *et al.*, JOSA B, **10** (7), 1180 (1993)
[10] G. Almási *et al.*, Optics Comm, **88**, 231 (1992)
[11] G. Almási and S. Szatmári, Appl. Phys. B **60**, 565 (1995)
[12] T. S. Luk *et al.* , Optics Letters, **14**, 1113 (1989)

0.125 Terawatt Kilohertz Laser System

Sterling Backus, Charles Durfee, Margaret Murnane, and Henry Kapteyn

Center for Ultrafast Optical Science
University of Michigan
2200 Bonisteel Blvd., Ann Arbor, MI 48109-2099
Phone: (313) 936-0248; FAX: (313) 763-4876; E-mail: sbackus@eecs.umich.edu

Recently there has been significant progress in the development of high repetition rate, high peak power Ti:sapphire systems. [1] Many experiments in high field science require peak powers of 0.1-1.0 TW, and therefore this new generation of high-average power lasers will have a great impact on the quality and utility of experiments in this area. For example, recent experiments in high harmonic generation (HHG) have demonstrated that with sufficiently short laser pulses (~ 20 fs), laser energies of 2 - 10 mJ can be used to generate very high order harmonics, with photon energy up to 240 eV. [2,3] However, to date, the lasers used to generate very high-order harmonics have typically been low repetition-rate (10 Hz) systems. A kHz repetition-rate laser with sufficient peak power for high harmonic generation would result in a 100 times increase in x-ray flux, with vastly improved signal-to-noise ratios. In addition, other processes such as low-order harmonic generation in gases[4] become even more efficient with millijoules of laser energy, and will be capable of generating sufficient flux for application experiments in chemical dynamics.

We have developed a Ti:sapphire amplifier system that generates a peak power of 0.125 TW, at 1 kHz repetition rate, with 2.5 mJ of energy, in a 20 fs pulse duration. The laser system is shown in Figure 1, and consists of two stages of amplification. The first stage is a ring multi-pass amplifier, which has been demonstrated previously. [1] It is pumped by 9 mJ from an intra-cavity doubled Nd:YLF laser (Quantronix 527). The output from the first stage is 600 μJ, which is passed through a Pockels cell, before injection into the second stage. The second stage has a similar design to the first stage, and is pumped by the residual 7.5 mJ from the first pump laser, together with 12.5 mJ from a second Nd:YLF laser. The amplifier crystal used in the second stage is a 4.5 mm thick, 1 cm diameter, 0.25% doped Ti:sapphire crystal cut for normal incidence, anti-reflection coated for 800 nm, and temperature stabilized at 15 deg C. In high repetition rate systems, the average power that is deposited in the amplifying medium can cause a radial change in the refractive index, and can also cause stresses which deform the crystal surface. These changes act as a lens element in the amplifier, changing the pump-seed overlap, and thus dramatically reducing the energy extraction from the rod. The thermal lens changes as a function of pump power, which can also lead to a changing position for an intermediate focus within the ring amplifier as the pump power is increased. By placing a negative (-300 mm focal length) lens at the back surface of the Ti:sapphire crystal, the thermal lensing can be corrected.

The output pulse energy from the second stage of amplification is 4.0 mJ, giving an extraction efficiency of 23%. This value is close to our theoretically predicted value of 30% - the discrepancy arising from inexact thermal lens compensation at the present time. Further work is in progress to correct this. Residual forth order dispersion in our amplifier is compensated by a pair of SF18 glass prisms, which are placed directly after the stretcher, [5] giving us a fifth order limited pulse. We fully characterize our output in amplitude and phase using the new technique of transient grating frequency resolved optical gating (TG-FROG). This technique has allowed us to remove several non-optimum optics from our amplifier chain, and obtain very high quality output pulses. Figure 2 is a direct measurement of the intensity profile of our output. The energy after compression is 2.5 mJ, with a 20 fs pulse duration, to give a 0.125 TW peak power output pulse. We hope in the near future to reach output energies of 7 mJ after compression, which would correspond to a peak power of 0.350 TW.

References

1.S. Backus, J. Peatross, C. P. Huang, M. M. Murnane, H. C. Kapteyn, "Amplification of 20 fs, kHz pulses to the millijoule level," Opt. Lett. **20**, 2000 (1995).

2.J. Zhou, J. Peatross, M. Murnane, H. Kapteyn, I.P Christov, "Enhanced High Harmonic Generation using 25 Fs Laser Pulses," Phys. Rev. Lett **76**, 752 (1996).

3.I. P. Christov, J. P. Zhou, J. Peatross, A. Rundquist, M. M. Murnane, H. C. Kapteyn, "Non-Adiabatic Effects in High Harmonic Generation with Ultrashort Pulses," Phys. Rev. Letter **77**, 1743 (1996).

4.S. Backus, J. Peatross, M. Murnane, H. Kapteyn, "16 fs ultraviolet pulse generation in air: 1 μJ pulses at 257nm at 1 kHz," Opt. Lett. **21**, 665 (1996).

5.J. P. Zhou, C. P. Huang, C. Shi, H. C. Kapteyn, M. M. Murnane, "Generation of 21 fs millijoule-energy pulses by use of Ti:sapphire," Opt. Lett. **19**, 126 (1994).

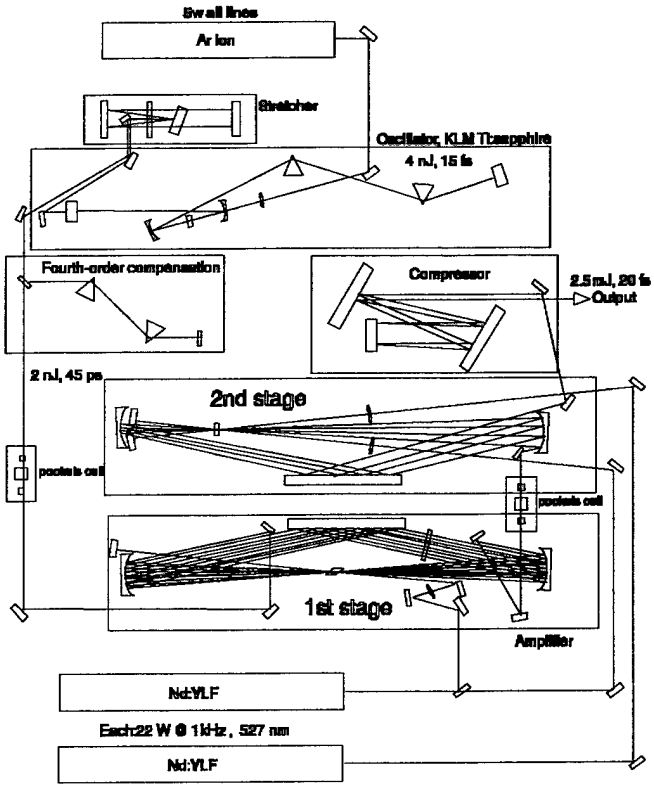

Figure 1: TW level, kilohertz repetition rate Ti:sapphire laser system capable of delivering 2.5 mJ in 20 fs, or a peak power of 0.125 TW.

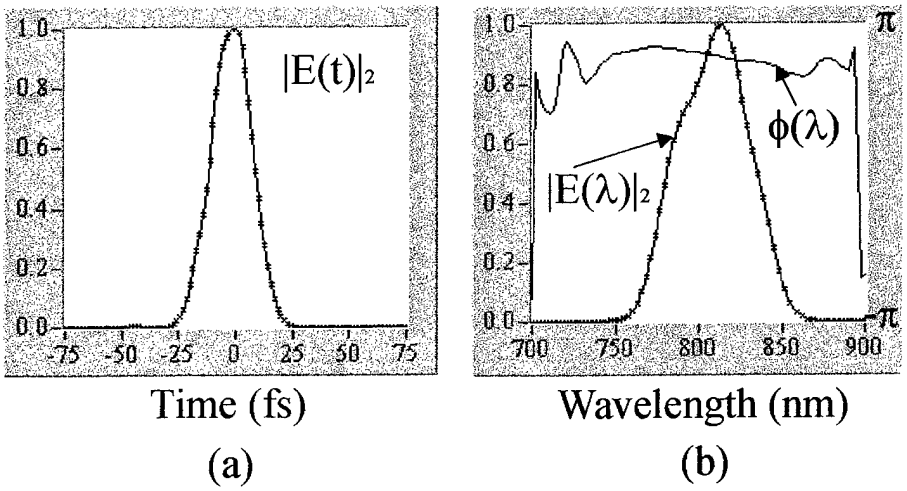

Figure 2: 20 fs compressed pulse output from the laser system, measured using transient grating FROG: (a) Pulse intensity profile, (b) spectrum and phase of the pulse.

X-Ray Magneto-Optical Kerr Effect and Its Applications

Chi-Chang Kao

National Synchrotron Light Source

Brookhaven National Laboratory

Upton, New York 11973

Tel: 516-344-4494

Fax: 516-344-3238

E-Mail: kao@BNL.GOV

It is well-known that the origin of the magneto-optical Kerr effect (MOKE) is spin-orbit coupling of electrons. The effect is relatively small in the visible light region because of the weak spin-orbit coupling of conduction electrons. On the other hand, the effect can be enhanced significantly in the x-ray region by tuning the x-ray energy through some core electron absorption edges of the sample, since the spin-orbit coupling can be much stronger for these core-electrons.

As an example, recent results from a thin bcc Co film will be presented. In the Kerr effect measurement, specular reflectivity as a function of incident angle and photon energy was measured using both linearly polarized and circularly polarized x-ray. In the case of linearly polarized light, specular reflectivity was measured in the transverse configuration; while in the case of circularly polarized light, the measurement was carried out in the longitudinal configuration. In both cases very large changes in reflectivity, up to 40% in the linearly polarized case and 75% in the circularly polarized case, were observed near the Co L_{II} and L_{III} absorption edges upon reversal of the direction of the magnetic field (see figure).

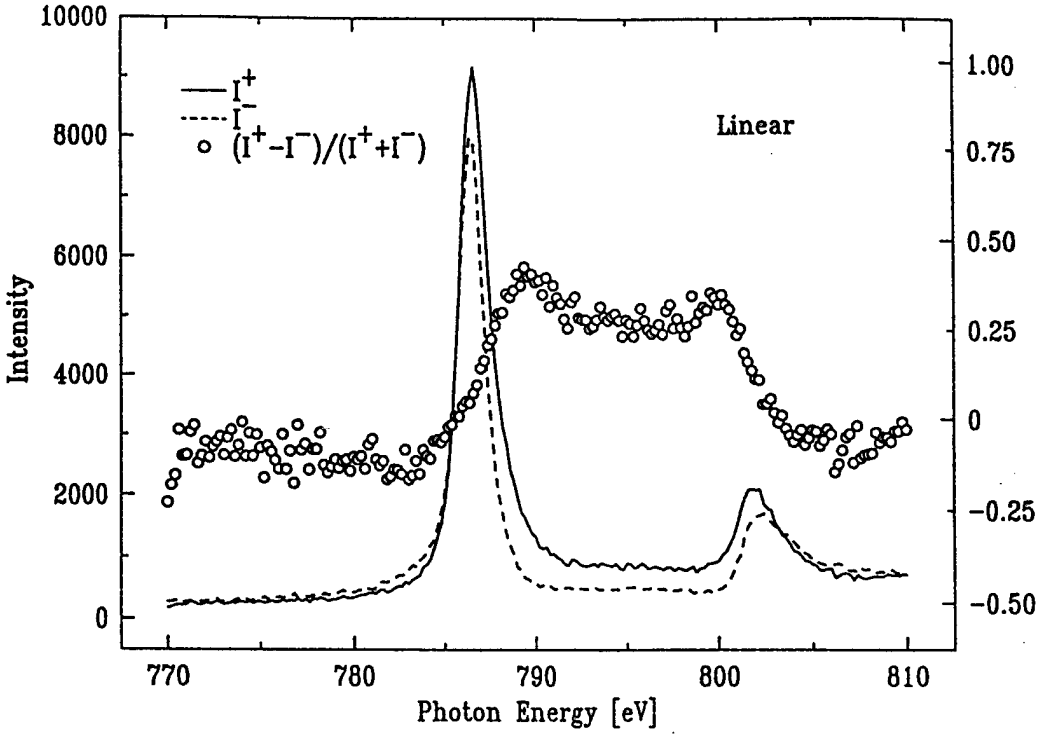
10000
8000
6000
4000
2000
0
Intensity
I^+
I^-
$(I^+-I^-)/(I^++I^-)$
Linear
1.00
0.75
0.50
0.25
0
−0.25
−0.50
770
780
790
800
810
Photon Energy [eV]

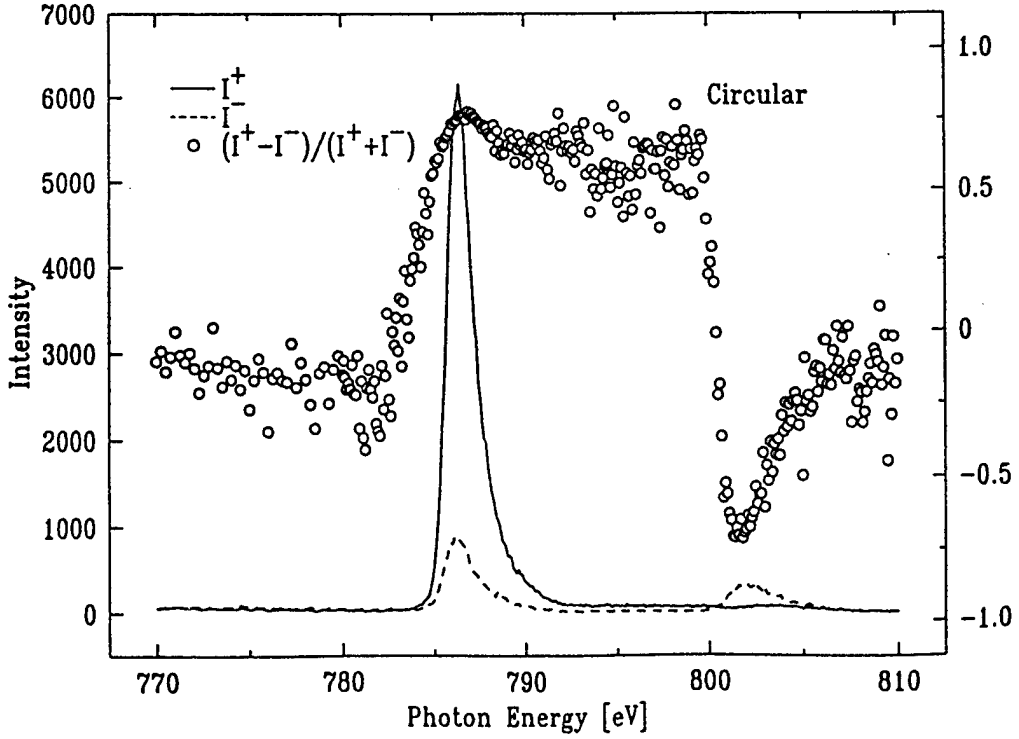
7000
6000
5000
4000
3000
2000
1000
0
Intensity
I^+
I^-
$(I^+-I^-)/(I^++I^-)$
Circular
1.0
0.5
0
−0.5
−1.0
770
780
790
800
810
Photon Energy [eV]

The large enhancement of the MOKE effect and the element-specific nature of core-electron excitations make x-ray MOKE an important new experimental technique in the study of magnetic thin films and multilayers. For example, it has been used to measure magnetization density profile of magnetic thin films, element-specific hysteresis loop of heteromagnetic systems, and magnetic structure of magnetic multilayers. Recent examples will be given.

Barrier-Suppression Ionization of Complex Atoms and Diatomic Molecules

V.P. Krainov
Moscow Institute of Physics and Technology,
141700 Dolgoprudny, Moscow Region, Russia
tel.: 7-095-911-1191; fax: 7-095-408-6336; e-mail: krainov@theory.mipt.su

Theory of tunneling ionization of atoms and atomic ions by strong low-frequency laser radiation was developed in Ref.[1] (so called ADK-approach). This theory is based on the conception of the quasi-stationary electromagnetoc field producing tunneling ejection of valence electrons. A complex atom or an atomic ion is considered in the frames of quantum defect method; its wave function is an asymptotic wave function at the large distances from the atomic core. In Ref.[2] the angular and energy distributions of ejected electrons in tunneling ionization were obtained.

The above results are valid for tunneling ionization when the field strength of laser radiation is small compared to the barrier-suppression field strength [3]. The generalization of this approach to barrier-suppression ionization has been made in Ref.[4] for ground state of hydrogen atom perturbed by circularly polarized laser radiation.

The goal of this talk is to generalize the theory to the case of arbitrary complex atoms, atomic ions and diatomic molecular ions, and to obtain simple analytical formulas for energy and angular distributions of the ejected electrons in the barrier-suppression ionization. Of course, the obtained expressions coincide with the results of ADK approach in the limit of a weak low-frequency radiation. In order to obtain correct pre-exponential factors in the transition amplitude, the Coulomb correction [5] for the Volkov wave function of the final continuum state is taken into account, using the semi-classical perturbation theory.

Everywhere we use the atomic system of units: $e = \hbar = m_e = 1$. In the case of circularly polarized radiation we obtain the next expression for barrier-suppression ionization rate of an atomic system with the charge of the atomic core Z and energy of the bound state $E_n = -Z^2 / 2n^2$ (here n is the effective principal quantum number) by low-frequency laser radiation with the field strength amplitude F:

$$w_{BSI} = \frac{Z(2F)^{1/3} D^2}{2n^2} \left\{ Ai'^2(k) - kAi^2(k) \right\}, \qquad (1)$$

where $Ai(...)$ is Airy function, and the notations are introduced

$$k = \frac{Z^2}{n^2(2F)^{2/3}}; \qquad D = \left(\frac{4eZ^3}{Fn^4}\right)^n. \tag{2}$$

This result is valid for initial *s*-state. It reduces to ADK expression with correct pre-exponential factor in the limit of a weak field $F << Z^3 / n^4$. The ionization rate of *p*-state is 3 times larger than of *s*-state. Details of tunnel ionization can be found in the book [6] while details of barrier-suppresion ionization are described in review paper [7] .

In the case of linear polarization of the radiation we obtain more cumbersome expression for the barrier-suppression ionization rate:

$$w_{BSI} = \frac{4\sqrt{3}FD^2}{\pi n(2F)^{1/3}} \int_0^\infty Ai^2\left(k + x^2\right)x^2 dx. \tag{3}$$

In the limiting case of tunneling ionization it reduces to ADK result as it should be.

The ratio of barrier-suppression ionization rate by ADK-rate is shown in Fig.1.

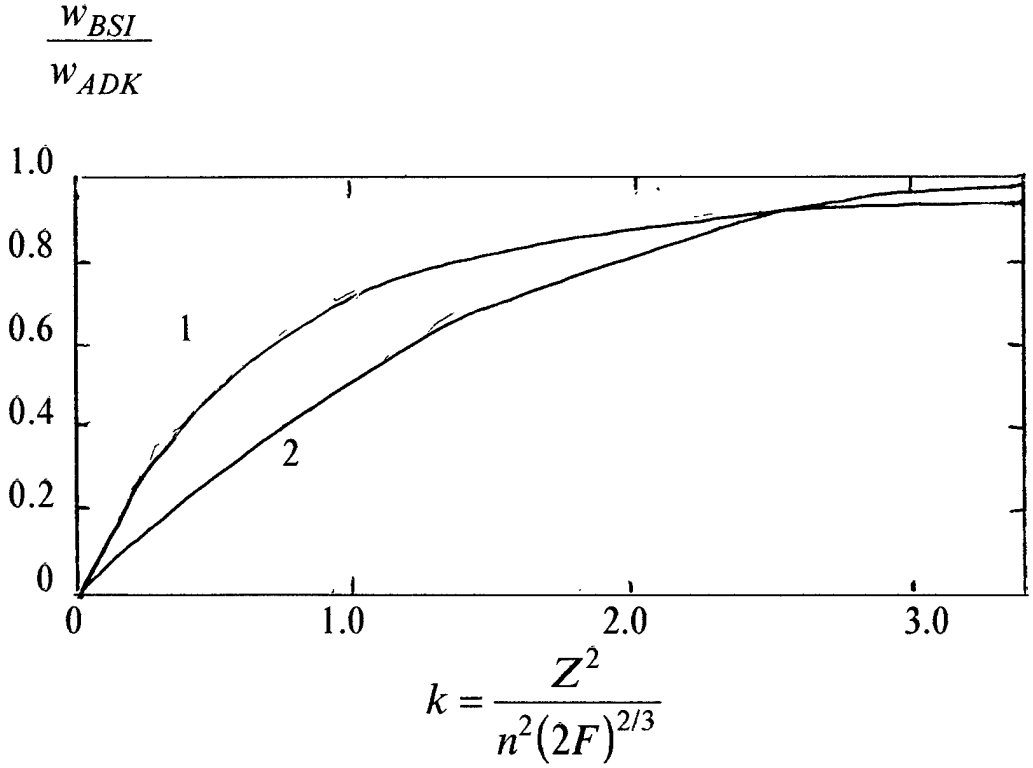

Fig.1.

The curve 1 is corresponding to circular polarization, the curve 2 - to linear polarization. Tunneling limit is corresponding to the case of $k >> 1$.

It is seen that BSI-ionization rate is less than the extrapolation of ADK expressions for the region of BSI-fields.

Now we consider the resonance tunneling in diatomic molecular ions. It takes place when the energy of lower state in one potential well is

approximately equal to the energy of higher state in the other potential well. The picture of resonance tunneling ionization of a diatomic molecular ion is shown in Fig.2.

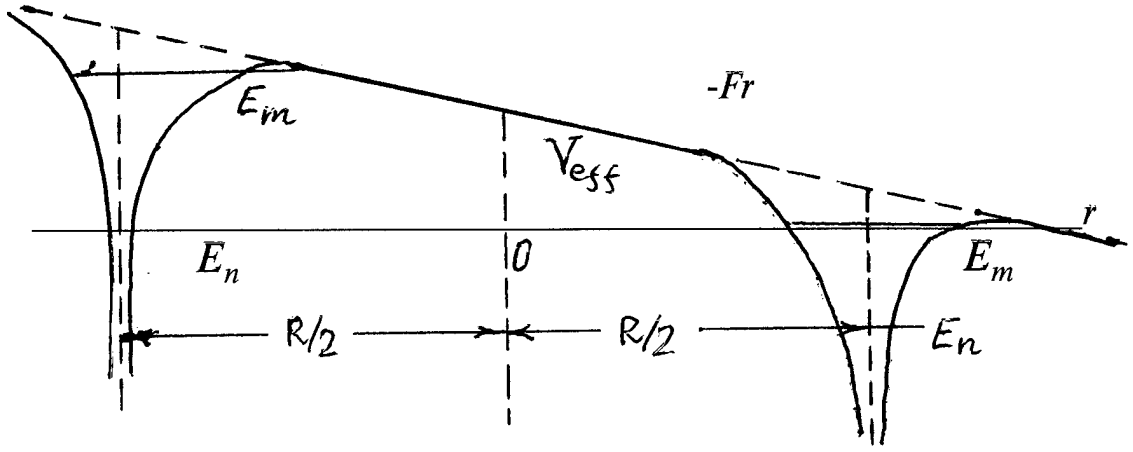

Fig.2.

The ionization rate of resonance tunneling for diatomic molecular ion is

$$w_{res} = \frac{FD^2}{4\pi Z}\left\{1+4\sin^2\left[\frac{\pi m^3}{2}\left(\frac{1}{n^2}-\frac{1}{m^2}\right)\right]\cdot\exp\left[\frac{2Z^3}{3F}\left(\frac{1}{n^3}+\frac{1}{m^3}\right)\right]\right\}^{-1} \quad (4)$$

The maximum rate in exact resonance does not contain any exponentially small terms:

$$w_{res}^{\max} = \frac{FD^2}{4\pi Z}. \quad (5)$$

References

1. Ammosov M V, Delone N B and Krainov V P 1986 *Sov. Phys. - JETP* **64** 1191-1194
2. Corkum P B, Burnett N H and Brunel F 1989 *Phys. Rev. Lett.* **62**, 1259-1262
3. Augst S, Meyerhofer D, Strickland D and Chin S L 1991 *J. Opt. Soc. Am. B* **8** 858-867
4. Krainov V P and Shokri B 1995 *Sov. Phys. - JETP* **80** 657-661
5. Reiss H R 1992 *Progr. Quantum Electr.* **16** 1-72
6. Delone N B and Krainov V P 1994 *Multiphoton Processes in Atoms* (Berlin: Springer)
7. Krainov V P 1995 *J. Nonlinear Opt. Phys. and Materials* **4** 775-798

PRECISION TESTS OF LASER-TUNNELING IONIZATION MODELS

B. Buerke[a], J. P. Knauer, S. J. McNaught[a], and D. D. Meyerhofer[a,b]

Laboratory for Laser Energetics
University of Rochester
250 E. River Rd.,
Rochester, NY 14623.

[a] also Dept. of Physics and Astronomy
[b] also Dept. of Mechanical Engineering

We have used a 1.5 ps, 1 μm laser with intensities up to 10^{18} W/cm^2 and two electron spectrometers to test laser-ionization models in the tunneling regime.

We have used circularly polarized light to ionize hydrogenic helium and have measured both the ion yield and electron energy distribution. The electron energy distribution is measured with a retarding potential spectrometer. A fully relativistic Monte Carlo simulation shows that while traversing the focus the electrons pick up 96% of the available energy ($2U_p$) at ionization. This intensity-to-energy calibration permits precise tests of tunneling theories.[1] A quasi-classical tunneling theory[4] predicts a peak energy lower than the observed peak. We compare the electron energy distribution to a variety of ionization models to elucidate the validity of quasi-classical models in the ionization of hydrogenic helium.

We have used a magnetic spectrometer[5] to measure the electron energy distribution during ionization with elliptically and linearly polarized laser light and to infer the initial condition of electrons injected into the field by tunneling ionziation. In strong laser fields, the ionization of atoms can be described quasi-classically. In an a.c tunneling model of ionization with linear polarization,[4] the electrons are ionized near the peak field of the optical cycle, with an optical phase width around the peak. The initial phase distribution with respect to the optical cycle determines the electron's initial condition. The angular distribution of high energy electrons in the plane of polarization has an asymmetry which is a function of this initial condition. We have measured the asymmetry in the angular distribution (in the plane of polarization) of electrons produced during the ionization of Neon leading to the Ne^{6+} - Ne^{8+} charge states. We find that the electrons must be born with a phase-spread of ~0.53 rad (FWHM) around the peak field of the optical cycle to explain the observed ~2:1 asymmetry in electron number. The phase spread is consistent with that predicted for a.c. tunneling models.[4, 6] This is an important confirmation of the quasi-classical models used to explain high-order harmonic generation.[7]

This work is supported by the National Science Foundation.Additional support was provided by the U.S. Department of Energy Office of Inertial Confinement Fusion under Cooperative Agreement No. DE-FC03-92SF19460, the University of Rochester, and the New York State Energy Research and Development Authority. The support of DOE does not constitute an endorsement by DOE of the views expressed in this article.

References

1. P.H. Bucksbaum, L.D. Van Woerkom, R.R. Freeman, and D.W. Schumacher, Phys. Rev. A **41**, 4119-4122 (1990).

2. S. Augst, D. D. Meyerhofer, D. Strickland, and S. L. Chin, J. Opt. Soc. Am. B **8**, 858-867 (1991).

3. L.V. Keldysh, Sov. Phys. JETP **20**, 1307 (1965).

4. A.M. Perelomov, V.S. Popov, and M.V. Terent'ev, Sov. Phys. JEPT **23**, 924-934 (1966).

5. C.I. Moore, "Observation of the transition from Thomson to Compton scattering in optical multiphoton interactions with electrons," PhD thesis, University of Rochester (1995).

6. M. V. Ammosov, N. B. Delone, and V. P. Krainov, Sov. Phys. JETP **64**, 1191 (1986).

7. P.B. Corkum, Phys. Rev. Lett. **71**, 1994-1997 (1993).

Tunneling ionization of molecules

B.A.Zon

394693, Russia, Voronezh University; e-mail: zon@niif.vucnit.voronezh.su

The Ammosov–Delone–Krainov theory (ADK, [1]) is a wide-spread theory for describing the tunneling ionization of atoms in high light field. It is an important detail of this theory that the ionization probability is determined not only by the exponential factor, but also by the pre-exponential factor which depends upon the electron orbital momentum and magnetic quantum number.

An application of this theory to the case of molecular tunnel ionization is rather complicated. This fact is due to that the valence electron in a molecule has no determined values of orbital and magnetic quantum numbers. Moreover, the explicit dependence upon the angular variables is difficult to display from the molecular wavefunctions constructed by methods of quantum chemistry. In this regard, the simplest molecules of H_2^+ type provide an exception.

There are two cases in molecular theory when the dependence of the electron wavefunction upon the angular variables is determined in rather general form. They correspond to the electron motion in the field of several δ-potentials [2] and in the field of Coulomb+point dipole potential [3]. In the present work, a theory of tunneling ionization is developed for the second case; this theory, strictly speaking, is applicable to the Rydberg electrons in polar molecules. In this case, apart from the Coulomb potential of the molecular core, its dipole moment is taken in account exactly.

For d. c. electric field we use Smirnov–Chibisov method [4], moreover, we show the connection of this method with the R-matrix theory, which has been extensively used recently for describing the interaction of atoms with powerful laser radiation [5]. The approach to the a. c. field is implemented using the technique proposed in Ref. [6]. To find the asymptotic constant of the electron wavefunction in quantum defect approximation, we used the results of Ref. [7].

References

[1] M. V. Ammosov, N. B. Delone, V. P. Krainov, *Zh.Eksp.Teor.Fiz.* **91**, 2008 (1986) [*Sov.Phys. JETP* **64**, 1191 (1968)].

[2] R. Subramanyan, *JETP* **55**, 363 (1968); Ju. N. Demkov, V. S. Rudakov, *JETP* **59**, 2035 (1970); G. F. Drukarev, *Electron Collisions with atoms and molecules* Moscow, Nauka, 1978.

[3] B. A. Zon, *Zh. Eksp. Teor. Fiz.* **102**, 36 (1992) [*Sov.Phys. JETP* **75**, 19 (1992)]; J. K. G. Watson, *Mol.Phys.* 81,227,1994.

[4] B. M. Smirnov, M. I. Chibisov, *Zh. Eksp. Teor. Fiz.* **49**, 841 (1965).

[5] C. J. Joachain, Report on The 7th International Comference on Multiphoton processes (ICOMP VII) 30 Sept. – 4 Oct., 1996, Garmish-Partenkirchen, Germany.

[6] A. M. Perelomov, V. S. Popov, M. V. Terent'ev *Zh. Eksp. Teor. Fiz.* **50**, 1397 (1965).

[7] B. A. Zon, V. E. Chernov, *J.Phys.B* **29**, 4161 (1996).

Spectral Structure in High Harmonic Emission

Hai-Wen Wang, Zenghu Chang, Andy Rundquist, Henry Kapteyn, Margaret Murnane
Center for Ultrafast Optical Science
University of Michigan
Phone: 313-763-0573; Fax: 313-763-4876; E-mail: kapteyn@eecs.umich.edu

Ivan P. Christov
Department of Physics, Sofia University
1126 Sofia, Bulgaria

There has been considerable effort, both experimentally and theoretically, devoted to understanding the process of high harmonic generation. Much of this effort has been focused on understanding the existence of the plateau region, and the position of the cutoff. More recently, theoretical work has attempted to predict the spectral structure of the harmonic peaks, in order to better understand the mechanism of high harmonic generation. In this work, we present data from the first detailed experimental study of the fine spectral structure of high harmonic emission. We studied the harmonic lineshapes as a function of pressure, density and chirp, using 25 fs laser excitation pulses. We observed dramatic changes in the spectral shapes of the harmonic peaks as these experimental parameters were changed.

There are many difficulties preventing the observation of fine structure in the harmonic peaks. One major difficulty is that the laser energy can fluctuate from shot to shot, which washes out the fine structures if we average the data, because the spectral (blue) shift of the high harmonics is very sensitive to the pulse energy. In our work, we used a high-resolution x-ray spectrometer (Hettrick Scientific) to observe the harmonic emission. The spectrometer has a flat-field output, and allows us to record a single-shot spectrum of the high harmonic emission, as shown in Figure 1. An imaging microchannel plate (MCP) x-ray detector is used to record the data, which is coupled to a phosphor screen and a CCD camera easy readout.

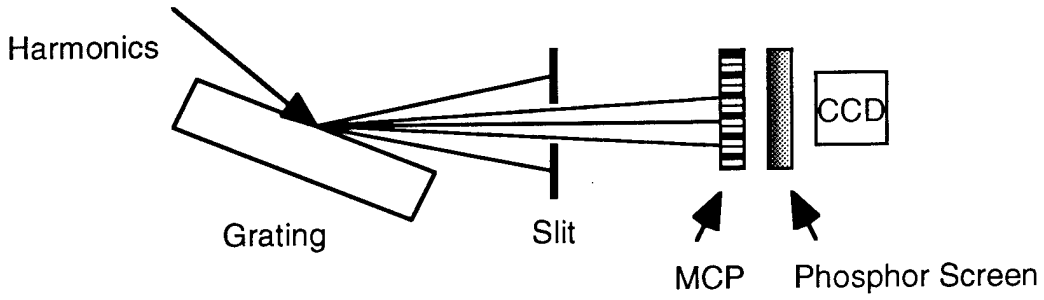

Figure 1: Experimental setup for single-shot spectrum recording.

We use a 26 fs, 10 Hz repetition rate, Ti:Sapphire laser in our experiments.[1] The laser beam is focused onto an argon gas jet, produced by a piezo-electrically driven gas nozzle. The spectrum of each individual harmonic is both blue-shifted and broadened when the laser energy is increased, to such an extent that the spectra of adjacent harmonics eventually merge and form a continuum spanning the soft-x-ray region. The

blue-shifting and broadening of the 25th harmonic of argon (the right-hand-side peak is shown in Figure 2). The peak on the right is the 24th harmonic. Both sides of the spectrum are artificially cut off by the exit slit.

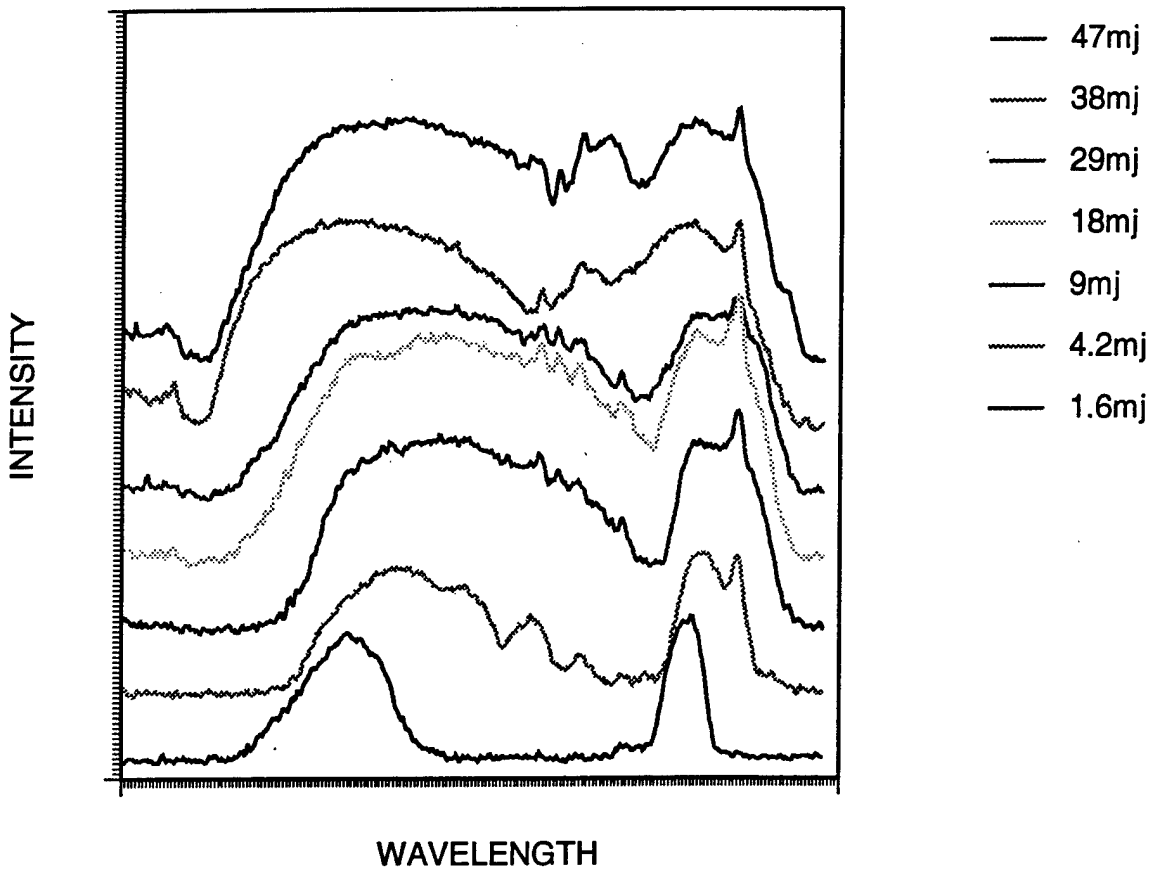

Figure 2: Spectral broadening and blue-shifting of the 25th harmonic in argon.

We also found that there are several smaller peaks on the blue (short wavelength) side of each individual harmonic in the mid-plateau region. The side peaks of the 29th harmonic of argon are shown in Figure 3. The left peak is part of the 31st harmonic, which is artificially cut off by the exit slit. To determine if this fine structure is a single-atom effect, we varied the gas pressure, and observed that the shape was insensitive to decreases in pressure down to < 10 torr.

Using a 3-D quantum mechanical model, we found that the mid-plateau harmonics generated by a very short (sub-100 fs) laser pulse, would be expected to display significant spectral structure. These effects may be due to symmetry-breaking by the ultrafast 25 fs rising edge of our excitation pulses. Other theoretical work has demonstrated[2] that the mid-plateau harmonics should display fine structure as a result of the two possible trajectories that a given energy electron may have, and as a result of secondary re-encounters of the electron with the ion. It is worth noting that none of the above theories exactly match our experimental data. However, our new results may lead to further refining of the theories of high harmonic emission.

1. J. P. Zhou, C. P. Huang, M. M. Murnane, H. C. Kapteyn, Opt. Lett. **20**, 64 (1995).
2. C. Kan et al., Phys. Rev. A **52**, R4336 (1995).

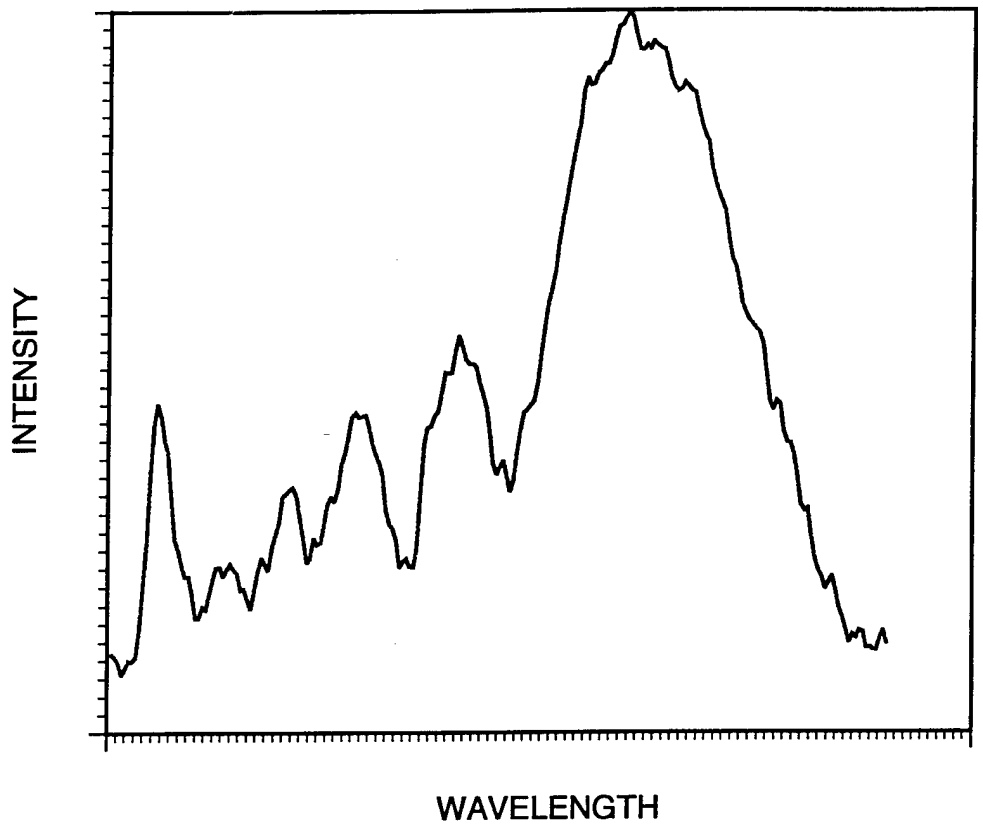

Figure 3: Fine structure of the 29th harmonic generated in argon. The left peak is part of the 31st harmonic, which is artificially cut off by the exit slit.

Enhanced harmonic generation using pulse shaping

Andy Rundquist, Erik Zeek, Haiwen Wang, Zenghu Chang, Margaret Murnane
and Henry Kapteyn
Center for Ultrafast Optical Science, University of Michigan, Ann Arbor, MI 48109-2099
Phone: (313) 763-0573; FAX: (313) 763-4876; E-mail: kapteyn@umich.edu

Ivan Christov
Department of Physics, Sofia University, 1126 Sofia, Bulgaria

Harmonic generation from ultrafast, ultra-intense lasers has proven to be an excellent source of coherent radiation in the soft x-ray regime.[1,2] Our recent work[3,4] has shown that very short driving pulses can generate broad bandwidth harmonic peaks, which are tunable, and with a cut-off at wavelengths substantially shorter than harmonics produced with longer duration pulses. In this work, we show how shaping the amplitude and phase of our laser pulses, to ensure faster risetimes and and optimal shapes, can enhance the efficiency of harmonic generation, as well as extend the plateau to even shorter wavelengths. We employ novel shaping techniques, using birefringent filters, and spectral shaping elements, to produce these effects.

Analytically, it is easy to understand how a birefringent material for example can shape a pulse. Consider the initial field in time to be given by -

$$\vec{E}_{initial}(t) = A(t)e^{i\omega_0 t}\hat{x}$$

Consider the birefringent material to be a multiple order wave plate oriented with the slow axis at an angle θ with respect to the x axis.If n is the order of the wave plate, the fields at the output of the wave plate are given by -

$$\vec{E}'_o(t) = A(t)e^{i\omega_0 t}(\hat{x}\cos\theta + \hat{y}\sin\theta)$$

and

$$\vec{E}'_e(t) = A(t + \tfrac{n\pi}{\omega_0})e^{in\pi}e^{i\omega_0 t}(\hat{x}\sin\theta - \hat{y}\cos\theta)$$

After passing through the final polarizer which is oriented along the x axis, the final field is given by -

$$\vec{E}_{final}(t) = \left[A(t)\cos\theta - A(t + \tfrac{n\pi}{\omega_0})\sin\theta\right]e^{i\omega_0 t}\hat{x}$$

For small n, corresponding to time separations much smaller than the pulse duration, almost all of the energy is sacrificed; this is especially true for zero order half wave plates (n=1). When θ is 45 degrees, the two waves have the same amplitude and the output is a symmetric double pulse with the second pulse having a much faster rise time than either pulse alone (see Figure 1a). In laboratory experiments, we have already shown that faster risetimes enhance both the efficiency of harmonic production as well as extend the plateau. Thus, producing faster risetimes is very desirable (see Figure 2). However, the very large prepulse in the case of θ = 45 will pre-ionize the atoms, so that harmonic generation will only occur during the first pulse. The rise time of the prepulse is very close to that for either pulse alone, so there would be no gain in harmonic efficiency or quantity for this case. We wish to produce a shaped pulse which has a modest prepulse, does not lose too much energy, and has a faster rise time and shorter duration than the original pulse. By adjusting θ we can depress the prepulse and compromise by increasing the rise time. In Figure 1 we

plot the final field intensity envelope for several combinations of n and θ, where we take A(t) to be a gaussian envelope with a FWHM of 25 fs.

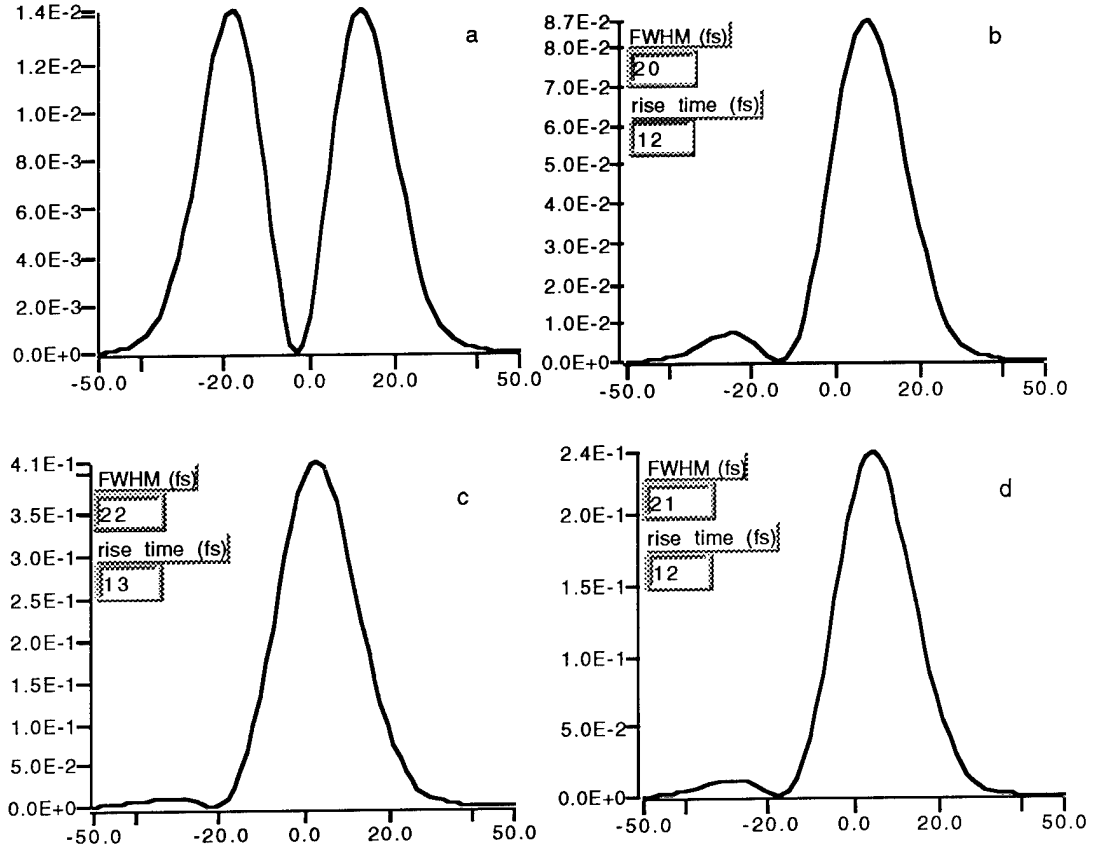

Figure 1. Birefringent shaping of a 25 fs gaussian pulse

The fastest risetimes are accompanied by the greatest energy loss, while the modest prepulse can always be obtained for a given n by adjusting θ. Figure (1a) shows the case for n = 5 and θ = 45deg, (1b) shows n = 7 θ = 40deg, (1c) shows n = 15 θ = 31deg, and (1d) shows n = 11 θ = 35deg, where the x axis is in femtoseconds and the y axis is normalized to the peak intensity of the original pulse. For n less than 11, the rise time is very short but the peak intensity is below 10% of the input. For values of n greater than 11, the peak intensity can approach 50% of the input, but the rise times approach that of the original pulse. For these reasons we have chosen n = 11 with θ = 35 degrees as the optimum settings. This combination gives an output with 25% of the input peak intensity, a 10% pre-pulse, a risetime of 12 fs, and a pulse duration of 21 fs.

Other methods of producing and using shaped pulses for enhanced x-ray generation will also be presented.

1. A. L'Huillier, P. Balcou, Phys. Rev. Lett. **70**, 774 (1993).
2. J. J. Macklin, J. D. Kmetec, C. L. Gordon III, Phys. Rev. Lett. **70**, 766 (1993).
3. J. Zhou, J. Peatross, M.M. Murnane, H.C. Kapteyn, I.P. Christov, Phys. Rev. Lett **76**, 752 (1996).
4. I. P. Christov, J. P. Zhou, J. Peatross, A. Rundquist, M. M. Murnane, H. C. Kapteyn, Phys. Rev. Letter **77**, 1743 (1996).

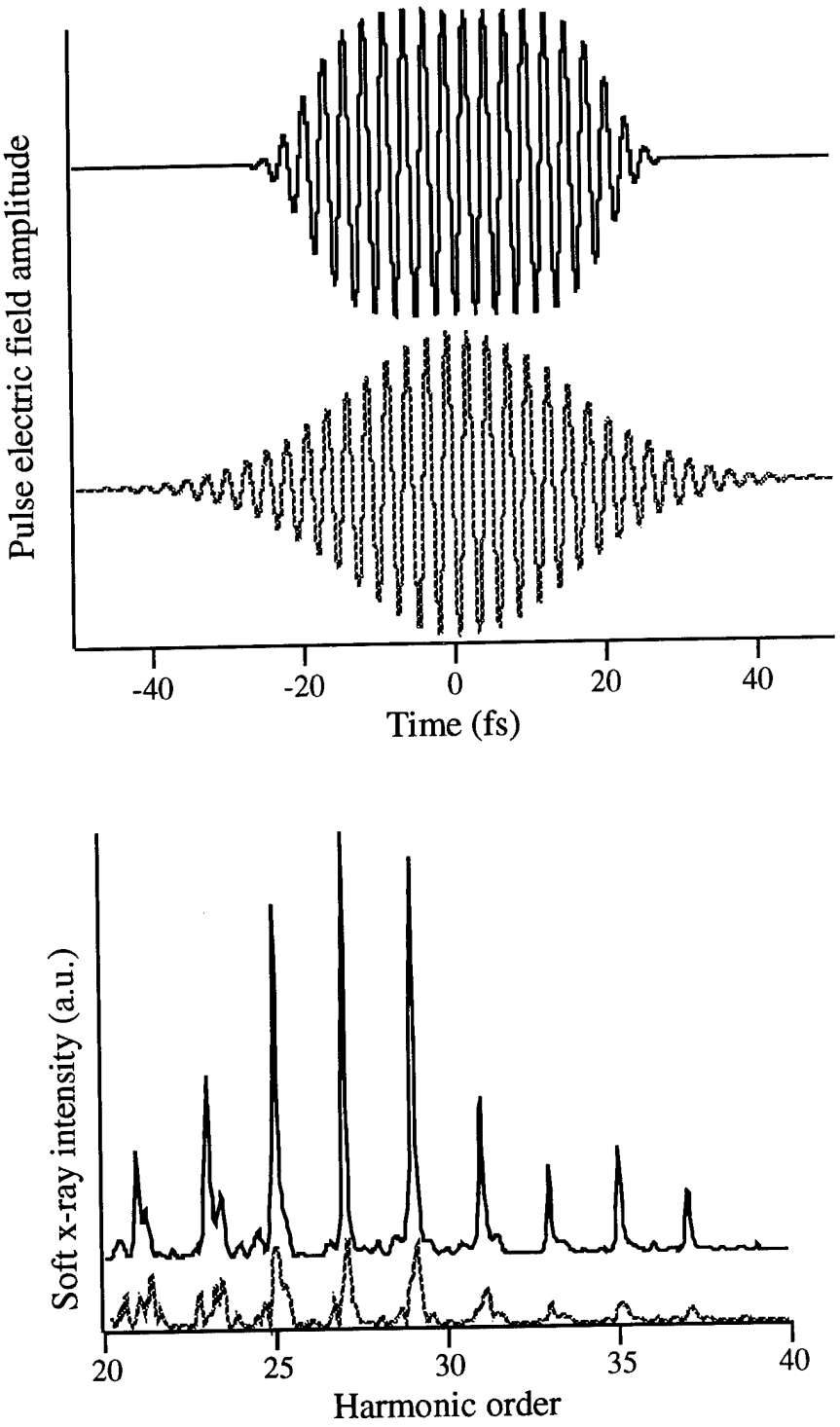

Figure 2: (Top) 20 fs Super-Gaussian and Gaussian pulse shapes for use in harmonic generation; (Bottom) Harmonic emission corresponding to the two pulses above, illustrating that control of pulse shape can significantly increase the efficiency of high-harmonic generation.

Time-dependent Schrödinger equation for the interaction between a laser pulse and a one-dimensional metal

P. Martin and G. Petite
Commissariat à l'Energie Atomique, DSM/DRECAM/SRSIM, CEN Saclay,
91191 Gif sur Yvette, France
e.mail : martin@santamaria.saclay.cea.fr
phone : (33) 0169084374

As well known, solving the time-dependent Schrödinger equation allows an accurate non pertubative description for the interaction between an intense optical field and an electron in a potential [1].

In this work, we apply this method to the case of a linear chain of atoms which mimics the periodic potential « seen » by a test electron in a quasi-free electron metal. This « crystal » potential is built as a series of screened coulombic potentials. Outside the « crystal », the potential is constant and adjusted in order to reproduce the work function of the metal considered. After diagonalization we obtain well known band structures with characteristic gaps at the end of each one dimensional Brillouin zones (figure 1). For eigenstates below the vacuum level, we obtain typical Bloch functions extending in the whole « crystal ». Above the vacuum level, we find, as normal, that, the electron has a larger probability to be outside the « crystal ».

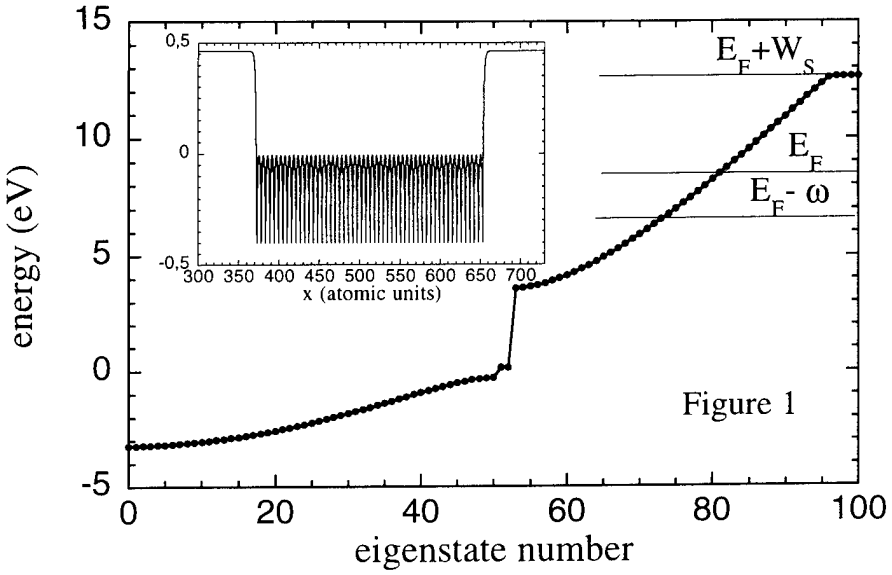

Fig1 : Eigenvalues corresponding to the potential in the inset.. E_f : Fermi level location, Ws : vacuum level, ω : photon energy

The laser is supposed to impinge on the chain at grazing incidence and the electric field is parallel to the chain. The electric field is, in the case of metallic reflection, space dependent : constant in vacuum and damped on a length taken equal to the skin depth inside the chain. In this framework, the notion of « surface » appears naturally because the laser irradiates only one side of the chain. This has some important consequences especially on the harmonic spectra because, despite of fact that we are dealing with a fully centro-symetric static potential, the electric field introduces a non symmetric

component in the (time-dependent) wave-function, allowing for the observation of odd and even harmonics. As well known, this is not the case in atoms.

In order to simulate the interaction properly, we must take into account the fact that only the eigenstates between the Fermi level and the Fermi level minus the energy of the photon must be propagated. In that case, only transitions between unoccupied states take place and this accounts for the Pauli exclusion principle. On the other hand, because we adopt a one-electron potential model, we must sum the contributions from each level in an incoherent way for electron as well as harmonics spectra.

We present now a few examples of calculations which have been performed for 1.55 eV photons and 24 optical cycles. The width of the (trapezoidal) laser pulse is in that case of the order of 50 fs. The calculation is performed for a chain of 200 unit potentials which represents an improvement compared to the calculation of reference [2] (50 atoms and 16 optical cycles). Below the vacuum level, the spacing between two successive levels is inversely proportional to the number of atoms included in the calculation. Around the Fermi level, this spacing is of the order of 50 meV. This is, of course, considerably larger than for a real metal, but, considering the energy broadening of the laser pulse, this is enough to consider that each transition presents a quasi-resonant character. Under these conditions, we propagate up to 26 eigenstates. The skin depth is for Aluminum and for 1,55 eV photons, of the order of 100 atomic units.

We present in figure 2 (a,b), electron spectra for two laser intensities. For $I=1x10^{10}$ W/cm^2, we note that the width of the spectrum is less than the photon energy showing that only levels requiring a minimum number of photons (3 in our conditions) to overcome the 4.2 eV corresponding to the work function contribute to the photo-current. For $I=5x10^{11}$ W/cm^2, we note that the spectrum is « hotter » because it involves a small contribution from deeper states (4 photons needed to reach the vacuum for levels around Ef-ω) and a high energy contribution from Fermi electrons having absorbed 4 photons.

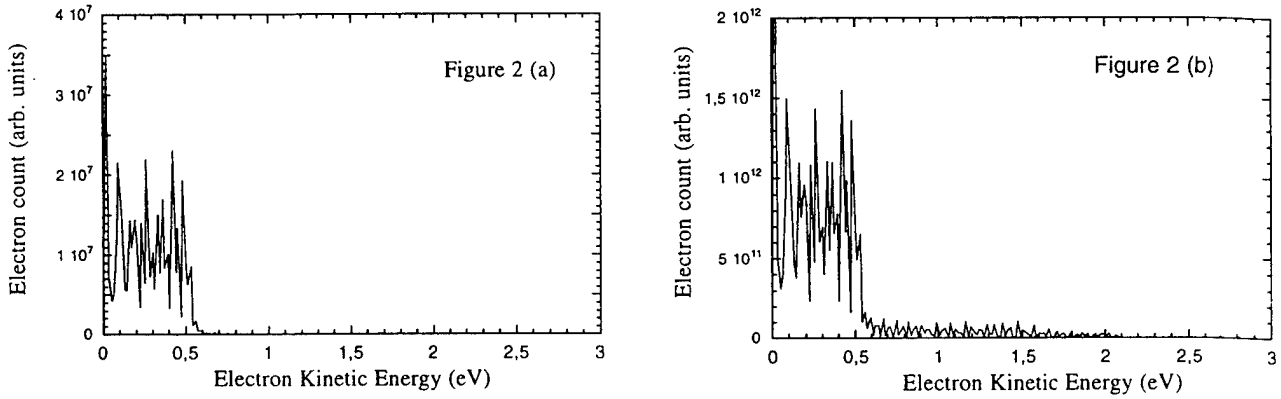

Figure 2 : electron spectra for For $I=1x10^{10}$ W/cm^2 and For $I=5x10^{11}$ W/cm^2

We present also, in figure 3 (a,b,c), the harmonic spectra obtained for three intensities.

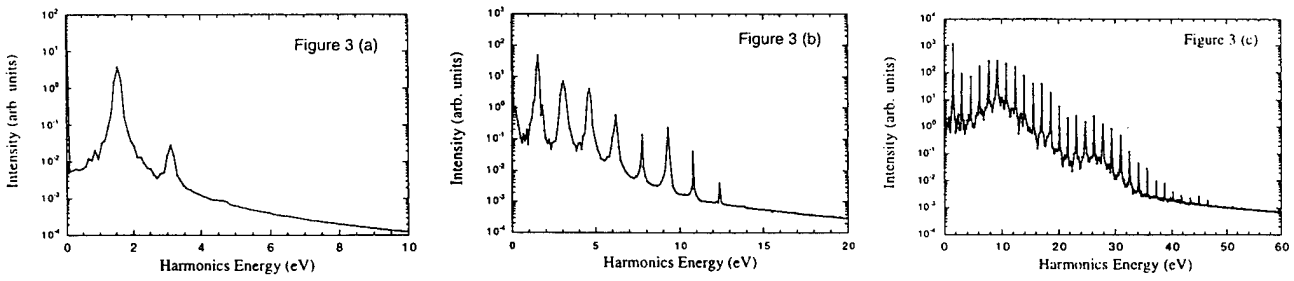

Figure 3 : harmonics spectra for For $I=1x10^{10}$ W/cm^2, $5x10^{11}$ W/cm^2 and $1x10^{13}$ W/cm^2

We observe well resolved harmonic spectra through the whole range of intensities explored. In particular, for $I=1x10^{13}$ W/cm^2, we note a « double plateau » structure which was already present in the 50 atoms calculation where the harmonic structure was barely visible.

Figure 4 shows the dependence of the total current on the laser intensity. Below, $I=1x10^{12}$ W/cm^2, the log-log plot shows a lowest order perturbative behavior, the slope being equal to 3. However, we observe a saturation of the current for higher intensities. This is due to two important and intricate points: the first one is that for such intensities, the initial population is depleted (we will come back to this point) and, the second is that we have reached the so-called Keldysh regime. The Keldysh parameter (ratio of the time necessary for an electron to tunnel trough the barrier over the half optical period) is equal to 0.2. This regime appears earlier than in an atom for two main reasons : the electron velocity around the Fermi energy (12 eV) is high and the work function (i.e. the analog of the ionization potential) is low (4.2 eV).

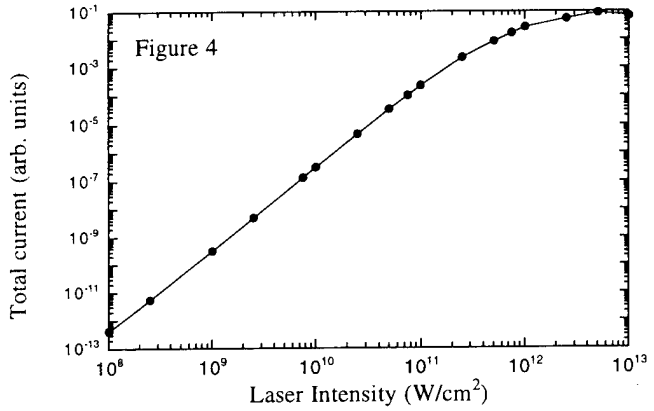

Figure 4 : Total ionization rate as a function of the laser intensity. The slope of the straight line is equal to 3.

The model presented above has the advantage of simplicity. However, many improvements are needed if we want to perform more accurate simulations of the interaction of a laser beam with a metal. Pragmatically, two of them can be added : in a metal, the life-time of an electron hole pair close to the Fermi level is in general very short compared to the laser pulse duration. That means that during all the interaction, the propagated levels are never depopulated. This is not the case here, especially in high intensity limit. This can strongly influence the conclusions on the « Keldysh regime ». On the other hand, the role of the lattice vibrations is very important because the associated phonons can supply momentum to the electron during transitions and thus probably increase the total photocurrent.

[1] Kulander K., Schafer K.and Krause L., *Atoms in Intense Laser Fields*, (Gavrila M. ed) Academic press, San Diego, 1992

[2] P. Martin, J.Phys.B : At. Mol. Opt. Phys, **29**, L635, 1996.

Determination of the Duration of UV Femtosecond Pulses.

J.-F. Ripoche, B. S. Prade, M. A. Franco, G. Grillon, R. Lange and A. Mysyrowicz

Laboratoire d'Optique Appliquée
ENSTA-École Polytechnique, Batterie de l'Yvette,
F-91761 Palaiseau, France
tel.: (33) 1.69.31.02.20; fax: same; e-mail: mysy@enstay.ensta.fr

The determination of the duration of visible or near-infrared optical pulses with subpicosecond duration has become a routine operation in ultrafast time-resolved spectroscopy. Several experimental methods have been demonstrated, which all rely on the same principle, transforming a time measurement requiring an ultrafast detector into a length measurement using a slow detector [1]. By far the most commonly used technique is the measurement of the sum frequency radiation which yields the autocorrelation of the pulse from which the pulse duration is extracted, assuming the pulse timeshape known. Recently, more sophisticated methods have been developed to obtain more precise knowledge of the pulse characteristics, such as its phase and amplitude [2-3]. However, to extend such measurements to the ultraviolet (UV) domain is a nontrivial task [4-5], for instance because of phase-matching or group velocity dispersion issues.

We present an approach based on the same general principles, which has the advantage that it can be easily implemented in the UV (and in principle in the far UV as well). It is based on spectral analysis following cross phase modulation. Since the non-linear process is described by a symmetric term of the third-order non-linear susceptibility tensor, it does not require frequency up-conversion nor any phase-matching conditions.

The principle of the method is shown in figure 1. The pulse to be analysed is divided in two parts: the pump beam containing most of the energy and a weak probe beam. After passing one of the beams through an optical delay, both beams are made to overlap in a common region of a non-linear sample. The sample consists of any transparent, centrosymmetric medium with instantaneous Kerr response, here a thin plate of fused silica.

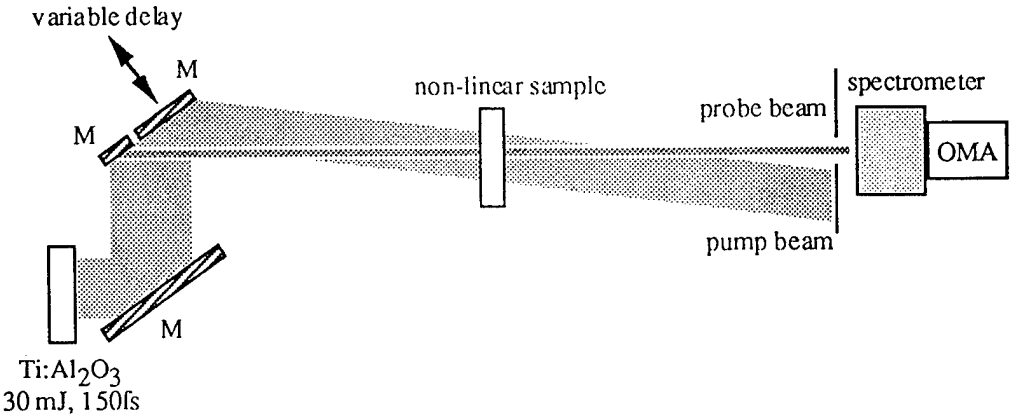

Figure 1: Principle of experimental set-up. M: mirrors.

The spectrum of the probe beam is then recorded in the presence of the pump beam as a function of time delay between pump and probe. The pump pulse induces a change of the probe spectrum, which is a sensitive function of the time delay during the pulse overlap. As we show now, by simply recording the change in the centre of gravity of the probe beam spectrum, the derivative of the autocorrelation function is directly obtained.

The centre of gravity of the probe spectrum is given by: $g(\tau) = \frac{\int \nu |F(\nu,\tau)|^2 d\nu}{\int |F(\nu,\tau)|^2 d\nu}$ (1), where τ is the delay between the pulses, ν is the frequency and $F(\nu,\tau)$ the Fourier transform of the probe beam complex electric field in the time domain. Noting that the denominator in (1) is the energy of the laser E and integrating by parts, one finds that $g(\tau)$-g_0 is proportional to the derivative of the autocorrelation function $A(\tau)$: $g(\tau) - g_0 = \frac{2\pi z n_2}{\lambda E} \frac{dA(\tau)}{d\tau}$ (2) where $g_0=g(\tau=0)$, λ is the laser central wavelength, n_2 the sample's non-linear index and z its thickness.

To test the method we have performed two experiments, the first with near IR and visible optical pulses already well characterised by other standard techniques, the second with UV pulses obtained by harmonic generation, for which the results could be compared to predictions since the pulse duration at the fundamental frequency was known.

We first used a Ti:sapphire oscillator-amplifier providing up to 30 mJ in about 150 femtoseconds at 800 nm and an amplified CPM dye laser working at 615 nm with an energy of 2 mJ per pulse and pulse durations as short as 80 femtoseconds. Experimental spectra in figure 2a (figure 2b) show very clearly that red (blue) components are added to the spectrum when the pump intensity increases (decreases) with time. The data were fitted to equation (2) using a Levenberg-Marquardt method. Assuming a pulse shape of the $(sech)^2$ form, we obtain a pulse duration t_{FWHM} (full width at half maximum) of 139 femtoseconds for the Ti:sapphire and 196 femtoseconds for the dye laser (showing significant residual chirp) in good agreement with a characterisation of the same lasers by autocorrelation via second-harmonic generation or via the ENSTA method [3].

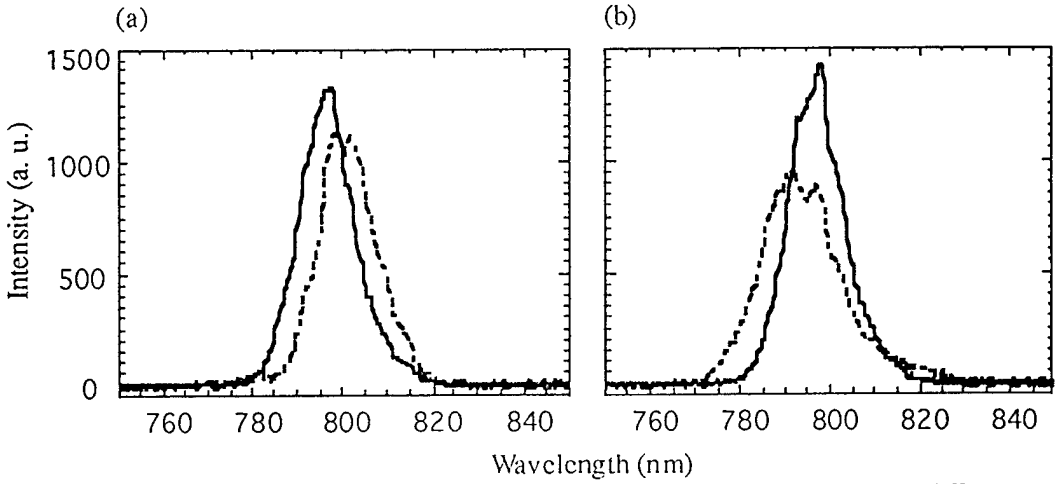

Figure 2: Experimental spectra of the probe beam from the Ti:sapphire chain at different time delays, without the pump beam (solid line) and in presence of the pump beam (dashed line). (a) τ=-100 fs. $g(\tau)$-g_0=3.9 nm. (b) τ=117 fs. $g(\tau)$-g_0=-3.0 nm.

For the second series of experiments, the same laser is used together with a KDP crystal (100 µm thickness) to generate harmonic pulses at 307 nm. An energy per pulse of 10 µJ was obtained in the UV. Figure 3 displays the shift of the centre of gravity of the probe spectrum as a function of time delay. Each point of the curve corresponds to an average over twenty shots within a predetermined window (±10%) of the pump and probe pulse energies. The obtained pulse duration (126 femtoseconds) is in good agreement with what is derived from the fundamental pulsewidth.

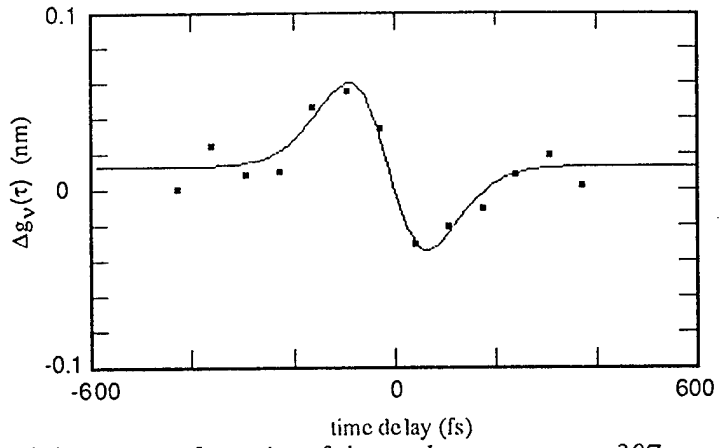

Figure 3: Change of the centre of gravity of the probe spectrum at 307 nm as a function of time delay between pump and probe in 3 mm of fused silica (Suprasil). The full line is a fit assuming an (sech)^2 pulse shape, the retrieved pulse duration is 126 femtoseconds.

One could extend this method further in the UV to vacuum-ultraviolet (VUV) domain by using, for example, a cell filled with gas (Xenon) as the non-linear sample. The lower non-linear index n_2 in gases, due to the lower density of the medium, can be compensated for, to some extent, by a long interaction length since the dispersion is small.

In conclusion, we have demonstrated a general method for measuring the derivative of the autocorrelation function of a femtosecond pulse which is valid from the near-infrared to the ultraviolet.

[1] E. P. Ippen and C. V. Shank, Ultrashort Light Pulses - Picosecond Techniques and Applications, S. L. Shapiro Eds. (Springer - Verlag, Berlin, 1977) 83.

[2] D. J. Kane and R. Trebino, IEEE. J. Quantum Electronics. 29 (1993) 571.

[3] B. S. Prade, J. M. Schins, E. T. J. Nibbering, M. A. Franco and A. Mysyrowicz, Opt. Comm. 113 (1994) 79.

[4] D. J. Kane, A. J. Taylor, R. Trebino and K. W. DeLong, Opt. Lett. 19 (1994) 1061.

[5] J. M. Schins, P. Breger, P. Agostini, R. C. Constantinescu, H. G. Muller, A. Bouhal, G. Grillon, A. Antonetti and A. Mysyrowicz, J. Opt. Soc. Am. B 13 (1996) 197.

INCREASED COHERENCE LENGTH IN HIGH ORDER HARMONIC GENERATION BY A SELF-GUIDED BEAM

H.R.Lange, A. Bouhal, J.-F. Ripoche, and A. Mysyrowicz
Laboratoire d'Optique Appliquée
ENSTA - Ecole Polytechnique - 91125 Palaiseau, FRANCE
P. Breger and P. Agostini
Service des Photons Atomes et Molécules
Centre d' Études de Saclay 91191 Gif sur Yvette FRANCE
lange@enstay.ensta.fr
phone: ++33-1-60.10.03.18 fax: ++33-1-60.10.60.85

High-order harmonics as a potential source of coherent XUV have resulted in extensive studies of this effect. One of the limitations to the efficiency of the generation process is the phase shift occurring at the focus of a gaussian beam (Goyd factor) [1]. This can be minimized by using long focal length and setting the atomic jet either before or after the focus. Self-guided beams are an attractive alternative to focused beams since they can, in principle, be made intense enough while their phase front remains flat in the high intensity region. This is because the curvatures of the wavefront due to diffraction and the Kerr effect compensate each other.

In this contribution we report on the generation of harmonics in Xenon up to the 15th order by a self-guided optical filament generated in air by 120 fs laser pulses of 0.9 mJ per pulse (in the filament).

The laser pulse from a Ti:Sapphire CPA laser is focused into air and leads to a self-guided beam of a diameter of about 300 μm [2]. A coupling efficiency of about 15% from the initial beam into the filament leads to intensities of about 10^{13} W/cm^{-2} in the filament. The harmonics are generated in a gas cell of variable length filled with Xenon at variable pressure and detected through photoionization of a target gas. The photoelectron are produced and analyzed in a magnetic bottle spectrometer [3].

The length of the cell has been varied from 5 to 20 mm and the xenon pressure from 1 10^{-2} to 5 10^{-1} bar while monotoring the harmonics spectrum. The observed cutoff is consistent with the maximum intensity in the filament (5 10^{13} W/cm^{-2}). In an estimation the number of generated photons for a cell length of 20 mm is increased by a factor of 10 with respect to the usual thickness in jets (1 mm) for optimized pressures of Xenon in both the lense and filament cases. For a given length, there is an optimum gas pressure. Fig. 1 shows a typical spectrum and the observed dependence on the cell length for a constant pressure. The observations are compared to the results of numerical simulations using propagation codes which solve the wave equations through a finite difference scheme: for the

self-guided beam we take into account diffraction, the Kerr effect and a simple ionisation model [4] while ionization is included in the harmonic generation code [5].

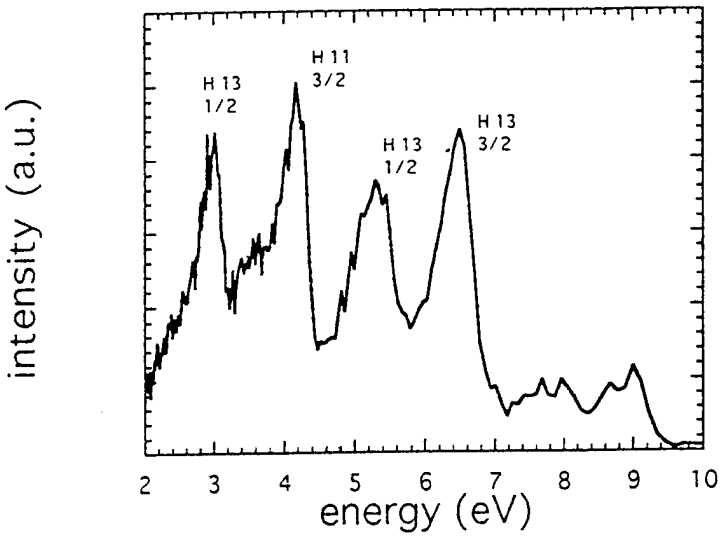

Fig. 1: Spectrum of Higher Harmonics Generated in Xenon

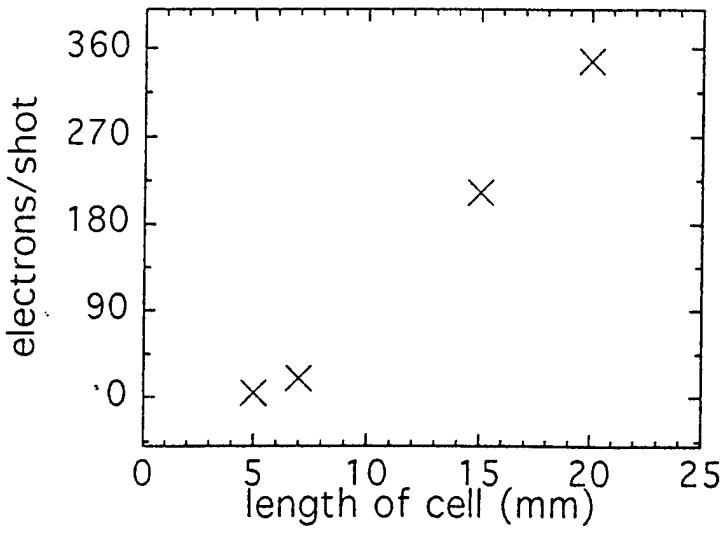

Fig. 2: Increase of electron numbers per shot as a function of the length of the Xenon gas cell

[1] A. L'Huillier et al.: Atoms in Intense Laser Fields, M. Gavrila ed. Academic Press(1992).
[2] A. Bouhal et al. JOSA B, submitted for publication
[3] Nibbering et al., Optics Letters, Vol 21, No 1, 63 (1996)
[4] A. Chiron et al., Solid-State Lasers For Application to Inertial Confinement Fusion, Paris, 22-25 October 1996, abstract book P73
[5] P. Salieres et al. , Physics Review Letters 75, 3776 (1995)

Spectral-Spatial Measurements of Fundamental and Third Harmonic Light Scattered from Ionizing Gas in the Focus of a 25fs Laser Pulse

J. Peatross
Dept. of Physics & Astronomy, 277 FB
Brigham Young University
Provo, UT 84602-4360
Phone: (801) 378-5043, FAX: (801) 378-2265
peat@byu.edu

S. Backus, J. Zhou, M. M. Murnane and H. C. Kapteyn
University of Michigan, Center for Ultrafast Optical Science
2200 Bonistell Blvd., Ann Arbor, MI 48109-2099
Phone: (313) 763-5574, Fax: (313) 763-4876
murnane@eecs.umich.edu

We recently reported[1] a ~0.1% efficiency for converting 800nm, 25fs laser pulses into the third harmonic at 267nm by simply focusing 1mJ pulses in air or in other gases such as argon. Most importantly, the UV pulses were measured to be very short in duration (~16fs). For our laser conditions, we found third harmonic conversion to be most efficient when focusing with a relatively loose geometry (f/30-f/40). During the interaction, a plasma is produced in the focus, and the laser beam undergoes blueshifting and spatial distortions as ionization of the gas takes place.[2-4] The goal of the present work is to gain insight into this complex interaction (i.e. propagation and distortion of the fundamental as well as the generation and propagation of third harmonic light) via a study of the spectral and spatial properties of the emerging light.

We present spatially and spectrally resolved measurements of light emerging from the focus. The spectral-spatial maps were recorded for various pressures and pulse energies in argon and air. These are the first measurements of this type. The experiments indicate that the optimal spatial quality of the third-harmonic beam occurs at the pressure and laser intensity for which the highest conversion efficiency takes place.[1]

S. C. Rae[5,6] performed two-dimensional calculations of a 1ps pulse interacting with argon gas under tight focusing conditions (f/5 optics). He produced spectral-spatial maps of the emerging laser light similar to those that we have obtained experimentally and present in this paper. However, our results cannot be compared directly with the calculations of Rae because we used a much shorter pulse duration and larger f-number. Also, for our 25fs pulses, the slowly varying pulse envelope approximation that he used is no longer valid. In addition, we produced spectral maps for third harmonic light, and this is outside of the frame work of his model.

Experimental Setup

The quality of the laser spatial profile is of particular importance in our experiments because small distortions in the laser profile can translate into severe azimuthal asymmetries in the spatial structure of the radiation emerging from the interaction region. To be able to interpret meaningfully the spatial structures of the emerging radiation, it is necessary to achieve a very clean and well characterized beam. The degree to which the emerging radiation shows cylindrical symmetry is a good indication of whether this is achieved. With this aim, we spatially filtered the beam of a 2-TW Ti:Sapphire system (800nm),[7] at the expense of the majority of the pulse energy. Under vacuum, the 12mm beam was clipped by a 4mm hard circular aperture and then focused through a pinhole. The beam was then refocused with an f-number of ~40 inside a backfilled chamber.

The beam profile was measured to focus to within about 6% of the theoretical diffraction limit. The pulse duration was measured by autocorrelation to be in the range of 25-30fs. The energy delivered into the gas cell was varied up to about 1mJ, with an uncertainty of about 20%.

Under vacuum, 1mJ corresponds to a peak intensity in the focus of about 5×10^{15} W/cm^2, or about 20 times above that necessary to ionize Ar.[8]

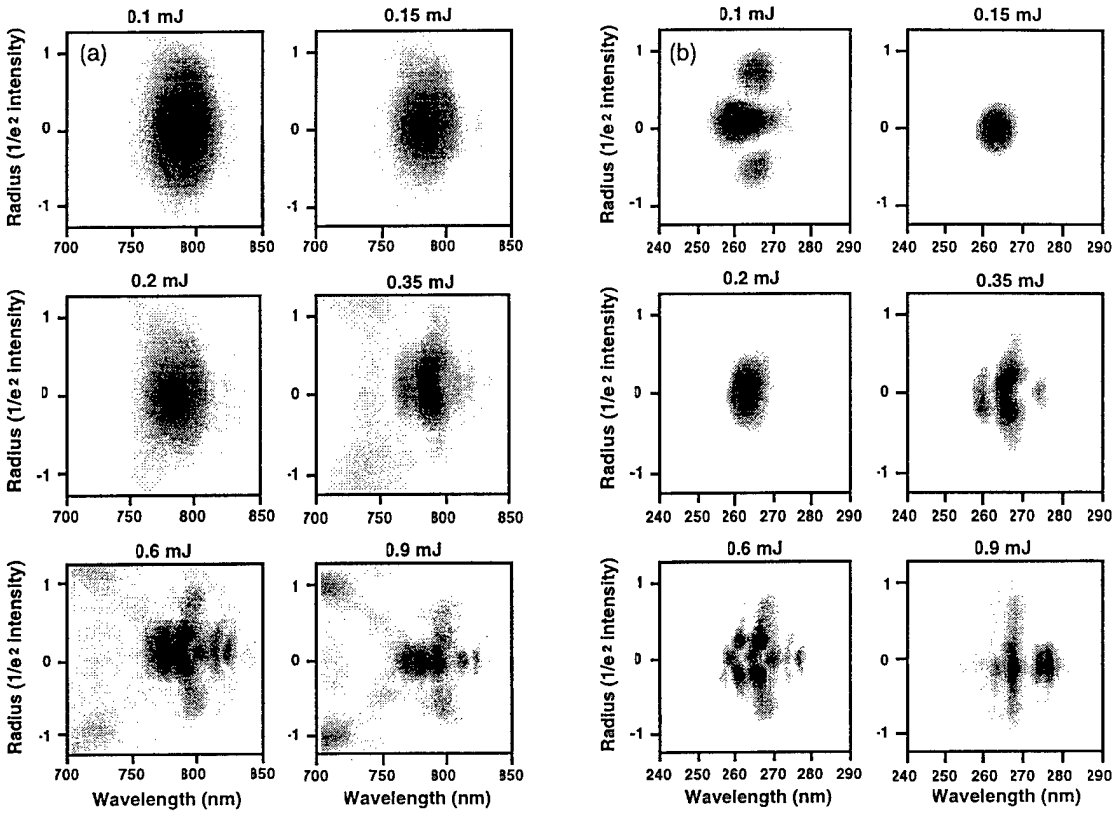

Figure 1. The (a) fundamental and (b) third harmonic spectra plotted against beam radial position for various pulse energies focused in 1000 Torr of argon. Position is expressed in units of 1/e^2-intensity radius of the beam when the gas cell is evacuated. The brightness of the images should not be compared from frame to frame.

Spatial-Spectral Measurements

We positioned a spectrometer in the far-field of the beam exiting the gas cell. The slit of the spectrometer sampled a narrow strip of light through the center of the beam, and this light was spectrally resolved in the orthogonal dimension. Using this setup, we recorded spectral-spatial maps of the emerging light as a function of pulse energy and pressure in the gas cell. Figure 1(a) shows a series of maps near the fundamental wavelength (800nm) captured when laser pulses of various energies are focused in a cell back-filled with 1000 Torr of argon. Figure 1(b) shows a similar series of maps for wavelengths near the third harmonic (267nm). Each frame records an individual laser shot.

Both the fundamental and third harmonic maps show a general trend of increasing complexity from lower to higher pulse energy. At the lowest pulse energy, 0.1mJ, the nominal peak intensity in vacuum is about 5×10^{14} W/cm^2, a factor of two above onset of ionization.[21] Below this energy, the third harmonic signal quickly diminished, making it difficult to detect with our instrument. Not indicated by the figure, the peak brightness (not integrated energy) of the third harmonic map for the 0.1mJ case is more than an order of magnitude below that of the 0.15mJ case. Above this value, the peak brightness in the third harmonic map continues to increase from frame to frame, but only by an additional factor of 5 by the final frame (0.9mJ).

The map of the fundamental beam at a pulse energy of 0.1mJ is very similar to the case of focusing in vacuum. However, as the pulse energy is increased, the beam undergoes significant

distortions as parts of the fundamental beam are blue-shifted. Perhaps the most striking feature within the maps of the fundamental wavelength is a well defined ring of blueshifted light which develops at the highest intensities.

Similar maps were generated for different pressures at fixed pulse energy. The efficiency of converting the fundamental into the third harmonic was observed to be highest (0.15%) in argon at a pressure in the range of ~300Torr.[1] The spatial measurements revealed that this pressure range also yields a well behaved Gaussian-like third harmonic beam profile.

Similar spectral-spatial maps were obtained using air. Although there are many distinctions, the results have many traits in common with those obtained with argon. This suggests that much of the physics involved in the interaction process is species-independent. The efficiency of converting fundamental light into the third harmonic in air was generally measured to be about half of that in argon.

Discussion

It appears that the onset of ionization in the focus is linked to the strong emission of third harmonic. Whether the act of ionization is linked directly with the bulk of the third harmonic emission or whether ionization plays an indirect role through the breaking of disadvantageous phase-matching symmetries is unknown. Nevertheless, we found that 20% of the initial beam energy is unaccounted for in the light emerging after the focus. In fact, if the laser were to focus in the manner that it does in a vacuum, there would be insufficient energy in the pulse to remove one electron per atom in the volume wherein the intensity reaches the ionization threshold.

An interesting feature of the data at high intensity and pressure is the development of a strongly blueshifted ring in the fundamental spectral map. The blueshifting presumably arises from rapid ionization in the focus.[2-4] We have calculated using Fresnel diffraction the field pattern necessary to create such a ring structure in the far field, assuming that the light originates from a plane at or near the focus. Under this scenario, the calculation indicates that the pattern comes from a spot surrounded by rings of alternating phase. The direct occurrence of this specialized pattern in the focus seems unlikely. An emission pattern which begins already in the form of a ring seems more plausible since a cylinder of plasma is formed in the focus. However, a ring near the focus does not transform into a ring pattern in the far field, assuming azimuthally uniform phase. A ring structure can be preserved, however, if the emission originates from a plane several Rayleigh ranges after or before the focus (or an effective focus).

These measurements are the first of this type and are performed with a laser beam of exceptional spatial quality. In addition, the extreme shortness of the laser pulse duration provides a unique regime for this type of experiment, where standard slowly varying envelope approximations are questionable. The process of focusing an intense laser into a gas cell is complicated, and these measurements may be useful for comparisons with numerical simulations which often employ simplifying approximations. We are working on such calculations and plan to report on them in the future.

1. S. Backus, J. Peatross, E. Zeek, A. Rundquist, G. Taft, M. M. Murnane, and H. C. Kapteyn, Opt. Lett. **21**, 665-667 (1996).
2. C. W. Siders, N. C. Turner III, M. C. Downer, A. Babine, A. Stepanov, and A. M. Sergeev, J. of Opt. Soc. of Am. B (1995).
3. Wm. M. Wood, C. W. Siders, and M. C. Downer, Phys. Rev. Lett. **67**, 3523 (1991).
4. T. Auguste, P. Monot, L.-A. Lompre, G. Mainfray, and C. Manus, Opt. Commun. **89**, 145 (1992).
5. S. C. Rae, Opt. Commun. **97**, 25 (1993).
6. S. C. Rae, Opt. Commun. **104**, 330 (1994).
7. J. Zhou, C.-P. Huang, M. M. Murnane, and H. C. Kapteyn, Opt. Lett. **20**, 64 (1995).
8. S. Augst, D. Strickland, D. D. Meyerhofer, S. L. Chin, and J. H. Eberly, Phys. Rev. Lett. **63**, 2212 (1989).

Coherence Properties of Ultrashort High-Order Harmonics

P. Salières†, Ph. Antoine†‡, A. L'Huillier§, B. Carré† and M. Lewenstein†

† Commissariat à l'Energie Atomique, DSM/DRECAM/SPAM, Centre d'Etudes de Saclay,

91191 Gif-sur-Yvette, France,

Tel: (33) 169086339, Fax: (33) 169089063, Email: psalieres@cea.fr

‡ Laboratoire de Physique Atomique et Moléculaire, Université Catholique de Louvain,

chemin du Cyclotron, 2 B-1348 Louvain-la-Neuve, Belgium

§ Department of Physics, Lund Institute of Technology, S-221 00 Lund, Sweden

Recently, high-order harmonic generation has attracted considerable interest for the possibility of generating ultrashort XUV pulses. With the advent of intense lasers that produce pulses of duration a few tens of fs, harmonic pulses of duration below 10 fs can be generated. To pass the limit of the (optical) fundamental period, different schemes have been proposed. Antoine *et al.* [1] showed that propagation in the macroscopic medium could lead to a phase locking of the different harmonics, resulting in emission of a train of attosecond pulses. Corkum *et al.* [2] proposed to use the extreme sensitivity of the harmonic efficiency on the polarization of the fundamental field to "extract" a single pulse from such a train.

Another scheme, due to Schafer and Kulander [3], involves the phase characteristics of harmonics generated by an ultrafast pump laser. By numerically integrating the time-dependent Schrödinger equation, they observe that harmonics located in the cutoff region of the spectrum exhibit a very regular phase that depends quadratically on time. This linear chirp can be compensated for with a grating pair leading to "compressed" harmonics of duration less than one period of the fundamental. This peculiar behaviour is attributed to the rapid change of the intensity during the pulse which makes a non negligible variation over one optical period. On the rising edge of the pulse, the electron in the continuum experiences an additional acceleration before returning to the parent ion, which leads to a blueshift of the generated harmonic field. Similarly, the falling edge of the pulse is associated to a harmonic redshift.

The different schemes mentioned above will be discussed. In particular, the question of adiabaticity/non adiabaticity of these phenomena will be addressed. We show that a quadratic temporal dependence of the phase is consistent with an adiabatic assumption, for which the full response is simply given by the integration of the instantaneous response over time. Indeed, the intrinsic phase of the harmonic dipole moment is related to the action acquired by the electron on its trajectory in the continuum, and thus depends on the fundamental intensity [4]. For the

emitted harmonic field, this results in a phase modulation which becomes more important as the laser pulse is shorter.

This effect in time has also consequences in space: due to the radial distribution of intensity in the laser focus, the harmonic emission phase front is curved, resulting in a divergence bigger than the one predicted by perturbation theory. Another important effect due to the temporal distribution of intensity is that the phase front curvature changes in time. The correlation in time of the electric fields in two points (taken non-symmetrically) in the harmonic beam is thus degraded. In other words, the harmonic beam is not fully spatially coherent and presents a finite coherence length. Ionization is an additionnal cause of distorsion of the spatial coherence. We will present the results of our extensive simulations of the degree of coherence of the harmonic beam generated in different experimental conditions.

[1] Ph. Antoine, A. L'Huillier and M. Lewenstein, *Phys. Rev. Lett.* 77, 1234 (1996).
[2] P. B. Corkum, N. H. Burnett and M. Yu. Ivanov, *Opt. Lett.* **19**, 1870 (1994).
[3] K. J. Schafer and K. C. Kulander, Proceedings of ICOMP VII (1996).
[4] P. Salières, A. L'Huillier et M. Lewenstein *Phys. Rev. Lett.* **75** 3776 (1995).

SPATIAL COHERENCE MEASUREMENT OF HIGH ORDER HARMONIC RADIATION

T. DITMIRE, E. T. GUMBRELL, R. A. SMITH, J. W. G. TISCH,
D. D. MEYERHOFER*, AND M. H. R. HUTCHINSON

Blackett Laboratory, Prince Consort Road,
Imperial College of Science, Technology, and Medicine
London, SW7 2BZ, United Kingdom

**Department of Mechanical Engineering*
University of Rochester
Rochester, New York 14624-1299

Though a vast number of studies have been conducted on the various properties of intense field high order harmonic radiation, there have been no studies of the actual spatial coherence of optical harmonics at short wavelengths (< 1000 Å). Measurements of harmonic far field profiles have suggested that the harmonics exhibited high coherence [1,2,3], but harmonic profile measurements alone are inadequate in determining the spatial coherence of the harmonic beam [4]. To address this aspect of the harmonic generation, we have conducted a series of two-slit interference measurements on harmonics in the 270 Å to 480 Å range to determine unambiguously their spatial coherence properties.

For the majority of the measurements, we studied the coherence of harmonics produced in a helium gas jet by a frequency doubled, Nd:glass, chirped pulse amplification laser (λ_0 = 527 nm). Previous studies have indicated that this configuration yields good conversion efficiency into harmonic energy in the soft x-ray region below 500 Å [5]. The laser, which had a pulse width of 2 ps, was focused with an f = 75 cm lens into the output of a solenoid valve gas jet. The Gaussian spatial profile of the laser beam was apertured to a diameter of 1.5 cm before the lens. Up to 140 mJ of 527 nm light was focused into the jet yielding a peak intensity of up to 7 x 10^{15} W/cm^2, well above the ionization saturation intensity of He.

The slit pairs for measuring the spatial coherence were placed 5 cm from the gas jet. Spatial scans of a single slit at this position indicate that the harmonics have a spatial width of roughly 200 μm. The harmonics were spectrally resolved in one dimension; the fringe pattern on each harmonic could then be observed in the other dimension. The harmonics were detected with a dual CsI coated micro-channel plate detector located 180 cm away from the slits. The slits were laser drilled in 20 μm thick Ti. Each slit had a width of roughly 8 ±1 μm, and slit-spacings of between 27 and 100 μm were used.

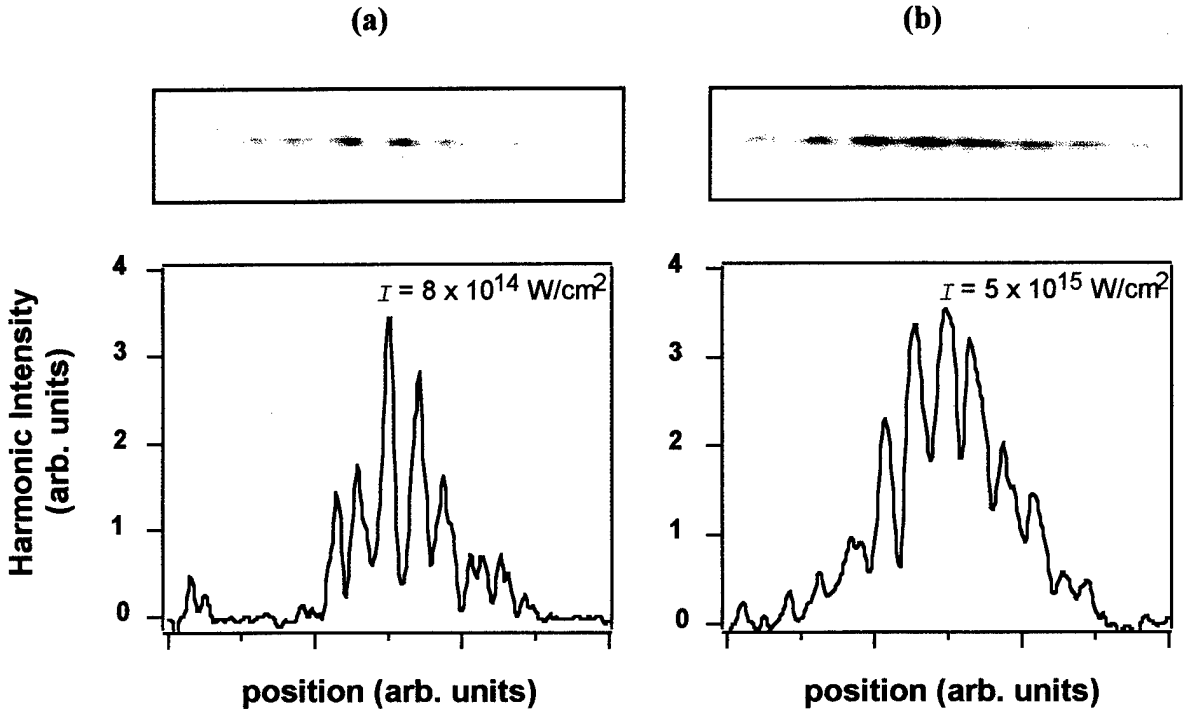

Figure 1: Interference fringes of the 11th harmonic of 527 nm light generated in helium from two slits separated by 50 μm. The images above the lineouts show the raw data containing the interference pattern.

Typical data generated from a slit pair with a spacing of 50 μm is shown in figure 1. Here the interference fringes of the 11th harmonic of the 527 nm light ($\lambda_{q=11} = 479$ Å) produced in a helium jet backed by 800 psi of pressure are shown at two intensities. As can be seen here, the fringe visibility, which is a measure of the light's coherence and is defined as $\mu = (I_{max} - I_{min})/(I_{max} + I_{min})$ [4], is very good. When the harmonic is generated with a peak intensity below the saturation intensity in helium, the fringe pattern, shown in figure 1a, exhibits a visibility that is ~ 0.8, indicative of near perfect coherence over the spacing of the slit pair. At an intensity above ionization saturation, the fringe pattern, shown in figure 1b, exhibits a somewhat lower visibility, ~ 0.5. We believe that this degradation in the harmonic's coherence is the result of free electron production by tunnel ionization during the harmonic generation process. We observe this coherence degradation on all the harmonics we studied, out to the 19th harmonic ($\lambda_{q=11} = 277$ Å).

Despite the deleterious effects of ionization, we find that the harmonics can be produced at high intensity and good conversion efficiency with good spatial coherence. In fact, the observed spatial coherence of the soft x-ray harmonics is substantially superior to the spatial coherence of collisionally pumped x-ray lasers. We find, for example, that the effective size of a thermal source with the same coherence as that measured for the

harmonics with wavelength 270 - 400 Å is < 10 μm, smaller than the laser focal spot size (60 μm) and significantly smaller that the measured effective source size of x-ray lasers which typically exhibit an effective coherence source size of > 100 μm [6]. Consequently, our measurements indicate that the high order harmonics represent a source of soft x-rays with the highest spatial coherence ever reported.

References

1. J. W. G. Tisch, R. A. Smith, J. E. Muffet, M. Ciarocca, J. P. Marangos, and M. H. R. Hutchinson, Phys. Rev. A **49**, R28 (1994).
2. P. Salières, T. Ditmire, K. S. Budil, M. D. Perry, A. H. L'Huillier, J. Phys. B: At. Mol. Opt. Phys. **27**, L217 (1994).
3. J. Peatross, and D. D. Meyerhofer, Phys. Rev. A **51**, R946 (1995).
4. M. Born, and E. Wolf, *Principles of Optics: Electromagnetic Theory of Propagation, Interference, and Diffraction of Light*, (Oxford: Pergamon, 1989).
5. T. Ditmire, J. K. Crane, H. Nguyen , L. B. DaSilva, and M. D. Perry, Phys. Rev. A **51**, R902 (1995).
6. J. E. Trebes, K. A. Nugent, S. Mrowka, R. A. London, T. W. Barbee, M. R. Carter, J. A. Koch, B. J. MacGowan, D. L. Matthews, L. B. DaSilva, G. F. Stone, and M. D. Feit, Phys. Rev. Lett. **68**, 588 (1992).

Application of MeV X-rays from Femtosecond Laser-Produced Plasmas to the Study of Photonuclear Effects

H. Schillinger, Ch. Ziener, R. Sauerbrey
Institut für Optik und Quantenelektromik
Friedrich-Schiller-Universität Jena
Max-Wien-Platz 1, D-07743 Jena, Germany
phone: 49-3641-636281
fax: 49-3641-636278

H. Langhoff
Universität Würzburg
Am Hubland, D-97074 Würzburg, Germany

Femtosecond laser-produced plasmas are sources of superhot electrons and consequently of hard radiation in the multi-MeV range via bremsstrahlung [1, 2]. These sources offer the potential to observe nuclear effects using ultrashort laser pulses. Although still at the beginning these techniques might lead to a new femtosecond spectroscopy of nuclei.

We measured X-ray spectra from laser-produced plasmas in the energy range from 200 keV to 7 MeV with a NaI(Tl) scintillator crystal and a pulse height analysator. The spectra show typically two distinct spectral components with approximately exponential behavior, one with mean photon energies of a few hundred keV and another consisting of MeV x-rays. The hard part of the emission beyond 1.7 MeV could be optimized by intentionally increasing the prepulse energy 13ns before the main pulse. The total yield of photons above 200 keV was found to be on the order of 10^{-4} of the incident laser energy. The yield of the high energy component is correlated with very strong $3/2\omega$-harmonic emission. Therefore, collective plasma excitation is the most likely mechanism for the production of the MeV electrons. The lower energy x-rays in the several hundred keV-range can be attributed to acceleration of electrons

in a single cycle of the laser electric field.

We conclude that at focussed intensities above 10^18 W/cm^2 about 10^6 photons per shot with energies in excess of 1.7 MeV are emitted. This value is in agreement with theoretical estimates. This high energy photon yield should be sufficient to produce photonuclear processes with this source, despite the generally small cross sections for photonuclear reactions. The applications to nuclear physics that we discuss are the photoneutron effect in Beryllium and Deuterium (threshold 1.67 MeV and 2.2 MeV, respectively), and nuclear resonance fluorescence in Lithium.

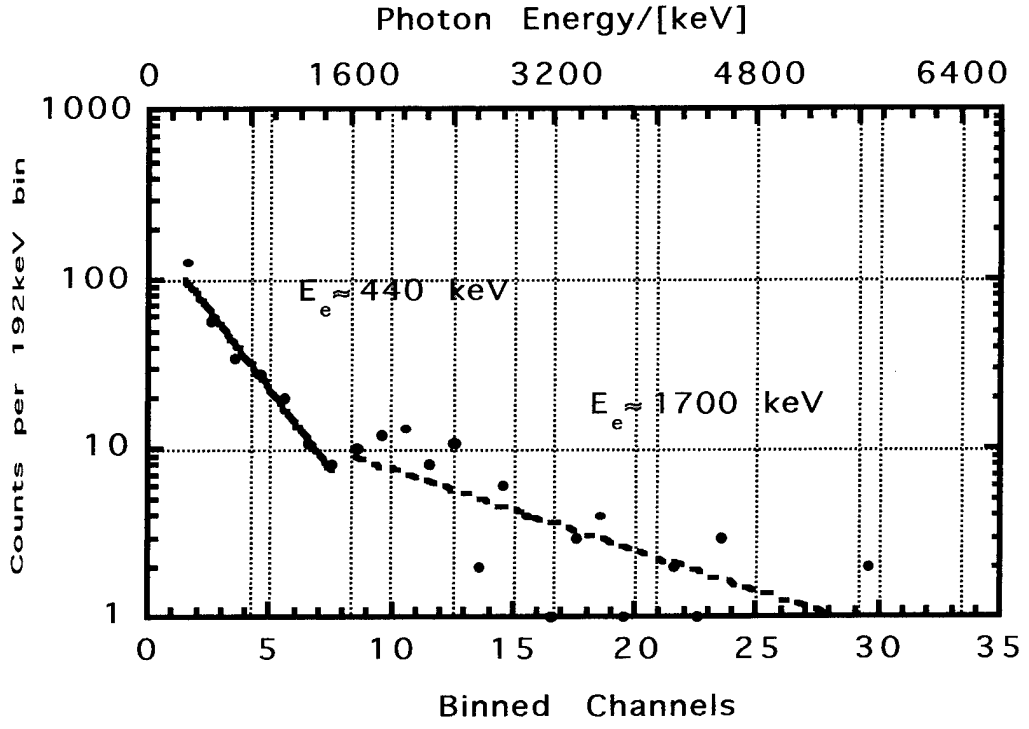

Fig.1: X-ray spectrum from a Tantalum target irradiated by a 110 fs, 2 10^{18} W/cm^2 Ti:Sapphire laser.

References:

[1] G.Malka, J.L. Miquel; Phys. Rev. Lett. 77, 75 (1996)

[2] J.D. Kmetec, C.L. Gordon III, J.J. Macklin, B.E. Lemoff, G.S. Brown, S.E. Harris; Phys. Rev. Lett. 68,1527 (1992)

ULTRA-INTENSE LASERS FOR FAST IGNITION IN INERTIAL CONFINEMENT FUSION AT ILE, OSAKA

T. YAMANAKA, Y. KATO, Y. KITAGAWA, R. KODAMA, H. TAKABE,
H. FUJITA, T. KANABE, M. NAKATSUKA, and K. MIMA
Institute of Laser Engineering, Osaka University,
2-6 Yamada-oka, Suita, Osaka 565, Japan
+81-6-879-8721, tyama@ile.osaka-u.ac.jp

1. Introduction

Progress in high power short pulse laser using a chirped-pulse amplification technique[1] is opening the possibility of an additional heating concept "fast ignition" [2] in Inertial Confinement Fusion (ICF). In the concept, the compressed fuel with a high fuel density created by a conventional laser implosion is heated by an ultra-intense short pulse laser (a few ps) before a core is disassembled (< a few ten ps). The concept will give us reduction of the required laser energy and the implosion uniformity for ignition in ICF.

In this paper we report two aspects related to the fast ignition. First we investigate the ignition condition with a 2-dimensional hydrodynamic code for the isochoric implosion with off-center ignition. Second, present status of CPA in our GEKKO MII and GEKKO XII lasers for fast ignition experiments are reported with preliminary experiments such as the hole boring with a 100 ps laser pulse on a plane target.

2. Evaluation of ignition condition in fast ignition

The ignition condition was studied using a 2-D hydrodynamic code ILESTA with alpha particle heating included for the isochoric implosion for the central as well as the off-center ignitions. First the validity of the 2-D code was tested in the 1-D configuration for the central spark ignition for the isobaric and isochoric implosions. The isochoric implosion requires higher spark temperature of approximately 10 keV in comparison to 5 keV for the isobaric implosion with the areal density ρR of 0.5 g/cm^2 which is slightly higher than 0.3-0.4 g/cm^2 for the isobaric implosion.

The simulation for burn-wave propagation for the off-center ignition shows that the ignition condition for the off-center ignition is very close to that for the central ignition, since the velocity of the burn wave propagation is very high (2-3x10^{8}cm/s) compared to the sound

velocity. The spark energy (the internal energy in the spark region) depends critically on the fuel density; it is 2-3 kJ for 400 g/cm^3 and 15-20 kJ for 200 g/cm^3. Thus higher density is preferable for reducing the ignition energy, but the core gain decreases due to the higher energy required for higher density compression.

The core gain of 2,000 is achieved with the fuel energy of 50 kJ, corresponding to the fusion gain of 200 with the 500 kJ driver for the hydrodynamic efficiency of 10%. The fast igniter beam of $\sim$50 kJ will be required in this case if $\sim$30 % coupling efficiency is achieved to make an igniter. This energy could be reduced to 6-10 kJ when the fuel is compressed to 400 g/cm^3.

3. High power short pulse laser constructions

To experimentally study the phenomena related to the fast ignition, we are constructing two high power short pulse lasers for efficient heating of the compressed fuel. Using a single mode optical fiber front end system, we have previously generated a 1ps-30TW pulse from the GEKKO MII (two beams system)[3]. Now the front end is replaced by the combination of a mode-locked Ti:sapphire oscillator and a Ti:sapphire regenerative amplifier to obtain a 50 TW output. The beam with a diameter of 140 mm, limited by the pulse-compression grating, will be focused with an off-axis parabolic mirror onto a target at intensities above 10^{18} W/cm^2. This facility will be used to investigate laser-matter interaction, laser boring of overdense plasmas, and high energy particle generation from underdense plasmas.

In the first test experiment, we are going to irradiate a plastic foil target to see the energy coupling between laser and solid density plasma. We are also preparing the measurement of the transfer efficiency of $10^{19}\sim10^{20}$ W/cm^2 ps pulse through a solid density plasmas. According to the simulation results, a 10^{20} W/cm^2 laser pulse makes a channel in an overdense (n/n_c = 7) plasma slab with 2μm-thickness and 90% of the pulse energy comes out in the rear side. In the preliminary experiment using a 100 ps pulse on planar target we observed the beam propagation into the overdense region where the laser is self-focused in underdense region to drill a hole through the overdense region and deposits its energy near the solid density surface. [4].

Another ultra-intense short pulse laser is constructing as the 13th arm of the GEKKO XII (twelve beams system), as shown in Fig. 1. The purpose is to experimentally verify the fast ignition. A mode-locked glass oscillator and a Ti:sapphire regenerative amplifier are used as the front end system. Preamplification is with 4-pass glass rod amplifier. The final 35 cm disk amplifier of a Cassegrainian type 3-pass geometry provides the output of 1 kJ in 300 ps to 7 kJ in 3 ns with a beam diameter of 200 to 350 mm. After the grating-pair compression, the

system will provide a 100 TW with an energy of 100 J for a beam diameter of 200 mm. The system is expected to provide 1 PW by enlarging the beam diameter to 350 mm. The new 13th beam is to irradiate the spherical target, pre-imploded with 12 beams. The additional heating effects such as neutron yield enhancement will then be investigated.

We appreciate LLNL for fabrication of the large aperture grating for pulse compression.

References

[1]B.C.STUART et al., "Chirped-Pulse Amplification in Ti:Sapphire Beyond 1 μm", IEEE J. Quantum Electron. **31**(1995) 528.

[2]M.TABAK et al., "Ignition and High Gain with Ultrapowerful Lasers", Phys. Plasmas **1**(1994) 1626.

[3]K.YAMAKAWA et al., "Prepulse-free 30TW, 1-ps Nd:glass Laser", Opt. Letters **16**(1991) 1593.

[4]R.KODAMA et al., "Study of laser hole-boring into an overdense plasma", 24th ECLIM, PT 26 (Madrid, June 3-7, 1996).

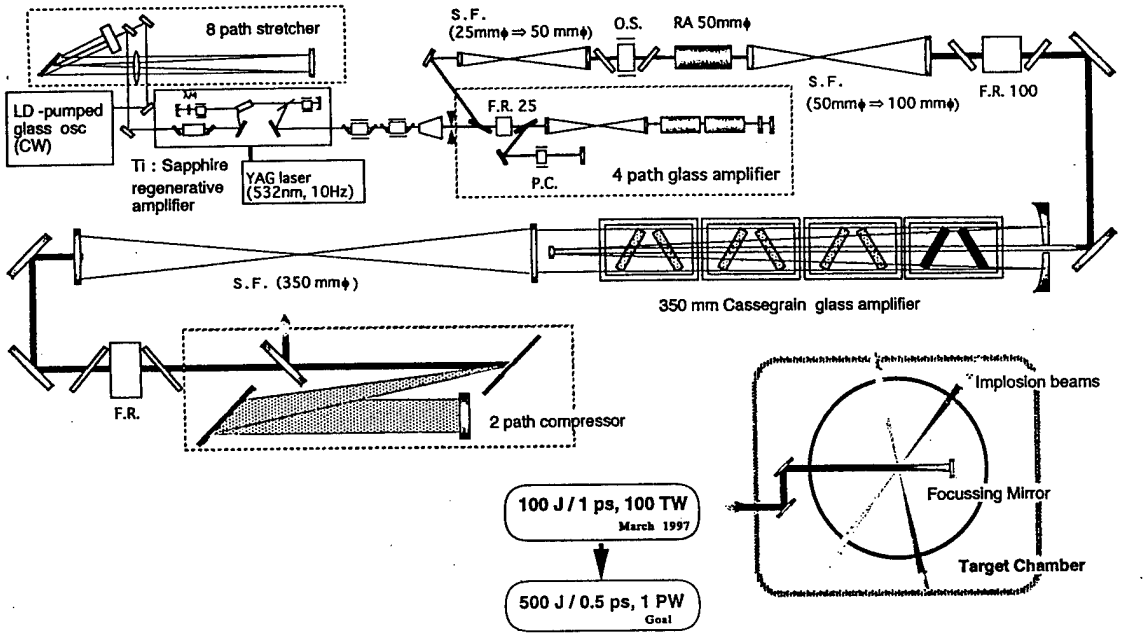

Fig. 1. Petawatt laser module as the 13th beam of the GEKKO XII laser system. This laser is used to heat the high density plasma compressed with 12 beams from the GEKKO XII laser system. 3 pass Cassegrainian type amplifier is introduced as a main amplifier.

Conical Emission of a Femtosecond Pulse Undergoing Self-focusing and Ionization in Air

O.G. Kosareva, A.Brodeur [1], V.P. Kandidov and S.L. Chin [1]

International laser center, Physics Department, Moscow State University, 119899, Moscow, Russia,
fax: +(095)939-3113, tel.: +(095)939-3091, e-mail: kosarev@synapse.ru

[1] *Centre d'optique, photonique et laser, Departement de physique, Universite Laval, Quebec, Canada, G1K 7P4, fax: +(418)656-2623*

Recently, the phenomenon of intense femtosecond light pulse filamentation over distances of several tens of meters was observed [1,2]. The study of long-interaction-length intense laser pulses has interesting applications including laser-induced lightning, laser-pumped x-ray sources, and laser-plasma based accelerators.

Measurements of the near-axis energy in the filament and numerical simulations performed in [3] showed that the filamentation process originates from the joint influence of the instantaneous Kerr nonlinearity of air and the plasma produced by the pulse itself in the course of propagation. The optical - field - induced ionization of air components stops the contraction of the beam and leads to severe divergence of the trailing part of the pulse [4].

One of the interesting phenomena accompanying filamentation in air is the conical emission [2]. In normally dispersive medium with the electronic Kerr nonlinearity the conical emission is attributed to four-photon coupling [5]. However, under the conditions of self-consistent plasma production due to multiphoton or tunnelling ionization, the order of the nonlinear process is much higher than three. Therefore, the models based on four-photon coupling are not applicable here.

Here we report the results of numerical and experimental studies of the conical emission from the filament created by a femtosecond pulse in air. We show that the self-produced plasma is a determining factor in the transformation of spatial-temporal spectrum of the pulse in the course of propagation.

The propagation is described by the two-dimensional (cylindrical symmetry is assumed in radial direction) nonlinear Srödinger equation. The nonlinear term includes instantaneous Kerr nonlinearity, plasma contribution, which grows with time, and energy loss due to plasma production. The electron density is calculated in each space-time point according to the models [6], [7] depending on the intensity. The parameters of the input pulse in simulations correspond to those in the experiment, where Ti:Sapphire chirped-pulse-amplification laser system was used to generate pulses with the central wavelength 800 nm, the duration 250 fs and the energy 10 mJ. For calculations the input pulse shape was chosen to be Gaussian with Gaussian transverse distribution of the laser intensity.

In the course of propagation highly nonlinear medium response causes large phase gradients in space in time. Figure 1 shows the resulting spatial-temporal spectrum of the pulse which reveals the following peculiarity: at the anti-Stokes side shorter wavelengths propagate at larger angles to the laser axis (z - axis). A simple interpretation of the complicated plot in

Fig. 1(b) is shown in Fig. 2. The picture demonstrates the conical emission at a distance of 20 m from its source.

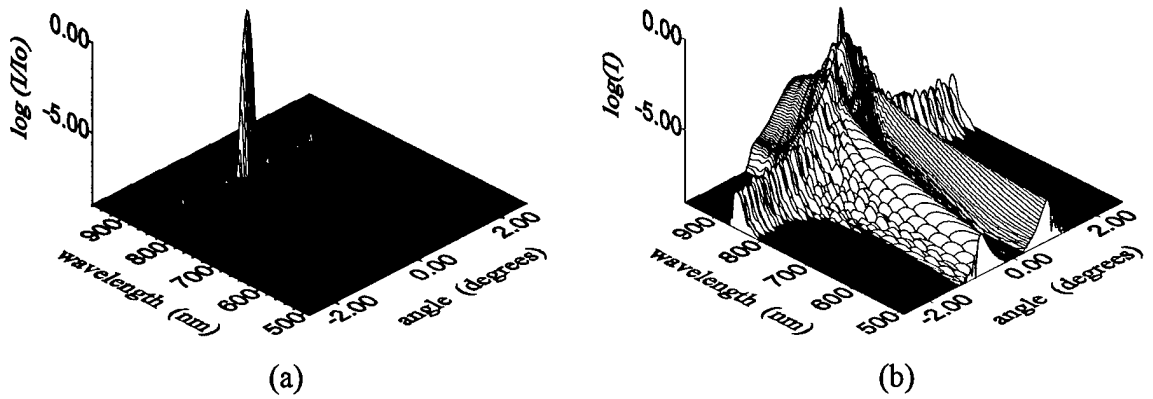

Fig. 1. Spatio-temporal spectra of the pulse undergoing filamentation in air.
(a) Spectrum of the input pulse ($z = 0$), (b) spectrum of the pulse at $z \approx 0.52 z_d$

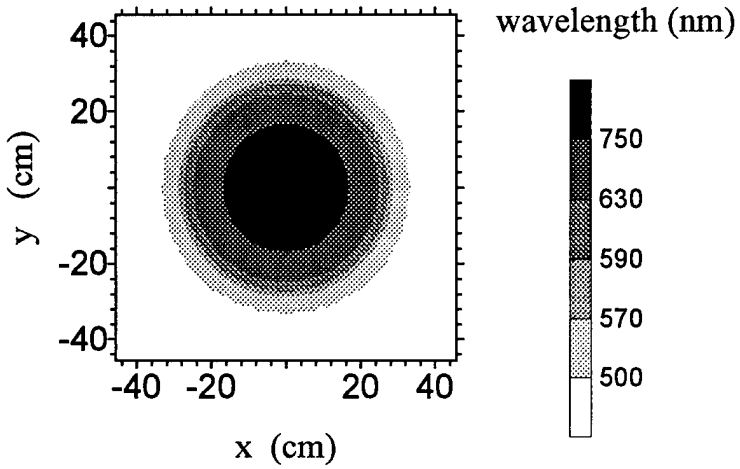

Fig. 2. The conical emission at a distance of 20 m from its source.

In the experiment the conical emission was observed in the following way: at the output of the optical compressor, the beam was sent into a long hallway using two transport mirrors. The second transport mirror was located 17.7 m from the compressor. After this mirror, the beam propagated freely to the end of the hallway for a total propagation distance of 111 m (diffraction length $z_d \approx 96$ m) . The conical emission was seen on a white screen placed in the beam path at a distance $z = 70$ m $\approx 0.72 z_d$ from the output of the compressor and at a distance of 20 m from its source located at $z \approx 0.52 z_d$. To select a particular wavelength, an interference filter (10 nm bandwidth) was inserted in the beam path, in front of the screen. The setup was organized in such a way that the CE source was restricted to a length of 2 meters thus making possible to reduce the angle measurement error to 10%.

The nonlinear mechanism responsible for the conical emission is the time-dependent growth of the density of free electrons produced by high-intensity laser field. The plasma leads to the blue spectral broadening. Therefore, conical emission at the Stokes side of the pulse spectrum was observed neither in simulations nor in the experiment.

In conclusion we note, that experimentally obtained and simulated conical emission angles, scaled by the initial divergence of the corresponding input beam, are in good agreement with each other. Three typical features of the conical emission found both in the experiment and simulations should be pointed out:

- For distances larger than the self-focusing distance for the central slice of the pulse and smaller than the diffraction length emission angles are independent of the position of the conical emission source.
- No conical emission was observed at the Stokes side of the pulse spectrum.
- The largest spectral broadening occurred in the conical emission. Indeed, colors covering the entire visible spectrum were seen in the conical emission, while only red could be seen in the central part of the beam.

References

1. A.Braun, G.Korn, X.Liu, D.Du, J.Squier, and G.Mourou, Opt. Lett.,**20**, 73 (1995).
2. E.T.J. Nibbering, P.F.Curley, G.Grillon, B.S. Prade, M.A. Franco, F. Salin, and A.Mysyrowicz, Opt. Lett., **21**, 62 (1996).
3. A.Brodeur, O.G.Kosareva, F.A.Ilkov, V.P.Kandidov, S.L.Chin, submitted to Opt. Lett.
4. O.G.Kosareva, and V.P.Kandidov, *in* Book of Abtracts of 7th International Conference on Multiphoton Processes, (Sept. 30 - Oct. 4, 1996, Germany), p. B35.
5. G.G. Luther, A.C. Newell, and J.V. Moloney, Opt. Lett., **19**, 789 (1994).
6. A. Szoke,. *in* Atomic and Molecular Processes with Short Intense Laser Pulses, p. 207, edited by A.D. Bandrauk, Plenum, New York, 1987.
7. M.Ammosov, N.B.Delone, and V.P.Krainov, Sov.Phys.JETP, **64**, 1991 (1986).

A THREE DIMENSIONAL PONDEROMOTIVE TRAP FOR HIGH ENERGY ELECTRONS

J.L. Chaloupka[a], T.J. Kessler, and D. D. Meyerhofer[a,b]

Laboratory for Laser Energetics
University of Rochester
250 E. River Rd.,
Rochester, NY 14623.
jcha@lle.rochester.edu
[a)] also Dept. of Physics and Astronomy
[b)] also Dept. of Mechanical Engineering

Electrons injected into a high intensity laser focus by tunneling ionization quickly escape due to the strong ponderomotive force. This limits the probability of observing harmonic radiation from free electrons oscillating in the field[1] and other nonlinear effects. Two dimension(radial) optical confining schemes have been proposed to increase the life-time of the electron in the intense field.[2, 3] These do not confine the electron in the direction of the laser propagation which limits their effectiveness. In intense fields the electrons have significant momentum in this direction.[4] To our knowledge, neither of these schemes have been demonstrated.

We have developed a three-dimensional ponderomotive optical trap suitable for high intensity lasers by using a phase mask to change the phase of half of the beam near-field pattern by π. In this case, the laser intensity has a minimum at the best focus allowing electrons to be ponderomotively trapped. The phase mask has been created by cutting a disk out of a zeroth order half-wave plate, rotating it by 90° and reinstalling it. The inner disk covers approximately 50% of the beam near field. We have used equivalent target plane images to demonstrate the trapping potential and show that the peak intensity at the trap boundaries is approximately 20% of the peak intensity of the beam without the phase mask. By changing the relative angle of the two wave-plate sections, the trap depth can be varied.

This work is supported by the National Science Foundation.Additional support was provided by the U.S. Department of Energy Office of Inertial Confinement Fusion under Cooperative Agreement No. DE-FC03-92SF19460, the University of Rochester, and the New York State Energy Research and Development Authority. The support of DOE does not constitute an endorsement by DOE of the views expressed in this article.

References

1. E.S. Sarachik and G.T. Schappert, Phys. Rev. D **1**, 2738-2753 (1970).
2. U. Mohideen and et al., J. Opt. Soc. Am. B **9**, 2190 (1992).
3. C.I. Moore, J. Mod. Optics **39**, 2171 (1992).
4. C.I. Moore, J.P. Knauer, and D.D. Meyerhofer, Phys. Rev. Lett. **74**, 2439 (1995).

X-laser induced nuclear decay: Resonance internal conversion

B.A.Zon and V.E.Chernov

394693, Russia, Voronezh University; e-mail: zon@niif.vucnit.voronezh.su

The behaviour of nuclei in intense electromagnetic field is a subject of great theoretical interest. Considerable changes in these processes (e. g. in internal conversion, IC) could be achieved by resonanse interaction between nuclei and their electronic shells, when the correspondent nuclear and electronic levels are sufficiently close and the defect of resonance is compensated by laser radiation. As an example of such processes, the resonance internal conversion (LIDIC) in metastable nuclei [1, 2, 3] can be considered. Experimental study of the laser field interaction with metastable nuclei can provide an information about important nuclear characteristics, such as energies and multipolarities of nuclear transitions, anomalous internal conversion coefficients etc., which are not well identified for some nuclei. Moreover, of certain interest can be an acceleration of nuclear decay due to the LIDIC-process, and even (at sufficiently high intensities of the laser field) a coherent X-ray radiation due to electron transition into the deep vacancy created by LIDIC-process or (at still higher intensities) a coherent γ-radiation due to the nuclear transitions.

Some evaluations for LIDIC-process in ^{235m}U [1] and ^{229m}Th [2] were carried out. But one of the most experimentally attractive isomers can be ^{99m}Tc [3, 4], which is widely used in the medical radiodiagnostics and produced in macroscopic amounts.

The K- and L- conversion in ^{99m}Tc is forbidden by the energy conservation law, and the M-conversion is the main channel of the metastable level decay. However, the L-conversion becomes possible if a $\sim 500\,\mathrm{eV}$ photon is absorbed from an external radiation. In the work [4] we considered a highly-stripped Tc ions, where the same process would require the photon energy of a few eV. The obtained numerical estimations show that the laser radiation of a comparatively low intensity $I \sim 10^7\,\mathrm{W}\cdot\mathrm{cm}^{-2}$ can double the activity of $^{99}\mathrm{Tc}^{32+}$ ions. But a plasma of such ions has rather short lifetime normally, so the neutral Tc atom seems to be an object not less appropriate for the experimental study of LIDIC process [3].

The cross-section of the LIDIC-process can be evaluated in the hydrogen-like approximation, when then the wavefunctions of the deep electron shells are characterized by some effective charges which can be obtained from self-consistent calculations of atomic structures. Our rough calculations show that the X-ray radiation with $\omega \sim 500$–$600\,\mathrm{ev}/\hbar$ results approximately in the same cross-section values as for LIDIC in highly-stripped Tc ions. Although such powerful X-ray sources at the mentioned frequences are not available yet, it should be kept in mind that a multiphoton LIDIC could be more probable in high X-ray field. The calculations of such processes are rather complicated, but they can be carried out using the Coulomb Green function which was used in refs. [3, 4] for one-photon LIDIC calculations.

Let us note another interesting property of ^{99}Tc: it has a short-lived nuclear level lying below the metastable one. So the coherent γ-radiation due to $7/2^+ \rightarrow 9/2^+$ nuclear transition could be realized when the incident radiation intensity is sufficiently high. Our numerical estimations for a coherent single-pass amplification yield $I \sim 10^{22}\,\mathrm{W/cm^2}$.

It should be noted that ^{99}Tc is not unique nucleus for LIDIC process; the resonance conditions can also be satisfied, e.g., for ^{105}Ag, ^{189}Os, ^{191}Os, ^{191}Au, ^{193}Ir, ^{205}Pb. Some estimations for external laser photon energies required for LIDIC into rydberg electron states of the above mentioned nuslei are presented in the table [5]. LIDIC-process in these nuclei can take place in rather wide spectral range of the external radiation — from soft VUV up to X-Ray.

Nucleus	Transition energy	Lowest initial subshell for usual IC	External photon energy	Possible initial subshell for LIDIC
^{105}Ag	25.47 keV	L	44 eV	K
^{99}Tc	2.71 keV	M	500 eV	L
^{189}Os	69.54 keV	L	4.3 keV	K
^{191}Os	74.38 keV	L	400 eV	K
^{191}Au	13.7 keV	L_2	200 eV	L_1
^{193}Ir	80.3 keV	K	4 keV	K
^{205}Pb	2.330 keV	N	150 eV	M
^{229}Th	3.5 eV	Q_2	1 eV	Q_1
^{235}U	76 keV	Q	4 eV	Q

References

[1] B. A. Zon and F. F. Karpeshin, *Sov. Phys. JETP* **70** (1990) 224.

[2] F. F. Karpeshin, I. M. Band, M. B. Trzhaskovskaya, and B. A. Zon, *Phys. Lett. B***282** (1992) 267.

[3] B. A. Zon and V. E. Chernov, *Phys. Lett. B* **383** (1996) 367.

[4] B. A. Zon and V. E. Chernov, *Sov. Izvestia RAN* **60** (1996) 189.

[5] *Table of Isotopes, 7-th edition* (ed. by C. M. Lederer and V. S. Shirley), Wiley–Interscience Publication, New-York, 1978.

Laser Wakefield Acceleration Experiments

H. Kotaki[1], K. Nakajima[1,2], M. Kando[4], H. Ahn[1], T. Watanabe[3], T. Ueda[3], M. Uesaka[3], H. Nakanishi[2], A. Ogata[2], K. Kinoshita[3] and K. Tani[1]

[1]Japan Atomic Energy Research Institute (JAERI),
2-4, Shirakatashirane, Tokai, Ibaraki, Japan
Tel. +81-29-282-5237, FAX +81-29-282-6057

[2]National Laboratory for High Energy Physics (KEK)
1-1, Oho, Tsukuba, Ibaraki, Japan
Tel. +81-298-64-5248, FAX +81-298-64-3182

[3]Nuclear Engineering Research Laboratory (NERL),
The University of Tokyo,
2-22, Shirakatashirane, Tokai, Ibaraki, Japan
Tel. +81-29-287-8473, FAX +81-29-287-8471

[4]Institute for Chemical Research, Kyoto, Japan, Kyoto University,
Uji, Kyoto, Japan
Tel. +81-774-32-3111, FAX +81-774-33-5509

E-mail addresses

H. Kotaki	: kotaki@hikari.tokai.jaeri.go.jp
K. Nakajima	: nakajima@kekvax.kek.jp
M. Kando	: kando@hikari.tokai.jaeri.go.jp
H. Ahn	: ahn@hikari.tokai.jaeri.go.jp
T. Watanabe	: wata@utnl.gen.u-tokyo.ac.jp
M. Uesaka	: uesaka@utnl.gen.u-tokyo.ac.jp
H. Nakanishi	: nakanishi@kekvax.kek.jp
A. Ogata	: ogata@kekvax.kek.jp
K. Kinoshita	: kino@utnl.gen.u-tokyo.ac.jp
K. Tani	: tani@apr.jaeri.go.jp

Laser-driven particle accelerators have been conceived over the past decade to be the next-generation particle accelerators, promising super-high field particle acceleration and a compact size compared with conventional accelerators [1]. Among a number of laser accelerator concepts, laser wakefield accelerators have great potential to produce ultra-high-field gradients of plasma waves excited by intense ultrashort laser pulses [2]. Recently wakefield excitation of the order of ~10GeV/m in a plasma has been directly confirmed by the use of a table-top-

terawatt (T^3) laser [3].

Our project aims at achieving high energy particle acceleration to energies more than 1 GeV in a table-top scale owing to a channel-guided laser wakefield acceleration (LWFA) scheme by the use of 100 fs, 2 TW T^3 laser system.

We have demonstrated the self-channeling of ultrashort laser pulses with a relativistic intensity over a few cm [4]. We have achieved synchronization of a 10 ps electron beam with a 100 fs laser pulse within a few ps in order to accelerate injected electrons firmly due to wakefield induced by laser pulses in the rate of 10 Hz [5].

Fig. 1 shows the distribution of the energy gain of accelerated electrons at the Helium pressure of 20 Torr for the laser peak power of 0.5 TW. The energy gain of 100 MeV was obtained from this figure.

As a next step, we are planning to measure the frequency and the amplitude of the plasma wakefield by using interferometry technique [3].

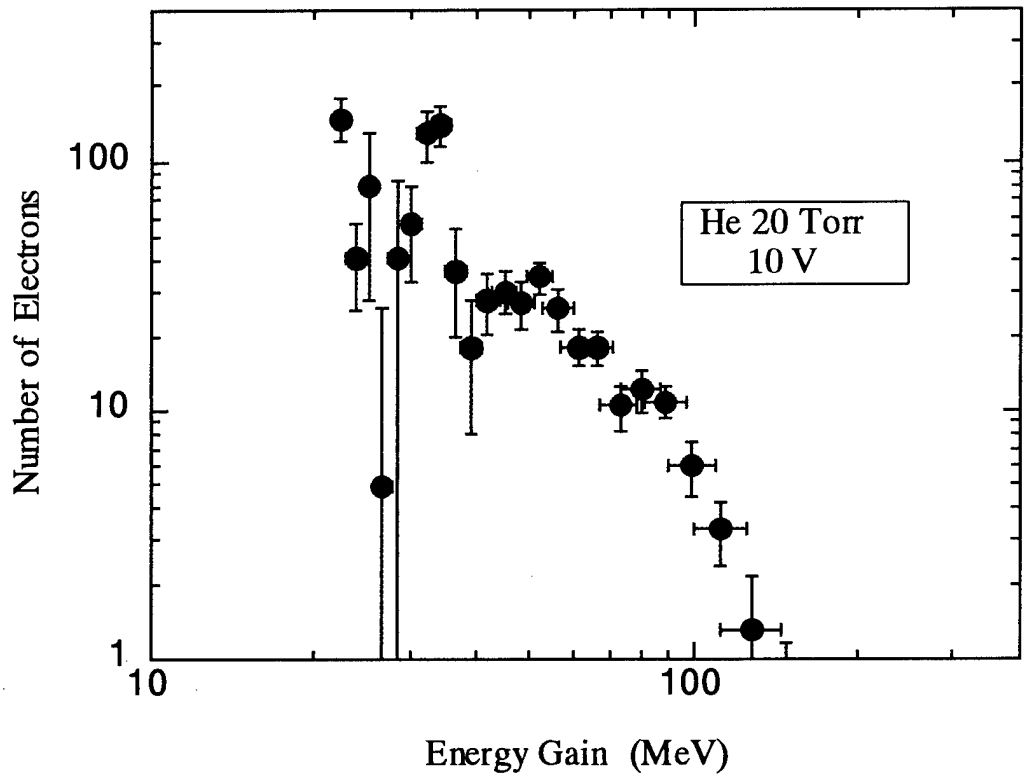

Fig. 1 Distribution of the energy gain of accelerated electrons at the Helium pressure of 20 Torr for the laser peak power of 0.5 TW.

References

1) T. Tajima and J. M. Dawson, Phys. Rev. Lett., **43**, 267 (1979)
2) K. Nakajima et al., Phys. Rev. Lett., **74**, 4428 (1995)
3) J. R. Marques et al., Phys. Rev. Lett., **76**, 3566 (1996) ; C. W. Siders et al., Phys. Rev. Lett., **76**, 3570 (1996) ; C. W. Siders et al., IEEE Trans. Plasma Sci., **24**, 301 (1996)
4) M. Kando et al., contributed to " '96 Advanced Accelerator Concepts", Lake Tahoe, California, USA, Oct. (1996)
5) M. Uesaka et al., contributed to " '96 Advanced Accelerator Concepts", Lake Tahoe, California, USA, Oct. (1996)

INFLUENCE OF RELATIVISTIC STRUCTURE AND RETARDATION IN TWO-PHOTON TRANSITIONS IN HYDROGENIC SYSTEMS

C. Szymanowski†, V. Véniard, R. Taïeb, and A. Maquet

Laboratoire de Chimie Physique - Matière et Rayonnement ,
11 rue Pierre et Marie Curie , Université P. et M. Curie Paris VI ,
F - 75 231 Paris Cedex 05 , France
†e-mail: szymanow@ccr.jussieu.fr ; phone +33-1-44-27-62-78 ; fax +33-1-44-27-62-26

The experimental realization of powerful sources of coherent X-ray radiation [1] opens for the first time the possibility to perform two-photon bound-bound absorption experiments involving inner shells in heavy atoms or ions. This would considerably broaden the scope of traditional, (single-photon) X-ray Absorption Spectroscopy (XAS) and related techniques. From the theoretical point of view it is clear that the usual non-relativistic dipole treatment of the atom-field interaction is no longer valid: By considering the two-photon $|1^2S_{1/2}\rangle \rightarrow |2^2S_{1/2}\rangle$ transition in hydrogenic systems, we test the inherent limitations of such a simplified approach as compared to a treatment taking full care of relativistic and retardation effects.

Our treatment is based on the computation of the relevant second-order perturbative amplitudes, the perturbative approach being certainly valid in view of the expected intensities of the currently developed X-ray sources as compared to typical electric field strength in heavier atoms. Its distinctive feature is that the infinite sums over the complete set of states, which enter the second-order amplitudes, are performed exactly by using a discrete, Sturmian-like, expansion of the Dirac Coulomb Green's function. While Sturmian expansions are widely exploited in non-relativistic applications, comperatively few applications have been reported in a relativistic context. However, the close similarities between the *second-order* Dirac equation and the non-relativistic Schrödinger equation enable the use of corresponding techniques as well in relativistic calculations [2,3]. Using Sturmian functions of the *second-order* Green's function, we give a compact explicit expression for the *first-order* Dirac Coulomb Green's function which has proven to be very useful in actual two-photon calculations.

The retarded Dirac Coulomb green's function $G_E^{(1)}$ with energy parameter E obeys

$$\left[c\vec{\alpha}\vec{p} + \beta mc^2 + U - E\right] G_E^{(1)}(\vec{r}_1, \vec{r}_2) = -\beta\, \delta(\vec{r}_1 - \vec{r}_2)\,, \tag{1}$$

where U stands for the Coulomb potential. The introduction of the projection operator on the positive energy subspace yields a second order differential equation which can be solved analogously to the non-relativistic case. Retaining the notation of Sturmian functions for the second order equation, the following expression for the Green's function of first order is obtained:

$$G_E^{(1)}(\vec{r}_1, \vec{r}_2) = \sum_{jlmnq} \begin{pmatrix} c_1 & c_2 \\ c_3 & c_4 \end{pmatrix}, \tag{2}$$

where the four coefficients c_i are

$$
\begin{aligned}
c_1 &= \frac{Z^2\alpha^2}{4q\lambda}\Big[\Big(-\frac{E(\kappa+q\lambda)}{\eta(mc^2-E)}-1+\frac{\eta-q\lambda}{\nu r}\Big)\langle\vec{r}_1|S_n^r\rangle \\
&\quad -\frac{1}{\nu r}\sqrt{(n+1)(n+2\zeta)}\langle\vec{r}_1|S_{n+1}^r\rangle\Big]\,\frac{\langle S_n^r|\vec{r}_2\rangle}{n-\eta+\zeta}\,\Omega_{jlm}(\hat{e}_1)\Omega_{jlm}^{\dagger}(\hat{e}_2)\,; \\
c_2 &= \frac{Z\alpha}{(\kappa+q\lambda)}c_1\,(-i\vec{\sigma}\hat{e}_2)\,; \\
c_3 &= \frac{Z^2\alpha^2}{4q\lambda}\frac{\kappa+q\lambda}{\alpha Z}\Big[\Big(-\frac{E(\kappa-q\lambda)}{\eta(mc^2+E)}-1+\frac{\eta-q\lambda}{\nu r}\Big)\langle\vec{r}_1|S_n^r\rangle \\
&\quad -\frac{1}{\nu r}\sqrt{(n+1)(n+2\zeta)}\langle\vec{r}_1|S_{n+1}^r\rangle\Big]\,\frac{\langle S_n^r|\vec{r}_2\rangle}{n-\eta+\zeta}\,(-i\vec{\sigma}\hat{e}_1)\,\Omega_{jlm}(\hat{e}_1)\,\Omega_{jlm}^{\dagger}(\hat{e}_2)\,; \\
c_4 &= \frac{Z\alpha}{(\kappa+q\lambda)}c_3\,(-i\vec{\sigma}\hat{e}_2)\,. \qquad (3)
\end{aligned}
$$

Here the following abbreviations are used: Ω_{jlm} denote the spherical spinor harmonics, κ is the eigenvalue of the spin-orbit operator, $\lambda=\sqrt{\kappa^2-Z^2\alpha^2}$. The index $q=\pm1$, and $\eta=Z\alpha E(m^2c^4-E^2)^{-1/2}$. The generalized Sturmian functions for the radial components of the second-order Dirac equation are

$$
\langle\vec{r}|S_n^r\rangle\equiv\sqrt{\frac{n!(2\nu)^2}{\Gamma(n+2\zeta)Ze^2}}\,(2\nu r)^{\zeta-1}\,\exp(-\nu r)\,L_n^{2\zeta-1}(2\nu r)\,, \qquad (4)
$$

where $\zeta\equiv\lambda+1/2+q/2$, $\nu\equiv(\sqrt{m^2c^4-E^2})/\hbar c$ and L_b^a denote generalized associated Laguerre polynomials.

The question of the competing influences of retardation and relativistic effects, as compared to the simpler non-relativistic dipole approximation, is still a matter of active discussion. Most discussions have dealt with single-photon ionization where it was observed that the non-relativistic dipole (angle-integrated) cross section is accurate enough far beyond its expected range of validity [4]. A commonly accepted argument to account for this property of one-photon bound-free transition amplitudes, starting from an initial s-state, is the occurrence of partial cancellations between the various contributions (retardation, multipole, relativistic,...), to the cross sections. Concerning two-photon processes, the state of the discussion is much less advanced. There is however a notable exception for Rayleigh $|1^2S_{1/2}\rangle\rightarrow|1^2S_{1/2}\rangle$ scattering amplitudes. In this case, a detailed analysis [5], indicates that the conclusions drawn from the previous analysis cannot be transposed without care, as the presence of the Green's function in the second-order amplitude modifies the interplay between the contributions of retardation and relativistic effects.

We investigate this point here in the case of the two-photon $|1^2S_{1/2}\rangle\rightarrow|2^2S_{1/2}\rangle$ absorption by comparing the results of our relativistic (retardation included) calculation with those of non-relativistic dipole, non-relativistic with retardation and relativistic dipole simplified calculations.

In table 1 the modulus of the matrix element M in atomic units (a.u.) multiplied by Z^4, which is the dependence of the leading non-relativistic dipole (NRD) contribution, is given as a function of nuclear charge Z for four selected ions of the periodic table.

Z	NRR	RD	RR
1	−1.963406	−1.963324	−1.963312
32	−1.950904	−1.871599	−1.859651
63	−1.915941	−1.608297	−1.568383
94	−1.861272	−1.174384	−1.109617

The non-relativistic dipole result is $|M_{\mathrm{NRD}}| \times Z^4 = 1.963414$ a.u.. The numerical values are converged to one part in 10^6. The non-relativistic treatment including retardation (NRR) starts to depart significantly from the dipole approximation around $Z = 25$, where the difference amounts to $\approx 0.4\%$. Regarding the influence of relativity, one notes that its overall contribution is to significantly lower the magnitude of the amplitudes when considering higher Z and, correlatively, higher frequencies. This is true for both the relativistic dipole (RD) and relativistic with retardation treatments (RR). For a given Z, the ratio of the results for the dipole approximation to the ones with retardation included, is the same to within a fraction of a percent, for both the non-relativistic and relativistic treatments.

To summarize, the results of our original calculations show that, for two-photon bound-bound transitions, relativistic contributions are indeed significant, starting even before $Z = 20$. It appears also that no significant cancellations take place when adding up the contributions of retardation and relativity. Furthermore, the overall influence of relativity is to decrease the magnitude of the transition amplitudes as compared to the usual non-relativistic dipole treatments. Such an influence is opposite to the one observed in the case of single-photon bound-free transitions, where relativistic effects tend to increase the cross sections [4].

CS acknowledges a fellowship HSP II / AUFE from the German Academic Exchange Service (DAAD) financed by the German Ministry of Education, Science, Research and Technology. This research is supported as well in part by the European Union under the HCM contract ERB CHRX CT 940 470. The Laboratoire de Chimie Physique – Matière et Rayonnement is Unité de Recherche Associée au CNRS (URA 176).

[1] see, for instance, the special issue of *J. Opt. Soc. Am.* **B 13** (1), January 1996.
[2] B. A. Zon, N. L. Manakov and L. P. Rapoport, *Yad. Fiz.* **15**, 508 (1972) [*Sov. J. Nucl. Phys.* **15**, 282 (1972)]
[3] S. A. Zapryagaev and N. L. Manakov, *Izv. Akad. Nauk SSSR* **45**, 2336 (1981)
[4] A. Ron A., I. B. Goldberg, J. Stein, S. T. Manson, R. H. Pratt, and R. Y. Yin, *Phys. Rev. A* **50**, 1312 (1994)
[5] A. Costescu A., P. M. Bergstrom Jr., C. Dinu, and R. H. Pratt, *Phys. Rev. A* **50**, 1390 (1994)

Self-Guiding Without Focusing Nonlinearity: Leaking Mode Self-Effect due to Field-Induced Saturable Ionization

A.M.Sergeev, M.Lontano*, and A.V.Kim

Institute of Applied Physics of the Russian Academy of Sciences
603600 Nizhny Novgorod, Russia
e-mail: ams@ufp.appl.sci-nnov.ru
**Istituto di Fisica del Plasma, Consiglio Nazionale delle Ricerche*
EURATOM-ENEA-CNR Association, 20133 Milano, Italy
e-mail: lontano@ifp.mi.cnr.it

Creation of elongated plasma structures for guiding of powerful ultra-short laser pulses is a challenging scientific problem and an important application in the area of superstrong field interaction with matter. Self-channeling regimes recently observed in experiments[1-4] have been attributed to the focusing nature of relativistic and Kerr nonlinearities that cause an increase of the refractive index and deviation of light rays toward stronger field regions. In the case of gas ionization at the axis of a Kerr-effect induced waveguide[3-5] the influence of focusing nonlinearity should be especially strong since it is not only to prevent the divergence of rays due to linear diffraction but also to balance refraction of radiation from the axis, that is caused by emerging plasma. Experimentally observed extra-long waveguides produced by few mJ, 100 fs laser pulses at ionization of atmospheric air[3,4] have been interpreted as plasma structures having a core where the ionization nonlinearity prevails and an outer cladding where the dominating Kerr nonlinearity generates opposite-in-sign positive variations of the refractive index and hence keeps the radiation from divergence.

In this report we demonstrate that the saturable ionizaton nonlinearity alone, without any focusing nonlinearity, is a sufficient mechanism for self-channeling of an ultrashort laser pulse. At first sight, this statement looks absurd since in accord with a common concept a nonlinearity with a growing dependence of the refractive index on the field intensity is needed for the self-guiding effect. The idea of self-guiding at defocusing ionization nonlinearity consists in the following. Owing to a strong dependence of the field ionization rate on the field intensity a laser pulse can produce a plasma distribution that is smooth near the axis and sharply bounded at the periphery of the cross-section (a plasma filament with sharp boundaries). This distribution in spite of a negative variation of the refractive index at the axis can guide an electromagnetic wave in the form of a leaking mode with exponentially small losses over the distances of many free-space Rayleigh lengths. As distinct from the common self-guiding effect where the field localization is acieved due to the total internal reflection at the periphery of a guide, in this case the quasi-localization is obtained due to a strong reflection of the trapped wave from the plasma boundary that is sharp as compared to the transverse scale (transverse wavelength) of this wave. Hence, the leakage losses are an inherent feature of the plasma waveguide though these factor may have only a minor contribution to the overall wave dissipation as compared for example to the ionization losses. Note that the leaking wave radiation has been measured in the recent experiment[4], however the authors have interpreted the observed channeling as a self-effect due to the Kerr nonlinearity.

Formation of a channel with a quasi-rectangular radial plasma profile can be facilitated in the case of saturation of the ionization, which is typical for this nonlinearity and corresponds to the complete depletion of one or several electronic states in atoms. The result of saturation is a flattening of the plasma profile near the axis and a corresponding decrease of refraction in the center of the channel where the main part of the laser energy is propagated. This regime seems easier to be implemented in single-species gases at not so high pressures when the saturation can be reached before the free electron concentration becomes too large and leaves no chance to balance the strong refraction.

A combination of two factors, a sharp dependence of the ionization rate and a strong saturation, allows us to compose a simple analytical model for the self-guiding[6]. Assuming the electron concentration to be saturated at a level N_0 everywhere inside the induced plasma waveguide with the radius a, so that $(k_0 a)^{-2} << \frac{N_0}{N_{cr}} << 1$, we obtain for the spatial decrement h of the self-trapped leaking mode the following expression

$$h \approx \frac{6}{k_0^2 a^3 \sqrt{N_0/N_{cr}}}, \qquad (1)$$

where $k_0 = \omega/c$ and $N_{cr} = m\omega^2/4\pi e^2$. For a quite powerful laser pulse focused on the gas in a spot with the size a_0 we expect that the ionized region is wider than the radiation beam, $a > a_0$. The ratio of the leakage distance $z^* = 1/h$ to the free-space Rayleigh length z_d can be presented in the form

$$\frac{z^*}{z_d}=\frac{k_0 a^3}{a_0^2}\sqrt{\frac{N_0}{N_{cr}}}. \tag{2}$$

This expression demonstrates the physical requirements for the long distance channeling $(z^*/z_d >> 1)$.

We have also performed a detailed computational study of the new self-guiding effect. For the optical field with the scalar complex amplitude E in the paraxial approximation we have used the equation

$$2ik_0\frac{\partial E}{\partial z}+\frac{\partial^2 E}{\partial x^2}+\frac{\partial^2 E}{\partial y^2}-\frac{4\pi e^2 N}{mc^2}E+ik\Gamma E=0 \tag{3}$$

that includes the factors of diffraction in the transverse (x, y) directions, ionization nonlinearity, and dissipation due to the plasma production. The electron density N has been governed by a simple dynamical equation

$$\frac{\partial N}{\partial \tau}=(N_0-N)f(|E|) \tag{4}$$

that describes the ionization with the field-dependent rate $f(|E|)$, saturated at the level N_0. The time $\tau = t-\frac{z}{V_{gr}}$ has been counted from the pulse arrival at a given point along the propagation path z. Below we present some results in the case of tunneling ionization with the well known dependence of the ionization frequency on the field amplitude[7]

$$f(|E|)=\frac{4\gamma}{\left|\frac{E}{E_a}\right|^{2n-3/2}}\exp\left(-\frac{E_a}{|E|}\right). \tag{5}$$

The values of the atomic field E_a, the quantum number n, and the frequency γ may range in wide intervals dependent on the concrete kind of the ionized species.Here we present the results obtained for $\gamma=1.2\cdot10^4/\tau_0$, n=3, $N_0=9.5\cdot k_0 a_0^2 N_{cr}$, and the collimated incident laser pulse with the Gaussian temporal and transverse distributions of intensity $|E|^2(z=0,x,y,\tau)=0.16E_a^2\exp\left[-\frac{x^2+y^2}{2a_0^2}-\frac{2\tau^2}{\tau_0^2}\right]$.

In Fig.1-3 the transverse distribution of the field intensity in the middle of the temporal profile, the transverse distribution of the plasma density after the pulse passage and the radiation frequency shift averaged over the whole profile at each cross-section point are shown for different distances from the gas boundary. The field intensity at the axis in the middle of the pulse is demonstrated in Fig.4 versus the distance z. In these pictures the self-trapping of the ionizing laser pulse in the induced cylindric plasma channel is distinctly seen.

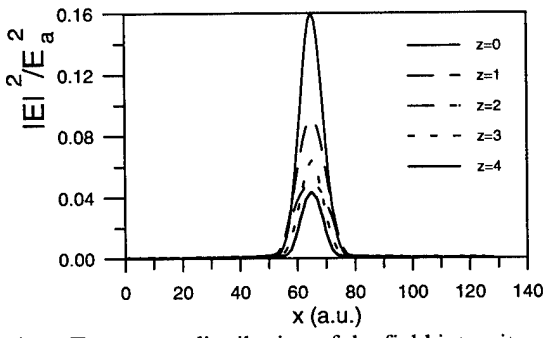

Fig.1 Transverse distribution of the field intensity in the plasma channel for different propagation distances z measured in Rayleigh lengths

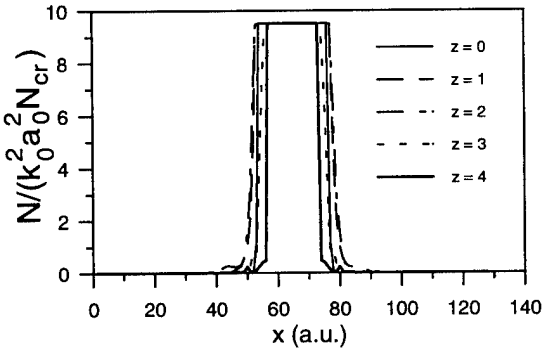

Fig 2. Transverse distribution of plasma density in the channel for different distances z measured in Rayleigh lengths.

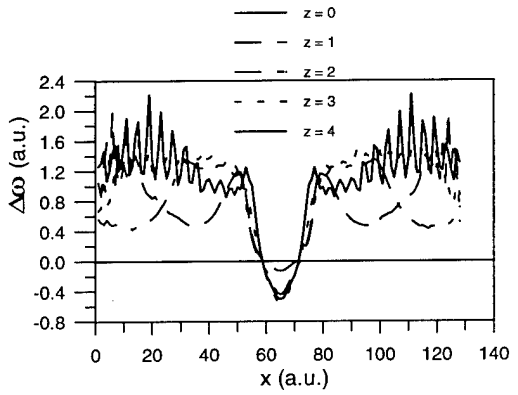

Fig.3 Radiation frequency shift averaged over the temporal pulse profile at different z measured in Rayleigh lengths.

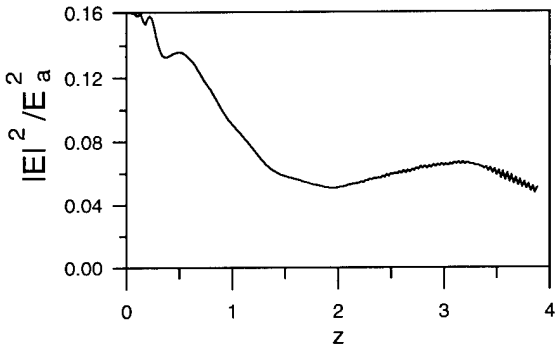

Fig.4 Field intensity at the axis of the channel in the middle of the temporal profile of the pulse as a function of propagation distanse z measured in Rayleigh lengths.

The self-guiding effect under the investigation is characterized by several remarkable features. First of all it concerns the form of the plasma filament. Due to the decrease of the intensity caused by the wave leakage, the area of the cross-section, occupied by the field capable of strong ionization, is gradually narrowing. As a result with receding from the boundary the plasma filament becomes thinner (see Fig.2) and takes ultimately the form of a sharpened needle. Hence, the decrease of the energy transmitted through the nonlinear guide is accompanied by a narrowing of the channel itself, which is rather unusual for self-guiding waves.

Another important feature that can be proved directly in an experimental observation is a specific transverse distribution of the frequency shift acquired by the guided wave. It is well known that any group element of the wave producing ionization experiences a blue shift of the frequency[8,9]. In the central part of the channel (near the axis), a strong blue shift is acquired only at the leading front of the pulse due to gas ionization to the saturation level whereas the rest major part of the pulse propagates at a fixed frequency in the pre-formed plasma. On the contrary, at the periphery of the channel the radiation increases the frequency due to a gradual ionization over the time of the full pulse duration. If one evaluates the frequency shift averaged over the pulse at different positions from the axis, a frequency gradient directed toward the channel periphery will be readily seen. This effect is even more pronounced if we take into account that short-scale (i.e. high frequency) components trapped in the channel have a greater leakage coefficient at reflection from the sharp plasma boundary as compared to the large-scale transverse components. These two factors results in a remarkable effect: the radiation frequency averaged over the pulse at the axis of the channel is decreasing in spite of the strong ionization whereas the radiation propagating at the channel periphery is essentially blue-shifted (see Fig.3).

Summarizing, we have proposed and described an unusual opportunity for self-guiding of an ultrashort laser pulse without a focusing nonlinearity. This effect is attributed to the specific properties of ionization nonlinearity in the superstrong optical fields and is promising for creating long distance plasma channels for applications.

REFERENCES

1. A.Sullivan et al., Opt.Lett., **19**, 1544 (1994).
2. A.B.Borisov et al., JOSA **B 11**, 1941 (1994).
3.A.Broun et al., Opt.Lett., 20, **73**, (1995).
4. E.T.J.Nibbering et al., Opt.Lett., **21**, 62 (1996).
5. D.Anderson et al., Phys.Rev.**E 52**, 4564 (1995).
6. A.A.Babine et al., Izv.VUSov Radiofizika, **39**, 713 (1996).
7. M.V.Ammosov et al., Sov.Phys.JETP **64**, 1191 (1986)
8. W.M.Wood et al, Opt. Lett., **13**, 984, (1988)
9. V.B. Gildenburg et al., JETP Lett., **51**, 104 (1990).

All-Optical Femtosecond Electron Acceleration

J.-K. Kim, E. Dodd and D. Umstadter
Center for Ultrafast Optical Science,
University of Michigan, Ann Arbor, MI 48109
(313) 764-2284, (313) 763-4876 (fax), dpu@umich.edu

The recent development of compact high-peak-power lasers has spurred renewed interest in electron acceleration by the use of the ultrahigh-electric-field gradients of laser-driven plasma waves [1]. In fact, the field gradient of a plasma wave has recently been demonstrated to exceed that of an RF linac by four orders-of-magnitude ($E \geq 200$ GV/m) and has been used to accelerate electrons with over 1-nC of charge per bunch in a low-emittance beam (1 mm-mrad) [2]. However, the energy spread of such beams is 100%, due to the method of injection, which is self-trapping of background electrons with random phases with respect to the accelerating buckets. In order to reduce this energy spread, it is generally thought that the required pre-acceleration can only be accomplished with a conventional RF linac. The difficulty is that the wakefield accelerating buckets are 30 fs in duration and the injection bunch must be a small fraction of that. The shortest pulses from laser-triggered photocathode RF guns are much longer, currently 0.5 ps in duration, and have jitters of more than a picosecond. Besides, RF linacs are large and expensive.

We show instead that the problem can be simply solved with an additional laser pulse, derived with a beamsplitter from the same laser. The basic idea is that once a laser wakefield is excited by one laser pulse (the pump pulse), a second injection pulse can then be used to locally alter the trajectories of some of the plasma wave electrons such that they become in phase with the wave's electric field and thus accelerated to the trapping velocity [3]. The injection pulse acts as a switch, turning on the injection at just the right time and thus producing the requisite low electron-energy-spread. We refer to the concept as Laser Injected Linear ACcelerator (LILAC). Besides the aforementioned advantages, improved electron beam emittance may result from the increased field gradient in the first acceleration stage, by minimizing the time during which electrons are non-relativistic and thus most susceptible to space charge effects. In fact, since the emittance scales inversely with the field gradient, in theory the beam emittance can may be four orders-of-magnitude lower than a conventional RF gun. Both the energetic electrons and the high-energy photons into which they can be converted have numerous industrial, medical and scientific applications. For instance, this technique produces a *single* ultrashort-duration (fs) electron or x-ray pulse (without the need for pulse selection or beam compression), which is synchronized with an ultrashort laser pulse, and thus suitable for the study of ultrafast dynamics on femtosecond timescales.

Several geometries have been considered, collinear and orthogonal injection [3]. The dephasing comes about by the action of the ponderomotive force of the injection laser and/or

it's wakefield. We present the results of fully relativistic numerical particle-in-cell (PIC) code computer simulations, which include collective effects. The latter are either one or two dimensional spatially and three dimensional in velocity space.

The pump pulse has wavelength 1 μm, and pulse length 10 μm, or 33 fs. The injection pulse is linearly polarized such that its magnetic field is set to be parallel to that of the pump pulse. The injection pulse has a spatial profile given by a Gaussian shape with a spot radius of 5 μm. The spatial domain size for the simulation is $10\lambda_p$. A simulation was run with $a_0 = 1$ ($\phi = 0.7$). The position and the intensity of the injection pulse were varied in order to find the optimal trapping threshold intensity. Fig. 1 shows the velocity of one of these trapped electrons as a function of time, along with the phase space trajectory plotted in the inset of Fig. 1. A value of $b_{\rm th} = 1.6$ was found by increasing b_0 until we obtain one or more trapped electrons. As can be seen in Fig. 1, the gradual velocity-dephasing along the z direction by the injection pulse gave the electron enough boost for trapping.

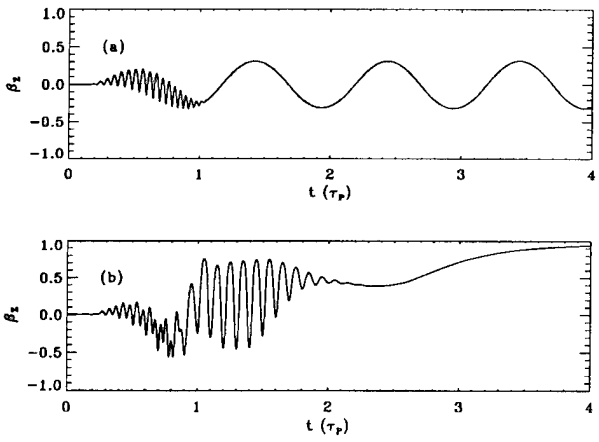

Figure 1: (a) Velocity of an electron in the plasma wave without injection pulse and (b) velocity of an electron that becomes trapped plotted as a function of time (in unit of a plasma period τ_p).

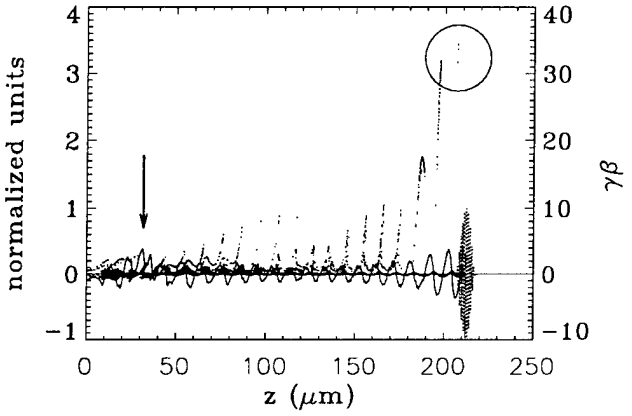

Figure 2: A PIC simulation with an injection pulse of $b_0 = 2.0$; shown are: the pump intensity **a**, the wake field, and the longitudinal momentum $(\gamma\beta)_z$ of a number of the simulation electrons.

Fig. 2 shows the output from a simulation with $b_0 = 2$; shown are: the pump intensity **a**, the wakefield, and the longitudinal momentum $(\gamma\beta)_z$ of a number of the simulation electrons. The field of the pump and the wake are normalized to the quiver velocity. The pulse width of the injection pulse is equal to τ_p. The normalized momentum $(\gamma\beta)_z$ distinguishes the electron beam from fast background electrons. Electrons that are not trapped by the second bucket (circled), 70 fs behind the pump pulse, fall into the next buckets. The plasma wave appears to be damped by beam loading. The average field gradient is 0.85 GeV/cm, which is 85% of the maximum field gradient, 1 GeV/cm. Of course, a longer acceleration

distance results in a narrower energy spread, both in absolute terms (from bunching) and relative terms, from higher final energies. For instance, the trapped electrons eventually obtain an average energy of 100 MeV, with an energy spread of 0.3%. We estimate a value of greater than 10^7 for the number of trapped electrons. In another simulation, by use a second anti-resonant pump pulse to create only a single acceleration bucket, we have eliminated the electrons that get trapped in the later buckets. The lilac electron beam parameters are summarized in Table 1.

$\varepsilon_{\perp n}$	$.16\pi$ mm·mrad
$\varepsilon_{\parallel}$	$.3 \times 10^{-9}$ eV·sec
τ_b	1.3 fs (.4 μm)
$\Delta E/E$@100 MeV	0.3%
n_b	1.5×10^7 per bunch (2 pC)

Table 1: A summary of lilac electron beam parameters.

References

[1] T. Tajima and J. M. Dawson, Phys. Rev. Lett. **43**, 267 (1979).

[2] D. Umstadter, S.-Y. Chen, A. Maksimchuk, G. Mourou, and R. Wagner, Science **273**, 472 (1996).

[3] D. Umstadter, J. K. Kim, and E. Dodd, Phys. Rev. Lett. **76**, 2073 (1996).

High-intensity subfemtosecond sub-cycle pulses, solitons and shock waves *via* cascade SRS and "EM-bubbles" generation

A. E. Kaplan (*) and P. L. Shkolnikov

Dept. of Electr. & Comp. Eng., The Johns Hopkins University, Baltimore, MD 21218
Tel:(410) 516-7018, Fax:(410) 516-5566; e-mail: sasha@super.ece.jhu.edu

** also at Abteil. Quantenphysik, Univ. Ulm, Germany, on sabbatical leave from JHU, till Feb.'97*
ph: ++49 (731) 502-3079; fax: ++49 (731) 502-3086; e-mail: kap@physik.uni-ulm.de

We review here our recent work on the formation of extremely powerful near- and subfemtosecond (sub-*fs*) pulses based on two new principles:

- The phase-locking [1] of multiple components of stimulated cascade Raman scattering (CSRS), that can produce an almost periodic train of powerful sub-*fs* pulses, with pulses as short as ~ 0. 2 *fs* and spaced by ~ 8 *fs*.
- The generation of powerful "EM-bubbles" (EMBs) [2], unipolar very short solitary pulses of EM-radiation propagating in a gas of two-level or classically nonlinear atoms. This effect can generate a single EMB, or a few EMBs with controllabe parameters, easily separable into individual EMBs.

Using available sources [lasers and existing half-cycle pulses (HCPs) in terahertz domain], one can attain $\sim 10^{-16}\ s$ (or $\sim 0.1\ fs$) long pulses with the intensities up to $10^{14} - 10^{16}\ W/cm^2$. These are sub-cycle (in particular, unipolar, or half-cycle) solitons or soliton-like pulses which can exist in both quantum and classical nonlinear systems. Most of them were obtained as the exact solution of full 1D Maxwell and full either Bloch (without rotating wave approximation) or nonlinear classical oscillator equations.

CSRS (known for many years [3]) is a process whereby laser light with the frequency ω_L, propagating in the Raman-active medium with the Raman frequency, ω_R, $\omega_R \ll \omega_L$, excites many cascade-induced Stokes and anti-Stokes components with the frequencies

$$\omega_j = \omega_L + j\omega_R\,; \quad j = \pm 1,\ \pm 2,\ \pm 3 \ldots .$$

The idea of using multi-frequency CSRS for generating sub-*fs* pulses is based on CSRS having tremendously broad spectrum, with up to ~15-20 ***equidistant*** lines being spread from far infrared to very far ultraviolet, and having very high (up to 40%) conversion efficiency. If all these CSRS components were properly phased-locked, this broad spectrum radiation could result in time-domain in the train of sub-*fs* pulses, with each of individual pulses having the length (time duration) of the order of half-cycle of the highest-frequency component, ω_{max} (which can be much shorter the cycle length of the pump radiation), and extremely high intensity. This sub-*fs* pulse train would then have spacing $\Delta\tau$ between pulses, the length of an individual pulse, τ_p, and (ideally) the ratio of the pulse intensity, I_p, to that of a laser, I_L, as:

$$\Delta\tau \approx \pi/\omega_R\,; \quad \tau_p \approx \pi/\omega_{max}\,; \quad (I_p/I_L) \sim (\omega_{max}/\omega_R)^2 .$$

The main problem to be solved is to "lineup" the multiple CSRS components, i. e. to phase-lock them and force them to propagate with the same group velocity to overcome walk-off effect. All the participating CSRS components interfere coherently only if they overlap in space/time over sufficiently long path; however, their linear group velocities over such a large spectral stretch can be substantially different, which may result in a strong walk-off effect.

We have recently shown [1,4] that this problem can be solved by the feasible formation of multi-component CSRS solitons, whereby all the CSRS components are mode-locked within a 2π soliton (a multi-photon generalization of self-induced transparency solitons), and thus they propagate with the same group velocity. These solitons have a new, Lorentzian intensity profile, the same for all the CSRS components. (Note that ***all*** the frequency components of the

new soliton are so called bright solitons.) The set of the Maxwell equations for the field components interacting through the Raman transition, and the Bloch equations generalized in application to multiple two-photon processes, were solved by us analytically [1]. In general, they give rise to a rich family of solutions: solitary waves, stationary traveling fronts, bright and dark solitons, periodic stationary waves, etc. Bright solitons are fundamental eigensolitons of this family of solutions. In the case of hydrogen gas (with $\lambda_0 \approx 2.4\ \mu m$) pumped by the third harmonics of Ti:Sapph laser ($\lambda_L \approx 0.28\ \mu m$), exciting 12 CSRS components, the total mode-locked field consists of the train of sub-fs pulses, each ~0.2 fs long, spaced by ~8 fs and having the peak intensity of up to $10^{14} - 10^{15}$ W/cm^2.

The cross-sections of stimulated Raman scattering (and CSRS) are directly related to the probability of two-photon interactions, and thus to the quantum levels other than (two-level) Raman transition (for example, SRS is prohibited in an ideal two-level atom); furthermore, they are most efficient when the resonant dipole interaction of light with Raman transition is prohibited. However, two-level systems with strong dipole momentum that can be excited by EM-field directly through a single-photon interaction, proved to be equally capable of producing high-intensity non-envelope EM-pulses.

We showed [2] that atomic gasses can support solitary pulses of unipolar, non-oscillating EM-field ("EM-bubbles") of up to atomic and even larger amplitude with their length ranging from ~10^{-9} s to ~10^{-16} s, which propagate without dispersion and are stable and insensitive to the change of gas density. As a result of nonlinear propagation in two-level media, these pulses can be transformed into single non-envelope solitons. The theory of these pulses based again on full Maxwell equation and full Bloch equations for two-level system (solved exactly, without using rotating wave approximation, similarly to super-driven two-level atom [5]), gives exact soliton solution for these pulses [6], [2]). However, the use of a two-level model is limited by the amplitudes smaller than an atomic unit.

As the EMB field approaches the atomic field, the ionization potential dominates the EMB formation, limiting EMB length and amplitude. With the amplitudes approaching photoionization, the atom can be considered as an almost classical object, with the appropriately chosen potential. In this case Bloch equations are to be replaced by a classical equation for the electron motion. We have found analytical soliton solution (in quadratures) for an ***arbitrary*** classical potential. A rough idea about feasible numbers can be given by an example with a classical "box" potential of the ionization potential U_0, and the width, $2x_0$. The EM-bubble maximal field strength, E_{max}, and shortest pulse length, τ_{min}, due to over-the-barrier ionization, are then:

$$\tau_{min} = (x_0/c)\sqrt{m_e c^2/2U_0}\,; \quad E_{max} = U_0/ex_0\,;$$

which for $x_0 = 1$ Å and $U_0 = 13\ eV$ gives $E_{max} \sim 1.3\times10^9\ eV/cm$ ($I \sim 5\times10^{15}\ W/cm^2$), and $\tau_{min} \sim 0.5\times10^{-16}\ s$. For an atom with a given U_0 and atomic number, Z, we have $x_0 \sim r_e Z(mc^2/U_0)$, and

$$\tau_{min} \sim (2r_e Z/c)\times(mc^2/U_0)^{3/2}\,; \quad and \quad E_{max} \sim (U_0/mc^2)^2\times(mc^2/er_e Z);$$

here $r_e = e^2/m_e c^2$ is the classical electron radius. Assuming $U_0 \approx 24\ eV$ and $Z=2$, as in He, one obtains: $\tau_{min} \sim 0.1$ fs, $E_{max} \sim 2\times10^9$ V/cm.

One of the ways to generate EMBs is to use existing HCPs to launch much shorter EMBs in a nonlinear medium. We found that, given the amplitude, E_0, and length, t_0, of the incident HCP, a threshold (minimal) amplitude of HCP required to attain a single EMB, is $E_{thr} = 2\hbar/t_0 d$, where d is a dipole moment of a two-level system; for Xe and $t_0 \sim 400$ fs, $E_{thr} \approx 60\ KV/cm$. In our most recent work [7] we showed that the strongest (and fastest) EMB, EMB-precursor, has its amplitude, E_{EMB}, and length, t_{EMB}, as:

$$E_{EMB} \approx 2E_0 - E_{thr}\,, \quad t_{EMB} \approx t_0\,/\,(t_0 E_0 d/\hbar - 1).$$

Thus, to attain intense and short EMBs, there is no need to use a very short incident HCP pulse; the only prerequisite is a sufficiently high amplitude of HCP. We also found that, in the case when more than one EMB is generated, their total number is proportional to the incident HCP area, $E_0 t_0$, and the distance of the first EMB formation is inversely proportional to E_0^3.

We have found that atomic gasses can also support an EM shock wave (a precursor of *dc*-ionization), with its amplitude close to the atomic unit. We found an exact solution for such a wave and showed that the front duration can again be in the vicinity of 0.1 fs. A shock-like wave can appear even in a non-ionizing wave, if the number of EM-bubbles is sufficiently large (more than 6-8); moving with different speeds, the EM-bubbles, due to constructive interference form a semblance of shock wave, which after some distance breaks info individual EM-bubbles.

The domain of sub-*fs*, EM-pulses of non-oscillation nature, with the intensities approaching or exceeding 1 *au*, is largely new and unchartered territory. The familiar effects associated with coherent light-matter interactions are likely to take on entirely different forms. We demonstrated recently [8,9] the feasibility of a qualitatively new quantum effect, backward and multi-echo field ionization, in the interaction of new pulses with atoms and quantum wells. We explain this effect [8,9] by a simple, "resonator-like" picture of the phenomenon.

Feasible applications of new "superpulses" range from research tools and novel spectroscopies to medical imaging and other X-ray-emulating imaging techniques. We briefly discuss time-resolved spectroscopy of transient chemical processes, e. g. dissociation and autoionization -- on a *fs* time scale, in particular, quantum control of chemical transformation; frequency upconversion due to large Doppler shift of a counter-propagating light backscattered by high-gradient refractive index in superpulses or shock waves; a "global" spectroscopic technique *via* a shock-like excitation across the entire atomic spectrum; the ionization by a pulse shorter than the orbital period which would bridge a gap between conventional field ionization and collisional ionization by a particle, etc. Based on differential transparency for these new pulses, new imaging techniques can be envisioned, such as monitoring of processing of high-density computer chips, screening food products and luggage in the airports and concealed weapons; medical tomography, etc. With 8 fs-spaced trains of superpulses one can also envision *Petahertz* time-domain spectroscopy; ***stroboscopic imaging*** of the expansion of solid-density laser plasma for the diagnostics of inertially-confined fusion and X-ray lasing; X-ray production at surfaces by sub-*fs*-pulses (*via* formation of fast electrons and Bremsstrahlung radiation of these electrons in solids), These pulse trains hold also a promise of communication speed approaching *Terabit*/s (10^{15} *bit*/s).

This work is supported by AFOSR. AEK is also a recipient of Alexander von Humboldt Award by the AvH Foundation of Germany.

[1] A. E. Kaplan, Phys. Rev. Lett. 73, 1243 (1994).

[2] A. E. Kaplan and P. L. Shkolnikov, Phys. Rev. Lett. 75, 2316 (1995).

[3] R. W. Terhune and P. D. Maker, Phys. Rev. 137A, 801 (1965).

[4] A. E. Kaplan, P. L. Shkolnikov, and B. A. Akanaev, Opt. Lett. 19, 445 (1994).

[5] A. E. Kaplan and P. L. Shkolnikov, Phys. Rev. A. 49, 1275 (1994).

[6] R. K. Bullough and F. Ahmad, Phys. Rev. Lett. 27, 330 (1971).

[7] A. E. Kaplan, S. F. Straub, and P. L. Shkolnikov, submitted to Opt. Lett.

[8] A. E. Kaplan and P. L. Shkolnikov, in *Advanced Program of the OSA Annual Meeting* , Rochester, 1996, ThHH1; also in in *Abstracts of ICOMP VII* , 1996, A52.

[9] P. L. Shkolnikov and A. E. Kaplan, ***this conference***,

Backward and multi-echo field ionization by intense non-envelope "superpulses"

P. L. Shkolnikov and A. E. Kaplan *

Electrical and Computer Engineering Department

The Johns Hopkins University, Baltimore, MD 21218

Tel. (410) 516-7220 FAX (410) 516-5566 e-mail peter@super.ece.jhu.edu

* *also at Abteil. Quantenphysik, Univ. Ulm, Germany, on sabbatical leave from JH U, till Feb.'97 ph: ++49 (731) 502-3079; fax: ++49 (731) 502-3086*

Recently, we have proposed two avenues to generating ultrashort (potentially, sub-femtosecond) and intense (up to atomic fields) nonoscillating pulses: a high-repetition train of such pulses can be produced in multicomponent stimulated Raman scattering [1], and a single pulse ("electromagnetic bubble" -- EMB) or several of them can result [2,3] from the propagation of an initially broad unipolar pulse (half-cycle pulse -- HCP [4]) in an appropriate nonlinear medium. Such pulses could cause a substantial "shake-up" excitation or ionization of an atomic system within the time much smaller than any characteristic time of the system. These "superpulses" would open a new chapter in nonlinear optics and atomic and molecular physics, both as a new probing tool and a source of new effects. In the present paper, we consider one of them: backward and multi-echo field ionization [5].

According to the above definition, the HCPs [4], with their duration of about half of a picosecond, could be approximated as superpulses for highly excited Rydberg atoms. In fact, research on HCP ionization of Rydberg atoms [4,6] has already revealed many drastic differences with atomic ionization by oscillating optical fields. Superpulses capable of impulse-field ionization of a single low-lying atomic eigenstate may produce new effects of essentially quantum nature. One such effect is multiple ionization "echoes"; we theoretically show that photoelectrons born by unipolar superpulse field ionization, would be emitted in several, well-separated in space and time bunches, in both forward and backward directions.

As the most fundamental example, we consider a hydrogen atom ionized from its ground state by an EMB. Treating the interaction as instantaneous, and therefore modeling the electric field of the pulse by the Dirac δ –function, $\vec{E} = \vec{E}_0\,\delta(t)$, one immediately obtains a simple relation between the initial (before the pulse, at $t = 0-$), Ψ_0, and "after-kick", Ψ, wavefunctions as

$$\Psi(\vec{r}, 0+) \approx exp(i\vec{q}\vec{r})\Psi_0(\vec{r}, 0-), \quad \vec{q} = \vec{E}_0, \tag{1}$$

where $\vec{q}$ is the momentum transfer in atomic units. The modifying term, $exp(i\vec{q}\vec{r})$, is, in fact, independent of the particularities of the quantum system, due to δ-kick [7], and was used in so-called impulse approximation in collision theory and lately in the theory of HCP ionization [8,9]. Further, after-kick, evolution of the wavefunction $\Psi(\vec{r}, 0+)$ is determined by the unperturbed Coulomb hamiltonian H_0. In particular, the spatial density of the photoelectron cloud is described by $|\Psi_{ion}(\vec{r}, t)|^2$, the wavefunction $\Psi_{ion}(\vec{r}, t)$ being determined by the exact (within the impulse approximation) expression:

$$\Psi_{ion}(\vec{r},t)=\int d\vec{k}\, a_{\vec{q}}(\vec{k})\psi_{\vec{k}}(\vec{r})\, exp(-itk^2/2)\ ,\ a_{\vec{q}}(\vec{k})=\int d\vec{r}\,\psi^*_{\vec{k}}\Psi(\vec{r},0+) \qquad (2)$$

where $\psi_{\vec{k}}(\vec{r})$ is an eigenfunction of H_0 for the positive energy $k^2/2$. Calculated according to Eq. (2), the spatial distribution of the photoelectrons along the direction of the momentum transfer is shown in Fig. 1a at $t=5$ *a. u.* after the superpulse with $E_0=0.4$ *a. u.* and duration $\tau_0 \ll 1$ *a. u.* interacted with a hydrogen atom in the ground state. One can easily see a sequence of well-separated peaks resulting in strong spatio-temporal inhomogenuity of the photoelectron cloud. These multiple ionization echoes may be observed using e. g. the imaging technique [10].

Another example considered by us is an electron in a one-dimensional quantum well. The superpulses required could be relatively long for shallow wells. In Fig. 1b, a distinctive double-echo is seen in the computer simulation of the ionization of an electron from the ground state of a model quantum well (0.1 *eV* deep, *140* Å wide), by a *4* fs-long unipolar pulse of *350* kV/*cm* amplitude.

This effect can be explained by a simple, "resonator-like" picture of the phenomenon. Immediately after a δ-kick, the wavefunction corresponds to a moving particle with the average momentum determined by the momentum transfer. The consequent (quantum) motion of this particle is in effect a chain of scatterings off the walls of the atomic potential. During each scattering, part of the wavefunction "splashes out" over the edge of the potential, which is reminiscent of the short EM pulse part of which is radiated away through a semi-transparent mirror of a resonator. This creates an electron bunch propagating in "forward" direction. At the same time, part of the wavefunction is reflected, leading, after the next scattering, to a bunch propagating in the opposite, backward, direction. This results in a series of photoelectron peaks moving alternatively in the forward and backward directions, with steadily diminishing amplitudes.

In conclusion, we demonstrate the feasibility of a qualitatively new quantum effect, backward and multi-echo field ionization, in the interaction of superpulses with atoms and quantum wells.

This work is supported by AFOSR; AEK is a recipient of Alexander von Humboldt Award by the AvH Foundation of Germany.

References

[1] A. E. Kaplan, Phys. Rev. Lett. 73, 1243 (1994); A. E. Kaplan and P. L. Shkolnikov, JOSA B 13, 412 (1996).

[2] A. E. Kaplan and P. L. Shkolnikov, Phys. Rev. Lett. 75, 2316 (1995); also in Int. J. of Nonl. Opt. Phys. & Materials, 4, 831 (1995); A. E. Kaplan, S. F. Straub, and P. L. Shkolnikov, to appear in Opt. Lett.

[3] P. L. Shkolnikov and A. E. Kaplan, in Proceedings of this Topical Meeting.

[4] R. R. Jones, D. You, and P. H. Bucksbaum, Phys. Rev. Lett. 70, 1236 (1993).

[5] A. E. Kaplan and P. L. Shkolnikov, in *Advanced Program of the OSA Annual Meeting* , Rochester, 1996.

[6] C. O. Reinhold, H. Shao, and J. Burgdorfer, J. Phys. B 27, L469 (1994).

[7] L. D. Landau and E. M. Livshits, *Quantum Mechanics* (Academic Press, NY, 1966), Ch. VI.

[8] P. Krtic and Y. Hahn, Phys. Lett. A 192, 47 (1994).

[9] A. E. Kaplan and P. L. Shkolnikov, in *Abstracts of ICOMP VII* , 1996, A52.

[10] H. Helm, N. Bierre, D. L. Huestis, and M. Saead, Phys. Rev. Lett. 70, 3221 (1993).

Fig. 1. Multiple ionization echoes in superpulse ionization.

(a) Spatial distribution of the photoeletrons along the direction of the momentum transfer at $t=5$ *a. u* after the ionization of a ground-state hydrogen atom by a superpulse with the amplitude $E_0=0.4$ *a. u.* and duration $\tau_0 << 1$ *a. u.*. The atom is located at $z=0$.
(b) One-dimensional photoelectron distribution after superpulse ionization of an electron from the ground state of a model quantum well (0.1 *eV* deep, *140* Å wide) by a *4* fs-long unipolar pulse of *350* kV/*cm* amplitude. x is in units of well width, the well is located at $x=0$.

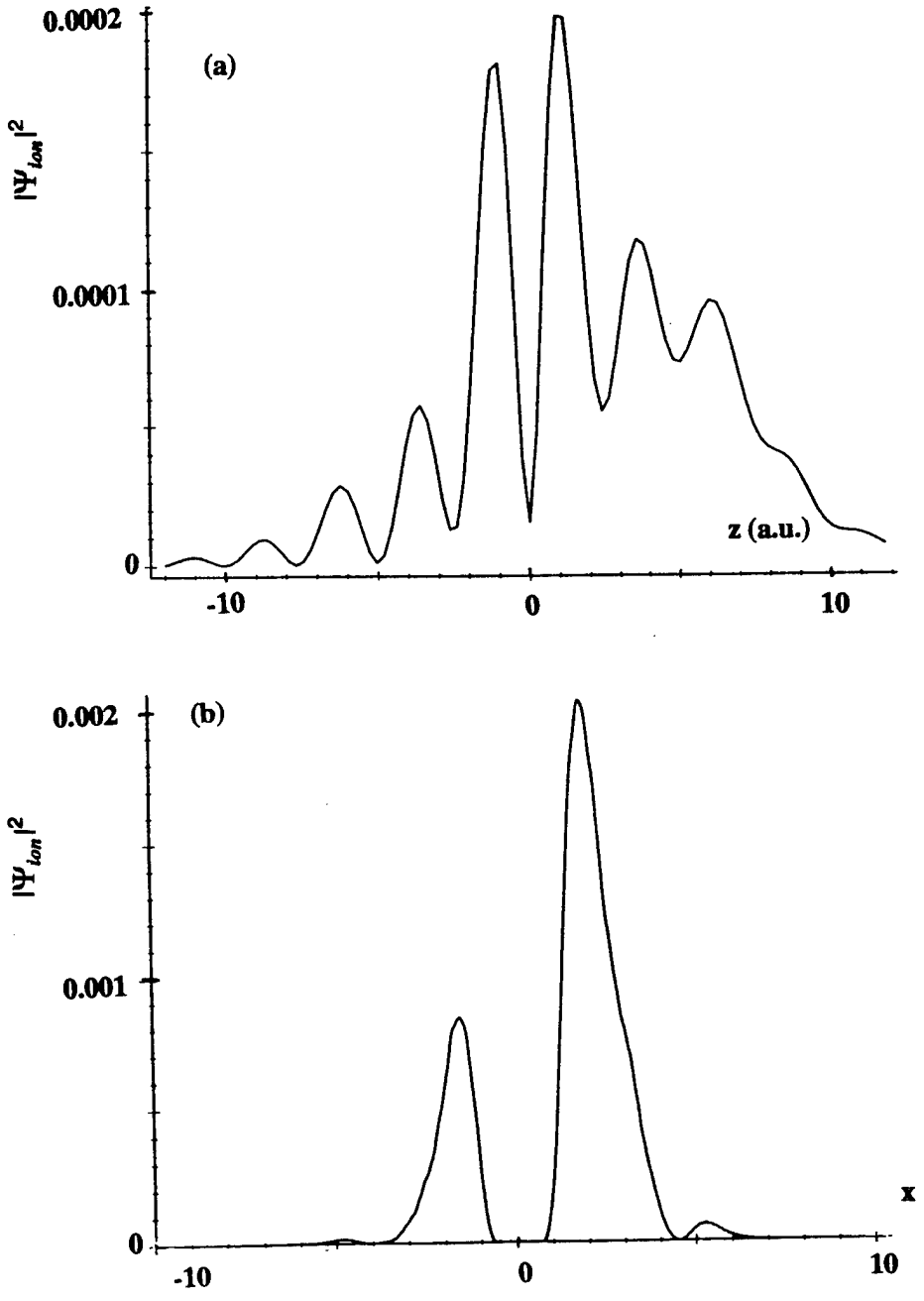

Absorption of high intensity femtosecond laser pulses in solids and the production of suprathermal electrons

T. Feurer, W. Theobald, R. Sauerbrey
Institut für Optik und Quantenelektronik, Friedrich-Schiller-Universität
Max-Wien-Platz 1, D-07743 Jena, Germany, Tel.: 03641-636281
I. Uschmann, D. Altenbernd, U. Teubner, P. Gibbon, E. Förster
Max-Planck-Gruppe: Röntgenoptik, Friedrich-Schiller-Universität
Max-Wien-Platz 1, D-07743 Jena, Germany
G. Malka, J.L. Miquel
Commissariat a l'Energie Atomique, Centre d'Etudes de Limeil-Valenton,
94195 Villeneuve-Saint-Georges Cedex, France

Femtosecond high power laser systems offer the posibility to create plasmas with high electron densities and short scale lengths at relatively moderate energies. One possible application of such lasers is the recently proposed 'fast ignitor' [Tab94]. The basic idea of this scheme is to seperate the compression phase from fuel ignition that leads to lower requirements on the driver lasers. After compressing the fuel by a factor of several hundred the ignition is performed by a burst of electrons that are created by an intense subpicosecond laser pulse. Such suprathermal electrons can be produced by several mechanisms. For laser intensities where the quiver energy equals or even exceeds the electron rest energy $m_e c^2$, relativistic effects become important. Now magnetic fields are no longer negligible and the longitudinal component of the Lorentz force accelerates electrons in the longitudinal direction [Wil92]. The experiments were performed with the frequency doubled P102 laser at CEA/L-V in Limeil. The laser delivers up to 8 J in about 300 to 400 fs at 528 nm. The conrast ratio is better than 10^{12}, therefore no preplasma, even at the highest intensity, is created on the target surface before the main pulse. The pulses were focused using an off-axis parabola leading to a minimum focal spot size of 5 μm. The central spot contained about 20 % of the full energy on target, the maximum intensity therefore was about $2 \cdot 10^{19}$ W/cm^2 . The remaining part of the energy is distributed over a large spot.

For the absorption measurements the targets were 0.9 μm aluminium evaporated on glass substrates. The absorption measurements were performed for s- and p-polarized light and for a variety of angles of incidence. The fraction of the absorbed energy was determined by measuring 1) the fraction of backscattered light 2) of specular reflected light and 3) of diffuse reflected light. The diffuse reflected light was collected by an Ulbricht sphere and the linearity of the sphere has been carefully checked prior to the measurements.
The absorption at $2 \cdot 10^{19}$ W/cm^2 for the different directions of polarization is only slightly different and peaks at 25 deg reaching values of about 40 to 45 % for p-polarized light (see figure 1). In figure 2 the ratio of diffuse and specular reflected light as a function of the incident laser intensity is displayed.

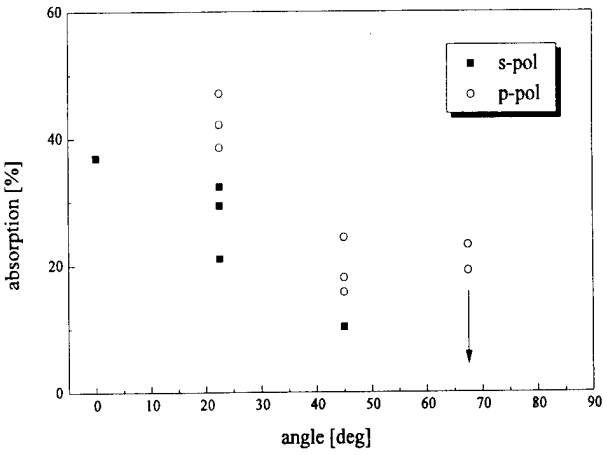

Figure 1: *Absorption as a function of the angle of incidence for s- and p-polarized light.*

The plot contains all data points measured at 22.5 and 45 deg for s– and p–polarized light. It can be seen that the fraction of the diffuse reflected light increases dramatically with intensity indicating that holeboring may play an important role.

In order to characterize the bursts of suprathermal electrons produced during laser irradiation two detector arrangements were used. First a 0.4 to 3 MeV electron spectrometer with six channels where the energy window of each channel is about 100 keV. Second, a 'von Hamos' spectrometer with cylindrically bent Lithiumfluoride crystals of (200) and (420) orientation was used to measure the K_α emission of thin foil targets. The targets were various combinations of thin metal foils. For a target of 400 nm aluminum evaporated on a 7.6 μm copper foil and assuming a Maxwellian electron distribution the temperature of the suprathermal electrons obtained from is 420 keV. The total number of electrons is about 10^9 sr^{-1} and the total energy carried by the electrons is estimated to 0.6 mJ.

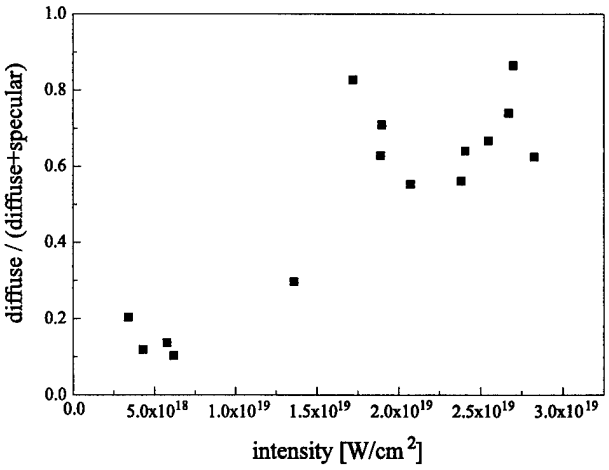

Figure 2: *Ratio of diffuse reflected and diffuse plus specular reflected light.*

In order to characterize the suprathermal electrons by detecting the K_α emission of multilayer targets [Rou92] the following target combinations have been used: Ni/Cu/Zn, Zn/Ni/Cu, Cu/Zn, and Cu. In practice the experimental results were compared to simulations which consider the K_α line production by electrons penetrating the target with energies from 10 keV up to 1 MeV. For all target combinations only the K_α line radiation originating from the top layer has been observed. Although the excitation energy of the K–shell of the three elements is different, for all lines the number of photons emitted from the target was on the order of $0.7 \ldots 1.5 \cdot 10^{12}$ photons per shot. Due to the fact that no K_α line radiation from the second or third layer has been observed and assuming the electrons are penetrating almost perpendicular with respect to the target surface, the energy of the electrons producing the major part of the x–ray photons is lower than 60 keV (top layer: Cu) and lower than 90 keV (top layer: Ni). It should be mentioned that the number of electrons observed with the electron spectrometer is to low to produce enough photons which could be detected with the von Hamos spectrometer. Even if one assumes that the detected electrons belong to the high energy wing of a Maxwellian distribution with a temperature of 420 keV their number is to small to produce a detectable signal. Taking into account an average conversion efficiency of $\eta = 0.8$ % (for the conversion of electrons between 10 keV and 90 keV to K_α photons, which is the result of the simulation) the number of electrons produced per laser shot is on the order of $(0.9 \ldots 1.9) \cdot 10^{14}$. From that it is possible to calculate a conversion efficiency of the absorbed laser energy into suprathermal electrons of about 50 % and a conversion efficiency into K_α radiation of 0.4 %. This result might be explained by the fact that about 80 % of the laser energy has been focussed to an intensity much lower than $2 \cdot 10^{19}$ W/cm^2 resulting in a large number of electrons with lower energies than the ones detected by the electron spectrometer. Another explanation could be a non–isotropic emission of the suprathermal electrons, such that the major part of the electrons is emitted parallel to the target surface.

In order to further characterize the electrons contributing to the K_α production by electron impact, targets consisting of two layers, namely aluminum (100 nm to 1700 nm) on copper (7.6 μm) have been used. The Cu–K_α intensity has been recorded as a function of the thickness of the aluminum layer. For aluminum layers thicker than about 0.5 μm no Cu–K_α radiation can be detected. This result would be consistent with the simulations if the energy of the electrons is

lower than 15 keV. But in this case the extremely small conversion efficiency into K_α radiation would yield a conversion efficiency of laser energy to electron energy in excess of 100 %. An explanation of this effect could be that there is a strong electron velocity component parallel to the target surface which was also observed many years ago. With this assumption the extracted electron energy can be much larger than 15 keV and the conversion efficiency of laser energy to electron energy would be on the order of the observed values.

In addition to the above mentioned detectors two scintillator arrangements were used to measure the hard x–ray radiation in the energy range of 60 keV up to about 1 MeV. Aluminum targets evaporated on a glass substrate were used under various angles of incidence of p– and s–polarized laser light. The measurement of both detectors yielded an averaged total energy of hard x–rays of some μJ in the mentioned energy range. This corresponds to a conversion efficiency of the incident laser energy into hard x–rays of about 10^{-7}. The efficiency was derived under the assumptions of an isotropic radiating source and a Maxwellian velocity distribution of the suprathermal electrons in the plasma with a characteristic temperature of 420 keV. The energy coupling into hard x–rays is several orders of magnitude lower compared to other experimental results [Kme92]. The hard x–ray emission is due to bremsstrahlung from suprathermal electrons decelerated in the solid density plasma. The conversion efficiency η from electron kinetic energy E_k into energy E_x of bremsstrahlung radiation can be estimated for a Maxwell distribution according to with $\eta = E_x/E_k = 1.65 \cdot 10^{-9} Z k_B T_h$, where Z is the atomic number. For aluminum ($Z = 13$) and a characteristic temperature of 420 keV this yields an efficiency of $\eta = 0.9$ % for the bremsstrahlung production. Therefore, only about 10^{-4} of the laser energy contained in the central spot is converted into suprathermal electrons.

References

[Tab94] M. Tabak, J. Hammer, M.E. Glinsky, W.L. Kruer, S.C. Wilks, J. Woodworth, E.M. Campbell, M.D. Perry, R.J. Mason: Phys. Plasmas **1**, 1626 (1994)

[Wil92] S.C. Wilks, W.L. Kruer, M. Tabak, A. Langdon: Phys. Rev. Lett. **69**, 1383 (1992)

[Har79] J.D. Hares, J.D. Kilkenny, M.H. Key, J.G. Lunney: Phys. Rev. Lett. **42**, 1216 (1979)

[Kme92] J.D. Kmetec, C.L. Gordon, III, J.J. Macklin, B.E. Lemoff, G.S. Brown, and S.E. Harris: Phys. Rev. Lett. **68**, 1527 (1992)

Absolute measurement of the spectral brilliance of a subpicosecond UV-laser induced soft x-ray source

R. Häßner, W. Theobald, and R. Sauerbrey

Institut für Optik und Quantenelektronik, Friedrich-Schiller-Universität Jena, Max-Wien-Platz 1, D-07743 Jena, Germany

Phone:+49-3641-636281, Fax:+49-3641-636278, Email: sauerbrey@qe.physik.uni-jena.de

D. Altenbernd, U. Teubner, and E. Förster

Max-Planck-Arbeitsgruppe Röntgenoptik an der Friedrich-Schiller-Universität Jena, Max-Wien-Platz 1, D-07743 Jena, Germany

T. Wilhein, B. Niemann, and G. Schmahl

Forschungseinrichtung Röntgenphysik, Georg-August-Universität Göttingen, Geiststraße 11, D-37077 Göttingen, Germany

We have investigated the spectral brilliance of subpicosecond UV-laser-plasmas as a source for the soft x-ray microscopy in the so-called 'water-window'. The spectral range between the absorption K-edges of carbon (4.36 nm) and oxygen (2.32 nm) is termed 'water-window' . The absorption coefficient of both materials differ by one order of magnitude providing a high contrast of the biological samples in their natural environment [1].

The measurements were performed by a newly developed absolutely calibrated soft x-ray spectrograph with a resolution of $\lambda/\Delta\lambda \approx 1000$ at 2.4 nm. The imaging optics and the dispersive element are unified into a single elliptical off-axis reflection zone plate. The zone plate with a focal length of 1 m consists of two stripes (each 1×8 mm^2) with a total number of about 7000 line pairs. The absolute calibration was performed at the BESSY Synchrotron radiation source at Berlin. Additionally, other soft x-ray transmission grating spectrographs (TGS) were cross calibrated. The TGS consists of a toroidal nickel coated mirror, a free standing gold transmission grating and a microchannel plate detector [2]. The soft x-rays were produced by

subpicosecond KrF-laser pulses (20 mJ, 0.7 ps) with a wavelength of 248.5 nm focused to an intensity exceeding 10^{16} W/cm^2 onto carbon and boron nitride targets. These low Z materials produce a strong K-shell line and continuum radiation in the wavelength range from 2 to 4 nm. The ratio between line and continuum radiation strongly depends on the initial plasma parameters and can be controlled by the angle of incidence and the laser intensity [3].

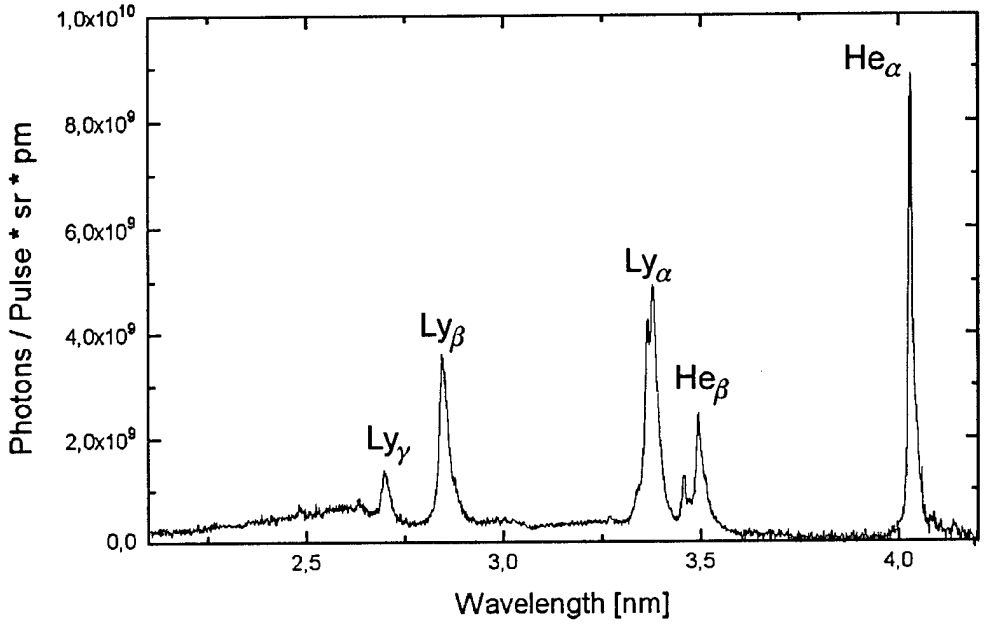

Fig. 1: Highly resolved soft x-ray spectrum of carbon obtained by the novel zone plate spectrograph. The laser light was p-polarized with respect to the plane of incident (30° incidence angle) with an average laser pulse energy of 20 mJ.

Fig. 1 shows a carbon spectrum taken with the zone plate spectrograph using about 4000 laser shots for the whole spectrum. Clearly visible are Heα (4.03 nm), Heβ (3.50 nm), Lyα (3.37 nm), Lyβ (2.85 nm), and Lyγ (2.70 nm) together with a continuum emission down to below 2 nm. A line width of 0.0124 nm FWHM for Heα and 0.0339 nm FWHM for Lyα can be inferred from the spectrum. The line broadening is predominantly due to stark broadening in the high density plasma. A photon number of 1.8×10^{11} per laser shot and solid angle is measured for the Lyα-line which is slightly higher than for Heα (1.3×10^{11}) due to the difference in line width. Fig. 2 shows a nitrogen spectrum obtained with a boron nitride target using 1900 laser shots for the whole spectrum. The obtained numbers for Heα (2.88 nm) and Lyα (2.48 nm) are of the order of 10^{10} photons per shot and solid angle for both lines. The intensity of

these nitrogen lines are one order of magnitude lower than that obtained for the carbon Heα and Lyα.

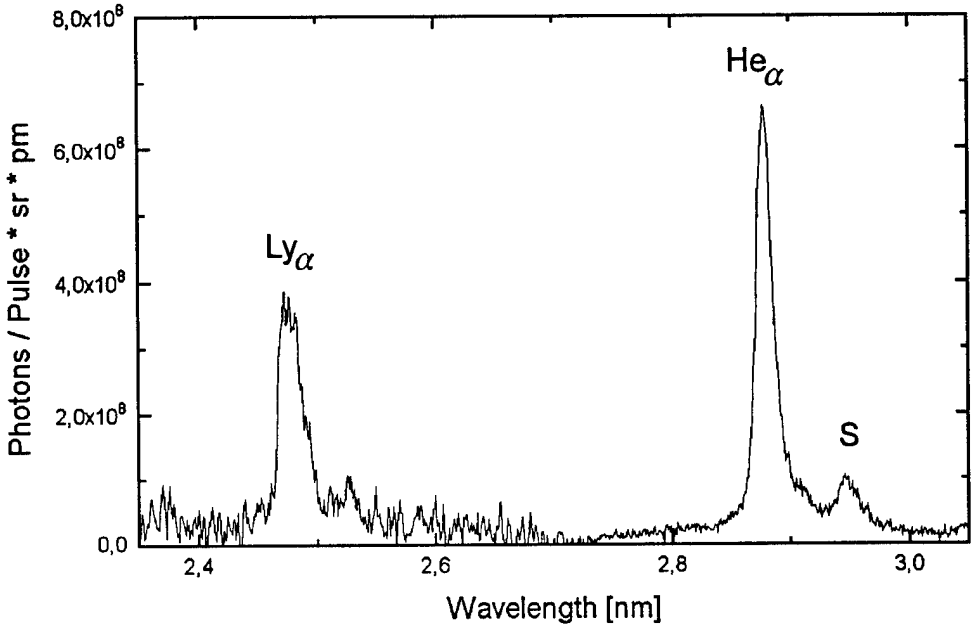

Fig. 2: A soft x-ray spectrum of boron nitride obtained by the novel zone plate spectrograph shows in the wavelength range from 2 to 3 nm the nitrogen lines of Lyα, Heα, and a spectral feature S which is contributed to lithium like satellite lines. The laser light was p-polarized with respect to the plane of incident (30° incidence angle) with an average laser pulse energy of 7 mJ.

[1] G. Schmahl and D. Rudolph: *X-ray microscopy*, Springer-Verlag, Heidelberg (1984).

[2] J. Jasny, U. Teubner, W. Theobald, C. Wülker, J. Bergmann, and F. P. Schäfer, *A single-shot spectrograph for the soft x-ray region*, Rev. Sci. Instrum. **65**, 1631-1635 (1994).

[3] U. Teubner, W. Theobald, and C. Wülker, *Mechanisms and origin of continuum and line emission from carbon plasmas produced by ultrashort laser pulses*, to appear in J. Phys. B (1996).

Control of the X-Ray Emission from High-Intensity Ultrashort Laser Produced Plasmas

U. Teubner, D. Altenbernd, E. Förster
Max-Planck-Arbeitsgruppe "Röntgenoptik" an der Friedrich-Schiller-Universität Jena,
Max-Wien-Platz 1, 07743 Jena, Germany
(Tel.: ++49-3641/635621; FAX: ++49-3641/636126;
email: uteubner@roentgen.physik.uni-jena.de)

The control of the X-ray emission from high-intensity laser-produced plasmas is a subject of current interest (see, e.g., [1]) and requires an understanding of the laser-pulse absorption, thermal transport and the X-ray conversion processes. Both depend on various factors (i.e., target material, angle of incidence, laser intensity, laser pulse duration etc.) and, in particular, ultrashort laser pulses offer the opportunity to generate ultrashort X-ray bursts of high brightness. Furthermore, these short pulse laser-plasma X-ray emitters are of fundamental interest because they allow to diagnose the laser-plasma interaction under unique conditions.

Here we report on a detailed study of the X-ray emission from plasmas produced by picosecond and femtosecond laser pulses on various solid target materials. For the experiments two different laser systems have been used, namely a KrF^*-laser system [2] (wavelength $\lambda_L = 248$ nm) and a Ti-sapphire system [3] ($\lambda_L = 800$ nm). The contrast ratio (i.e. short pulse intensity to background) was 10^{10} and 10^8 respectively and thus unwanted preplasma formation was avoided. By using well defined laser pulses with intensities up to 5×10^{17} W / cm^2 and various experimental conditions the plasma emission has been observed in the soft X-ray region (10-100 Å) by means of an absolutely calibrated single-shot spectrograph.

Some specific X-ray lines have been measured with high spectral resolution and absolute photon numbers have been deduced. As an example, Fig. 1 shows a spectrum from a carbon plasma produced by 248 nm laser light. The total number of photons per shot and steradian (sr) in full width at half maximum (FWHM) of the Ly-α and He-α line from this plasma is 10^{11} for both lines. Measurements made for comparison with 800 nm laser light but otherwise the same experimental conditions showed that the X-ray yield produced with the UV laser is more than one order of magnitude larger.

Several other experimental parameters have been changed as well, namely the laser pulse duration τ_L, intensity I_L, polarization, angle of incidence α and the target material. In some of the measurements a short prepulse was introduced. Finally, spectra obtained from a thin carbon foil target of 100 nm thickness have been compared to those of a solid carbon target.

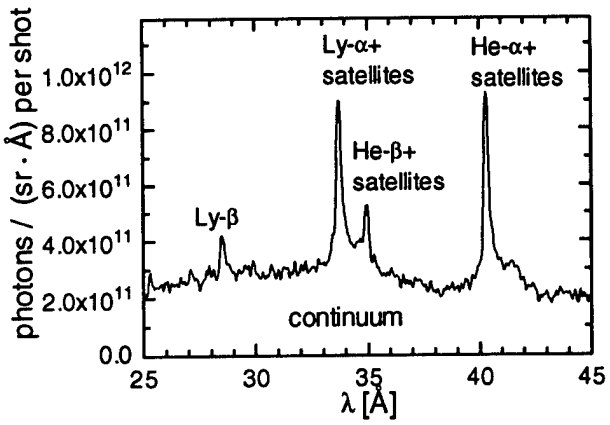

Fig. 1 X-ray spectrum from a solid carbon plasma produced by a $\tau_L = 0.5$ ps, *p*-polarized KrF^*-laser pulse focused to an intensity of $I_L = 10^{15}$ W/cm^2. The angle of incidence was $\alpha = 25°$ and the spot size was 20 μm.

The experimental results have also been compared to computer simulations. Using a hydrocode [4] the plasma parameters have been calculated as a function of time and space (in one dimension). The X-ray spectra have been simulated using these results as the input for a time-dependent atomic physics radiation code [5].

It has been found that the X-ray yield and the spectral characteristics may strongly depend on the pumping conditions. In particular, by changing the laser pulse duration from 100 fs-2 ps (for a *fixed laser energy*) a 700 fs pulse leads to the highest X-ray yield. This may be explained by the ionization dynamics and the coupling of the laser light with the plasma: for very short pulses (~100 fs) the plasma will be ionized less effectively due to the finite ionization time and for picosecond pulses the interaction of the laser pulse with the expanded plasma leads to a distribution of the absorbed energy over a larger volume and hence, results in a less effective ionization as well. In contrast to this, a short prepulse increases the emission (for *fixed laser energy and intensity*) due to the improved absorption in a larger electron density scale-length plasma.

The laser intensity, polarisation, angle of incidence and pulse duration have a distinct influence on the observed continuum and line emission for both laser wavelengths. The influence of these parameters has been related to the mechanism of laser pulse absorption, conversion process (of the absorbed energy into X-ray emission) and electron density and temperature in the emission volume. It has been found that line emission is mostly generated by laser light absorbed by inverse Bremsstrahlung and comes from an electron density not much larger than the critical density. However, the continuum may be produced *in addition* by collisionless absorbed light which becomes more and more important as the laser intensity is increased (in particular for *p*-polarized laser light at intermediate angles of incidence). Furthermore, the emission region is more extended, i.e. part of the continuum comes from high electron density regions.

This explains also 1) the observed much faster increase (with I_L) of the continuum emission ($\propto I_L^{1.6}$ for carbon) in comparison to the X-ray lines ($\propto I_L^{1.1}$ for carbon), 2) that the ratio of continuum to line emission shows a maximum at $\alpha = 45°$ and 3) that the observed continuum is more pronounced for a short laser pulse and/or a foil target (in comparison with a solid).

Hence, from this it is expected that the dependence of the continuum to line emission ratio for different experimental conditions effects the X-ray pulse duration measured in an experiment too: the measured value depends on which type of emission is dominant because the X-ray pulse duration [6] is significantly different for the continuum and the X-ray lines. The angle of incidence has also an influence on the line emission: at large α the width of the observed X-ray lines becomes smaller and the continuum is reduced like expected from the simulations.

The observed larger X-ray yield generated with UV-laser light with respect to red laser radiation may be explained by the higher electron density achieved in the first case (compare, e.g. Ref. [7]). In addition, part of the absorbed 800 nm pulse energy is transferred to suprathermal electrons (and thus not available for soft X-ray production) which is much less pronounced for UV-laser for laser intensities below 10^{17} W/cm^2.

In conclusion, the results show, that the X-ray yield, pulse duration, spectral region, bandwidth, ratio of continuum to line emission, source size, source bandwidth etc. depend strongly on the experimental conditions. Thus the X-ray parameters can be controlled and may be optimized by the proper choice of the pumping parameters. This may be also of practical relevance for applications exploiting the plasma as a short pulse plasma X-ray source of high brilliance.

References

[1] D. Kühlke, U. Herpers, D. von der Linde, Appl. Phys. Lett. **50**, 1785 (1987); J. C. Kieffer, M. Chaker, J. X-Ray Sci. Tech. **4**, 312 (1994); J. Workman *et al.*, Phys. Rev. Lett. **75**, 2324 (1995)

[2] Advanced version of the system described in S. Szatmari, F. P. Schäfer, Opt. Comm. **68**, 196 (1988); work done in collaboration with (in part) A. Andreev, R. Häßner, B. Niemann, R. Sauerbrey, R. Schmahl, W. Theobald and T. Wilhein

[3] C. LeBlanc *et al.*; Opt. Lett. **18**, 140 (1993); work done in collaboration with P. Audebert and A. Mysyrowicz

[4] FILM code; see P. Alaterre *et al.*, Phys. Rev. A **32**, 324 (1985); U. Teubner *et al.*, Phys. Plasmas **3**, 2679 (1996)

[5] FLY code, developped by R. W. Lee at Lawrence Livermore National Laboratory

[6] C. Wülker *et al.*, Phys. Rev. E **50**, 4920 (1994)

[7] P. Audebert *et al.*, Europhys. Lett. **19**, 189 (1992); U. Teubner *et al.*, Appl. Phys. B **62**, 213 (1996)

Solid to Plasma Transition in fs-Laser-Irradiated Fe: Collapse of the Spin-Orbit Gap

M. K. Grimes, Y. -S. Lee, M. C. Downer
The University of Texas at Austin,
Department of Physics, Austin, Texas 78712-1081, USA
e-mail: grimes@physics.utexas.edu, phone: 512-471-7251, fax: 512-471-9637

Quantitative measurements of the optical conductivity of iron under earth core conditions are important in modelling geomagnetism[1]. We approximate such conditions transiently[2] by exciting an Fe, and a control Al, surface in a vacuum or helium environment with 620 nm, 120 fs FWHM laser pulses with 10^5 peak-background contrast ratio at .6 ps focussed to peak intensities $10^{11} < I < 10^{15}$ W/cm^2 on target. Figs. 1 and 2 present p- and s- polarized self-reflectivity $R_{p,s}(\theta, I)$ for constant incident angle θ and peak intensity I, respectively. Geometric correction for the dependence of spot shape on θ has been made in plotting the data. Using very linear pulse energy reference monitors, reproducibility to within $\Delta R/R \leq 0.1\%$ was achieved. This allowed measurement of very slight reflectivity changes, as shown in the inset of Fig. 1. This figure also shows that the reflectivities of Fe and Al in the solid to plasma transition region ($10^{13} - 10^{15}$ W/cm^2) approach each other as I increases, consistent with their similar total conduction electron densities ($n_e \simeq 1.8 \times 10^{23}$ cm^{-3}) when the Fe d-electrons are included. This suggests qualitatively that progressive unbinding of the d-electrons dominates the changes in optical properties of Fe in this regime. Fig. 2 provides evidence that a density gradient develops during the laser pulse. It is well known[3] that θ_{min}, the angle at which the minumum p-polarized reflectivity occurs, shifts toward smaller angles as the density gradient scale length grows. Although the largest angle of incidence attainable in the experiment was smaller than θ_{min} under these conditions, the data clearly indicate a shift toward smaller values, seen for Fe in Fig. 2 as a crossing of the p-polarized data sets.

Quantitative analysis of the data requires that the perturbation of Fresnel reflectivity by small scale length ($L/\lambda \leq 0.1$) surface density gradients, if present during the pulse, be identified unambiguously and distinguished from ΔR caused by simultaneous intensity-dependent changes in dielectric properties of the plasma. We achieve this separation by calculating the reflectivity of such gradients under a wide range of conditions, and identifying those values of L/λ and the dielectric constant $\epsilon = \epsilon_r + i\epsilon_i$ that best reproduce the measured results. This reflectivity calculation numerically solves the Helmholtz wave equations[4] under the assumption that $\epsilon - 1$ varies linearly with density throughout the gradient. The qualitative features of the fit result are however reproduced when this assumption is relaxed to require only that ϵ drop monotonically toward the vacuum value of 1. The Riemann solution[5] $\rho(z) = \rho_0(1 - z/L)^3$, is used to describe the density profile, but no additional assumptions regarding the functional form of the dielectric constant are required. Fig. 3 shows the resulting values of ϵ_r and ϵ_i vs. laser intensity for Fe. The corresponding results for the density gradient scale length are shown in Fig. 4. Note that at the highest measured intensity the gradient scale length is still small compared to the laser wavelength, with $L/\lambda \simeq .1$.

The dielectric function of Fe at optical frequencies is well described at room temperature by a Drude-Lorentz model of the following form[6]:

$$\epsilon(\omega) = 1 + \epsilon_b - \frac{\omega_p^2}{\omega(\omega + i\nu)} + \frac{a^3}{\omega\omega_0}\frac{\omega + i\Gamma}{\omega_0^2 - (\omega + i\Gamma)^2}, \tag{1}$$

where $\omega_p = 4\pi n_e e^2/m^*$ is the plasma frequency with effective electron mass m^*, ω is the laser frequency, ν is the Drude collision frequency, and a describes the strength of the Lorentz oscillator

resonance centered at ω_0 of spectral width Γ. The term ϵ_b describes a frequency-independent background contribution to the polarizability. At the laser frequency $\hbar\omega = 2.0$ eV there is a convenient separation for Fe — the real part of ϵ is dominated by the free-electron, Drude term, and the imaginary part is dominated by the intraband, Lorentz term. This simplifies the interpretation of the changes in ϵ for low intensities. The nature of the interband, Lorentz resonance term is illuminated by the band-structure calculations of M. Singh *et al.*[7], which incorporate the effects of spin-orbit coupling critical to the description of the optical properties of transition metals. A collection of majority-spin states just below the Fermi energy and a collection of minority-spin states just above it lead to a joint density of states peaked at 2.4 eV.

The changing dielectric constant of Fe (Fig. 3) passes through three distinct stages as the intensity increases, each attributable to its own causes: first an initial decrease in both ϵ_r and ϵ_i, then a resonance feature, followed finally by a steep drop in ϵ_r and a milder decrease in ϵ_i. The initial drop in ϵ_r, the term dominated by the Drude free-electron term, is a consequence of a shrinking effective mass. At room temperature $m^* \simeq 8m_e$, but as the electron temperature rises with laser intensity the predominately d-orbital character of the conduction electrons in Fe will become more s-like. The greater mobility of these s-band states leads to a reduction in the effective mass and a corresponding increase in the collision frequency and $|\epsilon_r|$. The anticipated increase in collision frequency ν with temperature will offset this change somewhat, allowing the determination that at $I_{abs} = 10^{13}$ W/cm^2 the effective mass has dropped to $m^* \leq 5m_e$. In the second stage ($10^{13} < I < 10^{14}$ W/cm^2) the interband resonance term becomes dominant as the resonant frequency ω_0 drops from its initial value at 2.4 eV into the laser frequency at $I = 6 \times 10^{13}$ W/cm^2. This resonance is similar to those observed by Glezer, *et al.*[8] in fs-laser-induced bandgap collapse in GaAs. Finally, for $I > 10^{14}$ W/cm^2 ϵ_r becomes strongly negative again, indicating both collapse of the spin-orbit band gap and transition to a fully ionized plasma described entirely by the Drude model.

References

[1] J. A. Jacobs, *The Earth's Core*, Academic Press, London, 1987.

[2] M. C. Downer, H. Ahn, D. H. Reitze, D. M. Riffe, X. Y. Wang, in *Laser Interactions with Atoms, Solids, and Plasmas*, edited by R. M. More, Plenum Press, New York, 1994.

[3] O.L. Landen, D.G. Stearns, E.M. Campbell, Phys. Rev. Lett. **63**, 1475 (1989); O.L. Landen, B.T. Vu, D.G. Stearns, W.E. Alley, in SPIE Conference Proceedings Vol. 1413, *Short-Pulse High-Intensity Lasers and Applications* (1991).

[4] H. M. Milchberg, R. R. Freeman, J. Opt. Soc. Am. B **6**, 1351 (1989).

[5] Ya.B. Zeldovich and Yu.P. Raizer, *Physics of Shock Waves and High-Temperature Hydrodynamic Phenomena*, Ch. 1, Academic Press, New York, 1966.

[6] N.W. Ashcroft and K. Sturm, Phys. Rev. B, **3**, 1898 (1971).

[7] M. Singh, C.S. Wang, and J. Callaway, Phys. Rev. B **11**, 287 (1975).

[8] E.N. Glezer, Y. Siegal, L. Huang, and E. Mazur, Phys. Rev. B **51**, 6959 (1995).

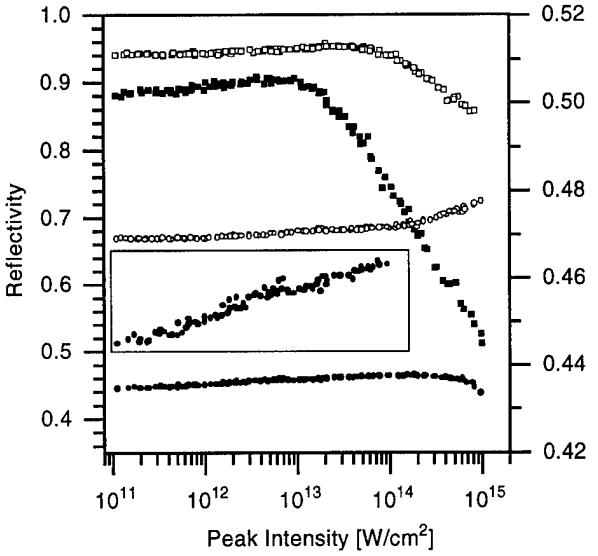

Figure 1: Reflectivity of 120 fs pulses from Al and Fe surfaces vs. peak pulse intensity, at a 45° angle of incidence. Al data are shown with squares, Fe with circles. Measurements with polarization parallel to the plane of incidence (p-pol.) are shown with filled points; open points are used for polarization perpendicular to the plane of incidence (s-pol.). A section of the Fe, p-polarized data is shown in the inset, magnified vertically as indicated by the right-side axis.

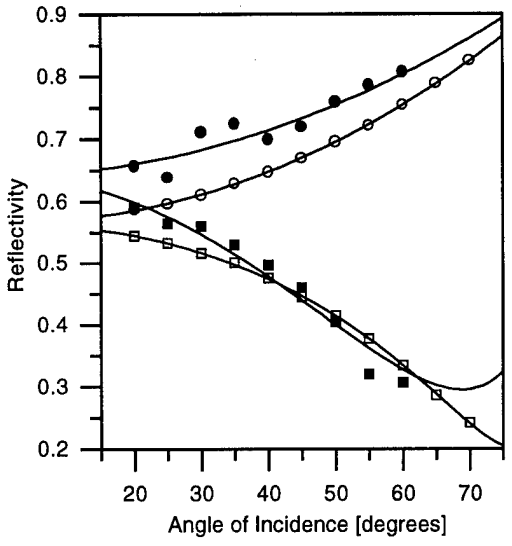

Figure 2: Reflectivity of Fe vs. angle of incidence at $I = 10^{11}$ W/cm^2 (open points) and 2×10^{14} W/cm^2 (filled points) for s-polarization (circles) and p-polarization (squares). The reflectivity of a density gradient calculated from the corresponding best fit results are shown with lines.

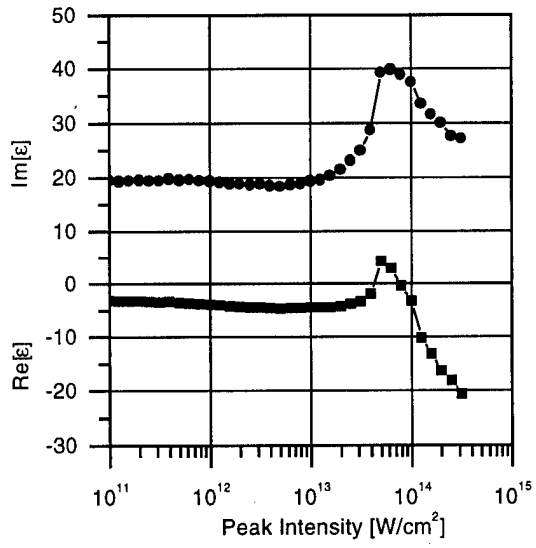

Figure 3: Best fit results for the complex dielectric constant ϵ of Fe vs. peak laser intensity.

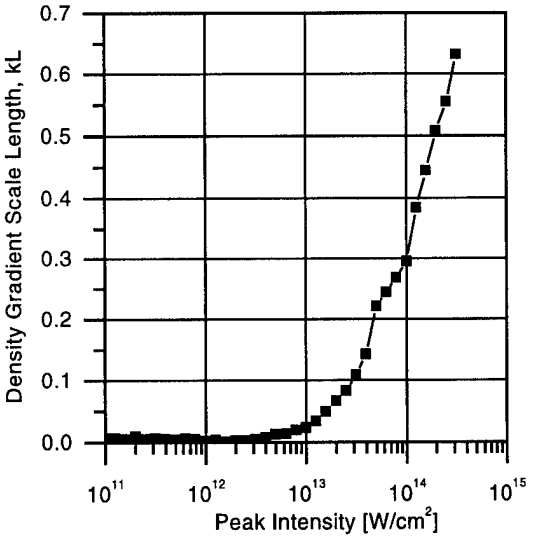

Figure 4: Best fit results for the dimensionless density gradient scale length $kL = 2\pi L/\lambda$ of Fe vs. peak laser intensity.

Anomalous Short Wavelength Emission by Optical Field Ionization of a Preformed Boron Plasma

Katsumi Midorikawa, Yutaka Nagata, Cornelius Wülker, and Koichi Toyoda

The Institute of Physical and Chemical Research (RIKEN)
2-1 Hirosawa, Wako-shi, Saitama 351-01, Japan
Phone:+81-48-462-1111
Fax:+81-48-462-4682
E-mail: kmidori@postman.riken.go.jp

1. Introduction

The use of optical-field ionization (OFI) allows to control both an ionic state and electron energy distribution, which is of importance for production of x-ray lasers[1-3]. We previously reported the observation of gain on the 13.5-nm Lyman-α transition of H-like Li ions by OFI of a preformed Li^+ plasma [4]. The measured electron temperature of less than 1.5 eV was significantly lower than what is expected by an above-threshold ionization model [5,6]. However, wavelength scaling of this scheme is not clear because the required pump laser intensity rapidly increases with decrease of x-ray laser wavelengths. The increase of the pump laser intensity additionally causes harmful heating of the plasma by nonlinear interactions. The increase of the pump laser intensity which results in the requirement of a huge pump device also makes it quite difficult to realize a tabletop x-ray laser operating below 10 nm.

In this paper, we report the reduction of pump laser intensity necessary for an OFI x-ray laser using the preformed plasma scheme. When a boron nitride (BN) target was used in place of the Li target, we observed anomalous short wavelength emissions, which originated from charge states far beyond that predicted by OFI of individual atoms or ions.

2. Experiment

The experimental arrangement for the measurement of time-integrated spectra is shown elsewhere[1]. In order to produce the initial boron plasma, a 20-ns KrF laser pulse with an output energy of 200 mJ was line-focused onto a rotating boron nitride (BN) disk target located in a vacuum chamber by using two cylindrical lenses. The focused laser intensity was 10^9 W/cm^2. After a certain delay with respect to the 20-ns KrF laser pulse, a linearly-polarized KrF laser pulse with a pulse width of 0.5 ps was focused inside the BN plasma column by using an f = 50 cm lens. The focus position and intensity were 0.5 mm from the BN target surface and 6×10^{16} W/cm^2, respectively. This intensity is 30 times lower than that required for production of fully stripped boron ions by OFI [7].

3. Results and Discussion

Figure 1 (a) and (b) show the spectra observed in BN plasmas produced by direct irradiation of the solid BN target with the subpicosecond KrF laser and by OFI of a preformed plasma, respectively. Because of the higher diffraction efficiency of the grating around 10 nm,

the 2nd or 3rd order signals are shown in the Figure. The OFI spectrum strongly differs from the spectrum observed in normal hot and dense expanding plasma produced by direct irradiation of the subpicosecond laser. When we used the OFI scheme, strong line emissions from H-like and He-like ions were observed, in spite of the low irradiation intensity of 6×10^{16} W/cm^2. For generation of those line emission by field ionization, the required laser intensity is calculated to be higher than 10^{18} W/cm^2. This fact indicates that the BN plasma containing fully stripped boron is not produced by the field ionization.

Time resolved spectrum observed with a streak camera is shown in Figs. 2. Due to low sensitivity of the homemade photo cathode and low signal intensity, time resolution is not good. However, the pulse width of the Lyman-α line could be estimated to be less than 10 ps. Although the time integrated spectrum of the He-α line is stronger than that of the Lyman-α line, the time resolved one is weaker than that of the Lyman-α line. This is presumably due to relatively long raiative life time of the He-α line. The He-α

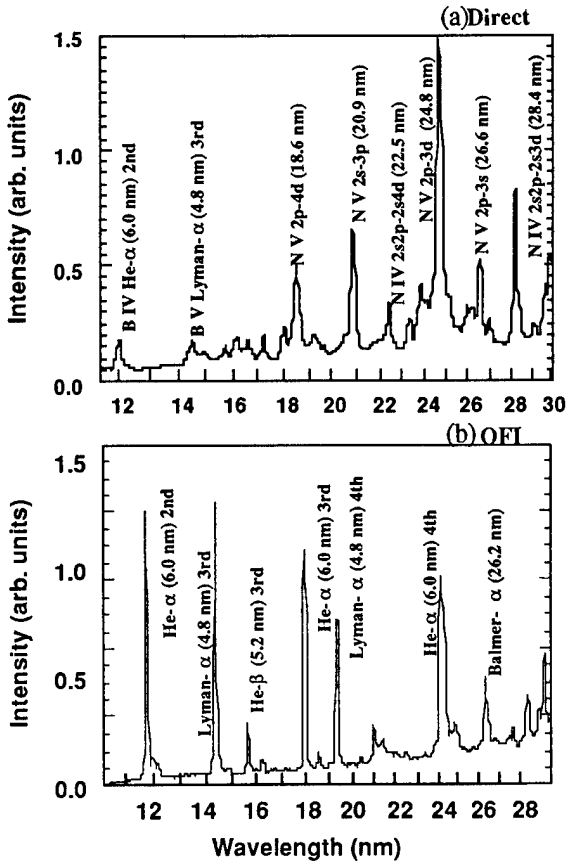

Fig. 1 Observed spectra (a) by direct irradiation of a subpicosecond KrF laser and (b) by OFI of a preformed BN plasma.

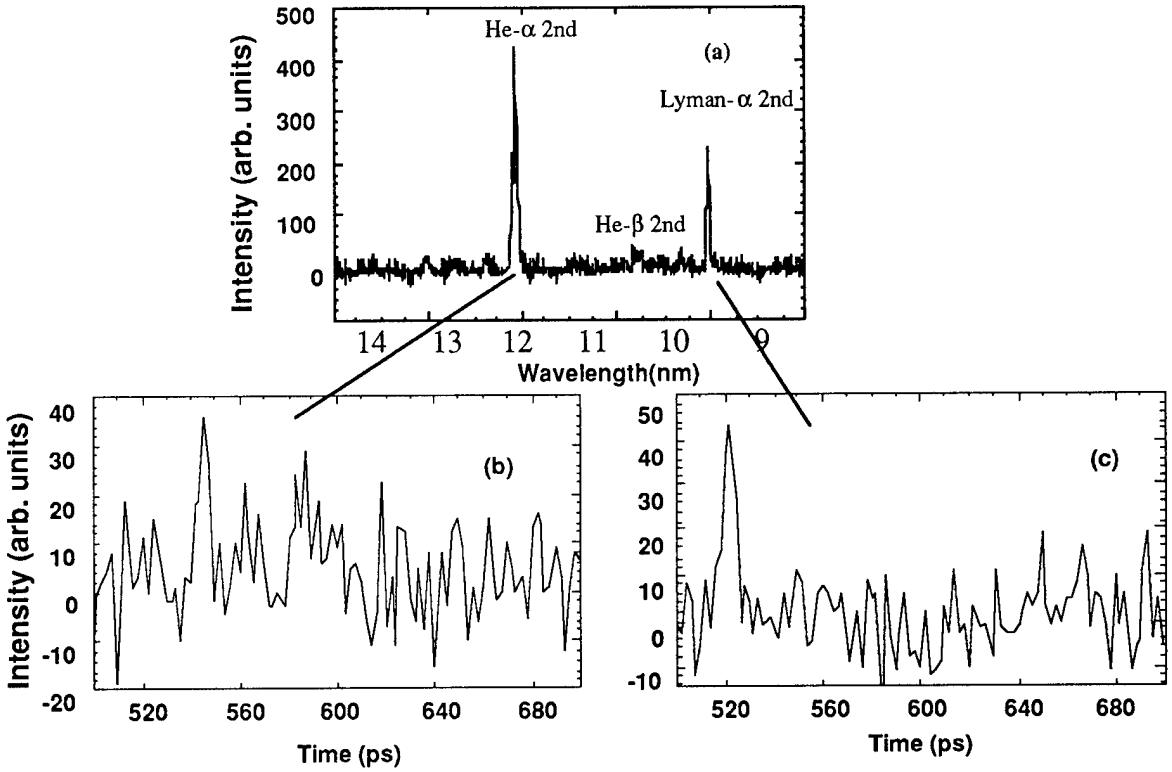

Fig. 2 (a) Time integrated and time resolved traces of (b) the He-α and (c) the Lyman-α lines of boron ions.

line appears 20 ps after the Lyman-α line. These results support that the OFI plasma is in a recombination dominated phase.

Figure 3 (a) shows delay time dependence of the boron plasma density and the time integrated Lyman-α line intensity. The)7th harmonics intensity was previously measured as a function of the delay between the ns and the subpicosecond KrF laser pulse. The plasma density was estimated from this harmonic signal intensity because the harmonics intensity is propotional to square of the plasma density. The Lyman-α signal rapidly increases around 700 ns and gradually decreases. Figure 3 (b) shows delay time dependence of the intensity ratio of the Lyman-α to the Balmer-α line. The large intensity ratio in the high density region indicates that collisional decay time of the Balmer-α transition is shorter than the radiative life time of it. This condition is satisfied at an electron temperature of about 10 eV, assuming the boron density of the order of 10^{17} cm^{-3}.

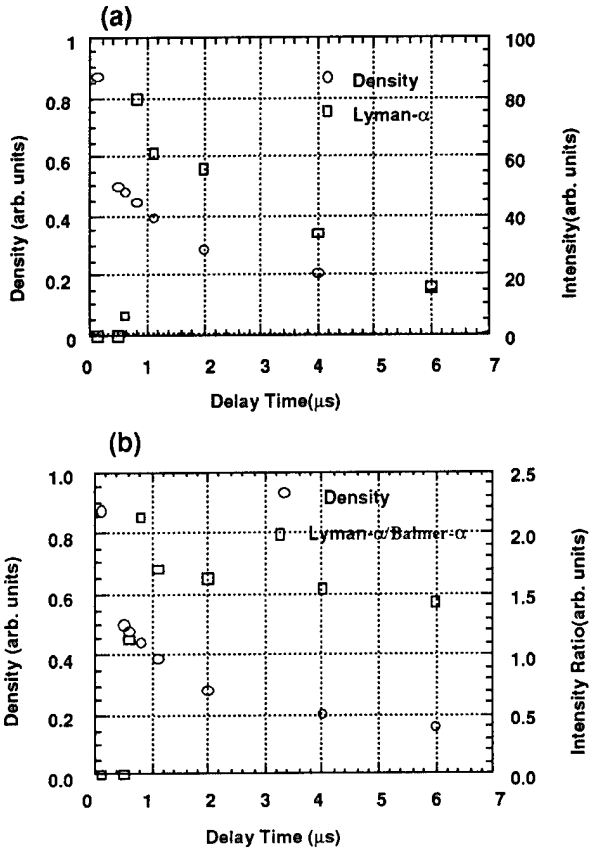

Fig. 3 Delay time dependences of (a) the plasma density and the Lyman-α line intensity: (b) the plasma density and the intensity ratio of the Lyman-α to Balmer-α line.

In conclusion, we have observed anomalous short wavelength line emission from a plasma produced by irradiation of high-intensity subpicosecond KrF laser pulses into a preformed boron nitride plasma. In spite of a low irradiation intensity of 6×10^{16} W/cm^2, strong line emissions from H-like and He-like boron ions which suggested generation of fully stripped boron were observed. More important, characteristics of the observed spectra indicated that the electron temperature of the plasma was much lower than that expected by collisional heating in clusters. The existence of both BN clusters and cold electrons in the preformed plasma may reasonably explain the spectral characteristics of the OFI plasma. In this case, the ion production occurs due to efficient absorption and collisional heating by the clusters [8,9]. The preformed cold electrons contribute to fast three-body recombination as in the lithium experiment [4].

References

[1] H. N. Burnett and P. B. Corkum, J. Opt. Soc. Am B **6** 1195(1989).
[2] H. N. Burnett and G. D. Enright, IEEE J. Quantum Electron. **QE-26** 1797(1990).
[3] P. Amendt, D. C. Eder, and S. C. Wilks, Phys. Rev. Lett. **66** 2589(1991).
[4] Y. Nagata, K. Midorikawa, S. Kubodera, M. Obara, H. Tashiro, and K. Toyoda, Phys. Rev. Lett. **71** 3774(1993).
[5] Y. Nagata, K. Midorikawa, S. Kubodera, M. Obara, H. Tashiro, K. Toyoda, and Y. Kato, Phys. Rev. A **51** 1415(1995).
[6] K. Midorikawa, Y. Nagata, S. Kubodera, M. Obara, and K. Toyoda, IEEE J. Selected Topics in Quantum Electron. **1** 931(1995).
[7] B. M. Penetrante and J. N. Bardsley, Phys. Rev. A **43** 3100(1991).
[8] A. McPherson, T. S. Luk T S, B. D. Thompson, K. Boyer, and C. K. Rhodes, Appl. Phys. B **57** 337(1993).
[9] T. Ditmire, T. Donnelly, R. W. Falcone, and M. D. Perry, Phys. Rev. Lett. **75** 3122(1995).

Overheating of Femtosecond Plasma in Freely Suspended Superthin Films

V.G.Babaev, M.S.Dzhidzhoev, V.M.Gordienko, M.A.Joukov, A.B.Savel'ev, A.A.Shashkov, A.P.Tarasevitch, R.V.Volkov

International Laser Center, Moscow State University, Vorobyevy gory, Moscow, 119899, Russia

Phone:+7-05-9395318, Fax:+7-095-9393113, E-mail:savelev@femto9.ilc.msu.su

Previously we proposed a new thin film target to obtain femtosecond plasma overheating using artificially limited thermoconductivity [1]. We discussed the results of computer modeling of interaction of superintense femtosecond laser pulse with freely suspended thin carbon film. It was shown that for film thicknesses of 50 nm and less the electron temperature rises up to 500 eV and even higher with decrease in thickness. This causes increase in x-ray yield from H- and He-like C ions.

In this paper we present for the first time the experimental results demonstrating the phenomenon for freely suspended carbon films as thin as 20-30 nm. It was obtained that for these superthin films x-ray yield increased more than twofold for p-polarized light. The comparison of the experimental results with predictions of the computer code shows good quantitative agreement and leads to the conclusion that there is threefold overheating of plasma layer up to 500 eV.

The possibility of widening the choice of target materials and promising advantage of superthin targets for considering relativistic intensities will be discussed as well.

The superthin film targets were placed onto specially designed flat grids of 175*175 μm^2 transparent cell with 350 μm period. We produced only one laser shot into each cell. The target then was translated in the plane coinciding with the plane of the grid. The film thickness was measured by a few techniques within 10 nm precision. We used a set of carbon films of different thickness in the range of 20-100 nm and «thick» 1 μm mylar film for reference.

Experiments were carried out using s- or p-polarized pulses (600nm, 200fs, angle of incidence 45°) produced intensities above 10^{15} W/cm^2 [2]. Temporal as well spectral

shapes of the laser pulse were measured for each laser shot. Energy contrast ratio was estimated to be not worse than 1000. It was tested, that interaction of the superluminiscent radiation with locked out femtosecond seed pulse with the superthin film has no effect on the film state.

The main part of total energy of x-ray yield form carbon target for plasma temperature above 100 eV is contained in two most bright lines of He-like (4,02nm) and H-like (3,37nm) ions [3]. Changes in plasma temperature cause changes in total x-ray yeild as well as in ratio between He- and H-like emission brightness. In our experiments we measured total x-ray yield from carbon plasma from both front and rear sides using filtered (250 nm Al filter) p-i-n x-ray diodes (see inset to Fig.1).

The results for the front-side detector as well as computer simulation results are plotted in Fig.1. The simulated curves were obtained using computer code described elsewhere [1] as a sum of x-ray yield from two lines mentioned above and recombination radiation from H- and He-like ions. Good quantitative agreement could be clearly seen from Fig.1 for experimental and simulated results. For 30 nm film x-ray yield enhances more than twice as compared to «thick» mylar film. In accordance with computer simulation this corresponds to temperature increase from 150 to more than 450 eV. This value could be compared to the figure of 170 eV obtained in [3] for carbon plasma under two orders higher laser intensity. It is worth noting, that while for mylar target He-like ions play dominant role, for 30 nm film the situation changes vise versa. For thinner targets the x-ray yield falls back: here film thickness become of the same order as skin-layer depth. The x-ray signal from rear side of the 30 nm film was twice as weak, whereas no signal was detected for mylar target's rear side.

Temporal shapes of the x-ray pulses obtained from superthin film targets are longer than those for the thick ones, but don't exceed few ps.

Finally, we discussed promising perspectives of using new type targets under action of up to relativistic intensities:

- Using superthin film targets made of the other materials (including heavier atoms) brings up the possibility of rising up x-ray yield in the range of

quanta energy larger than 1 keV.

- Preliminary estimations also show that overheated plasma could serve as efficient source of fast electrons bunches.
- Superthin film target could also serve as well-determined ion jet for efficient generation of high-order harmonics.
- Such phenomena as selfchanneling and selfinduced transparency could be investigated using relativistic intensities of 10^{18}-10^{20} W/cm^2 and superthin films.

1. M.S.Dzhidzhoev, V.M.Gordienko, V.V.Kolchin, S.A.Magnitskii, V.T.Platonenko A.B.Savel'ev, A.P.Tarasevich «Generation of incoherent x-ray pulses: resonant production and advantage of using thin films»JOSA B, 13 (1) 143 (1996).
2. R.V.Volkov, M.S.Dzhidzhoev, V.M.Gordienko, S.A.Magnitskii, V.T.Platonenko, A.B.Savel'ev, A.P.Tarasevitch, A.O.Timoshin «Two beam femtosecond high-field interactions with a solid target. Surface modification and second harmonic generation under the conditions of surface electromagnetic wave excitation», Quant.Electr. 26(5), 524 (1996)
3. U.Teubner, I.Uschmann. W.Theobald, E.Forster «X-ray emission from ultrashort UV-laser pulse produced plasmas», in Superintense laser fields, eds.: A.A. Andreev, V.M.Gordienko, SPIE proc., vol.2770, p.106, (1996).

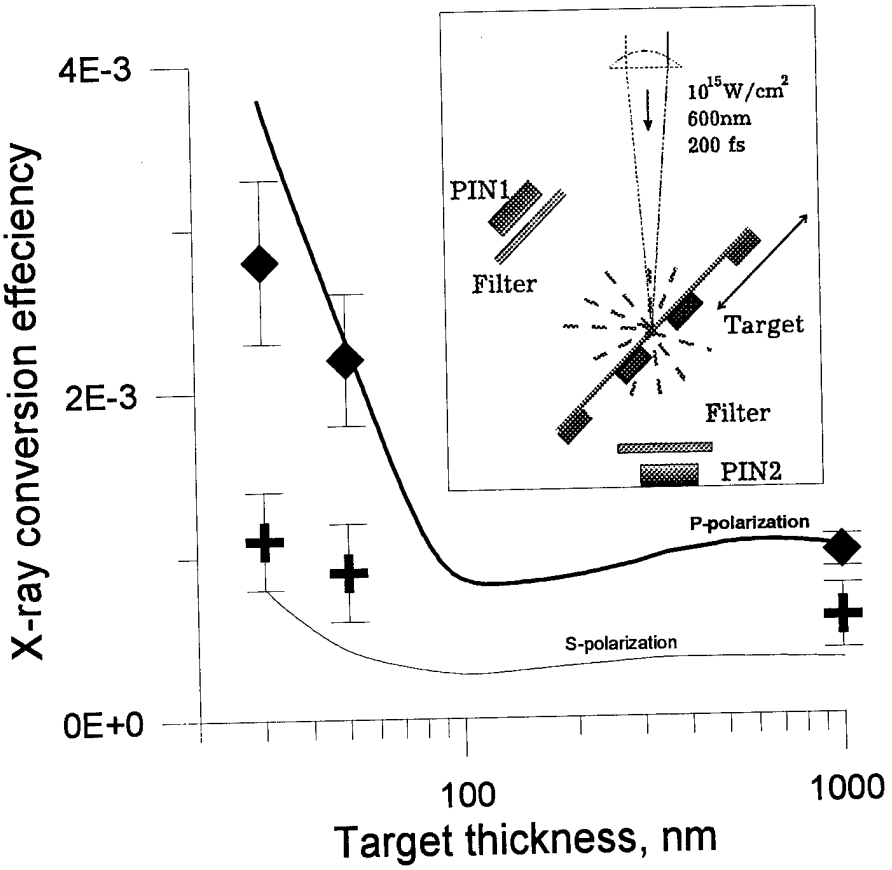

THE ROLE OF WAVEBREAKING IN SECOND HARMONIC GENERATION FROM FEMTOSECOND LASER-PRODUCED PLASMAS

D. von der Linde and T. Engers
Institut für Laser- und Plasmaphysik, Universität Essen
D-45117 Essen, Germany
Phone: 49 201 183 2564; Fax: 49 201 183 2567; e-mail: phy600@uni-essen.de

It is well known that an electromagnetic wave obliquely incident on a planar stratified inhomogeneous plasma couples with electron plasma oscillations when the electric field is polarized in the plane of incidence. The interaction is resonant at the critical density surface, and plasma waves of large amplitude may be generated. For a sufficiently strong driving field the condition of wavebreaking may be reached in a certain region around the critical density surface. Wavebreaking leads to efficient dissipation of collective wave energy and to the production of energetic electrons. The process is of fundamental importance as an absorption mechanism in high intensity laser-plasma interaction. Manifestations of wavebreaking have been seen in the electron energy spectra, x-ray emission, and optical absorption experiments.

In this contribution we wish to argue that time-resolved measurements of the second harmonic from a plasma produced by a short laser pulse on the surface of a solid target show evidence of the onset of wavebreaking in an early stage of plasma expansion, when the thickness of the plasma sheet corresponds to a small fraction of the wavelength of light.

Time-resolved measurements of the reflected second harmonic were performed using a pump-probe technique. Femtosecond laser pulses from an amplified CPM dye laser (λ = 620 nm) were focused on solid targets to generate a surface plasma. Delayed, weak probe pulses interacted with the plasma, producing coherent p-polarized second harmonic in the specular direction. The experimental parameters were as follows: Pulse duration 65 fs; spot diameter on the surface 8 μm; angles of incidence 40 degrees and between 45 and 60 degrees for pump and probe, respectively. The peak intensity on target of the s-polarized pump pulses was 10^{16} W/cm^2. The pump/probe energy ratio was 100:1, and otherwise the pump pulses and the probe pulses were the same.

Striking differences in the variation of the strength of the second harmonic as a function of the time delay were observed when s-polarized and p-polarized probe pulses were used. In the first case we observed a smooth increase of the second harmonic to a maximum between 2 and 4 ps, depending on the angle of incidence. This maximum was followed by a decay on a time scale of several picoseconds. On the other hand, for p-polarization we observed a very strong, sharp maximum of the second harmonic for a probe pulse delay of about 150 fs. This sharp feature at early times was not present for s-polarized probe pulses. For times greater than $\approx$ 300 fs the variation of the second harmonic for p- and s-polarization were very similar.

For an explanation of the experimental data we made the assumption that the dependence of the second harmonic on the delay time primarily reflects the changes of the plasma density profile during the free expansion into vacuum. Following this assumption we performed calculations of the reflected second harmonic as a function of the plasma scale length.

The simplest description of second harmonic generation in a plasma starts from a hydrodynamic model and applies perturbation theory [2]. It turns out that the results of perturbative calculations are in disagreement with the experimental results. The calculated variation of the second harmonic with the plasma scale length are very similar for both types of polarization. In particular, there is no distinct sharp feature of the second harmonic for p-polarization.

A perturbative treatment requires that the changes of the system in response to the perturbation are small. However, it turns out that, as a result of resonant coupling, this condition is violated in the critical density region. For the probe pulse intensities used in the experiment the amplitude of the induced electron density oscillations near the critical density are comparable with the unperturbed density, and it can be shown that the conditions for wavebreaking are reached.

We have developed an improved model of second harmonic generation based on the conjecture that, as far as the interaction of the electromagnetic waves is concerned, the principal effect of wavebreaking is a strong increase of the losses in the critical density region. Following a suggestion by Rae and Burnett [2] this aspect of wavebreaking can be modelled by introducing an *intensity dependent effective damping constant* in the dielectric function of the plasma.

Results of an extension of this approach to second harmonic generation are shown in Fig. 1. The calculated efficiency of the reflected second harmonic is plotted versus the normalized plasma scale length L/λ. The dotted and the dashed line represent, respectively, the second harmonic generated by s-polarized and p-polarized light in the limit of very low fundamental intensity (perturbation limit). As mentioned above, we find a smooth variation of the second harmonic for both polarizations, with p-polarization being about ten times more effective than s-polarization. The solid curve shows the second harmonic for a fundamental intensity of 1.3×10^{15} W/cm^2. In this case we obtain a very strong enhancement of the second harmonic for plasma scale lengths corresponding to a few percent of the wavelength. The solid line merges with the dashed line (perturbation limit) for $L/\lambda > 0.7$. Wave breaking does not occur in this range of scale length because tunnelling through a substantial plasma layer is required to reach the critical density. Tunneling leads to a strong attenuation of the driving field.

In Fig. 2 the experimental data for two different angles of incidence are compared with the calculations. The fitting parameters are the electric field of probe pulse ($E_0 = 1.5\times10^8$ V/cm) and for the conversion of the scale length axis to a time axis, the expansion velocity of the plasma ($v_{exp} = 2.5\times10^6$ cm/s in Fig. 2 a, and $v_{exp} = 3.5\times10^6$ cm/s in Fig. 2 b). The calculated curves were adjusted to the broad maximum of the measured second harmonic.

There is good qualitative agreement of the experimental data and the model calculations. In particular, the model reproduces quite well the observed striking differences of the time dependence of the second harmonic for p-polarized and s-polarized laser pulses, the conspicuous sharp spike at early times. The measured and the calculated times of the sharp maximum are, respectively, 170 fs and 70 fs in Fig. 2 a, and 60 fs and 45 fs in Fig. 2 b. The measured and calculated ratios of the maxima are 4:2 and 2:4.

These results suggest that the behavior of second harmonic generation provides direct evidence of the onset of wavebreaking during a early stage of the plasma evolution at very short scale lengths.

[1] D. von der Linde, in: *Laser Interactions with Atoms, Solids, and Plasmas*, ed. by R. M. More (Plenum Publ. Corpor., New York, 1994) p. 207

[2] S. C. Rae and K. Burnett, *Phys. Rev.* A 44: 3835 (1991).

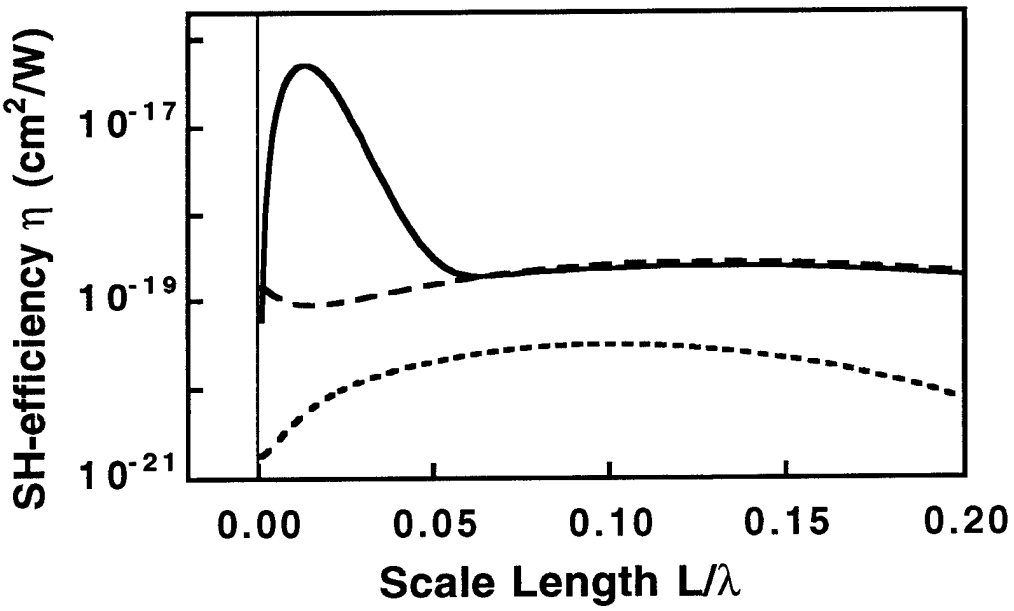
SH-efficiency η (cm²/W)
10⁻¹⁷
10⁻¹⁹
10⁻²¹
0.00
0.05
0.10
0.15
0.20
Scale Length L/λ

Fig. 1

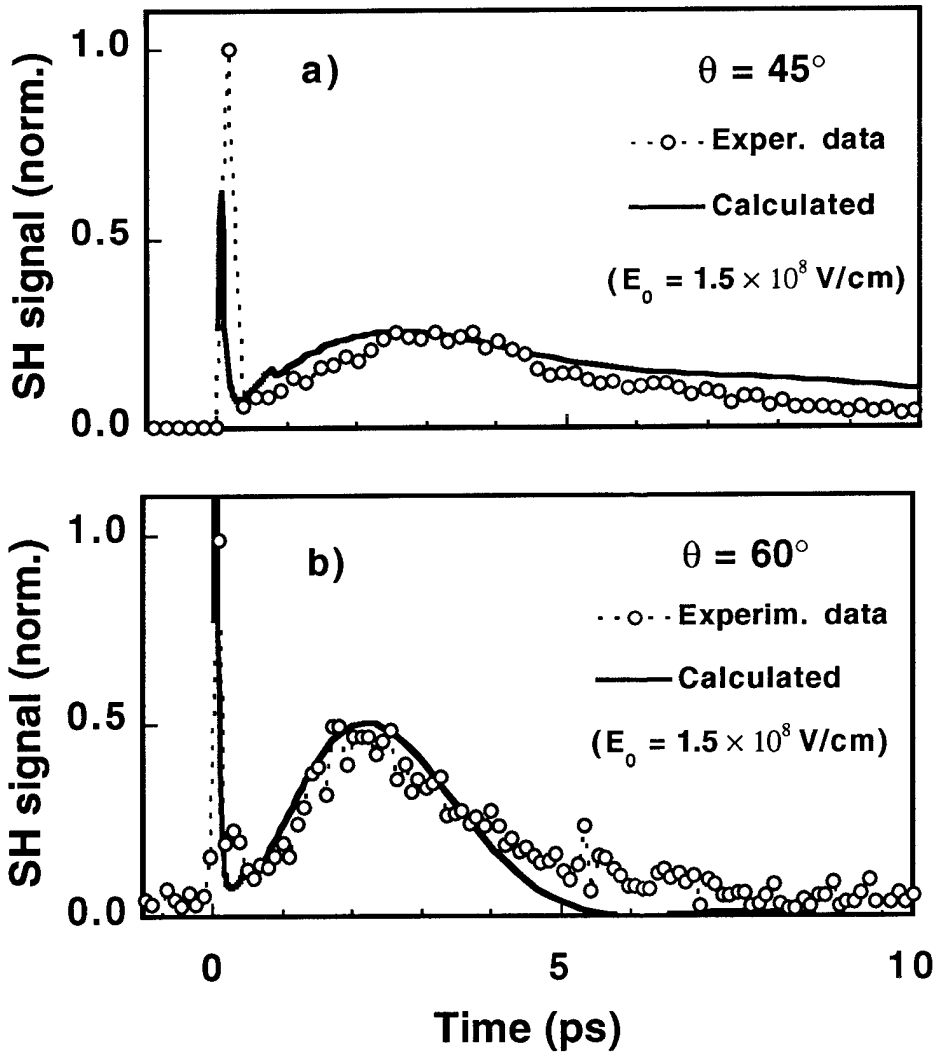
SH signal (norm.)
1.0
0.5
0.0
a)
θ = 45°
Exper. data
Calculated
(E₀ = 1.5 × 10⁸ V/cm)
b)
θ = 60°
Experim. data
Calculated
(E₀ = 1.5 × 10⁸ V/cm)
0
5
10
Time (ps)

Fig. 2

100 Femtosecond Laser Absorption in Solid Density Targets

Dwight F. Price, R. M. More, R. S. Walling, R. E. Stewart

Lawrence Livermore National Laboratory
P.O. Box 808 Mail Stop L-251
Livermore, California 94550
Phone (510) 423-6170 Fax (510) 422-2253
E-mail price4@llnl.gov

1. Introduction

Experimental short pulse lasers are rapidly approaching energy levels where target irradiances exceeding 10^{20} W/cm^2 are routinely achievable [1,2,3]. These high intensity levels will open up a new class of solid target interaction physics where relativistic effects must be included and non-traditional absorption mechanisms become significant. However much remains to be understood of the absorption physics at lower intensities where classical absorption is dominated by collisional and resonance absorption. If attention is paid to producing clean laser pulses that do not significantly pre-pulse interact with the target, it is possible to produce plasmas of sufficiently short scale length that near-solid density interactions are observable at intensities exceeding 10^{18} W/cm^2 for 100 fs laser irradiation.

We report here extensions to our previous efforts at normal incidence [4] that expand our observations to non-normal angles including the effect of polarization for several target materials. Between 10^{13} W/cm^2 and 10^{14} W/cm^2 we observe that the target absorption retains a signature of the intra-band atomic transitions. At higher intensities a more material independent ion-electron collisional absorption and short scale length resonance absorption dominate. P - polarized absorption in short scale length plasmas has been observed to exceed 60 percent.

2. Experiment

The experiment was performed on the 100 fs Ti:Sapphire laser of the USP facility at Lawrence Livermore National Laboratory. The Ti:Sapphire laser is capable of delivering 1 joule at 800 nm onto a target at intensities of 5×10^{19} W/cm^2 with a 1.5 times diffraction limited focus. In order to produce as low a level of prepulse as possible the current set of experiments where performed with frequency doubled 400 nm light. The pulse contrast is 10^{-7} one picosecond prior to the peak of the pulse; allowing near-solid density experiments to be performed. The compression of the CPA

pulse, its frequency doubling, and transport to the target are performed at vacuum. The light is focused with an off-axis parabolic mirror at f/4.8. Third order correlations are made on all shots to determine the pulse width used. Typical pulse widths are 120 fs to 130 fs.

The target, consisting of 1 micron thick e-beam deposited thin films on 1.5 mm thick glass plates, is raster scanned to ensure clean undamaged surface material on each shot. Intensity is varied by defocusing the target. The reflected, incident, transmitted, and back scattered light are measured on cross calibrated pyro-electric meters. Scattered light is monitored by an array of optical diodes, which are calibrated by the use of a Lambertian scatter of known scattering efficiency.

3. Observations and Conclusions

Observation were made in 10 degrees increments between 12.5 and 72.5 degrees angle of incidence. Both s and p - polarization where used. Absorption was inferred to be:

Absorption = 1 - Reflected - Transmitted - Scattered - Back Scattered

The previous results at 0 degrees angle of incidence agreed well with the low angle 12.5 degree shots, but significant improvement in absorption efficiency was noted for p - polarized light with increasing angle of incidence. This increase in absorption is due to resonance absorption in a short scale length expansion plasma. Unlike long scale length absorption, no notable maximum is observed in the p - polarized reflectivity (Figure 1.) up to the 72.5 degree limit of these experiments. The s - polarized absorptivity is observed to decrease with angle.

Considerable success has been achieved with simple non-hydrodynamic models of the plasma assuming resonance absorption and collisional absorption by varying the plasma expansion scale length and dielectric properties to achieve best fit. Improvements are expected when this absorption model is incorporated into a fully hydrodynamic model with wave-solving capabilities.

Previous experiments suggest that at intensities greater than 10^{16} W/cm^2 the s- and p - polarized light would reflect from the electron-ion "plasma mirror" with a nearly material independent reflectivity. We have investigated the atomic Z dependence of the absorption in the high intensity regime and find that absorption

increases with Z and is well modeled by our hydrodynamic calculations including resonance and collisional absorption.

Our future plans are to extend this work to higher intensities where non-classical absorption mechanisms become important.

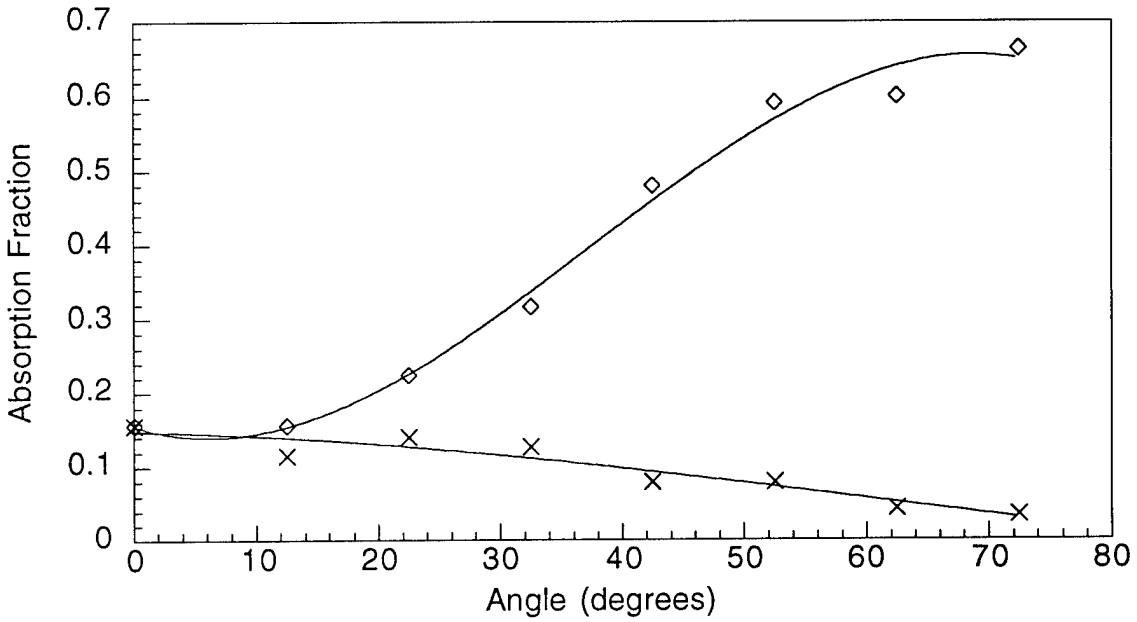

Figure 1. The experimental results for s and p - polarized absorption at 10^{16} W/cm^2 suggest that resonance absorption in short scale length plasmas plays a dominant role at high angles for p - polarized light. s - polarized (X symbol); p - polarized (diamond symbol).

This work was performed under the auspices of the U.S. Department of Energy by Lawrence Livermore National Laboratory under contract No. W-7405-Eng-48.

[1] M. Perry, Application of High Field and Short Wavelength Sources VII; Santa Fe, N.M., March 19-22 , 1997.

[2] C. P. J. Barty, et al., SPIE Vol. 2701, San Jose,Ca. 1996 (84).

[3] J. D. Bonlie et al., SPIE Vol 2701, San Jose,Ca. 1996 (107).

[4] D. F. Price et al., Phys. Rev. Lett. **75**, 1995 (252).

Propagation of sub-picosecond laser pulses through a fully ionized plasma

P.E. Young

Lawrence Livermore National Laboratory, L-251,P.O. Box 808, Livermore, CA 94551
Tel:(510)-422-5478, FAX:(510)-423-2505, e-mail:peyoung@llnl.gov

P.R. Bolton

Lawrence Livermore National Laboratory, L-251,P.O. Box 808, Livermore, CA 94551
Tel:(510)-422-8726,FAX:(510)-422-2263, e-mail:bolton1@llnl.gov

The development of high intensity lasers has led to the possibility of observing relativistic effects when a laser pulse interacts with a fully ionized plasma. The propagation of high intensity laser pulses through a fully ionized plasma has practical applications for compact x-ray lasers [1,2], laser-plasma-based particle accelerators [3], and advanced inertial confinement fusion schemes [4]. The relativistic filamentation instability [5] can lead to modifications of the propagating pulse by spatially modulating the laser intensity transverse to the direction of propagation; growth of the instability can lead to spreading of the beam as the result of the density modulation set up by the filamented ponderomotive force. The beam propagation needs to be understood before further nonlinear effects are investigated [6,7]. Previous experimental studies of high-intensity laser pulses have employed neutral gases which are ionized by the propagating pulse [8]. That technique is limited by technical constraints to relatively low electron densities ($\leq 10^{19}$ cm^{-3}) and introduces the possibility of the modification of the propagation behavior by the formation of an ionization front at the leading edge of the pulse [8].

In this Letter, we describe an experiment [9] in which a high intensity (up to 5 x 10^{18} W/cm^2), 600-fsec laser pulse propagates through a fully-ionized preformed plasma of substantial density (up to $0.5n_c$). When the laser intensity, I_L, and plasma density, n_e are sufficiently low such that relativistic filamentation does not grow, the pulse channels through the plasma. As I_L or n_e is increased, we observe the onset of relativistic filamentation, in which the beam breaks up into multiple hot spots, as opposed to whole-beam self-focusing, by analysing the light transmitted through the plasma and by 2-D pictures of the sidescattered laser light. If the plasma density or the laser intensity is high enough, the beam breakup occurs before the pulse reaches the peak plasma density. Along with the beam breakup, we observe time-dependent spectral modulation of the laser pulse transmitted through the plasma using a frequency-resolved optical gating (FROG) diagnostic. In the early part of the pulse we observe a spectral red-shift, consistent with electrons being moved out of the beam path, followed by a spectral blue shift, signaling the collapse of the channel.

The experiment was performed using the Janus laser facility at Lawrence Livermore National Laboratory. One beam of the laser produced a 0.53 μm wavelength, 45 J, 1.3 ns long, nominally square laser pulse that irradiated a 0.5 μm thick polypropylene exploding foil target (CH_2) which is supported by a 75-mm-thick Mylar washer. This beam is focused with an f/4 lens to a 400 μm diameter spot. After the plasma forming pulse has burned through the target and the

peak density has decayed below n_c, a second, interaction pulse counterpropagates relative to the plasma forming beam through the plasma. This pulse has a central wavelength of 1.053 μm with a bandwidth of 1.4 nm, and is compressed to a FWHM pulse width of ~ 600 fs. The 6.5 cm diameter beam is focused by a 30 cm focal length off-axis parabola to a focused spot with a FWHM diameter of 12 μm which was measured with an equivalent plane imaging system. At the highest input energies (6 J) the maximum intensity at best focus is ~ 5 x 10^{18} W/cm^2.

Light that is transmitted through the plasma is collected by the focusing lens of the plasma forming lens; 50% of the light goes to an energy calorimeter and 50% goes to a single-shot FROG diagnostic [10] which records the laser spectrum versus time with 10 fs resolution. The target plasma density distribution was measured by a folded wave interferometer throughout the experiment. The probe beam for the interferometer was 0.35 μm wavelength, 600 fs in duration, and was timed to within 50 ps of the arrival of the interaction pulse at the target. We also imaged the sidescattered 1.053 μm light transverse to the propagation direction of the ps pulse in order to locate the position of the maximum laser intensity.

The onset of relativistic filamentation is shown quite clearly in the scaling of the collected transmitted energy with the incident beam energy (see Fig. 1). As we found in earlier, 100 ps experiments [11], filamentation can result in the spraying out of the transmitted light to angles much larger than the vacuum propagation angle. In Fig. 1, we see that at low laser intensities, the transmitted laser energy equals the incident energy. Above an intensity of 10^{18} W/cm^2, the percentage of transmitted light is less as the filamentation instability increases. Varying the peak density changes the laser intensity at which the inflection point occurs. For a peak density of $0.1n_c$, the transition occurs near 0.15 J, while for a peak density of $0.05n_c$, it occurs near 0.7 J. The maximum amount of light backscattered into the parabola was 10% and cannot account for the transmission behavior.

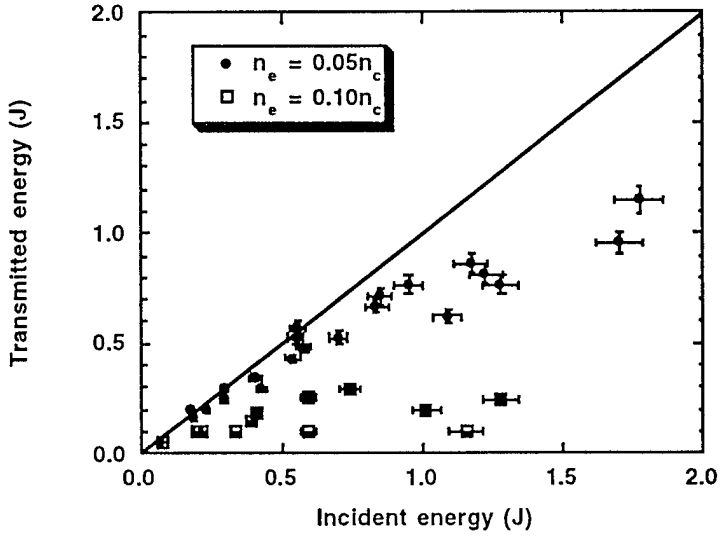

FIGURE 1. Measured energy transmitted through the plasma as a function of the incident energy for two different peak plasma densities.

The power at which the transition occurs in Fig. 1 is greater than the predicted critical power for relativistic self-focusing:

$$P_c = 17(n_c/n_e)\ \text{GW}. \qquad (1)$$

Substituting the measured peak densities into this equation gives critical powers of P_c = 340 GW or E_c = 200 mJ for $n_e = .05n_c$, and P_c = 170 GW or E_c = 100 mJ for $n_e = .1n_c$. The threshold energies are higher than those given by the theory probably because the theory is linear, whereas in the actual experiment the high intensity pulse can depress the background density.

We used filtered, high-speed infrared film to record the light outside the collecting lens. and show that as the energy was increased, the light sprayed to larger angles consistent with the observed decrease in the transmitted energy [11]. Most of the sprayed light has wavelengths close to the fundamental laser wavelength and the contributions from SRS are small. This result is consistent with the simulations of Ref. 12 which predict a 20% reduction of transmitted light due to SRS absorption and scattering. It has also been pointed out [13] that SRS will not occur in evacuated channels. These results are consistent with previous experiments [14], in which a single pulse interacts with a gas jet, have observed that as they increased the gas fill pressures (higher electron densities) they observed the reduction of the forward SRS anti-Stokes feature to the detection noise level which was accompanied by the exponential increase of the transmitted laser light, which they attributed to self-focusing and ionization induced refraction (which cannot occur in our experiment).

We would like to acknowledge useful conversations with M. Feit, J. Garrison, and A. Rubenchek. Important technical support was provided by J. Bonlie, W. Cowens, J. Foy, A. Hankla, J. Hunter, G. London, and B. Sellick. This work was performed under the auspices of the U.S. Dept. of Energy by Lawrence Livermore National Laboratory under contract W-7405-ENG-48.

REFERENCES

[1] C. E. Clayton *et al.*, Phys. Rev. Lett. **70**, 37 (1993).
[2] P. Sprangle and E. Esarey, Phys. Fluids B **4**, 2241 (1992), and references therein.
[3] N. H. Burnett and P. B. Corkum, J. Opt. Soc. Am. **6**, 1195 (1989); D. C. Eder *et al.*, Phys. Plasmas **1**, 1744 (1994).
[4] M. Tabak *et al.*, Phys. Plasmas **1**, 1626 (1994).
[5] C. E. Max *et al.*, Phys. Rev. Lett. **33**, 209 (1974); G. Z. Sun *et al.*, Phys. Fluids **30**, 526 (1987); P. Sprangle *et al.*, Trans. Plasma Sci. **PS-15**, 145 (1987);W. B. Mori *et al.*, Phys. Rev. Lett. **60**, 1298 (1988); X. L. Chen and R. N. Sudan, Phys. Rev. Lett. **70**, 2082 (1993); E. Esarey *et al.*, Phys. Rev. Lett. **72**, 2887 (1994); P. Gibbon *et al.* Phys. Plasmas **2**, 1305 (1995).
[6] P. Sprangle and E. Esarey, Phys. Rev. Lett. **67**, 2021 (1991).
[7] P. Monot *et al.*, Phys. Rev. Lett. **74**, 2953 (1995).
[8] R. Rankin *et al.*, Opt. Lett. **16**, 835 (1991); P. Monot *et al.*, J. Opt. Soc. Am. **B9**, 1579 (1992); A. J. Mackinnon *et al.*, Phys. Rev. Lett. **76**, 1473 (1996); P. R. Bolton *et al.*, J. Opt. Soc. B. **13**, 336 (1996).
[9] P.E. Young and P.R. Bolton, Phys. Rev. Lett. (in press).
[10] R. Trebino and D. J. Kane, J. Opt. Soc. Am. **A10**, 1101 (1993); D. J. Kane and R. Trebino, Opt. Lett. **18**, 823 (1993); D. J. Kane and R. Trebino, IEEE J. Quant. Elec. **29**, 571 (1993).
[11] S. C. Wilks *et al.*, Phys. Rev. Lett. **73**, 2994 (1994); P. E. Young *et al.*, Phys. Plasmas **2**, 2825 (1995).
[12] K.-C. Tzeng *et al.*, Phys. Rev. Lett. **76**, 3332 (1996).
[13] P. Mora and T. M. Antonsen, Jr., Phys. Rev. E **53**, R2068 (1996).
[14] C. A. Coverdale *et al.*, Phys. Rev. Lett. **74**, 4659 (1995).

Hot electron distribution from short pulse laser plasma

M. Schnürer, P. Ambrosi*, M.P. Kalachnikov, P.V. Nickles, R.Nolte*, Th. Schlegel and W. Sandner

Max-Born-Institut, Rudower Chaussee 6, 12489 Berlin, Germany
**Physikalisch-Technische Bundesanstalt, Postfach 3345, 38023 Braunschweig, Germany*

Tel.: 0049-30-63921321; Fax: 0049-30-63921329; E-Mail: mschnue@mbi.fta-berlin.de

Hot electron production and related Bremsstrahlung emission known in long pulse (tens of ps up to ns FWHM) becomes more important in short and ultra short (ps down to tens of fs FWHM) laser plasma interaction because some ten percent of the laser energy are being transferred to hot electrons, as theoretical (Wilks et al 1992, Gibbon 1994) and experimental (Schnürer et al 1995) studies have indicated. Measured hot electron distributions are compared to model predictions in order to gain more knowledge about the laser plasma absorption mechanism. A control of the hot electron production with the driving optical laser parameters is important for the Bremsstrahlung emission, if one wants to optimize short pulse hard X-ray sources. At relativistic driving laser intensities above 10^{19} W/cm^2 hot electron production is the key part in the fast ignitor concept for the inertial confinement fusion (Tabak et al 1994).

We analyze our experimental results from hard X-ray measurements on the basis of computer code calculations and phenomenological estimations. From literature one finds results (Malka and Miquel 1996, Kieffer et al 1996, Darrow et al 1995) and argumentations (Perry and Mourou 1994) for a Maxwellian distribution as well as for a non-Maxwellian distribution (Klem et al 1993) of hot electrons.

Experimental set-up

The experiments were carried out with the laser installation at the Max-Born-Institut in Berlin. The chirped pulse amplification system uses a Ti:Sa oscillator and a regenerative amplifier front end which is coupled to a glass power amplifier chain (Kalashnikov et al 1994). The main pulse parameters are : pulse width (0.7±0.2) ps FWHM, centre wavelength 1053 nm, aspherical lens with 123 mm focal length and amplified spontaneous emission background to main pulse contrast $\approx 10^{-6}$.

Tantalum targets 0.5 mm thick, with a non-polished surface with uniformly diffuse scattering properties were irradiated with $(3\pm2)*10^{17}$ W/cm^2. Thermoluminescence dosimeters (TLD's) (Ambrosi et al 1994) covered with different filters were used to detect the hard X-ray emission.

Results and discussion

In order to look at the X-ray emission with improved energy resolution a nine channel filter TLD-detector was used. The distance between the detector and the plasma spot X-ray source was 10 cm. X-ray emission from 22 laser shots with a total energy of 43 J was collected. Fig.1 shows the variation of the spectral fluence Φ_E (thick line) with photon energy. As indicated in fig.1 one can approximate the experimental distribution with two hot electron temperatures $T_h \approx$ 16 keV (dashed line) and $T_h \approx$ 70 keV (dotted line). As visible from fig.1 the signal at

photon energies above 100 keV gives an indication for hot electrons with energies also above 100 keV. Because of the very weak detected signals in this range no sufficiently reliable data could be obtained from the SAND unfolding algorithm (Mc Elroy et al 1967) which was applied to the measured values.

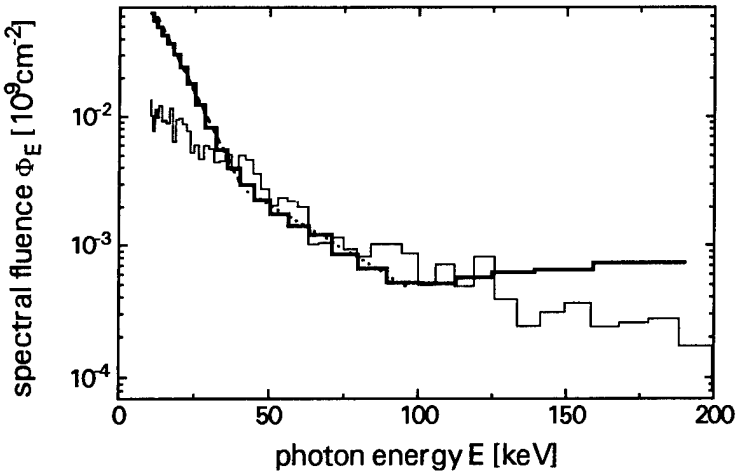

Fig.1 Spectral fluence (thick solid line) in different energy channels measured with the multi-filter detector and simulation (thin solid line), estimated hot electron temperatures: $T_h \approx$ 16 keV (dashed line) and $T_h \approx$ 70 keV (dotted line)

A hydrodynamic radiation coupled code was developed for the simulation of the laser plasma interaction at high laser intensities inclusive ponderomotive effects (Kalashnikov et al 1994). From the code we obtain the electron energies produced with the temporal laser intensity development. With the electrons produced one can calculate solid target Bremsstrahlung, provided that at electron energies above 10 keV the few microns thick plasma layer plays a minor role in the electron deceleration process.

The electron deceleration process in the thick target was calculated with the EGS4-Monte Carlo code (Nelson et al 1985). In addition we take tabulated scaled Bremsstrahlung cross sections (Seltzer and Berger 1986) for the X-ray emission calculation. The resulting spectrum from the theoretical electron energy distribution is also plotted in fig.1 (thin solid curve) which is scaled relatively to the experimental absolute spectral fluence values. The curve represents the angular emission (observation angle) which was relevant for the multi filter TLD-detector. Between 40 keV and 100 keV photon energy a similar shape to the experiment is visible. The hydrodynamic code does not predict as many low energy photons as seen in the experiment. That may be due to an overestimation of resonance absorption in the hydrodynamical radiation coupled code or a slight uncertainty in the absolute intensity distribution. The theoretically obtained hot electron distribution and the related X-ray emission can not be explained with a single temperature parameter.

In addition to measurements of spectral components of hot electron Bremsstrahlung we have recorded the spatial emission characteristic with a set of TLD´s . The distribution shows a slight maximum close to the direction of the target surface normal. The overall angular signal variation is between a factor 2 to 3.

As an additional effect from the Monte Carlo electron propagation and Bremsstrahlung coupled code one can calculate the temporal evolution of photon emission. So a Bremsstrahlung pulse duration estimation is possible. The temporal development of the Bremsstrahlung pulse integrated over all photon energies is shown in fig.2. The fit curve is an exponential decay function. It was assumed that all electrons from our theoretical distribution start at a time t=0. This idealized case at least gives than a lower bound of the Bremsstrahlung

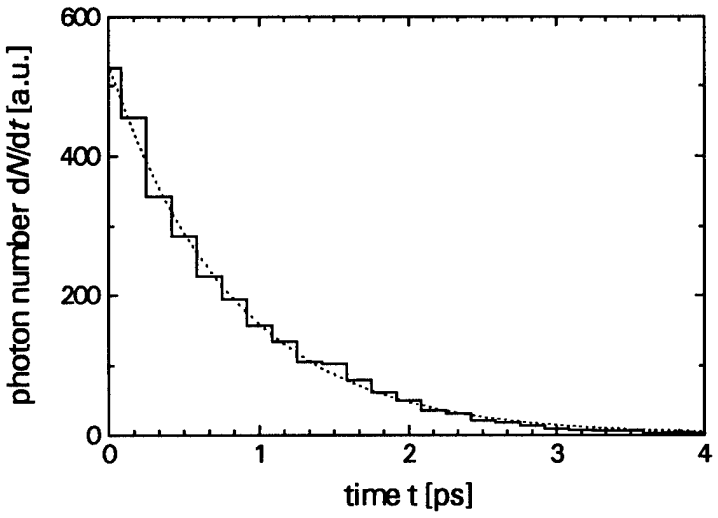

Fig.2 Theoretical calculation of the Bremsstrahlung pulse duration assuming a start of all hot electrons at t=0

pulse width due to multiple scattering and propagation of the electrons in a thick target in case of an energy distribution as we have taken. One can fold the laser and the idealized Brems-strahlung pulse in order to estimate the hard X-ray pulse duration. With our 0.7 ps laser driver one can expect an hard X-ray pulse of about 1 ps from a massive thick target.

Under our experimental conditions we have observed and verified theoretically a multi component hot electron temperature distribution characterizing the Bremsstrahlung emission of energetic electrons produced in short pulse high intensity laser plasma interaction.

References

Ambrosi P, Buchholz G, Böhm J, Griffith R V, Herrman D and Strachotinsky C 1994 Radiat. Protection Dosimetry **54** 5
Darrow C, Hay G, Zakharenkov Y, Nguyen H, Hammel B and Perry M D 1995 25th Anomalous Absorption Meeting, Aspen Colorado, unpublished
Gibbon P 1994 Phys. Rev Lett. **73** 664
Kalashnikov M P, Nickles P V, Will I, Billhardt F and Schnürer M 1994 Laser Part. Beams **12** 463
Kalashnikov M P, Nickles P V , Schlegel T, Schnürer M, Billhardt F, Will I and Sandner W Demchenko N N 1994 Phys. Rev. Lett. **73** 260
Kieffer J C, Jiang Z, Ikhlef A, Cote C Y and Peyrusse O 1996 J. Opt. Soc. Am. B **13** 132
Klem D E, Darrow C, Lane S and Perry M D 1993 SPIE Proceedings **1860**
Malka G, Miquel J L 1996 Phys. Rev. Lett. 77 75
McElroy W N, Berg S, Crockett T and Hawkins R G 1967 Report AFWL-TR-67-41, US Weapons Laboratory
Nelson W R, Hirayama H and Rogers D W O 1985 Report SLAC-265, Stanford Linear Accelerator Center (1985)
Perry M D and Mourou G 1994 Science **264** 917
Seltzer M S and Berger M J 1986 At. Data and Nucl. Tables **35** 345
Schnürer M, Kalashnikov M P, Nickles P V, Schlegel T, Sandner W, Demchenko N, Nolte R and Ambrosi P 1995 Phys. Plasmas **2** 3106
Tabak M, Hammer J, Glinsky M E, Kruer W L, Wilks S C, Woodworth J, Campbell E M and Perry M D 1994 Phys. Plasmas **1** 1626
Wilks S C, Kruer W L, Tabak M, and Langdon A B 1992 Phys. Rev. Lett. **69** 1383

Strong-Field Ionization of Molecules at 35 fsec.

G. N. Gibson, M. Li, C. Guo

University of Connecticut
Department of Physics
2152 Hillside Road, U-46
Storrs, CT 06269
(860) 486-3857, (860) 486-3346 (fax)
gibson@main.phys.uconn.edu

The multiphoton ionization of molecules in strong laser fields has been investigated for over 10 years. However, the interpretation of the experiments has been complicated by the vibrational time scales of the molecules. Specifically, when a molecules is ionized to 2+ or higher, it becomes unstable and starts to dissociation. At pulse durations longer that 100 fsec the dissociation occurs while the laser pulse is still on which complicates the interpretation of the results. Thus, there is great interest in performing these experiments with as short a pulse duration as possible. To this end we have constructed an ultrashort-pulse laser system which delivers 0.5 mJ in 35 fsec with good beam quality. Ensuring the latter required the careful design of a multipass amplifier.

There have basically been two approaches to designing amplifiers for ultrashort laser pulses: regenerative[1] and multipass[2]. Regenerative amplifiers have been used successfully, but have two drawbacks: they require active injection and extraction of the seed and amplified pulse, increasing the cost and complexity of the laser system. More importantly, the active elements consisting of a Pockels Cell and polarizer are traversed many times during the amplification. This amounts to a considerable quantity of optical material (potentially over 60 cm) seen by the laser pulse which introduces high order phase errors in the pulse's spectrum. While these phase errors can be compensated for in a sufficiently elaborate pulse compressor, it is not very convenient.

Alternatively, multipass amplifiers are attractive, as they are passive optical devices and contain only the amplifying crystal. An 8-pass amplifier with an 0.5 cm Ti:Sapphire crystal has only 4 cm of material. This is much easier to compensate. Ref. 2 presents a particularly simple multipass amplifier. However, to prevent degradation of the beam quality upon successive passes through the amplifier they had to place an aperture. Unfortunately, an aperture in the far field of a beam (i.e. not at the waist) can only affect the beam quality for a short distance, as it does not remove high spatial frequencies from the beam.

In order to correct these problems we have modified the design of Ref. 2 as shown in Figure 1. Instead of a three mirror ring amplifier, we used five mirrors. This allows us to independently adjust the angle of incidence on the curved mirrors. It is well know that a slab of glass at an angle with respect to the optical axis can compensate the astigmatism introduced by using mirrors off normal incidence. With complete control over the angle of incidence and using the Ti:Sapphire crystal at Brewster's angle we could completely

compensate the astigmatism in the amplifier. When we used a three mirror cavity, we noticed many of the effects mentioned in Ref. 2, such as the beam enlarging on each pass, attributed to thermal lensing, which was the purpose of aperturing the beam in Ref. 2. However, the five mirror cavity showed no adverse effects due to thermal lensing and the beam size and quality was maintained on each pass without any apertures. Indeed, our estimates of thermal lensing indicated that it should not be a problem.[3] Thus, we attribute the degradation of the beam quality in the three mirror amplifier design to astigmatism.

In addition to maintaining the beam quality without any apertures, we wanted to have full control over the modematching of the amplified beam with the pump volume. In Ref. 2, the central mirror was a single surface. This will complete the ring and have all of the beams overlap in the gain region only if the separation of the curved mirrors is equal to their radius of curvature. Eight passes is enough that the amplifier should be designed along the lines of a cavity, i.e. the waist of the beam which repeats without change will depend on the curved mirror separation. With a single central mirror the curved mirror separation is fixed, and thus, so is the beam waist. In order to lift the constraint on the beam waist, we had to allow the curved mirror separation to change. This, in turn, means that the central mirror cannot be one flat mirror, as the beam waists would not all overlap in the crystal. We replaced the single flat central mirror with six independently controllable mirrors, one for each pass. In addition, the first pass is controlled by the input beam and the fifth pass by a vertical retroreflector (see Figure 1). Thus, the overlap of the individual beams in the crystal could always be maintained. With these changes in place, the amplified beam was essentially identical to the unamplified beam at the exit of the amplifier.

As noted above, an important reason for producing such short laser pulses is to investigate strong-field ionization of molecules. One apparently puzzling observation has been that when molecules ionize and fragment, the kinetic energies of the ion fragments is always systematically less than what would be expected if the ionization occurred at the internuclear separation of the ground state neutral molecule, R_e.[4] Recent theories[5] offer a good explanation for this, in that calculations show that the ionization rate of a

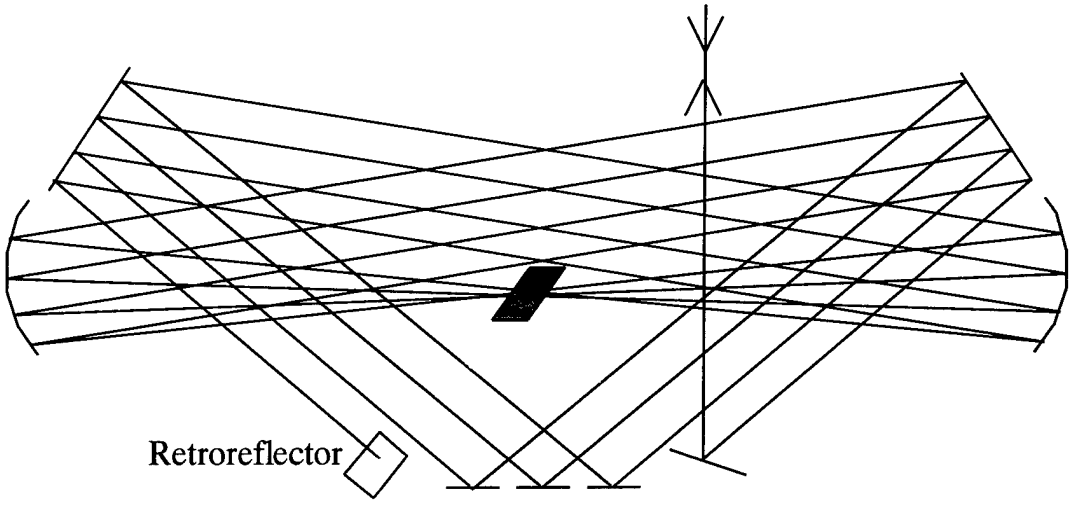

Figure 1: Eight pass amplifier. The retroreflector displaces the beam in the vertical direction. The incoming and out going beams are at different heights.

molecule depends strongly on the internuclear separation and, in fact, peaks strongly at a critical separation, R_c, which is about 2-3 times R_e. If the molecule expands sufficiently during the laser pulse through dissociation to reach R_c then most of the ionization will occur at this point and yield lower energy fragments. The intent of using very short pulses is to complete the ionization process before any dissociation can occur, and thus, be able to separate out these effects. Figure 2 shows our recent measurements of the kinetic energies of the ion fragments of nitrogen following strong-field ionization. The energies were recorded using a standard time-of-flight chamber. It is remarkable that even at very short pulse durations, the ion fragments have precisely the same energies as measured at 100 fsec and 1 psec. We now plan to take more extensive data to further test the model of ionization taking place at a critical separation.

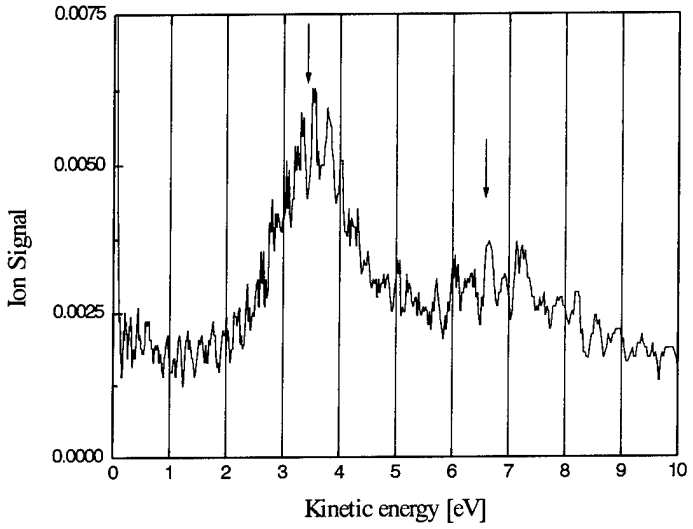

Figure 2: Energy distribution of N^{1+} ions following strong field ionization. Arrows indicate measured values from Ref.4.

References:

1) K. Wynne, G. D. Reid, and R. M. Hachstrasser, Opt. Lett. **19**, 895 (1994).

2) S. Backus, J. Peatross, C. H. Huang, M. M. Murnane, and H. C. Kapteyn, Opt. Lett. **20**, 2000 (1995).

3) K. F. Wall, R. L. Aggarwal, M. D. Sciacca, H. J. Zeiger, R. E. Fahey, and A. J. Strauss, Opt. Lett. **14**, 180 (1989).

4) C. Cornaggia, J. Lavancier, D. Normand, J. Morellec, and P. Agostini, Phys. Rev. A **44**, 4499 (1991).

5) M. Ivanov , T. Seideman , P. Corkum, Phys. Rev. A **54**, 1541 (1996).

Intensity Dependent Probabilities for Strong Field Ionization of Xenon

M.A. Walker, P. Hansch, and L.D. Van Woerkom
Department of Physics
The Ohio State University
174 W. 18th Avenue
Columbus, OH 43210-1106
voice: 614-292-4286
fax: 614-292-7557
e-mail: maw@mps.ohio-state.edu

We have employed a novel method, Intensity Selective Scanning [1, 2], to measure time-of-flight mass spectra of ions produced by strong field laser ionization. The hallmark of this technique is that it eliminates a serious problem inherent in traditional experiments: the complex spatial distribution of intensities present in the ionizing pulse. As a consequence, it becomes possible to extract ionization yields as a function of intensity directly from the experimental data, without the previous complication of untangling them from a spatially averaged signal. We present results for xenon ionized by laser pulses at intensities ranging from 10^{13} to $4x10^{14}$ W/cm^2.

We recorded time-of-flight mass spectra of xenon using a 1 kHz Ti:Sapphire laser system, generating 120 fs, 800 nm output pulses with an energy of 700 mJ per pulse. The absolute peak intensity at the minimum beam waist was held fixed while spectra over the range were recorded via the ISS technique, which involves limiting the volume observed by placing an aperture at the end of the spectrometer's flight tube near the interaction region. Ions are detected only from positions in the laser focus which are in the direct line of sight of the detector.

By restricting the spatial extent of the region from which the observed signal originates, in these experiments to a 500μm wide rectangular "slice" along the longitudinal axis of the focus, we were able to reduce the usually complicated spatial distribution of intensities responsible for producing ions to essentially a one-dimensional radial distribution about the axis. This reduced dimensionality allows the deconvolution of the ion signal to be performed by a simple procedure, so that the ionization yields as a function of intensity could be deduced directly from the experimental data. Determination of the specific spatial characteristics of our focus was sufficient to allow this to be done. This is in contrast to

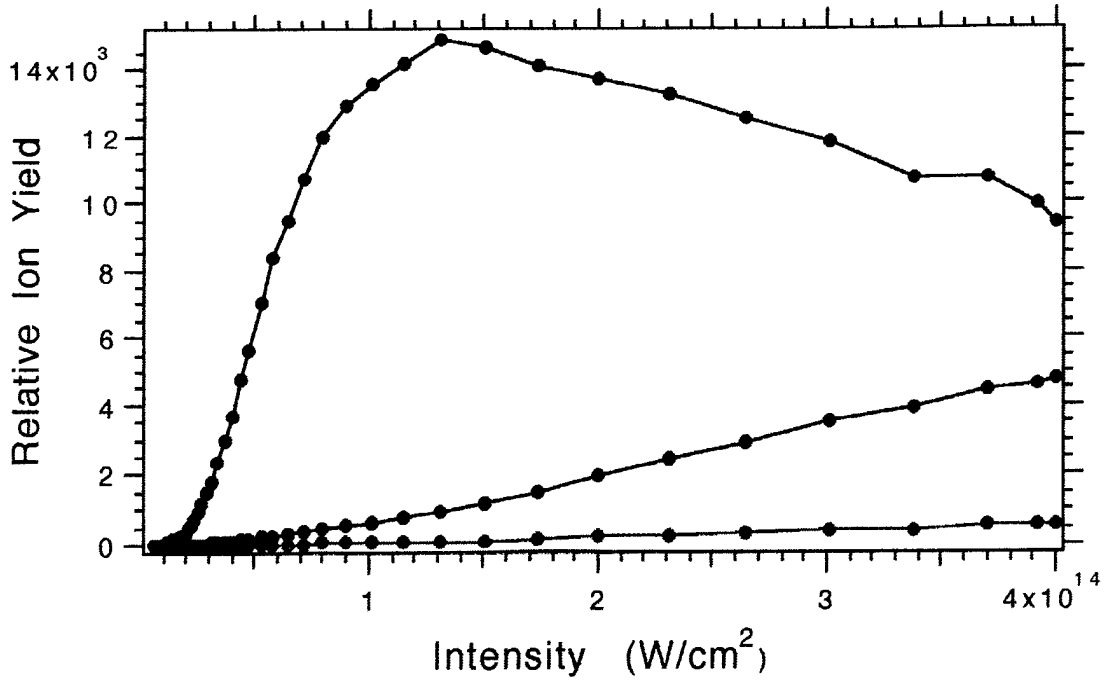

Fig. 1. Experimental ion yield curves vs. intensity found using the ISS technique. The higher charge state curves have been scaled to reflect the estimated relative efficiency of the ion detector.

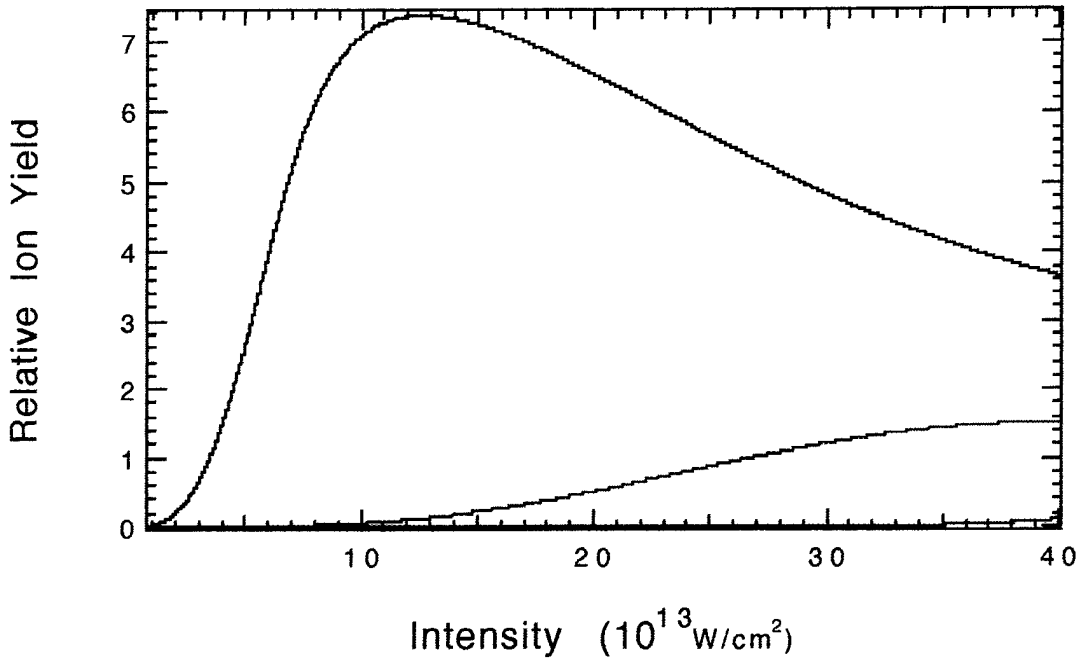

Fig. 2. Theoretical ion yield curves vs. intensity. The curves were generated by using a simple rate equation approach with rates estimated as multiphoton with effective cross section and order and integrating this signal over the radial intensity distribution.

This method makes it possible to directly observe the single-atom, single intensity response and then compare this with theory, rather than comparing averaged model predictions to averaged signals, which is the best that can be done otherwise.

Figures 1 and 2 represent a comparison of the experimental data with a simple theoretical model. The modeling approach was to solve a set of rate equations for the relative ionization after passage of the pulse, given a specific temporal peak intensity. This intensity was then varied to produce a plot of relative yield vs. intensity. The ionization rates were estimated as multiphoton with effective cross sections and orders. Figure 1 shows the experimental data obtained using ISS. It was necessary to scale the signal curves for the higher charge states using estimated values for the relative efficiencies of the multichannel plates used to detect the ions. The limitation of the signal source volume is evident in the rollover of the single ion curve around 1.3×10^{14} W/cm^2. This results from the saturation of the single ionization in the volume and subsequent depletion of single ions by double ionization.

The precise intensity control available with the ISS technique coupled with its simplification of the extraction of meaningful physical information from observed signals is an important step toward understanding ionization in high fields, in particular its behavior with intensity. Experiments can now be performed to collect data which is easily transformed to a representation directly compatible with theory, replacing the need to manipulate averaged theories to match averaged data so that they meet somewhere in the middle.

[1] P. Hansch, L. D. V. Woerkom, Opt. Lett. 21, 1286-1288 (1996).

[2] P. Hansch, M. A. Walker, L. D. V. Woerkom, Phys. Rev. A 54, R2559-R2562 (1996).

8- and 9-Photon Resonances in Above Threshold Ionization of Xenon

P. Hansch, M.A. Walker, and L.D. Van Woerkom
Department of Physics
The Ohio State University
174 West 18th Avenue
Columbus, OH 43210-1106
voice: 614-292-4286
fax: 614-292-7557
e-mail: hansch.1@osu.edu

We have observed for the first time higher order multiphoton resonances in xenon. The clear evolution through parity-allowed resonances at the 8- and subsequent 9-photon level demonstrates the validity of the transient resonance model up to the saturation intensity. At high laser intensities ($> 10^{12}$ W/cm^2) the ionization limit and high lying Rydberg states of xenon shift ponderomotively upward and ionization occurs via transient resonances with specific multiples of the incident photons [1]. We have observed a very clear evolution of transient 8-photon resonances showing the successive appearance of Rydberg states and a large enhancement in photoelectron signal when reaching the higher order 9-photon resonances. This observation furthers our understanding of the fundamental ionization process in strong fields.

We have recorded photoelectron time-of-flight spectra of xenon using a 1 kHz Ti:Sapphire laser system, generating 120 fs, 800 nm output pulses with an energy of 700 mJ per pulse. The absolute peak intensity at the minimum beam waist was held fixed while spectra at different intensities were recorded via Intensity-Selective-Scanning [2]. Using this technique, only a selected 'slice' instead of the entire Gaussian focal volume is exposed to the detector. By scanning the slice along the propagation direction we achieve precise intensity control, better signal-to-noise ratios, and signal gain at low intensities due to the volume increase of the diverging laser beam.

Fig. 1 shows the photoelectron kinetic energy spectra for the intensity range $2\text{x}10^{13}$ - $5\text{x}10^{13}$ W/cm^2. The ionization potential for leaving neutral Xe in the $^2P_{3/2}$ single ion state is 12.127 eV. Given 800 nm photons (1.55 eV), the first parity-allowed multiphoton resonance for the f-series Rydberg states occurs with the 8-photon level. As the intensity is raised beyond the threshold for observing the 4f-state, the overall signal keeps rising, yet the 4f-resonance becomes clearly the dominant spectral feature. Since low lying Rydberg states require higher ionization intensities, the 4f-ionization rate exceeds those of higher lying f-states and the 4f-peak dominates the spectrum (Figs. 1c, 1d), despite the smaller volume within which the 4f-resonance occurs.

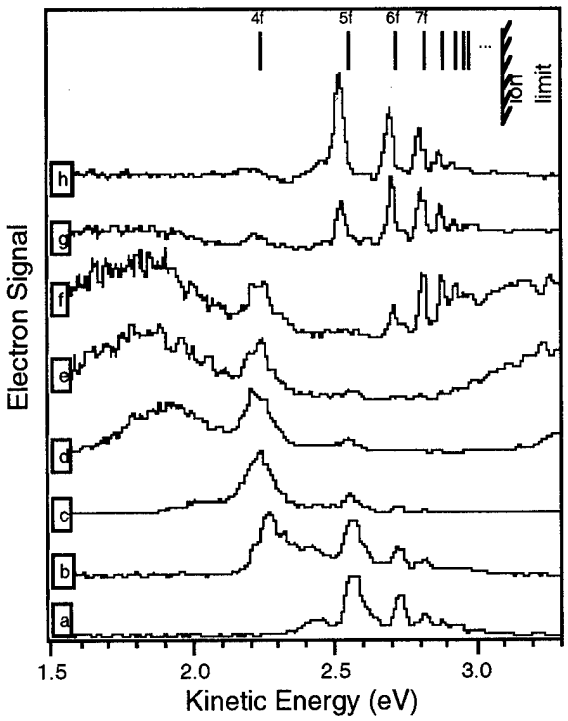

Fig. 1. High intensity photoelectron spectra showing the transition from 8- to 9-photon resonances in xenon using 800 nm light at intensities from $2x10^{13}$ - $5x10^{13}$ W/cm^2. All curves are vertically shifted and normalized to a common maximum amplitude.

In Figs. 1d, 1e a broad feature appears below the 4f-state. This region consists of a cluster of 7p-states as well as indications of nonresonant contributions to the ionization. Figs. 1f-1h display the sudden emergence of Rydberg g-states once the a.c.-Stark shift brings them into 9-photon resonance. Each curve is normalized to a common maximum amplitude for better comparison of relative effects. While the 8-photon 4f-state contribution remains fairly constant in Figs. 1e-1h, the effects of the 9-photon resonances at higher intensities increase dramatically and dominate the spectrum. The width of the 9-photon features is smaller than that of the 8-photon peaks. This is may be an indication of a longer lifetime for the 9-photon resonances.

In conclusion, we have observed for the first time higher order multiphoton ionization using Intensity-Selective-Scanning, a novel technique of photoelectron spectroscopy. Our measurements demonstrate a new level of precision in intensity control and signal-to-noise quality.

[1] R.R. Freeman *et al.*, *Phys. Rev. Lett.* **59**, 1092 (1987).

[2] P. Hansch and L.D. Van Woerkom, *Optics Letters* **21**, 1286 (1996).

Simulation of ionization ignition and inner atom shell ionization in ultrafast laser driven clusters

C. Rose-Petruck[a], K. J. Schafer[b], K. R. Wilson[a] and C. P. J. Barty[c]

(a) Department of Chemistry and Biochemistry
University of California San Diego, La Jolla, CA 92093-0339
phone: (619) 534-0290
fax: (619) 534-7654

(b) Department of Physics and Astronomy
Louisiana State University, Baton Rouge, LA 70803-4001
phone: (504) 388-0466

(c) Institute for Nonlinear Science,
University of California San Diego, La Jolla, CA 92093-0339
phone: (619) 534-2417

Gas clusters irradiated with ultrashort, high intensity laser pulses can exhibit "ionization ignition" which leads to very high charge states that are significantly higher than those for equivalent laser pulses applied to atoms in the gas phase [1, 2]. Moreover, such laser generated plasmas from clusters might serve as bright sources of ultrashort duration, hard x-rays [3-5]. Experimental shapes of the x-ray emission spectra are distinctly non-thermal and show evidence of multiple inner shell holes [6] and high electron kinetic energies [7].

The ionization dynamics of small rare gas clusters was studied using a Classical Trajectory Monte-Carlo (CTMC) model as described in detail elsewhere [8, 9]. 25-atom Ne clusters and 25-atom Ar clusters are modelled as irradiated by a 800 nm, 15 fs (fwhm) laser pulse with peak intensities ranging from $5x10^{15}$ to $5x10^{17}$ W/cm^2. While enforcing a chosen nearest neighbor distance, the atoms are initially randomly placed inside a boundary volume. This arrangement is subsequently equilibrated at T = 0 using Lennard-Jones potentials for the atom-atom interactions which leads to cluster geometries similar to experimentally found structures [10]. The cluster is placed in a laser field free region and the calculations are performed while the laser pulse passes through this volume. The output data for neon are subsequently used to calculate the inner shell electron impact ionization probabilities using Lotz' formula [11] normalized to a "classical atom size" of 74,500 pm^2. Due to the classical nature of this approximation and of our model, these probabilities are only used for comparison of the ionization dynamics of different atomic shells.

The atoms are modeled by placing electrons into classical orbits [8, 9] so that the ionization energies equal the experimental values. In order to prevent unphysical ionization, the interactions among bound electrons are restricted. Ions, outer shell electrons and ionized electrons interact via Coulomb forces. These charged particles simultaneously interact with the laser and the field of the other charged particles. The calculations are relativistic and thus include the magnetic forces of the laser field.

The ionization dynamics can be attributed to the laser field which initiates the cluster ionization and subsequently removes electrons from the cluster while the large field due to ionized

electrons and ions further enhances ionization. Only inner shell electrons are left which are too tightly bound to permit ionization.

As depicted in Fig. 1, the maximum average charge state reached rises very rapidly as the peak laser intensity is increased to about $5x10^{16}$ W/cm^2. Thereafter, as nearly the entire outer shell of neon is ionized, the slope levels off. While, at the lowest intensity, gas phase atoms would be singly ionized, a charge state of 2.5 is reached for a 25-atom cluster. This corresponds to 62 ionized electrons and, when compared to the total number of electron-ion collisions, shows that on average nearly every electron collides with an ion during the course of the laser cluster interaction. This leads to strong collisional heating of the electrons and causes their random motion. As the laser peak intensity increases, the number of electron-ion collisions decreases. The laser field gets increasingly stronger compared to the charged particle field inside the cluster and, therefore, can remove electrons from the cluster more efficiently. Due to the increasing laser intensity, the acceleration of the electrons increases which results on average in a larger energy gain per collision. Since collisional heating is dependent on the number of collisions and the energy gain per event, the strongest heating occurs at intermediate laser intensities around $5x10^{16}$ W/cm^2. This effect causes the maximum for the K shell ionization probability, as shown in Fig. 2. While the K shell electron impact ionization falls off at higher peak laser intensity, the L shell ionization probability remains approximately constant. To illustrate the effect of the cluster size on the L shell ionization, calculations for a 55-atom neon cluster are performed and the corresponding data point is reproduced in Fig. 2. It is important to note that the ionization probability is not just larger by a factor 2.2, the ratio of the number of atoms in the 55 and 25-atom clusters, but is about 5.5 times higher. This is due to the longer propagation time for the electrons to leave the cluster, which enhances the collisional heating. Nevertheless, at this laser intensity for the 55-atom cluster, no K shell ionization is found.

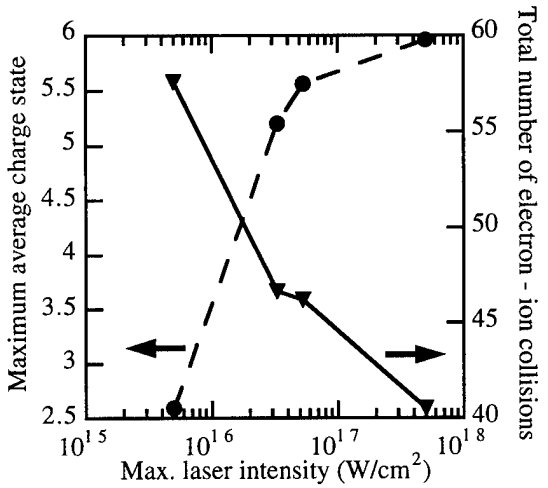

Fig.1: Maximum average charge state and total number of electron - ion collisions vs. peak laser intensity for a constant laser pulse width of 15 fs (fwhm) and for a 25 atom neon cluster. Prior to the interaction of laser pulse and cluster, the initial average nearest neighbor distance between the nuclei is 353 pm.

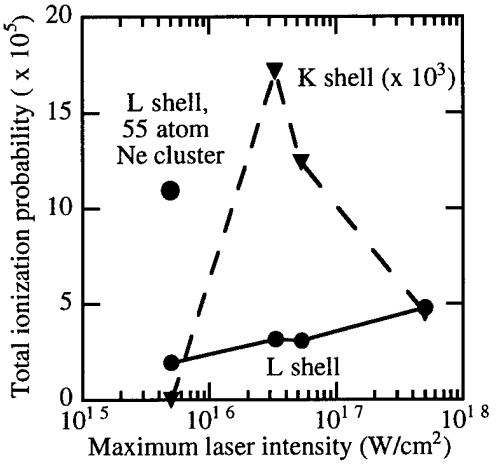

Fig.2: Total electron impact ionization probability of the K and L shells for the same calculations as shown in Fig. 1. Also shown is the L shell ionization probability for a 55 atom neon cluster.

Similar ionization characteristics as presented for neon clusters were also found for 25 atom argon clusters. The initial average nearest neighbor distance between the nuclei prior to the interaction of laser pulse and cluster is 382 pm. Upon illuminating such clusters by 800 nm, 15 fs (fwhm) laser pulses with a peak laser intensity of $5x10^{16}$ W/cm^2, the M shell of each argon atom is completely ionized, producing clusters of Ar^{8+}

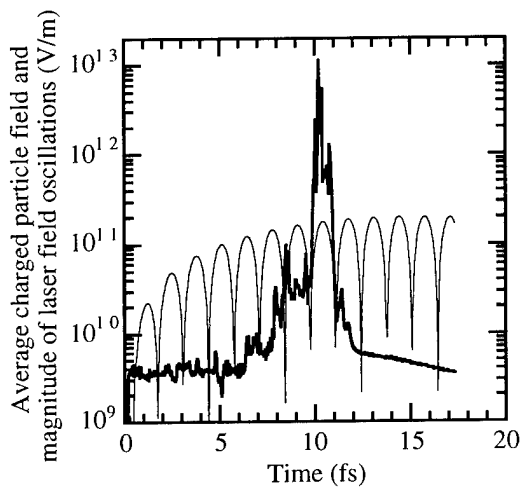

Fig.3: Average electric field from other ions and ionized electrons at the position of the nuclei of a 25-atom argon cluster. The cluster is illuminated by a 800 nm, 15 fs laser pulse with a peak intensity of 5×10^{15} W/cm^2 whose electric field oscillations are drawn as a thin line. Note the logarithmic scale.

ions within 11 fs after the beginning of the laser-cluster interaction. Collisional electron heating causes L shell electron impact ionization. Due to the high ionization potential of 3205.9 eV, no K shell vacancies are produced. For argon clusters as well as neon clusters the density drops to

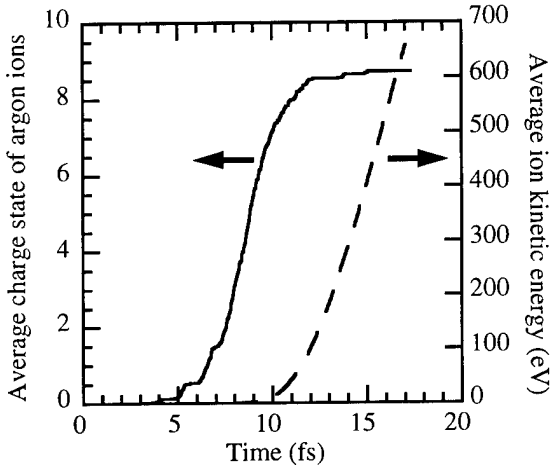

Fig.4: Average charge state of the cluster ions and average ion kinetic energy for the same calculations displayed in Fig. 3.

one tenth of its initial value within about 10 fs, due to the Coulomb repulsion. As depicted in Fig. 3, the average electric field at the position of each ion solely produced by surrounding ions and ionized electrons rises to values of up to 10^{13} V/m within 10 fs. This is much higher than the peak laser field of about 2×10^{11} V/m and shows the predominant influence of the charged particle field on the ionization dynamics. Considering this high field, it is not surprising that highly charged ions are measured in many related cluster ionization experiments [1, 2] and that their charge states are substantially higher than for equivalent laser pulses applied to gas phase atoms.

The electric field decreases as soon as a significant number of electrons have left the cluster and the ion density drops. The subsequent Coulomb explosion accelerates ions to substantial kinetic energies within 20 fs after the beginning of the laser pulse, as shown in Fig. 4. This is, again, a signature of "ionization ignition".

[1] J. Purnell, E. M. Snyder, S. Wei, and A. W. Castleman, Chem. Phys. Lett. 229, 333 (1994), .
[2] E. M. Snyder, S. A. Buzza, and A. W. Castleman Jr., Phys. Rev. Lett. 77, 3347 (1996), .
[3] C. Wülker, D. Theobald, D. Ouw, F. P. Schäfer, and B. N. Chichkow, Optics Comm. 112, 21 (1994), .
[4] A. McPherson, T. S. Luk, B. D. Thompson, A. B. Borisov, and C. K. Rhodes, Phys. Rev. Lett. 72, 1810 (1994), .
[5] T. Ditmire, T. Donnelly, R. W. Falcone, and M. D. Perry, Phys. Rev. Lett. 75, 3122 (1995), .
[6] A. McPherson, B. D. Thompson, A. B. Borisov, K. Boyer, and C. K. Rhodes, Nature 370, 631 (1994), .
[7] Y. L. Shao, T. Ditmire, J. W. G. Tisch, E. Springate, J. P. Marangos, and M. H. R. Hutchinson, Phys. Rev. Lett. 77, 3343 (1996), .
[8] C. Rose-Petruck, K. J. Schafer, and C. P. J. Barty, in Applications of Laser Plasma Radiation II, edited by M. C. Richardson and G. A. Kyrala (SPIE Publishing,Bellingham, WA, San Diego, 1995), Vol. 2523, p. 272.
[9] C. Rose-Petruck, K. J. Schafer, C. P. J. Barty, and K. R. Wilson, Phys. Rev. A (1996), in press.
[10] J. Farges, B. Raoult, and G. Torchet, J. Chem. Phys. 59, 3454 (1973), .
[11] A. A. Markowicz, in Handbook of X-ray Spectrometry: Methods and Techniques, edited by R. E. van Grieken and A. A. Markowicz (Marcel Dekker, Inc., New York, 1993), Vol. 14, p. 8.

Rare Gas Clusters in Intense Laser Fields

*M Lezius, S Dobosz, P d'Olivera, P Meynadier, and M Schmidt

CEA-Saclay, DSM/DRECAM/SPAM, Bat 524, 91191 Gif-sur-Yvette Cedex, FRANCE.

and

J-P Rozet and D Vernet

GPS - PIIM, Tour 13-23, Université Paris VI 2, place Jussieu, 75251 Paris Cedex 05, France

*(Phone: (33)-1-6908-2657, e-mail: lezius@droopy.saclay.cea.fr)

Recent experimental observations suggest that interaction of intense laser radiation with rare gas clusters jets provides an efficient source of X-rays and highly charged, energetic particles. Concerning the generation of X-rays the most prominent examples are the observation of: (i) Xe(M) an Kr(L) shell transitions with energies E up to 5keV reported by Rhodes and co-workers [1], (ii) non-coherent soft X-rays (E<500eV) on a nanosecond timescale reported by Perry and co-workers [2], and (iii) efficient high harmonic generation from Xenon clusters reported by Ditmire et al. [3]. Regarding the production of energetic particles, Ditmire et al. [5] have reported Xe^{q+}-ions with extremely high kinetic energies exceeding 100 keV when using 150fs pulses with intensities up to $10^{16}W/cm^2$. Interestingly, Snyder et al. [4] were able to detect high charge states such as Xe^{20+} in a time-of-flight mass spectrometer after applying 350fs pulses at intensities of only 10^{15} W/cm^2 to mixed He-Xe expansions. In a recent study of Argon clusters we have made very similar observations in a moderate intensity regime of $10^{14}W/cm^2$ [6] using 30ps pulses at 1064nm. Our experimental results suggest that the underlying mechanism is efficient electron-ion collisional heating of cluster-sized nanoplasmas, similar to the interpretation proposed by Perry et al [2].

In the present work, we have performed a extensive, quantitative study on the X-ray generation and ion production as a function of the laser intensity ($I<10^{17}W/cm^2$) and the clustering conditions. To this end, we have investigated large $(Ar)_n$, $(Kr)_n$, and $(Xe)_n$ clusters with estimated average sizes n of up to 1000 and more using 130fs pulses with a total energy of up to 40mJ at 790nm and 395nm. The laser light is focused into the cluster jet using an off-axis parabolic mirror. Ion charge states and energies have been characterized using time-of-flight mass spectrometry. X-ray photons ($E\geq 1keV$) are analyzed using a polarized Si(Li) junction.

We will present exact X-ray photon yield measurements as a function of the laser intensity, wavelength and pulse duration as well as on the mean cluster size. We obtain scaling laws which are in clear contradiction to previous experimental observations [1,2].

Références

[1] Thompson B D, McPherson A, Boyer K and Rhodes C K 1994 *J. Phys. B: At. Mol. Opt. Phys.* **27** p4391 Borisov A B, McPherson A, Thompson B D, Boyer K, and Rhodes C K 1995 *J. Phys. B: At. Mol. Opt. Phys.* **28** p2143

[2] Ditmire T, Donnelly T, Falcone R W, and Perry M D 1995 *Phys. Rev. Lett.* **75** p3122 Ditmire T, Donnelly T, Rubenchik A M, Falcone R W, and Perry M D 1996 *Phys. Rev. A* **53** (5) p3379

[3] Ditmire T, Donnelly T, Falcone R W and Perry M P 1995 *Phys. Rev. Lett.* **75** p17

[4] Snyder E M, Buzza S A, and Castleman A W, Jr. 1995 *Phys. Rev. Lett.Oct.* **75**

[5] Ditmire T, Tisch J W G, Springate E, Mason M B, Hay N, Smith R A, Marangos J and Hutchinson M H R 1995 *Proc. ICOMP VII (Garmisch-Partenkirchen, Germany)*

[6] Lezius M, Dobosz S, Normand D, Schmidt M Letter submitted to *J. Phys. B.: At. Mol. Opt. Phys* (Oct. 1996)

[7] Hagena O F and Obert W 1972 *Journ. Chem. Phys.* **56** (5) p793

Femtosecond stimulation of atomic and nuclear processes in high intensity laser plasmas

V. S. Rozanov[1], M. Richardson[2], N. Demchenko[1], S. Gus'kov[1] & D. Salzmann[3]

[1] P.N. Lebedev Physical Institute, Moscow, Russia

[2] Laser Plasma Laboratory, CREOL, University of Central Florida
4000 Central Florida Blvd., P.O. Box 162700, Orlando FL 32816-2700

[3] Soreq Nuclear Research Center, Yavne, Israel

Tel: 407-823-6819, Fax: 407-823-6819, Email: mcr@creol.ucf.edu

The interaction of intense femtosecond duration laser pulses with dense plasmas is replete with new plasma phenomena and exciting experimental opportunities. The intense fields within laser radiation with power levels in 10^{19} W/cm^2 range interacting with dense plasmas leads to the generation of enormous bursts of energetic electons (j ~ 10^{15} A/cm^2) that then give rise to the production of intense hard x-ray emission and unprecedented magnetic fields that could be in the GigaGauss range[1-3]. The role these phenomena play on the particle dynamics in these plasmas poses many interesting questions. As the development of femtosecond laser systems reaches these conditions[4,5] ,the examination of these phenomena becomes possible.

In this paper we examine the interaction of intense 100 fs laser light with targets of the heavy isotopes of hydrogen. The interaction is modeled with a hydrodynamic code (RAPID) that includes approximations for the radiation coupling physics and the subsequent particle transport and kinetics. In particular we examine the dynamics of the ions within the plasma, and the generation of neutrons in these plasmas. An example of the conditions predicted to exist in these plasmas is shown in Fig.1, which shows the spatial dependence of the electron and ion temperatures, the plasma density and pressure midway through the interaction of a 100 fs (FWHM) 850 nm, 1 J laser pulse focused to a 10 μm diameter spot on a C_8D_8 target . These conditions are expected to be generated by the upgraded CrLiSAF laser system currently nearing completion at CREOL [6]. Of particular interest are the extremely high pressures generated in the interaction region (~ 100 mJ/cm^3), and the very high ion temperatures predicted (~ 100 keV). These conditions give rise to the generation of a significant flux of neutrons. Neutron fluxes of ~ 10^8 are predicted for these plasma conditions.

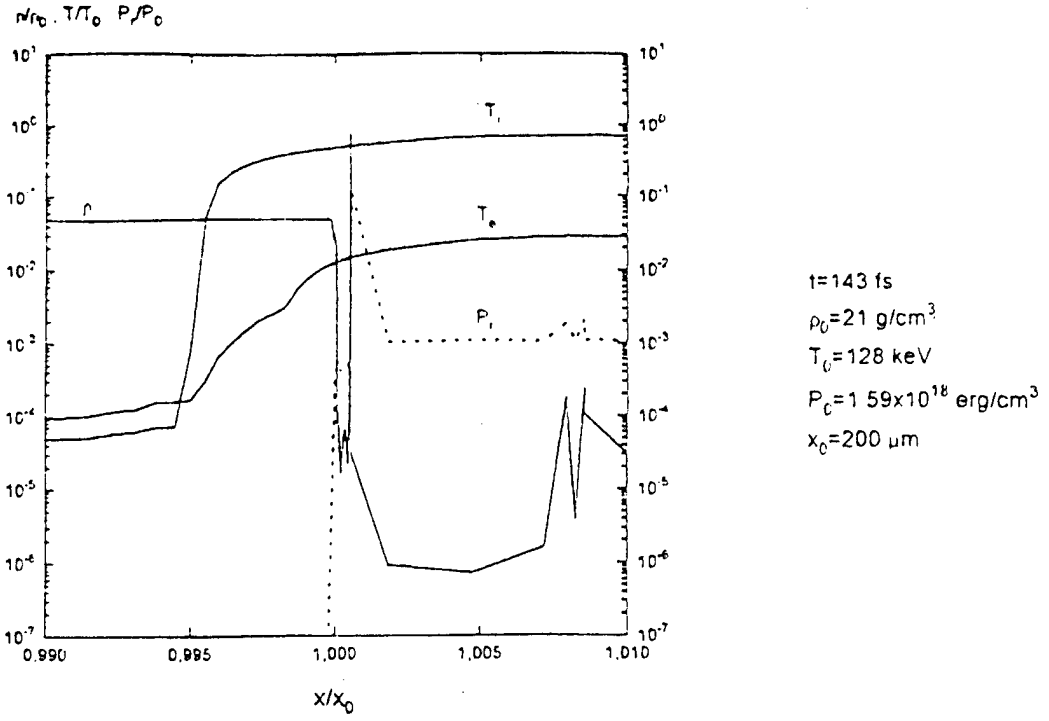

Fig 1. Hydro code simulations of the electron and ion temperatures T_e and T_i, and the plasma density , ρ, and pressure, P.

The extremely high electric and magnetic fields generated in the plasma will have a major impact on the atomic structure, and possible also the near nuclear field. Magnetic fields in the GigaGauss region will tend to create modified states of matter consisting of a distribution of atoms transformed into a pseudo-molecular state in which outer electron orbits of ions and atoms envelope other nuclei in directions normal to the field. The conductivity of this distribution will consequently be strongly dependent on the magnitude and direction of the field. These and other features of the interaction physics will be discussed.

References

1. S. Wilks Phys Fluids B 5, 2605, (1993): S,. C. Wilks, W. L. Kruer, M. Tabak & A.B. Langdon, Phys Rev Lett 69, 1383 (1992).

2. J. Denavit, Phys Rev Lett 69, 3052 (1992).

3. D. Salzmann & M. Richardson, (unpublished)

4. P.A. Beaud, M. Richardson & E.J. Miesak, IEEE, J. Quant. Electron, 31.317 (1995).

5. C.P. J. Barty, Laser Focus, p 93, June, 1996

6. M. Richardson, Steven Grantham, Kai Gabel, Gregory Shimkaveg and Paul Beaud, "A 10 Terawatt femtosecond laser plasma facility", SPIE Proc. 2633, pgs 324-337 (1995).

A debris-less laser-plasma source for EUV and XUV generation

David S. Torres, Christopher M. DePriest and Martin Richardson

Laser Plasma Lab
CREOL, University of Central Florida
4000 Central Florida Blvd.
Orlando, FL. 32816
phone 407) 823-6925, fax (407) 823-3570
email: dst@lorien.creol.ucf.edu

We have previously reported the development of a laser plasma EUV source, using mass-limited water droplets, based on the 13 nm and 11.6 nm O^{5+} lines, for EUV projection lithography [1]. The spectrum from this source is shown in Fig. 1. A vital feature of this approach [2 ,3] is the incorporation of a target limited in mass to the minimum number of EUV atomic radiators required. This feature has advantages for EUV lithography and other applications in minimizing the collateral debris and allowing for continuous operation without the need for periodic maintenance of the optics or target material replenishment. Debris effects were quantified by the measurement of the reflectivity of a Mo/Si multilayer mirror, placed 4 cm from the source, for $> 10^5$ laser shots, Fig. 2. The < 1 % variation in reflectivity allows us to predict that the system could run for up to 10^8 shots without any major degradation in performance.

We are now developing this source to emit at other wavelengths by using droplets of other materials. This investigation includes the use of liquids other than H_2O, liquid dyes and particles in liquid suspension. The variation of the target material and the irradiation parameters then provides a broad range of EUV to soft x-ray emission characteristics, while at the same time minimizing collateral damage from target debris. The short wavelength emission is in the form of line emission, Planckian light from the collisional plasma, or broadband or unresolved transition array emission from muli-ion species.

Although our initial studies involve a fixed nozzle diameter liquid jet, that produces droplets 20 μm in diameter, at a frequency of 1 MHz, we are now investigating the production of droplets with diameters from 400 μm at 1 kHz to 20 μm at 1 MHz. Variability of the target diameter will provide for greater options in source size and fluence, depending on the laser used to produce the plasma.

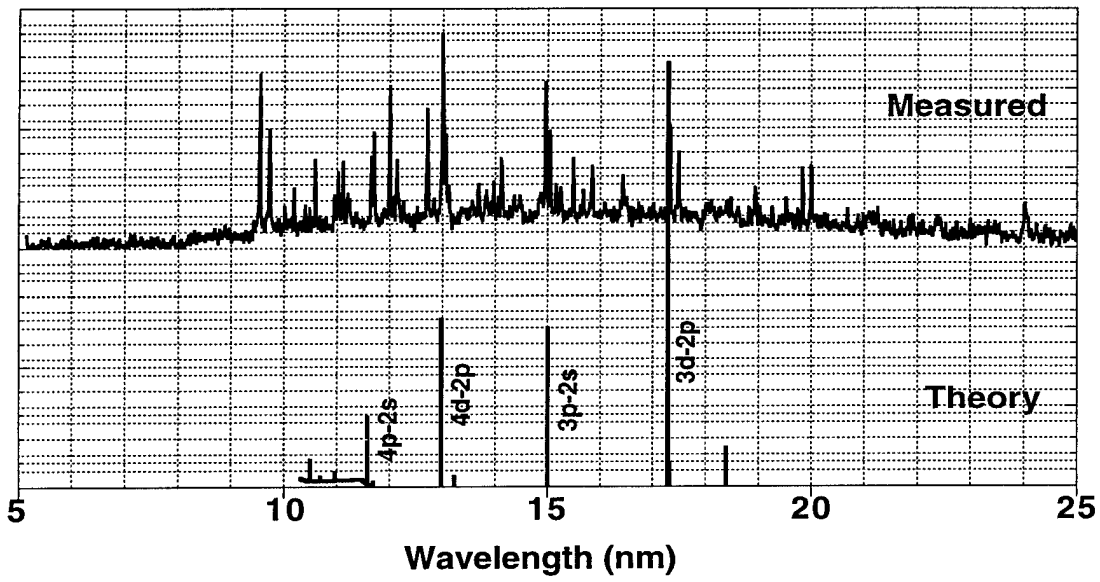

Figure 1. The Measured and Theoretical spectrum from the water droplet laser plasma source.

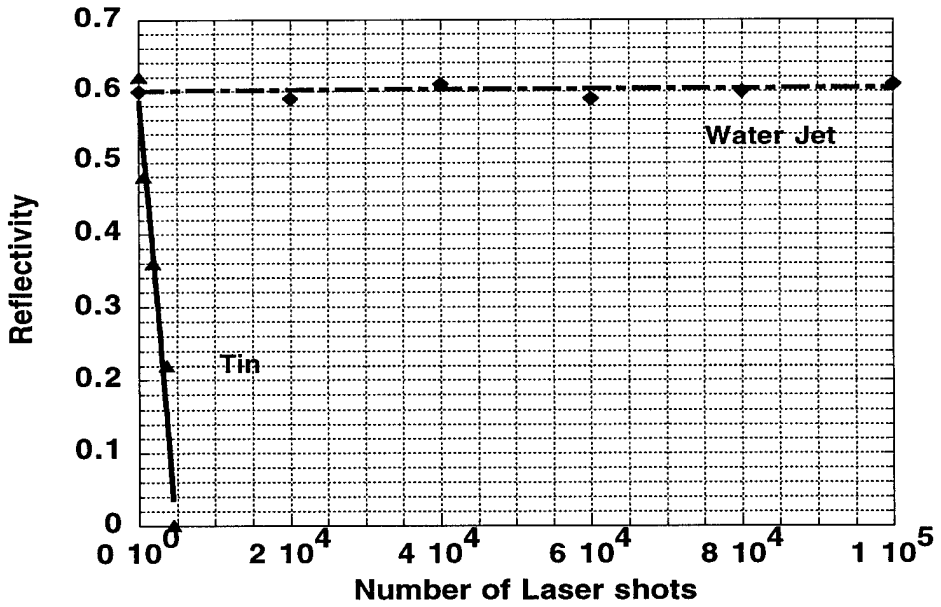

Fig. 2. The reflectivity vs. number of laser shots, for a Mo/Si multilayer mirror.

Concurrent with these experimental investigations detailed theoretical calculations are being made of the plasma characteristics using the one-dimensional hydrodynamic code Medusa [4,5]. In conjunction with the RATION [6] atomic physics code this permits an estimation of the line emission from the plasma, Fig. 1. In this paper we will report on detailed comparisons of these calculations with the experimental findings.

References

1. F. Jin, M. Richardson, G. Shimkaveg, and D. Torres, "An advanced EUV source from water droplet laser plasma", in TOPS on EUV Lithography, G. D. Kubiak and D. Kania eds. (Optical Society of America, Washington, DC, 1996), p. 89.

2. F. Jin, M. Richardson, G. Shimkaveg and D. Torres, "Characterization of a laser plasma water droplet EUV source", Proc. SPIE 2523, pp. 81 - 87, 1995.

3. M. Richardson, M. Kado, K. Gabel, F. Jin, "Water laser plasma x-ray point source and apparatus", U.S. Patent, 5,459,771.

4. J. P. Christansen, D. E. T. F. Ashby and K. V. Roberts, "MEDUSA A One-dimensional laser fusion code", Com. Phys. Comm. 7, 271 (1974).

5. D. Torres, F. Jin, M. Richardson, C. DePriest, "Characterization of mass-limited ice droplet laser plasmas", in TOPS on EUV Lithography, G. D. Kubiak and D. Kania eds. (Optical Society of America, Washington, DC, 1996) p. 75.

6. R. Lee "User manual for RATION", University of California and LLNL, (1990).

Guiding of sub-100 femtosecond pulses in preformed plasma channels.

S.P. Nikitin, T.R. Clark, H.M. Milchberg

Institute for Physical Science and Technology, University of Maryland, College Park MD 20742
tel: (301) 405-4816, fax (301) 314-9404, e-mail: milch@ipst.umd.edu

The guiding of 80 fs pulses over a 1 cm distance in a preformed plasma waveguide has been demonstrated. The guided pulses were produced by a Ti:sapphire laser system. The plasma waveguide was created in a neutral gas by using a separate laser system which consists of a 100 ps Nd:YAG oscillator seeding a Nd:YAG regenerative amplifier and two power amplifiers. In order to achieve stable guiding it was necessary to synchronize these two laser systems so that the time jitter between them is substantially less then time scale over which significant changes in the plasma waveguide can occur.

Our femtosecond laser system is based on the widely used chirped pulse amplification scheme [1] and consists of a Ti:sapphire oscillator, an all-reflective broadband stretcher, a Ti:sapphire regenerative amplifier and a diffraction grating compressor.

The oscillator contains a 10 mm long Ti:sapphire crystal which is pumped by 4 Watts of an Ar+ ion laser in the 'all lines' regime. At this pump level we typically have 300 mW of average power Ti:Sapphire oscillator output. The output pulse duration is < 50 fs (FWHM assuming gaussian pulse profile) while the spectrum width is typically > 25 nm FWHM centered at 780 nm.

The output pulses of the oscillator are stretched to ~200 ps by a single grating all-reflective design stretcher, similar to the one described in ref. [2]. The stretcher has a dispersion of 10 ps/nm and an 80 nm bandpass.

The output pulses of the stretcher are seeded into a 10 Hz repetition rate regenerative amplifier pumped by 35 mJ of the second harmonic output from a Q-switched Nd:YAG laser. Typical output of the amplifier is above 1 mJ. The Ti:sapphire oscillator is currently located in a separate room from the regenerative amplifier and the plasma waveguide producing Nd:YAG system. The resulting distance between the regenerative amplifier and oscillator is of the order of 10 m. Though this requires more careful alignment of the stretcher it was found to improve optical isolation between the regenerative amplifier and oscillator reducing the probability of leakage from the regenerative amplifier terminating the self mode-locked regime of the oscillator. Following pulse compression to ~80 fs, the energy is typically 500 μJ.

The output of this femtosecond system has been synchronized with a Nd:YAG laser system, which is described in detail elsewhere.[3] The Nd:YAG system consists of an actively mode locked oscillator driven by a 38 MHz signal. The output train of the Nd:YAG oscillator has a repetition rate at the doubled mode locker frequency which is 76 MHz. Single oscillator pulses of 100 ps duration are amplified by a flashlamp pumped Nd:YAG regenerative amplifier/power

amplifier system up to 500 mJ with a 10 Hz repetition rate. The output of this system is then used to produce plasma waveguides as described in [4] . Typical time scales for the plasma waveguide evolution is of the order of nanoseconds, which is known both from experimental observations and computer simulations [4]. Thus, in order to couple the output of a femtosecond system into the waveguide, these two systems should be synchronized to within ~1 ns.

The synchronization was realized by using a feedback loop which automatically adjusts the cavity length of the Ti:sapphire oscillator so that the repetition rate, or to be more exact, the phase of the pulse train generated by this oscillator is exactly the same as one from the Nd:YAG oscillator. Fine cavity length adjustment is done by putting one of the folding mirrors on a piezo-driven translator. A voltage applied to the PZT is produced by a phase comparator which compares phases of an electrical signal produced by the Ti:sapphire pulse train on a photodiode and the 38 MHz reference signal from the Nd:YAG oscillator, which is the doubled RF signal from the modelocker. Since long term cavity changes due to thermal variations may be larger than the range of a PZT, the end HR mirror is positioned on a motorized drive which allows the preliminary equalization of the cavity lengths 'manually' until the difference between them is within a PZT working range.

The time jitter between the two laser systems is within the 1 ns response time of the photodiode used for observation. Additionally, there was little shot-to-shot variation in the guided pulse spot size, proving the synchronization is sufficient for this experiment.

A typical output mode of an 80 fs pulse guided by the plasma waveguide is shown in Fig. 1. For this experiment 500 mJ pulses generated by Nd:YAG system were focused by a 35 deg. base angle axicon to an ~1 cm line focus in a 100 torr backfill of neutral N_2O. Approximately 1 ns after the plasma forming pulse, a femtosecond pulse at 0.1 mJ energy level was focused into the plasma waveguide with f/25 optics. Fig. 1 was obtained by imaging the output plane of the ~1cm long plasma waveguide to a CCD camera located outside of the chamber.

Finally, to measure the output pulse duration and chirp we use a FROG technique based on the polarization gating nonlinearity [5]. A PG FROG trace of the output pulse is shown in Fig 2. The pulse duration is measured to be 80 fs FWHM.

In conclusion, this experiment demonstrates the ability to propagate an intense femtosecond pulse over several centimeters in a preformed plasma waveguide. Applications of this technique include soft X-ray generation, plasma wake field particle acceleration, and studies of laser-plasma interaction at relativistic laser intensities.

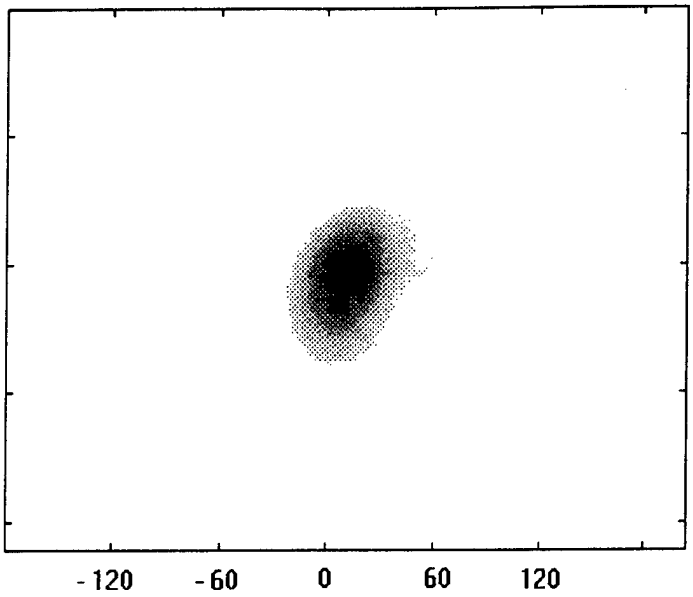

Fig.1

Spatial profile of the femtosecond laser pulse at the output of the plasma waveguide. N_2O at 100 torr, size is 50 microns FWHM.

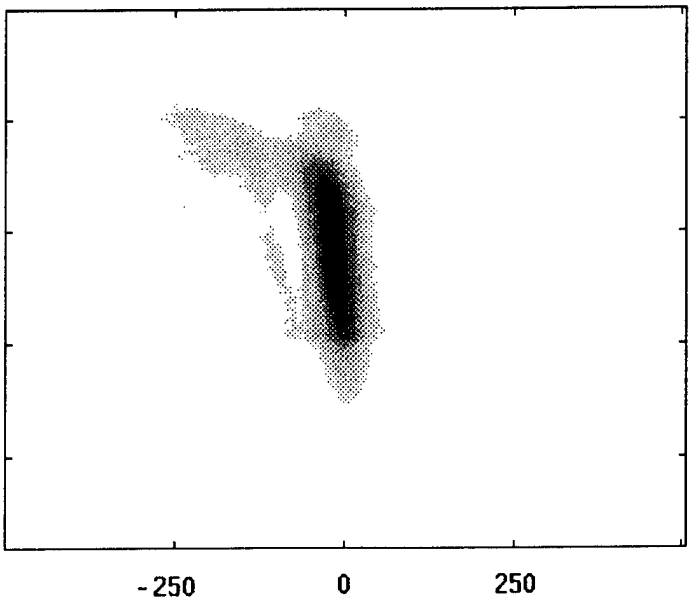

Fig. 2

PG FROG trace of the femtosecond pulse produced by Ti:sapphire system. Corresponding pulse duration is 80 fs FWHM.

References:

1. Mourou Opt com 85
2. G. Cheriaux, P. Rousseau, F, Salin, J.P. Shambaret, B. Walker and L. Dimauro, Opt. Lett. **21**, 414 (1996)
3. C. G. Durfee III, T.R. Clark and H.M. Milchberg, J. Opt. Soc. Am. **B13**, 59 (1996)
4. C.G. Durfee III, J.Lynch and H.M. Milchberg, Phys. Rev. **E51**, 2368 (1995)
5. D.J. Kane and R. Trebino, Opt.Letters **18**, 825 (1993)

Friday, March 21, 1997

Harmonics I

FA 8:30am – 10:15am
Zia A

P. Salieres, *Presider*
Centre d'Etudes de Saclay, France

PHOTOELECTRON SPECTROSCOPY WITH BROADLY TUNABLE FEMTOSECOND HARMONICS: APPLICATIONS IN PHYSICS AND CHEMISTRY

Richard Haight
IBM T.J. Watson Research Center
PO Box 218 Yorktown Hts., N.Y. 10598

High harmonics generated with a femtosecond laser provides virtually all of the properties that one would wish to apply to photoemission investigations of electronic states in materials. Harmonic light is monochromatic and polarized, as determined by the input laser. It is tunable over a wide range of photon energies. For even modest input intensities (0.5 mJ per pulse in our system) we have been able to generate harmonics with useful fluxes to 80 eV. The generated harmonic light is co-linear with the input laser so that reflective optics such as normal or grazing incidence gratings of reasonable size can be used to collect and select a particular harmonic of interest and then refocus this light onto the material under study. With efficient electron detection schemes useful photoelectron count rates can be obtained. With these properties alone, harmonics makes possible photoelectron spectroscopy experiments in the laboratory setting that were previously the sole domain of large scale synchrotron labs. But an additional, and singularly important, aspect of harmonic light is its femtosecond, and possibly even attosecond, time structure which opens avenues for investigations of the temporal evolution of excited electronic systems.

In the experiments to be described, an amplified dye laser system operating at a repetition rate of 540 Hz produces 0.5-0.6 mJ pulses of 610 nm, 200 fs light. When this light is focussed with a 200 mm lens into a burst of rare gas such as Ar or Ne, intensities of greater than $\sim 10^{14}$watts/cm^2 are achieved in the focal region leading to the generation of a comb of harmonics of nearly constant intensity. Fig. 1 shows a schematic of the light generation and transport system. A pulsed gas valve operating at 540 Hz is installed at the front end of a vacuum beam line. The fundamental and generated harmonics are directed to a grazing incidence toroidal grating which selects the harmonic of interest and refocusses the light onto a sample located in an ultrahigh vacuum (UHV) analysis chamber. Differentially pumped vacuum beam lines prevent significant amounts of rare gas from diffusing into the analysis chamber. Rotation of the grating permits selection of any harmonic of interest. The chosen harmonic passes through a reentrant aperture in the UHV system and hits the sample at an angle of 45° with respect to the sample normal. The excitation beam, generated by splitting off 10 to 20% of the fundamental, as shown in Fig. 1, is directed along the same path as the harmonic and impinges upon the sample at the same location.

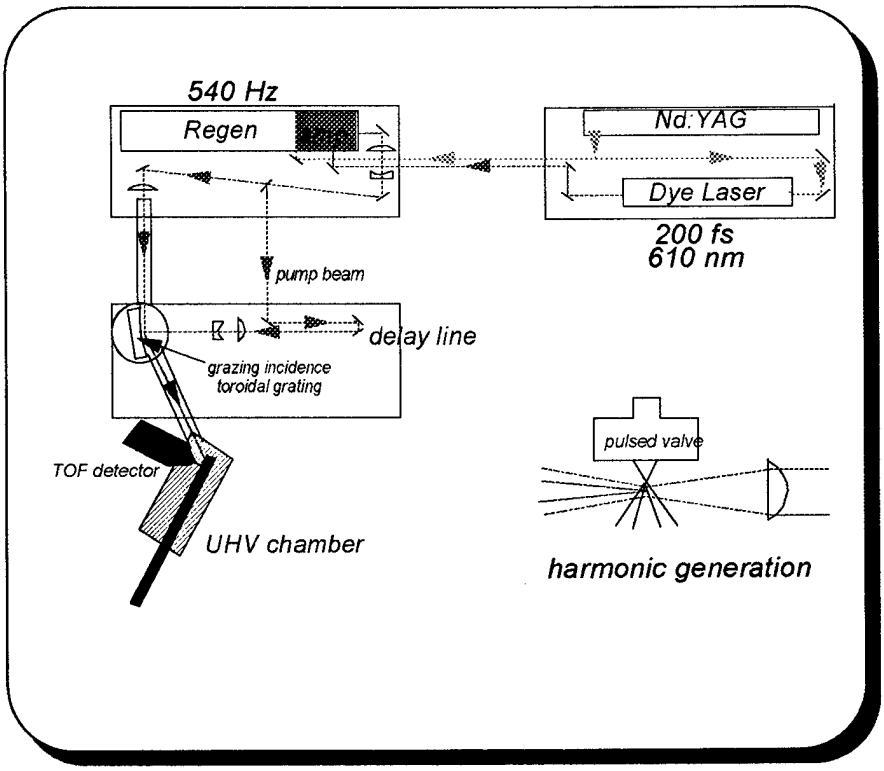

Fig. 1

Photoemitted electrons are collected in a parabolic mirror time-of-flight energy analyzer. The analyzer consists of a parabolic mirror that collimates, on reflection, the diverging electrons from the sample that sits at the focus of the mirror. The collimated electrons drift in a field-free tube until they strike an electron multiplier and multi-anode array. The resolution of the analyzer is 0.1 eV at a kinetic energy of 20 eV.

In condensed matter and surface physics a wide range of experiments designed to investigate surface and interfacial electron dynamics were performed. These involved photoemission experiments on the photoexcited clean semiconductor surfaces of cleaved GaAs (110) and Ge (111) and interfacial systems such as As terminated Ge. Ultrafast phenomena including surface intervalley scattering, non-radiative electron-hole recombination, surface trapping and passivation were observed and studied. In the area of bulk condensed matter systems, recent studies of layered chalcogenide materials such as $MoSe_2$ and WSe_2 led to the observation of energy dependent diffusion of electrons, a rapid process occuring within the first 1-2 ps after photoexcitation.

In chemistry, the high energies and tunability of harmonics have provided the opportunity to carry out high resolution studies of atomic core levels in the laboratory. Atomic core states are deeply bound levels which are not involved in chemical bonding but are observed to shift energetically in response to such bonding, when charge transfer occurs. The large binding energies of core levels typically require higher photon energies than that needed to study valcnce and conduction states.

Hence, high harmonics are critical to this application. In addition to chemical information, core levels are elementally specific allowing the identification of constitutents on or near a surface. Changes in core level shape and intensity gives direct physical evidence of changes in the chemical system.

In addition to core level spectroscopy with harmonics, recent experiments on the photoexcitation of, and subsequent photoemission from, thin organometallic films has shed new light on the dynamic behavior of electrons excited into the lowest unoccupied molecular orbitals (LUMO) of conductive organics. We have observed electrons photoexcited into the LUMO of tris-(8 hydroxy quinoline) Al (AlQ), an important electroluminescent material, and studied the dynamics of the excited electrons. Fig. 2 shows a spectrum of AlQ photoexcited with 3.5 eV photons used to drive electrons into the LUMO. For comparison, the LUMO intensity is enhanced by a factor of 80. As these materials become increasingly important in the technological arena, deeper understanding of transport and non-radiative recombination processes will be crucial. Harmonic laser photoemission is a powerful approach to studying these issues and others in a wide array of materials of fundamental and technological importance.

Fig. 2

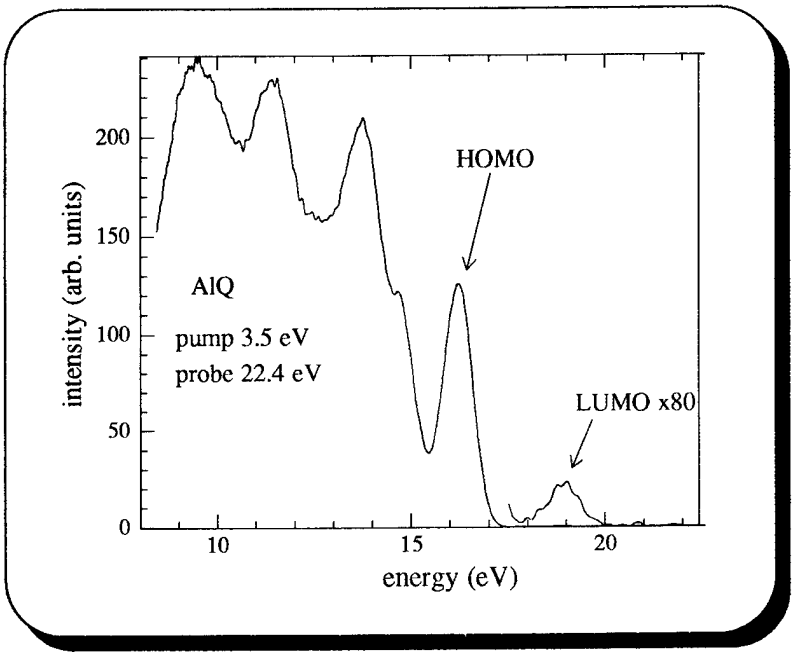

Temporal coherence of high-order harmonics

C.-G. Wahlström[1], C. Altucci[1], M. Bellini[2], M. B. Gaarde[1,3], T. W. Hänsch[4], A. L'Huillier[1], C. Lyngå[1], R. Zerne[1]

1. Department of Physics, Lund Institute of Technology
   P.O. Box 118, S-221 00 Lund, Sweden
   Tel: +46 46 2227655, Fax: +46 46 2224250, E-mail: claes-goran.wahlstrom@fysik.lth.se
2. L.E.N.S, Largo E. Fermi, 2, I-50125 Florence, Italy
3 Also at: Niels Bohr Institute, Oersted Laboratory, Universitetsparken 5, 2100 Copenhagen, Denmark.
4. Max-Planck-Institut für Quantenoptik, P.O. Box 1513, D-85740 Garching, Germany, and L.E.N.S, University of Florence, Largo E. Fermi, 2, I-50125 Florence, Italy

The generation of high-order harmonics in strong laser fields has been studied for several years and considerable progress has been made in the understanding of the physics involved. In different laboratories around the world, scientists are now beginning to explore the use of the harmonic radiation in novel applications in the extreme ultraviolet spectral region (XUV). In some applications, the lack of information regarding the coherence properties of the harmonic radiation is a restricting factor. We here present experimental results from an interference experiment, illustrating the potentials of harmonic radiation in applications requiring temporally coherent radiation in the XUV region.

For the generation of low-order harmonics (2nd, 3rd, 4th...), in gases or in nonlinear crystals, perturbation theory generally applies. In these cases, the phase of the single-atom harmonic emission follows that of the driving laser field (multiplied by a factor equal to the order of the process). High-order harmonic generation in gases, with its characteristic plateau of similar intensities for different orders, is a non-perturbative phenomenon. The phase of the single-atom high-order harmonic emission has been extensively discussed in the literature. It has become clear that this phase does not follow the phase of the driving field. It is strongly dependent on the intensity of the driving field. This rapid variation of the phase with the laser intensity, implying a rapid variation of the phase in the nonlinear medium as well as in time over the laser pulse, has raised questions concerning the possibility to use harmonic radiation in experiments requiring temporal coherence. The phase variation leads to a frequency chirp both for the single-atom response, and for the macroscopic response from the medium. This could be devastating for applications such as XUV interferometry and coherent spectroscopy.

We have therefore performed an experiment where we study the interference of two different harmonic sources produced by the same laser beam. The output from a 35 ps mode-locked Nd:YAG laser is split into two parallel beams, using a birefringent crystal. Each of these beams is focused into a pulsed Xe gas jet where harmonic radiation is produced. The distance between the two foci is about 200 μm, while the beam waist diameter in each foci is less than 50 μm. The two sources of harmonic radiation are hence well separated in space and independent of each other. Harmonic radiation of a particular order (ranging between the 7th and the 17th) are selected by a normal-incidence spherical grating and imaged onto a micro-

channel-plate detector (MCP), coupled to a charged-coupled device (CCD) camera. In principle, this experiment resembles the Young's double-slit experiment, but with a very fundamental difference: The emission from the two sources (foci) are *not* directly emerging from the same plane wave (as in the double-slit experiment), but are generated through the non-perturbative process of high-order harmonic generation. Even though the driving fields are locked in phase (originating from a common pump-laser beam), the phases of the harmonic emission from the two sources are not necessarily locked. If the peak intensities reached in the two foci are different, then at every instance during the laser pulse the single-atom dipole phases will be different. If this also applies to the phase of the macroscopic fields, then any interference pattern produced in the far field would be "washed out" when integrating over the duration of the laser pulse.

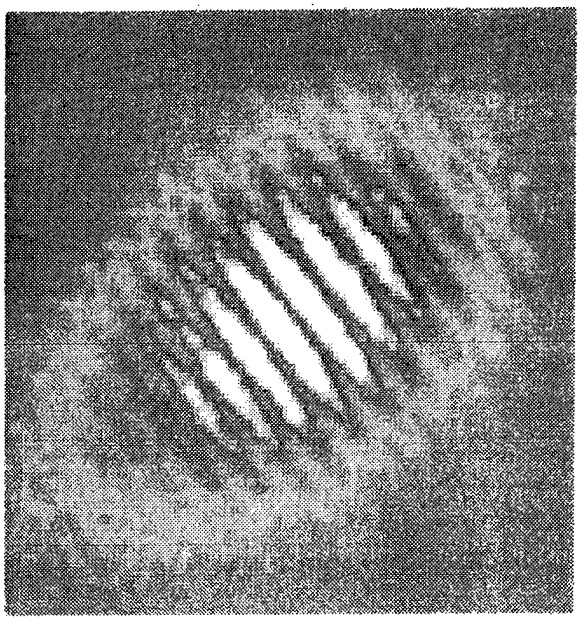

Figure 1. Far-field interference pattern created by overlapping in space two beams of the 13th harmonic, generated independently at different places in a xenon gas jet.

The results of our experiment are presently being analysed in details. An example of a recorded far-field pattern is shown in Figure 1. Interference fringes are clearly visible. This shows that, in spite of the intensity dependent single-atom phases, a stable temporal coherence is obtained. We find that the interference pattern is rather robust, and that it can be observed, with varying degree of contrast, even when the peak intensities in the two foci differ by almost a factor of two.

We find these results very promising for many future applications of harmonic radiation. For example, it might be possible to perform XUV interferometry without the use of complex XUV beam splitters. Ordinary beam splitters for visible radiation can be used, splitting the fundamental laser beam, *before* generating phase-locked XUV beams used for the actual interferometry. Our interference experiment, using beams of harmonic radiation generated in different places and with different peak intensities, shows that the strong variation of the dipole phase in the single-atom response does not destroy the temporal coherence of the harmonic fields. A theoretical analysis of these results is in progress.

Coherent, Tunable, X-Ray Emission at 5 nm using High-Harmonic Generation

Zenghu Chang, Andy Rundquist, Haiwen Wang, Henry Kapteyn, and Margaret Murnane
Center for Ultrafast Optical Science, University of Michigan,
Ann Arbor, MI 48104-1846
Phone: (313) 763-0573; FAX: (313) 763-4876; E-mail: kapteyn@eecs.umich.edu

Xiuqin Liu, Bing Shan
State Key Laboratory of Transient Optics Technology
Xi'an Institute of Optics and Precision Mechanics
Xi'an, 710000, P. R. China

In this work, we demonstrate that the technique of high-harmonic generation, using very short-duration driving pulses, can be used to generate photons of energy up to 240 eV (5 nm), which correspond to the 155th harmonic of the 800 nm driving laser.

The technique of high harmonic generation is relatively straightforward - a high peak-power femtosecond laser pulse is focused into an atomic gas, and the highly nonlinear interaction of the laser light with the atoms results in the emission of coherent high-order harmonics of the laser.[1,2] These harmonics can extend into the soft x-ray region of the spectrum under the right conditions. Many aspects of the physics can be understood using a semiclassical model of the motion of an ionized electron during the first optical cycle after it is ionized due to the strong laser field.[3,4] In this picture, the highest energy photon energy achievable is determined by the maximum kinetic energy of this electron as it return to the nucleus and (with some probability) recombines:

$$h\upsilon = I_p + 3.2\, U_p \qquad (1)$$

where U_p is the pondermotive energy, and I_p is the ionization potential of the atom. U_p is determined by the energy gained by the electron in the laser field, which is in turn determined by two factors: the atomic species (i.e. the ionization potential), and the laser intensity at which the atom ionizes. In previous work, we showed that, using very short-duration driving pulses, it is possible to generate photon energies substantially higher than in previous work.[5,6] This is because the atom ionizes at a high intensity for shorter laser pulses, and the electron then gains more energy in the laser field, and in turn can radiate high harmonic energies. In the work described here, we report further progress on generating harmonics at even high photon energies, and with broader tunability.

In past work we showed that, using 25 fs laser pulses, Neon and Argon can be used to generate harmonics up to the 133rd and 61st. However, in the case of helium (with ionization potential of 24.5eV), we would expect to generate harmonics with wavelengths as short as 4 nm, according to Eqn (1). Recently, we repeated these experiments with a better detector, to obtain substantially inproved results. We focus our 25 fs, 800 nm Ti:Sapphire laser into a He gas jet, produced by a piezoelectrically-driven pulsed nozzle. The gas target pressure was characteristed by observing the laser-produced fluorescence in the focal region. The x-ray harmonics are dispersed using a Hettrick 1.75 meter soft x-ray spectrometer, and then detected using a MCP intensifier made by Xi'an Institute of Optics and Precision Mechanics, China. The spectrum image is recorded using a CCD video camera connected to a framegrabber and/or videocassette recorder. Video-rate acquisition makes it possible to monitor the harmonics in real time, making optimization of the signal straigtforward.

Using 8 mJ of laser energy and a 1-meter focal length curved mirror to focus the laser, we generated harmonics up to 155 th order in He, which corresponds to a photon energy of 240 eV, or a wavelength of 52 Å, as shown by Fig. 1. To our knowledge, this is the shortest wavelength ever produced to date using nonlinear optical techniques. Fig.2 gives another experimental results which shows a better signal to noise ratio.

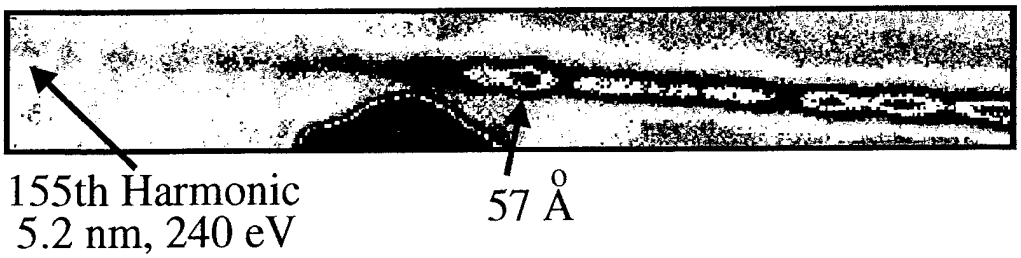

Figure 1: The 155th harmonics from He target

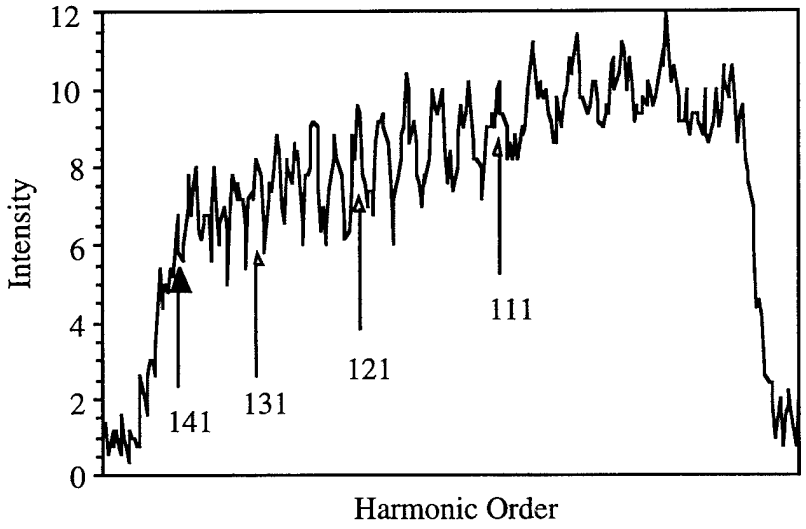

Figure 1: High harmonics from He target. The cut-off at short wavelengths is artificial, due to a light baffle in the spectrometer.

When we increase the laser intensity further, higher harmonic orders appear, but because of the limited resolution of our spectrometer in this wavelength range, it is difficult to resolve the harmonic orders. Work is in progress to improve spectrometer resolution in the 4-5 nm wavelength range and resolve the shorter wavelength harmonics. Modest further improvements in laser technology will make it possible to produce a reliable, table-top source of femtosecond x-rays with photon energy in excess of 300 eV. Ultrashort X-ray pulses in the "water window" (>270 eV photon energy) have great potential use in the study of ultrafast dynamics in organic and biological systems.

References

1. A. L'Huillier, P. Balcou, "High-Order Harmonic Generation in Rare Gases with a 1-ps 1053 nm laser," Phys. Rev. Lett. **70**, 774 (1993).
2. J. J. Macklin, J. D. Kmetec, C. L. Gordon III, "High-Order Harmonic Generation Using Intense Femtosecond Pulses," Phys. Rev. Lett. **70**, 766 (1993).
3. M. Lewenstein, P. Balcou, M. Y. Ivanov, A. L'Huillier, P. B. Corkum, "Theory of High Harmonic Generation by Low Frequency Laser Fields," Phys. Rev. A **49**, 2117 (1994).
4. K. C. Kulander, K. J. Schafer, J. L. Krause, *NATO 3rd Conference on Super Intense Laser-Atom Physics* , (Han-sur-Lesse, Belgium, 1993).
5. J. Zhou, J. Peatross, M. Murnane, H. Kapteyn, I. Christov, "Enhanced High Harmonic Generation using 25 Femtosecond Laser Pulses," Phys. Rev. Lett **76**, 752 (1996).
6. I. P. Christov, J. P. Zhou, J. Peatross, A. Rundquist, M. M. Murnane, H. C. Kapteyn, "Non-Adiabatic Effects in High Harmonic Generation with Ultrashort Pulses," Phys. Rev. Letter **77**, 1743 (1996).

Ultrafast Diffraction from Rydberg Wave Packets Using High Harmonics

Kenneth J. Schafer
Department of Physics and Astronomy
Louisiana State University, Baton Rouge, LA 70803-4001
504-388-0466; schafer@rouge.phys.lsu.edu

Jeffrey L. Krause
Quantum Theory Project
P.O. Box 118435, University of Florida, Gainesville, FL 32611-8435
352-392-6971; krause@qtp.ufl.edu

Rydberg wave packets have been the object of intense experimental and theoretical study over the past decade due to their many interesting semiclassical and quantum characteristics. Long-lived wave packets have been created in both hydrogen and alkali metal atoms, and localization in both the radial and angular dimension has been demonstrated [1]. It is also possible to apply the methods of quantum control to calculate optimally shaped laser pulses which create Rydberg wave packets that have a desired distribution in phase space at a specified "target" time [2]. This can take the form of, for instance, a "Schrödinger cat" state in which an electron is localized in several distinct regions of space simultaneously.

An important issue in Rydberg wave packet research is their detection. Normally the wave packet is localized in some interesting distribution only when it is far from the ion core in the nearly potential free region close to the outer turning point of the Coulomb potential. Since free electrons do not absorb or emit optical photons, this makes the wave packet distribution hard to detect with traditional pump-probe methods. Several alternative methods, each sensitive to different properties of the wave packet, have been used including wave packet interferometry [3], half-cycle pulses [4] and an "atomic streak camera" [5].

Rydberg packets typically have length scales 10-1000 nm and the orbital periods of several picoseconds. In this paper we present calculations which demonstrate that high order harmonics from a high repetition rate TW-class Ti:Sapphire laser interacting with a nonlinear medium can serve as an appropriate light source for ultrafast diffraction from Rydberg wave packets. The high harmonics from such a source are easily shorter than 100 fs and a wide range of wavelengths from 8-80 nm are available, making harmonic generation an ideal light source for time-dependent diffraction from these transient nanostructures.

In the first Born approximation the elastic cross section is proportional to the square of the atomic form factor, which has three contributions [6]

$$f(\vec{q},t) = n_0 f_0(\vec{q}) + n_{wp} f_{wp}(\vec{q},t) + f_{c.t.}, \tag{1}$$

where n_0 and n_{wp} are the population of the ground state and the wave packet, and f_0 and f_{wp} are the normalized ground state and wave packet form factors. The cross term $f_{c.t.}$, which results from the product of the ground state amplitude and the wave packet, oscillates on a time scale set

by the excitation laser. For XUV diffraction pulses that last much longer that the excitation laser period this rapidly oscillating cross term makes no contribution to the signal [2, 6].

For a wave packet with structure on the nanometer length scale, the optimal photon source has a wavenumber $k_0 \ll 1$ au. For these wavelengths the scattering from the ground state component is therefore isotropic. The scattered intensity, which is proportional to $|f(\vec{q},t)|^2$, can then be written as

$$I(\vec{q},t) \propto n_0^2 + 2n_0 n_{wp} f_{wp}(\vec{q},t) + \mathcal{O}(n_{wp} f_{wp})^2. \tag{2}$$

The signal oscillates about its average value with an amplitude proportional to the population of the wave packet, allowing us to extract f_{wp} which can then be inverted to give the spatial distribution of the wave packet.

Fig. 1 illustrates how $f_{wp}(\vec{q})$ changes as a function of time as an $\ell = 1$ radial wave packet with an average principle quantum number of $n \approx 50$ moves between its inner and outer turning points. We assume that $k_0 = .015$ au which corresponds to 22.2 nm radiation. The excitation laser is polarized parallel to the z axis, the XUV pulse propagates along the y axis, $q = 2k_0 \sin(\theta_q/2)$ where θ_q is the scattering angle in the $z-y$ plane, and the detector is assumed parallel to the $x-y$ plane. The wave packet's changing distribution is clearly reflected in the diffraction pattern at this wavelength.

Fig. 2 illustrates the diffraction from a shaped Rydberg wave packet, this one having a trident structure. Note the non-monotonic envelope of the form factor, which is due to the structure built into the packet at the target time. This feature is absent at later times when the wave packet disperses.

Recording a gas phase diffraction pattern such as Fig. 2 requires a very bright, short pulse source of photons. The cross section for electron-photon scattering is very small and there is no coherent enhancement due to periodic structure in the sample, though the wave packet axes are aligned by the pump laser which eliminates the need for rotational averaging. The experiment is feasible, however, because of the vastly different length scales in the problem (ground versus Rydberg state), and because the signal depends primarily on the form factor, not its square (Eq. 2). The best system for actually producing shaped wave packets would be an alkali metal atom since the excitation can be accomplished using optical wavelengths. This greatly aids the diffraction measurement since using an atom with Z_c core electrons alters the signal by replacing n_0 in Eq. 2 with $n_0 + Z_c$, raising the signal dramatically. For instance, in a sample with a density of $3\text{x}10^{12}$ atoms/cm^3 we estimate that more than 10 photons/second will be scattered by the sample.

References

[1] J. Parker and C. R. Stroud, Jr., Phys. Rev. Lett. **56**, 716 (1986); A. ten Wolde *et al.*, Phys. Rev. Lett. **61**, 2099 (1988); J. A. Yeazell *et al.*, Phys. Rev. A **40**, 5040 (1989); M. Kalinski and J. H. Eberly, Phys. Rev. Lett. **77**, 2420 (1996).

[2] J. L. Krause, K. J. Schafer, M. Ben-Nun, and K. R. Wilson, Phys. Rev. Lett. (1996) submitted.

[3] R. R. Jones *et al.*, Phys. Rev. Lett. **71**, 2575 (1993).

[4] R. R. Jones, D. You, and P. H. Bucksbaum, Phys. Rev. Lett. **70**, 1236 (1993).

[5] G. M. Lankhuijzen and L. D. Noordam, Phys. Rev. Lett. **76**, 1784 (1996).

[6] M. Ben-Nun, T. J. Martinez, P. M. Weber, and K. R. Wilson, J. Chem Phys. (1996), submitted.

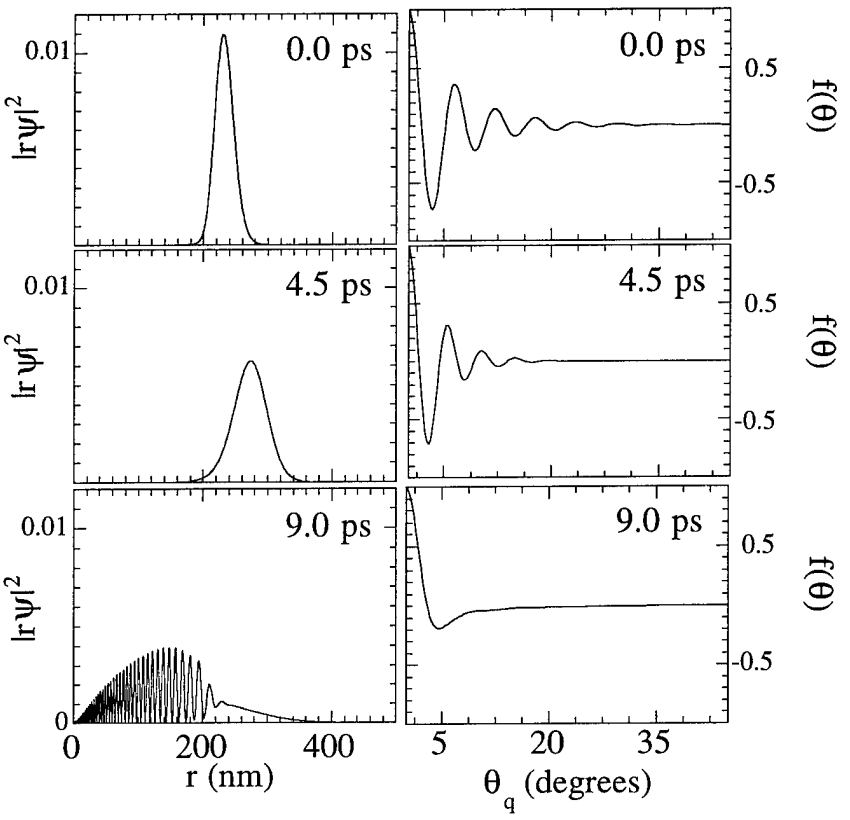

Fig1. Rydberg wave packet probability distribution as a function of time (left panels) and the form factor for scattering in the geometry described in the text (right panels). The wavelength is assumed to be 22.2 nm.

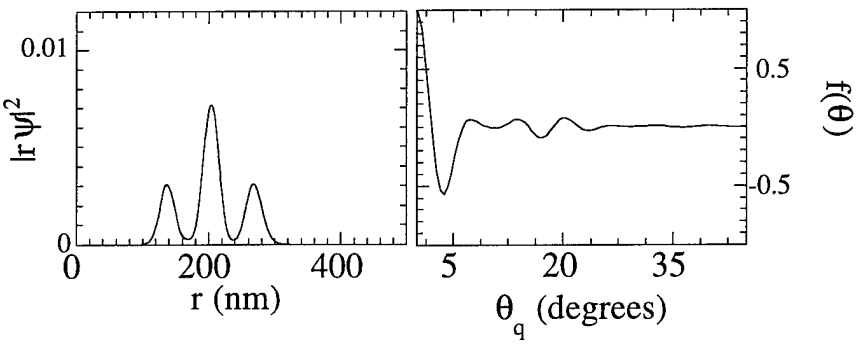

Fig.2. A three-peaked "tailored" wave packet at the target time (left panel) and its form factor (right panel). The wavelength is assumed to be 22.2 nm.

Ultrashort high harmonic pulse generated in a highly ionized gas

A. Bouhal[1], P. Breger[2], P. Salières[2], P. Agostini[2]
R. Constantinescu[3], H. G. Muller[3]
G. Grillon[1], A. Mysyrowicz[1], A. Antonetti[1],

([1]) Laboratoire d'Optique appliquée, ENSTA-école-Polytechnique, 91125 Palaiseau, France
Tel : (33). 01.60.10.03.18
mail : bouhal@enstay.ensta.fr
([2]) Service des Photons, Atomes et Molécules
Centre d'Etudes de Saclay, 91191 Gif Sur Yvette, France

High-order harmonics generation in rare gases is one of the most rapidly developing topics in the physics of atoms interacting with intense laser pulses [1]. At long wavelength and high intensity, high-order harmonic generation involves the excitation of electrons to the continuum and rescattering from the parent ion [2,3]. This implies a close relationship between harmonic generation and ionisation. Ionization actually influences the harmonic production through depletion of the ground state and defocusing of the fundamental beam caused by the free electrons.

This work investigates both experimentally and numerically the influence of ionization on the harmonics pulse duration.

Experimentally, the duration of one particular high-order harmonic was measured by a cross-correlation method described previously[4]. The harmonics were generated by fundamental pulses of durations ranging from 1 ps to 400 fs obtained by adjusting the compressor of the Ti:Saphire laser [5]. They were probed by a 120 fs pulse. The combination of long pump and short probe gives a good accuracy in the measurement. The 19th harmonic produced in Argon by a pump laser intensity of 2.5 10^{14} Wcm^{-2} was characterised by this technique. The cross-correlation gives a duration of 180$\pm$20 fs, 110 $\pm$ 20 fs and 90 $\pm$ 20 fs for a fundamental duration of 1 ps , 600 fs and 400 fs respectively.

On the other hand, the temporal profile of 19th harmonic generated in argon with an intensity peak greater than 2 10^{14} Wcm^{-2} has been calculated with the help of a code simulating the propagation of harmonics.

Ionization rates used as input in the code are evaluated in the tunnelling regime.

The computer simulations are in good agreement with the experimental results.

A typical result is shown in Fig. 1.

References:

[1] A. L'Huillier and Ph. Balcou, Phys. Rev. Lett. **70**, 774 (1993).
[2] J. L. Krause, K. J. Schafer, and K. C. Kulander, Phys. Rev. Lett. **68**, 3535, (1992).
[3] M. Lewenstein, Ph. Balcou, M. Yu. Ivanov, A. L'Huillier, and P. Cockum, Phys. Rev. A **49**, 2117 (1994).
[4] A. Bouhal et al. JOSA B 1996 (submitted).
[5] C. Le Blanc, G. Grillon, J. P. Chambaret, A. Migus, and A. Antonetti, Opt, Lett. **18**, 140 (1993)

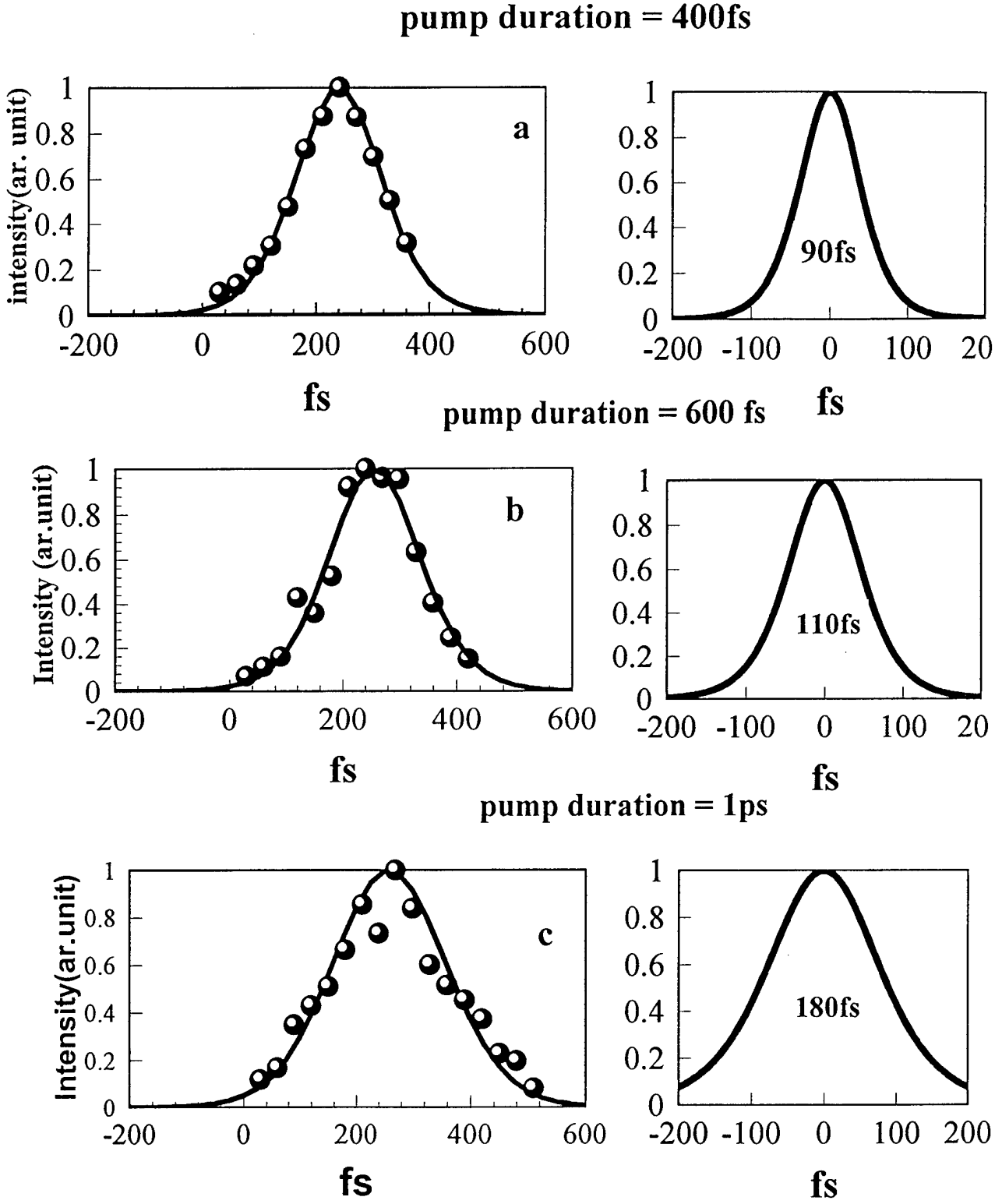

Experimental cross-correlation (dot) between the infrared laser and his 19th harmonic for tree different fundamental durations : (a) 400fs, (b) 600fs and (c) 1 ps.
The 19th harmonic duration is 90 fs, 110fs and 180 fs respectively

fig. 1

Friday, March 21, 1997

Harmonics II

FB 10:45am – 12:15pm
Zia A

Justin Peatross, *Presider*
Brigham Young University

Intense Laser Interactions: Hot Electrons and High Harmonic Ionization

L.D. Van Woerkom, S. Evans, P. Hansch and M.A. Walker
Department of Physics
The Ohio State University
174 W. 18th Avenue
Columbus, OH 43210-1106
voice: 614-292-9626
fax: 614-292-7557
email: lvw@mps.ohio-state.edu

We report on photoionization measurements made using intense 800 nm ultrashort pulse laser light and its high harmonics. First, we present photoelectron kinetic energy spectra showing prominent features at high kinetic energies that cannot be explained by the simpleman/rescattering theory, traditional Rydberg state resonances or other current theoretical treatments. Second, we report the first indications of multiphoton and multiple ionization using high harmonic radiation. We have measured what is believed to be two-photon ionization of both neutral and singly ionized Krypton. Ion charge state distributions for harmonic orders ranging from the 3rd to the 17th are presented for the noble gases.

I. Hot Electron Production

Two new unexplained effects have been seen: (1) We observe narrow dominant structures in the hot electron part of the photoelectron kinetic energy spectra for Xenon that suggest *resonant* ionization even at intensities as high as 1.9×10^{14} W/cm^2 and ponderomotive potentials above 10 eV. (2) We measure large enhancements in the electron production for kinetic energies near 20 and 35 eV. The high energy resonances appear within a very narrow intensity range between 1.2 - 1.9×10^{14} W/cm^2. Similar effects are also observed in Argon and Krypton in different kinetic energy regions. Our measurements represent a new level of resolution and signal to noise ratio for high intensity photoelectron studies.

Transient resonances account unambiguously for the low energy photoelectron structure found in experiments using linearly polarized light. For 800 nm light, Rydberg state resonances yielding kinetic energies up to the 2Up point can be clearly identified. Recently, electron signal beyond 2Up has been attributed to inelastic backscattering [1]. In the past, the repetitive ATI structure in the hot electron region has been considered due to nonresonant ionization. We have recorded high resolution spectra over the intensity range near 10^{14} W/cm^2 in fine intensity steps. Our data show surprising substructure within each ATI order for kinetic energies up to 50 eV. If these features resulted from nonresonant ionization, they would have to shift ponderomotively to lower kinetic energies as the peak intensity increased. In contrast, our measurements show that no such shift occurs and that the hot electron features appear over a small intensity range, indicating a resonant ionization process.

The spectra presented were obtained using a Positive Light, Inc. Ti:Sapphire laser system operating at a 1 kHz repetition rate. The 120 fs, 800 nm output pulses have an energy of 700 μJ per pulse and are plane-polarized. Spectra at different intensities have been recorded using Intensity-Selective-Scanning (ISS). This technique has been described elsewhere [2]. Briefly, a 500 μm pinhole is placed at the front of the TOF tube and only electrons traveling on the line of sight from the ionization volume to the detector are measured. This technique yields data from a one-dimensional radial intensity distribution, thereby reducing the problems associated with spatial averaging over the entire laser focal volume. By scanning a pinhole across the Gaussian ionization volume, specific peak intensities can be selected with high precision.

Fig. 1 shows a high resolution photoelectron kinetic energy spectrum of Xenon from 2-55 eV taken at 1.51 x 10^{14} W/cm^2. The spectrum consists of three basic regions: (i) 2-11 eV with well defined Rydberg structure, (ii) 11-28 eV with narrow structure appearing as a function of intensity, and (iii) 28-50 eV with prominent 'bumps' comprised of a number of ATI orders appearing as the intensity increases. It should be noted that the overall envelope of the electron signal does not monotonically decrease as predicted by various theoretical models. Although some calculations produce modulations in the spectrum for various kinetic energies [3, 4] the experimentally observed signal enhancement between 15-50 eV is at least an order of magnitude larger than any current model predicts.

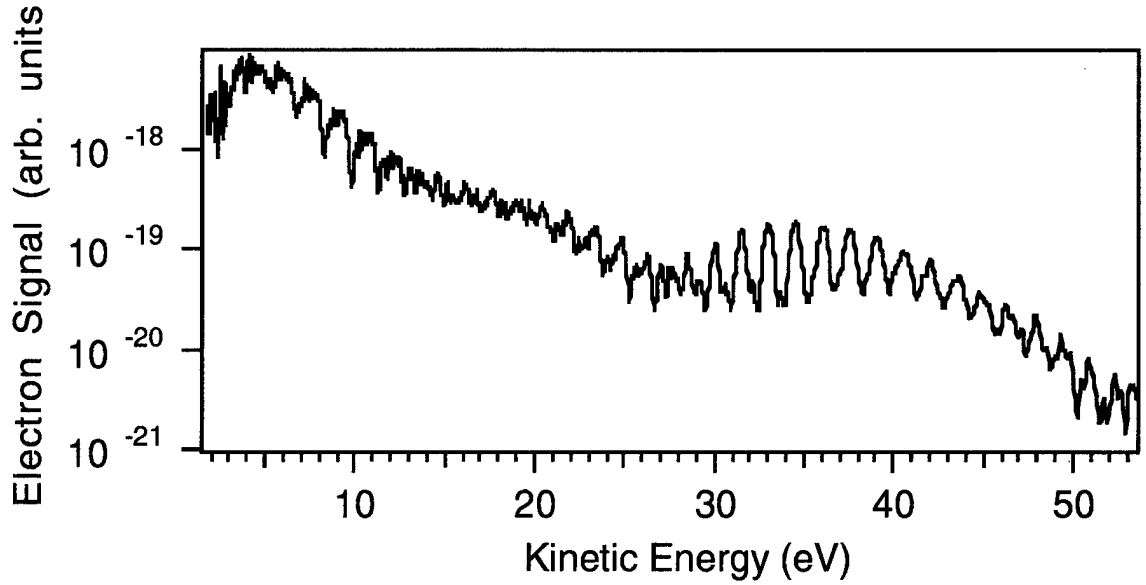

Fig. 1. High resolution photoelectron spectrum of xenon taken at 1.51 x 10^{14} W/cm^2.

We have performed measurements at a variety of intensities and observe no peak shifts. Rather, the peaks appear and grow in a fashion similar to the traditional Rydberg resonances at low kinetic energy. Furthermore, we observe at least two separate series of peaks near 35 eV that are shifted relative to each other by about 0.5 eV.

II. High Harmonic Photoionization

One important aspect in understanding the role of resonances in the production of hot electrons in ATI is the structure of the continuum. To probe the continuum we have utilized selected high harmonics to photoionize noble gases. The goal of this study is two-fold. First, we are searching for multiphoton effects using vacuum-ultraviolet wavelengths. Second, we are interested in understanding the continuum structure above one or more ionization limits.

These experiments were performed using a 10 Hz Ti:S laser system capable of producing 25 mJ pulses at 800 nm with about 140 fs duration. The harmonics and fundamental beam were separated using an f/4.5 VUV monochromator. The monochromator selected out a single harmonic and re-focused it into another high vacuum chamber which contains a time-of-flight (TOF) spectrometer. Krypton, Neon, Argon, and Xenon gases were successively backfilled into the interaction region to interact with a single harmonic.

Figure 2 shows the charge state distribution for the 7th harmonic irradiating Krypton gas. Two harmonic photons with energy 10.85 eV are required to ionize neutral krypton (I.P.=13.99 eV). Similar results were found for the 3rd and 5th harmonics. These data result from 10k laser shots,

but unambiguously demonstrate multiphoton ionization using high intensity harmonics. Due to the re-imaging of the harmonic out of the monochromator, the beam size in the interaction region was not at a minimum. This demonstrates that indeed the harmonics are quite short in order to maintain

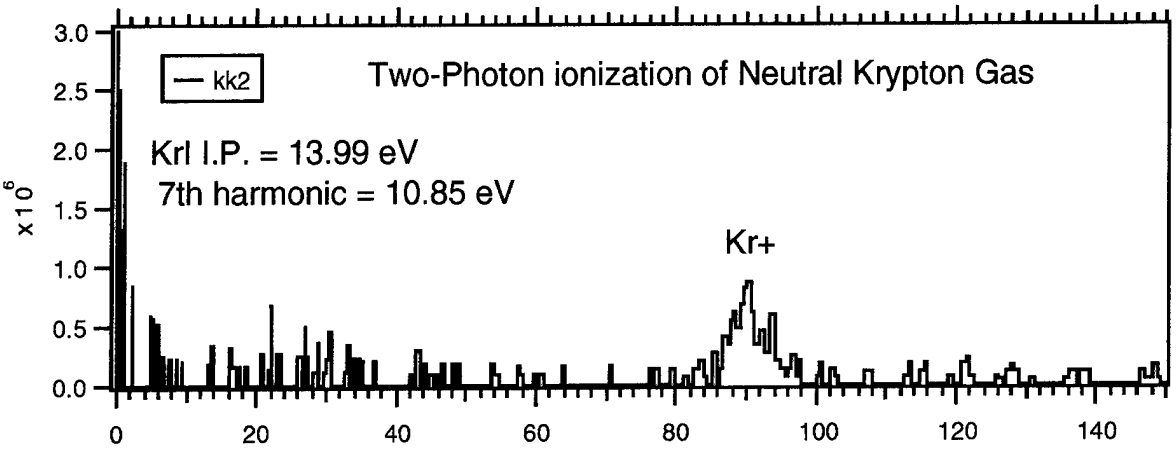

Fig. 2. Ion charge state distribution for multiphoton ionization of krypton with the harmonic of 800 nm light.

enough intensity for multiphoton ionization. By changing harmonics we were able to pass from the two-photon regime into single photon absorption. We saw an increase in single ionization at the 9th harmonic (13.95 eV) for ionizing Krypton at threshold.

Similar data have been collected for the other noble gases. For all gases the ionization appears to take place non-resonantly and via multiphoton absorption. Our data are restricted to the lower high harmonics due to the efficiency roll-off in the normal incidence monochromator. Further work is underway to extend these measurements to higher harmonics. For all cases the multiphoton ionization should be in the perturbative regime and cross-sections can be calculated in order to fit data.

In conclusion, we have observed for the first time prominent fine structure in hot electron production in high intensity photoionization of Xenon. The kinetic energy regions near 20 and 35 eV show a prominent enhancement in electron production. It is clear that a resonant process must be involved due to the lack of energy shifts with laser intensity. Furthermore, we have observed indications of multiphoton ionization using high harmonics of 800 nm intense laser light. Absorption of at least two-photons has been observed for the high harmonics near the 11th harmonic of 800 nm laser light. These measurements mark the beginning of a new era in nonlinear optical phenomena in the vacuum ultraviolet and soft x-ray regions of the spectrum. Much work remains to be done on both the experimental and theoretical sides in order to more fully explain these new phenomena.

[1] G. G. Paulus, W. Becker, W. Nicklich, H. Walther, J. Phys. B **27**, L703-L708 (1994).
[2] P. Hansch, L. D. VanWoerkom, Opt. Lett. **21**, 1286-1288 (1996).
[3] M. Lewenstein, K. C. Kulander, K. J. Schafer, P. H. Bucksbaum, Phys. Rev. A **51**, 1495-1507 (1995).
[4] G. G. Paulus, W. Nicklich, H. Xu, P. Lambropoulos, H. Walther, Phys. Rev. Lett. **72**, 2851-2854 (1994).

High harmonics as a probe for femtosecond laser-produced plasmas

W. Theobald, R. Häßner, and R. Sauerbrey

Institut für Optik und Quantenelektronik, Friedrich-Schiller-Universität Jena,

Max-Wien-Platz 1, D-07743 Jena, Germany

Phone:+49-3641-636281, Fax:+49-3641-636278, Email:sauerbrey@qe.physik.uni-jena.de

High harmonics produced by femtosecond lasers are a convenient source of ultrashort soft x-ray pulses and have been intensively studied in recent years [1]. We use high-order harmonics to measure time-resolved the electron density and the mean electron energy in femtosecond laser produced plasmas [2,3]. Differential absorption of the harmonics as a probe radiation allows to infer plasma free electron densities well above the critical density for the fundamental wavelength. It is shown that this pump-probe technique allows direct access to plasma parameters in conjunction with a time resolution of a few hundred femtoseconds.

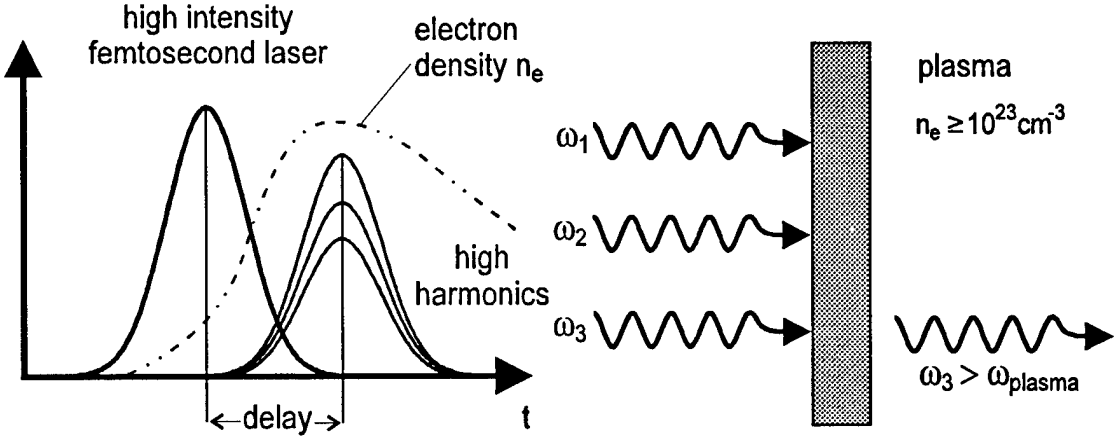

Fig. 1: Principle of the method.

Densities of up to 5×10^{23} cm^{-3} and initial electron energies of several hundred electron volts are reported. The measurement are compared with a detailed analysis of the plasma evolution

process including high density effects in several reaction cross sections. Furthermore, the technique offers the possibility to investigate non-Maxwellian effects in high-density plasmas.

Fig. 1 shows the principle of the method. The harmonics in the wavelength region between 60 nm to 15 nm are generated by a terawatt Ti:sapphire with 100 fs, 250 mJ pulses or a subpicosecond KrF-laser system (700 fs, 20 mJ) and irradiate a plasma generated by a femtosecond laser pulse in a 70-100 nm thin polycarbonat foil. The plasma of initially high electron density (N_e=10^{23}-10^{24} cm^{-3}) and high electron energy expands adiabatically after the foil had burned through. Depending on the electron density, high-order harmonics generated in an inert gas jet are transmitted through a femtosecond laser-produced plasma while lower-order harmonics are absorbed or reflected. The idea of this method is to measure the transmittance of a plasma at different frequencies in such away that some frequencies are below the plasma frequency while others are above.

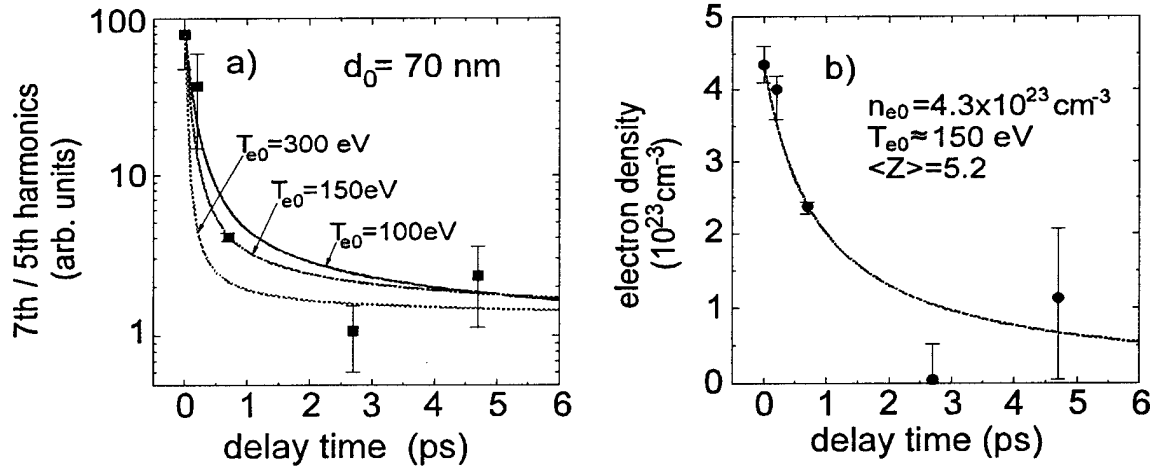

Fig. 2: a) Measured signal ratio of the fifth to seventh harmonic of a KrF-laser (solid squares) versus delay time and the calculated behavior assuming different initial electron temperatures (solid lines). b) Evolution of the electron density inferred from a) (solid dots) together with the calculation for an initial electron temperature of 150 eV (solid line).

Fig. 2 shows an experimental result obtained with the KrF-laser system derived from the relative transmitted intensities of the fifth (49.7 nm) and the seventh (35.5 nm) harmonics with a temporal resolution of about 0.5 ps. The solid curve corresponds to a calculation of the density versus time with an initial mean electron energy of 150 eV and an initial electron density of 4×10^{23} cm^{-3}. This simple method has the advantage of providing a direct access to ultrahigh electron densities and achieves a precision of better than 10% at zero time delay.

High-order harmonic generation provides coherent light pulses down to a wavelength below 10 nm, corresponding to a critical density of 10^{25} cm^{-3}, or about 1000 times solid density for a hydrogen plasma. Therefore this method is well suited for applications in the field of inertial confinement fusion (ICF), for soft x-ray laser development, and in general for the investigation of high density laser-produced plasmas.

[1] A. L'Huillier and Ph. Balcou, *High-order harmonic generation in rare gases with a 1-ps 1053-nm laser*, Phys. Rev. Lett. **70**, 774-777 (1993).

[2] W. Theobald, R. Häßner, C. Wülker, and R. Sauerbrey, *Temporally resolved measurement of electron densities ($>10^{23}$ cm^{-3}) with high harmonics*, Phys. Rev. Lett. 77, 298-301 (1996).

[3] J. C. Kieffer, Z. Jiang, A. Ikhlef, C. Y. Cote, and O. Peyrusse, *Picosecond dynamics of a hot solid-density plasma*, J. Opt. Soc. Am. B **13**, 132-137 (1996).

SHORT PULSE LASER DRIVE OF A SUPERSONIC RADIATION FRONT INTO SOLID MATTER

E. T. GUMBRELL, T. DITMIRE, R. A. SMITH AND M.H.R. HUTCHINSON

The Blackett Laboratory, Prince Consort Road,

Imperial College of Science, Technology and Medicine

London, SW7 2BZ, United Kingdom

e.gumbrell@ic.ac.uk

phone: 01715947516

An understanding of energy transport mechanisms is crucial to describing short pulse laser plasma interactions. On progressively longer time scales, electron thermal conduction, hydrodynamic expansion and shock wave propagation are thought to be the principle means by which deposited laser energy leaves the interaction region. Here we report the first observation of a supersonic ionisation front that is faster than any seen so far [1]. This can be explained by a radiative thermal conduction mechanism.

In our experiment a chirped pulse amplification Nd:Glass laser system was used to produce 2 psec pulses at wavelengths of 1054 nm and 527 nm. These were focused onto polished fused silica targets at intensities up to 10^{17} W/cm^2. A variety of target angles and polarisations were used. A small amount of light split from the main pulse was Raman shifted to 620nm and used for time and space resolved shadowgraphy in a plane normal to the target-vacuum interface, with temporal and spatial resolutions of approximately 1psec and 1μm. By varying the delay of the probe relative to the heating pulse we were able to image the formation of plasma overdense to the probe ($n_e \sim 3 \times 10^{21}$ cm^{-3}) inside the solid target.

Figure 1 shows images which are typical of the motion of the ionising front when 1054 nm heating pulses are used pulses. By measuring the maximum extent of the axial penetration as a function of time, we can determine the ionisation front velocity. Remarkably, the maximum velocity we observe is 8×10^8 cms^{-1} at an intensity of 8×10^{16} Wcm^{-2}, which is ~ 40 times that seen previously in experiments at lower intensity [2].

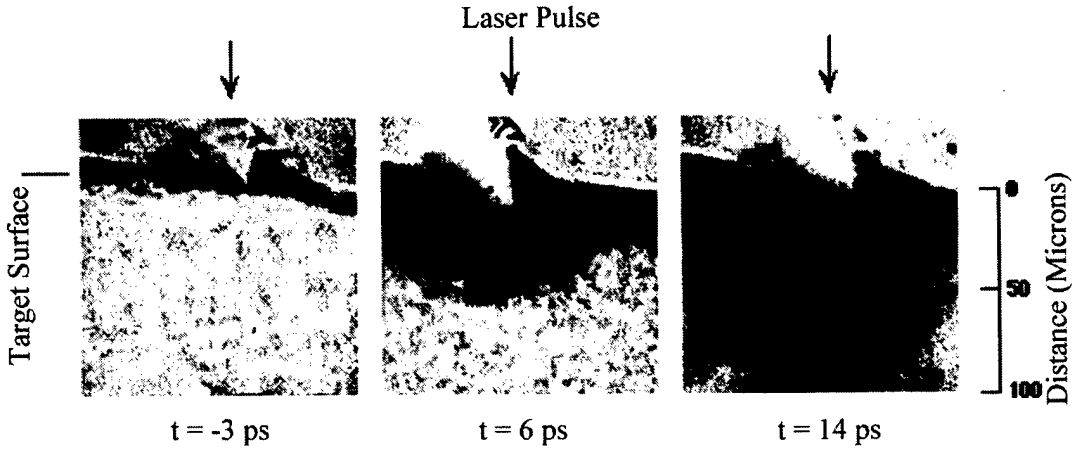

Figure 1: Profile of the inwards moving plasma at three different times relative to the heating pulse with a peak intensity of 6×10^{16} Wcm^{-2}.

We have performed modelling of the plasma kinematics by numerically solving the 1D nonlinear heat diffusion equation for the ionisation front penetration as a function of time - we use both Spitzer-Härm [3] theory for electron conductivity, and a standard form for the radiative conductivity [4]. To estimate the degree of ionisation at each time step we employ the local thermal equilibrium treatment of Reference 2. Appropriate free streaming clamps were applied to the heat flow.

In Figure 2 the ionisation wave penetration depth as a function of time is compared to the electron and radiative conduction predictions. The electron conduction predictions are clearly inadequate. The radiative heat flow model, however, accurately predicts the expansion of the heat front into the solid.

The nonlinear nature of the radiative conductivity means the heat front is very steep: according to our model, the plasma temperature rises to a few hundred eV over a distance of less than 5 μm from the leading edge of the front, where $T_e \sim 1eV$. This is the temperature to which our optical probing technique is sensitive. Therefore the ionisation front is a good indicator of the rapid speed at which energy is transported into the solid.

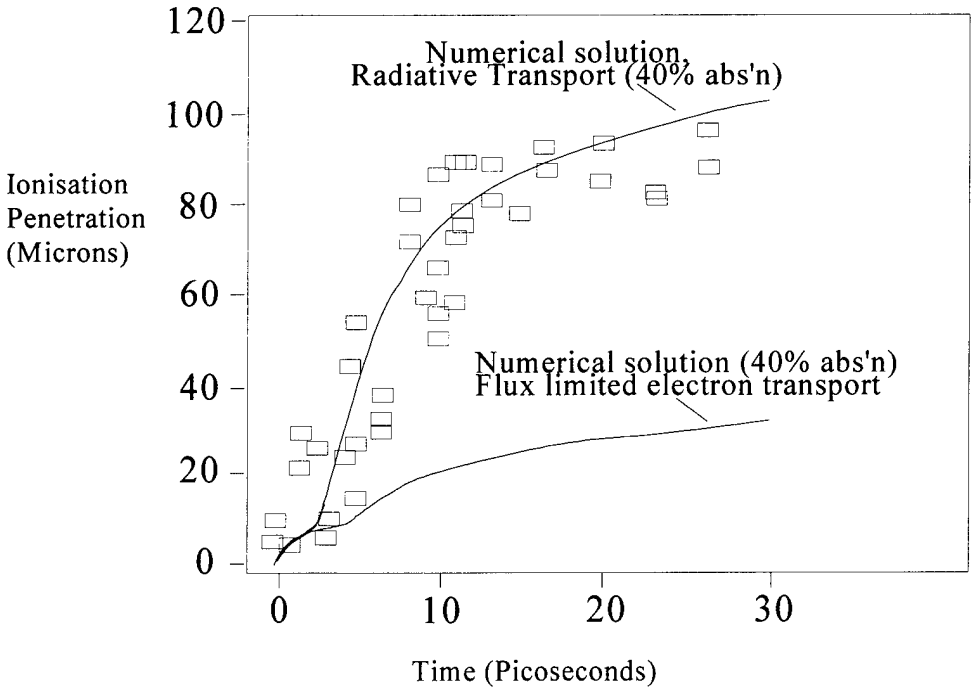

Figure 2: Measured ionisation front as a function of time for a peak intensity of 8×10^{16} Wcm^{-2}. The solid lines represent the flux limited numerical solutions, and the dashed lines the analytical solutions.

New studies of the radiation driven front using both 527nm and 1054 nm pulses have produced little evidence for dependence on polarisation and target angles. However, in the case of the 527nm pulse, although the penetration is not so pronounced axially, we now have observed strong radial energy transport as a function of time. Accounting for the focal spot size, the late time ratio of the radial to axial extent is ≥ 2.

References

1. T. Ditmire, E. T. Gumbrell, R. A. Smith, L. Mountford and M. H. R. Hutchinson. Phys. Rev. Lett. 77, 498 (1996)

2. B. T. Vu, A. Szoke and O. L. Landen, Phys. Rev. Lett. 72, 3823 (1994)

3. L. Spitzer and R. Härm, Phys. Rev. Lett. 89, 977 (1953)

4. Y.B. Zeldovich & Y.P. Raizer, *Physics of Shock Waves and High Temperature Hydrodynamic Phenomena* (New York: Academic Press, 1966)

Developments in XUV laser radiography of laser driven targets

M H Key , D H Kalantar , J Nilson , B A Remington , S V Weber
Lawrence Livermore National Laboratory , L-399 , PO Box 808 , Livermore , CA 94551
Tel. 510 424 2175, e-mail . key1@llnl.gov
E Wolfrum, D Neely, S J Rose
Rutherford Appleton Laboratory , Chilton, Oxon., OX11 OQX, UK
J Zhang , N S Kim , J S Wark
Clarendon Laboratory , Oxford University , Parks Road, Oxford , OX1 3PU , UK
CLS Lewis , A G Mac Phee , J Warwick
Physics Dept., Queens University, Belfast, N Ireland, UK
A Demir, J Lin, R Smith, G J Tallents
Physics Dept., Essex University ,Wivenhoe Park, Colchester, Essex, UK .

XUV lasers are being exploited for radiography with high space , time and amplitude resolution of perturbations in laser driven targets. Information of importance for research into the possibility of generating energy by inertially confined fusion has been obtained using a saturated 15.4 nm neon-like Yttrium laser [1,2,3]. More recently further work has been carried out with a neon- like Ge laser also operating at saturation with prepulse drive on the J=0-1 transition at 19.6 nm. This has enabled new avenues to be explored including the effect on the laser driven targets of single mode perturbations in the drive intensity and the transient behavior of thermal smoothing of the perturbations as illustrated by figures 1 and 2 . The change in XUV opacity of the dense shock compressed target material has also been studied and is of basic science interest as it gives the first direct measurement of the scaling with density of inverse Bremsstrahlung absorption in a strongly degenerate plasma [4].

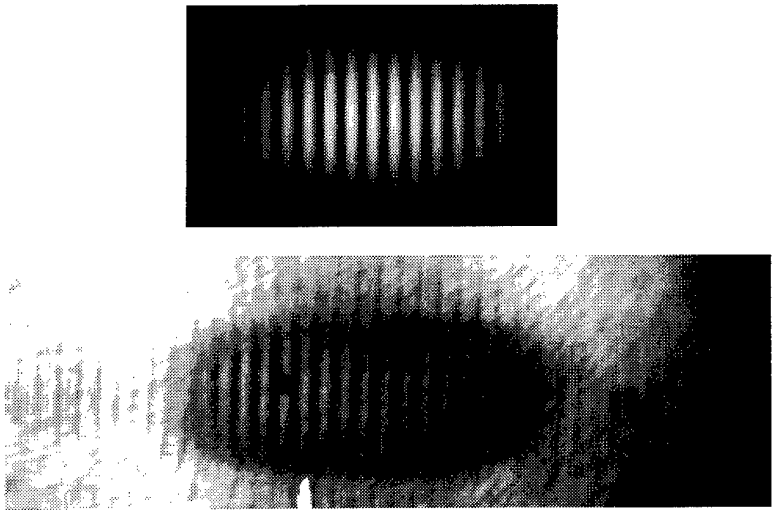

Figure 1 *Above is the computed form of a 1D optical mode pattern of 15 micron wavelength used to drive a 2 micron thick Al foil at* 210^{13} Wcm^{-2} *. Below is a Ge XUV laser radiograph with 50 ps exposure time recorded after 500 ps of drive . It shows perturbations induced in the foil which correspond to 5% variations in its thickness*

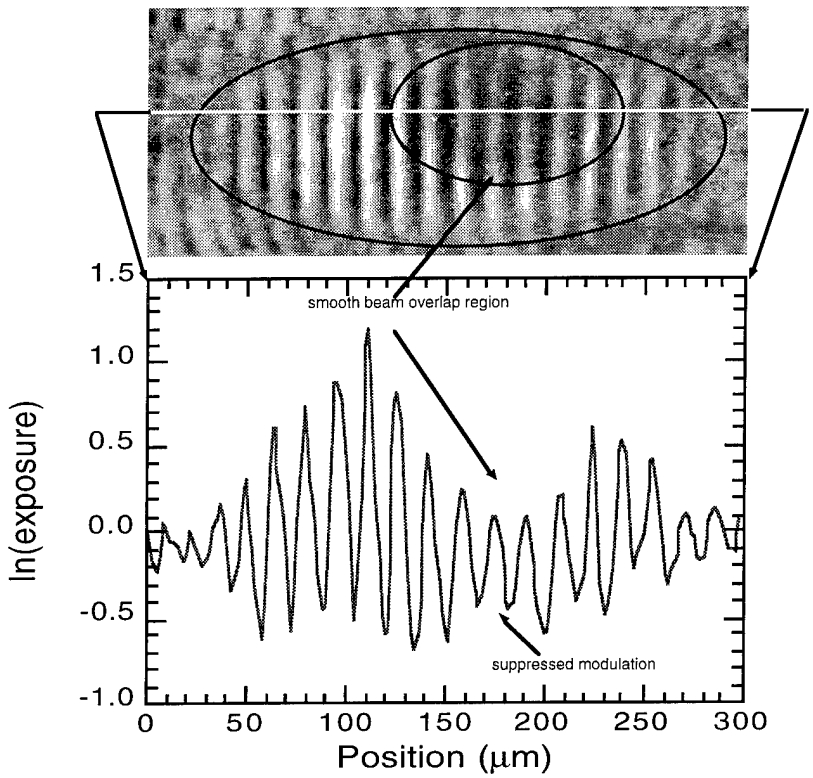

Figure 2 *Above is a radiograph similar to figure 1 but including a smaller region irradiated in addition by a uniform intensity twice that of the modulated drive . The relative timing of the uniform and modulated drive is varied to study the effect of a preformed plasma atmosphere on the efficiency of imprinting of hydrodynamic perturbations . A reduction in the imprint efficiency in the region of drive overlap is seen in the radiograph and quantified in the lineout of intensity shown below.*

In order to progress further we are giving new consideration to the characteristics of the XUV laser source . One area of investigation concerns the intrinsic speckle pattern of the XUV laser beam and we have made measurements of its amplitude and Fourier composition for the case of the Ge laser . The data give information on the temporal and spatial coherence of the laser .

We are interested also in the possibility of carrying out radiographic studies using shorter wavelength sources . Current work relies on probing materials whose L edge transmission window coincides with the XUV laser wavelength (Si for the Y laser and Al for the Ge laser). We aim to extend our research to probe thicker targets of CH plastic materials and for this purpose we are developing Ni-like lasers using prepulse drive .

The paper will summarize the new radiography results obtained with the Ge laser , discuss the speckle pattern of the laser and present the results of a current experiment to develop the Ni -like probe source .

1.M H Key et al. J. Quant. Spec. Rad. Trans. 54, 221, (1995).
2. D H Kalantar et al. Rev. Sci. Instr. 67, 781, (1996).
3. D H Kalantar et al. Phys. Rev. Lett. 76 , 3574, (1996)
4 . M H Key et al . J. Quant. Spec. Rad. Trans. (to be published)

Friday, March 21, 1997

High Field Laser-Electron Interaction

FC 1:45pm – 3:45pm
Zia A

Richard R. Freeman, *Presider*
Lawrence Livermore National Laboratory

Accelerator Based Source Development: Higher, Wider and Shorter

Erik D. Johnson
Brookhaven National Laboratory

A host of new sources are currently being pursued throughout the world which push the performance boundaries higher, wider and shorter than thought possible only a few years ago for accelerator based technologies. Various free electron laser configurations open the window to high power, sub-picosecond synchrotron radiation sources over a wide range of wavelengths. Storage ring sources still have some room for improvement within reason, and intense pulsed x-ray sources by Compton scattering are now being experimentally investigated. This talk will outline the scope of these developments as they relate to the production, and possible utilization, of novel sources of radiation based on accelerator technology.

Observation of nonlinear laser-electron and laser-photon scattering

C. Bamber, S. Boege, T. Koffas, T. Kotseroglou, A.C. Melissinos, D.D. Meyerhofer*, D. Reis, Dept. of Physics and Astronomy, University of Rochester, Rochester, NY 14627

C. Bula, K.T. McDonald, and E. Prebys Joseph Henry Laboratories, Princeton University,Princeton, NJ 08544

D.L. Burke, R.C. Field, G. Horton-Smith, J.C. Spencer, D. Walz, Stanford Linear Accelerator Center, Stanford University, Stanford CA

S. Berridge, W. Bugg, K. Shmakov, A. Weidemann, Dept. of Physics and Astronomy, University of Tennessee, Knoxville, TN 37966

*Presented by
D.D. Meyerhofer
Depts. of Mechanical Engineering and Physics and Astronomy
220 Hopeman Bldg.
University of Rochester
Rochester, NY 14627

Tel: 716-275-7769
FAX: 716-275-5960
email:ddm@lle.rochester.edu

Nonlinear laser-electron and laser-photon scattering has been observed during the interaction of an intense laser with 46.6 GeV electrons in the Final Focus Test Beam at SLAC. Nonlinear laser-electron and laser-photon scattering is characterized by two dimensionless parameters.[1-3] The first is η^2, defined as

$$\eta^2 = \frac{e^2 E_{rms}^2}{m_e^2 \omega_L^2 c^2} = \frac{e^2}{m^2 c^4} \langle A_\mu A^\mu \rangle,$$

where E_{rms} is the rms. electric field strength in the laboratory, ω_L is the laser frequency, and A_μ is the four vector potential. The second is

$$\Upsilon = \frac{2\gamma E_{rms}}{E_{crit}},$$

where $E_{crit} = \frac{m^2 c^3}{e\hbar}$, the QED critical field strength, is the field strength at which an electron is accelerated to its rest mass in a Compton wavelength.[4] γ is the Lorentz factor of the center momentum frame.

As η^2 approaches 1, nonlinear(multiphoton) Compton scattering

$$n\omega_L + e^- \rightarrow \omega_{sc} + e^-_{sc}$$

becomes probable. For 1μm laser light, this occurs at approximately 10^{18} W/cm^2. ω_L represents the laser photon and ω_{sc} the scattered photon, while n is the number of laser photons participating in the scattering.

If, in addition, $Y \rightarrow 1$, multiphoton pair production,

$$n\omega_L + \omega_2 \rightarrow e^+ + e^-$$

becomes possible. The critical field corresponds to an intensity in excess of 10^{29} W/cm^2, but the Lorentz boost associated with the 46.6 GeV electrons allows the critical field to be reached with an intensity of ~10^{19} W/cm^2.

We have performed an experiment interacting a high intensity laser with 46.6 GeV electrons in the Final Focus Test Beam at SLAC.[5] The laser system produces picosecond pulses with intensities in excess of 10^{18} W/cm^2 with 1.053 μm and 0.527 μm wavelength light at a repetition rate of 0.5 Hz.[6] Thus, both η^2 and Y approach one in these experiments.

We have observed both positron production by 0.527 μm wavelength laser light and nonlinear Compton scattering[5] with 1.053 μm and 0.527 μm wavelength light. Positron production requires a minimum of 4 laser photons due to the center of momentum energy requirement. Nonlinear Compton scattering has been observed with up to 4 laser photons participating in the interaction.

References

1. A.I. Nikishov and V.I. Ritus, Sov. Phys. Jetp **19**, 529-541 (1964).

2. N.B Narozhny, A.I. Nikishov, and V.I. Ritus, Sov. Phys. JETP **20**, 622-629 (1965).

3. V.B. Berestetskii, E.M. Lifshitz, and L.P. Pitaevski, *Quantum Electrodynamics* (Pergamon Press, Oxford, 1982), pp. sec. 101.

4. J. Schwinger, Proc. Nat. Acad. Sci. **40**, 132 (1954).

5. C. Bula, K.T. McDonald, E.J. Prebys, C. Bamber, S. Boege, T. Kotseroglou, A.C. Melissinos, D.D. Meyerhofer, W. Ragg, D.L. Burke, R.C. Field, G. Horton-Smith, A.C. Odian, J.E. Spencer, D. Walz, S.C. Berridge, W.M. Bugg, K. Shmakov, and A.W. Weidemann, Phys. Rev. Lett. **76**, 3116-3119 (1996).

6. C. Bamber, T. Blalock, S. Boege, J. Kelly, T. Kotseroglou, A.C. Melissinos, D.D. Meyerhofer, W. Ragg, and M. Shoup III, Laser Physics , submitted (1996).

High Energy Photon Generation in Colliding Laser Pulses

F.V. Hartemann, A.L. Troha, J.R. Van Meter, and N.C. Luhmann, Jr.
UC Davis Dept. of Applied Science, LLNL, PO Box 808, L-794, Livermore CA 94550
Phone : (510) 422-1481, Fax : (510) 422-2514, Email : fredh@gregor.llnl.gov
A.K. Kerman
Dept. of Physics and Center for Theoretical Physics,
Massachusetts Institute of Technology, Cambridge MA 02139

The acceleration of charged leptons to TeV energies is a problem of considerable importance. At these energies, electroweak spontaneous symmetry breaking and the Higgs mechanism are expected to play a dominant role in the interaction physics. Alternatively, short wavelength photons can also be used to probe this energy range, as exemplified by the γ–γ collider project [1].

To produce TeV electron beams over reasonable distances, extremely high accelerating gradients are required, and numerous laser-driven acceleration schemes have been proposed [2]. All of these essentially rely on the very high peak electric fields associated with tightly focused TW-class lasers using chirped pulse amplification (CPA) [3], as mediated by either plasmas [4] or structures in vacuum [2,5]. Among the different approaches, vacuum laser acceleration is of particular interest because of its simplicity and potential for extremely high gradients, and because it alleviates plasma control and stability issues [6]. Unfortunately, it is well-known that one of the simplest vacuum laser acceleration processes, ponderomotive acceleration [5], where the nonlinear axial force produced by the combined action of the laser transverse electric and magnetic fields accelerates electrons co-propagating with the wave, suffers from a severe drawback as no net energy gain can be imparted to the electrons without terminating the interaction with structures in close proximity to the beam. These structures may be damaged by the severe radiation environment and by high energy electrons, and this imposes serious restrictions on experimental designs, as noted by Sprangle [2].

In this work, we propose to combine vacuum ponderomotive acceleration [6] with Compton backscattering [7], to produce high energy photons with a high intensity laser and an electron beam of relatively modest energy. In this manner, the high energy

acquired by the electrons within the drive laser pulse is effectively extracted in the form of short wavelength photons by a colliding probe laser pulse, without requiring complex structures to terminate the interaction, thereby preserving the robustness and simplicity of vacuum ponderomotive acceleration. It will be shown that for this process, the photon energy scales as

$$h\nu \cong 4 \frac{hc}{\lambda_0} \gamma_0^2 A_\perp^4, \tag{1}$$

where λ_0 is the laser wavelength (pump and probe), γ_0 is the electron beam energy, and

$$A_\perp = \frac{e E_0 \lambda_0}{2\pi m_0 c^2} = \frac{e \lambda_0}{\pi m_0 c^{5/2}} \sqrt{\frac{I_0}{2 \varepsilon_0}}, \tag{2}$$

is the dimensionless amplitude of the 4-vector potential associated with the drive laser wave, as expressed in terms of the focused intensity I_0.

As a specific example, 1-TeV photons could be produced with an 8.5 10^{20} W/cm^2 drive pulse at 800 nm, interacting with a 550 MeV beam. These parameters correspond approximately to a normalized vector potential of 20. By comparison, a free-electron laser (FEL) [8] using the same laser wavelength for an electromagnetic wiggler would require over 200 GeV of beam energy.

The theoretical analysis of this interaction can be considerably simplified by noting that while the fields observed in the lab frame correspond to an interference between colliding laser pulses, the pulses are effectively decoupled in the electron frame because their respective Doppler shifts differ significantly : the drive laser fields are "frozen" and remain essentially constant during the Compton backscattering interaction.

The geometry of the interaction is illustrated schematically in Fig. 1. For the sake of simplicity, the main portion of the theoretical discussion is given in terms of plane waves ; however, three-dimensional effects are taken into account in the scaling of the process. In particular, because the transverse beam excursion in the drive laser field can be large, the preferred interaction geometry corresponds to a linearly polarized drive pulse focused in a slab configuration, as shown in Fig. 1.

The overall scaling of the process, for a slab geometry, is summarized in Fig. 2, where the following parameters are fixed : λ_0 = 800 nm, $\sigma_y = 5\ \lambda_0$, and where the pulse

duration is 20 fs FWHM. Using the frequency scaling, the relation between the intensity and the normalized vector potential, and the equation describing the transverse excursion, with the constraint that the drive pulse energy $W = I_0\,\sigma_x\,\sigma_y$, the photon energy can be expressed in terms of the electron beam energy γ_0, and the drive pulse energy W, as $\frac{h\nu}{e} \propto W^{4/3}\,\gamma_0^{2/3}$, or more accurately as

$$\varpi = 4\left(\frac{1}{4\pi^{2/3}}\,\frac{\lambda_0}{\sigma_y}\,\frac{W}{\Pi\,\Delta t}\right)^{4/3}\gamma_0^{2/3}, \qquad (3)$$

where we have introduced the parameter $\Pi = \frac{\varepsilon_0 m_0^2 c^5}{e^2} = 0.6931$ GW. For example, Eq. (3) and Fig. 2 indicate that when a realistic three-dimensional slab geometry is taken into account, 1-GeV photons can be produced with 10 J in the drive pulse and a 325 MeV beam ; 1-TeV could be reached with 1 kJ of laser energy and a 1 GeV beam.

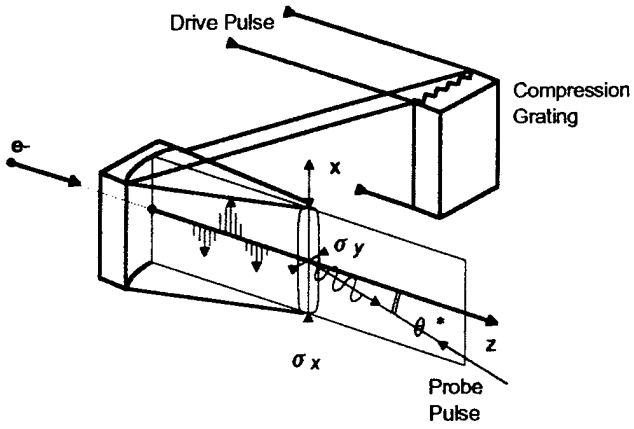

Fig. 1 *Geometry of the interaction process.*

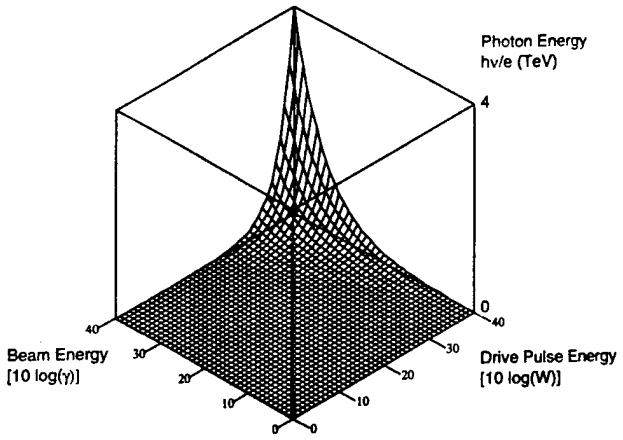

Fig. 2 *Photon energy vs. beam and drive laser energies.*

References

[1] K.J. Kim, *et al*, *"Gamma-Gamma Collider Based on Compton Backscattering"* , LBNL Report LBL-39325 (1996).

[2] P. Sprangle, E. Esarey, and J. Krall, Phys. Plasmas **3**, 2183 (1996).

[3] M.D. Perry, and G. Mourou, Science **264**, 917 (1994).

[4] C.E. Clayton, *et al*, Phys. Rev. Lett. **70**, 37 (1993).

[5] F.V. Hartemann, *et al*, Phys. Rev. **E51**, 4833 (1995).

[6] W.B. Mori, *et al*, Phys. Rev. Lett. **72**, 1482 (1994).

[7] F.V. Hartemann, *et al*, Phys. Rev. **E54**, 2956 (1996).

[8] C.W. Roberson, and P. Sprangle, Phys. Fluids **B1**, 3 (1989).

Single Pass Free Electron Lasers as Sources of Short Wavelength Coherent Radiation

Li Hua Yu

National Synchrotron Light Source

Brookhaven National Laboratory

Upton, NY 11973

516 344-5012

516 344 4745(fax)

yu@bnlls1.nsls.bnl.gov

Free electron lasers utilize a relativistic electron beam as the laser medium, which results in unique properties beneficial to the generation and amplification of short wavelength coherent radiation. Since the resonance condition can be adjusted by varying externally controlled parameters such as the electron energy or the wiggler magnetic field strength, these devices are well suited to produce sources with tunable wavelength. Also, there is no problem with the medium having undesirable absorption at particular wavelengths. Development of free electron laser oscillators utilizing optical cavities has proved very successful in the infrared. As one considers moving into the vacuum ultraviolet and x-ray regions, mirrors become more difficult, and it is worthwhile to consider devices based upon single pass amplification. One approach is to utilize an external laser to seed the FEL amplifier. At short wavelengths a seed at the operating wavelength may be unavailable, but one can use a subharmonic seed at longer wavelength and carry out harmonic generation in the FEL . This scheme has many merits especially in the ultraviolet region from 75nm-200nm. The temporal coherence of the output is inherited from the seed laser. Another approach is to start the FEL from the spontaneous radiation emitted at the beginning of the wiggler. This approach is viable at very short wavelengths where even subharmonic seeds are unavailable. Devices based on self-amplified spontaneous radiation are capable of delivering high intensity and good transverse coherence, but the frequency bandwidth cannot be as narrow as achievable in an oscillator or seeded amplifier.

In this paper we give an overview of the theory of FEL amplifiers and discuss their application to the development of sources of short wavelength coherent radiation. Intensity, brightness, wavelength tunability, and coherence of the source is described, and consideration is given to the projects under development at DESY, BNL and SLAC .

Friday, March 21, 1997

Strong Field Atomic Physics

FD 4:15pm – 6:00pm
Zia A

Wolfgang Sandner, *Presider*
Max Born Institute, Germany

Nonperturbative time-dependent theory of two-electron atoms in strong fields

Jian Zhang[1] and P. Lambropoulos[1,2]

1. Max-Planck-Institut für Quantenoptik
Hans-Kopfermann-str. 1, D-85748 Garching, Germany
Tel:+49-89-32905-705, fax:+49-89-32908-200, e-mail:pel@mpq.mpg.de
2. Foundation for Research and Technology-Hellas
Institute of Electronic Structure & Laser, P.O. Box 1527, Heraklion 71110, Crete,
and Department of Physics, University of Crete, Greece

We have developed an elaborate theoretical and computational approach for the study of strong field phenomena in two-electron atoms taking into account the electron-electron correlation in the dynamics of the process. The work grew in three stages. In the first stage, we developed the essentials of the approach which consists of a discretized L^2-basis of atomic states constructed in terms of B-splines. These are completely correlated two-electron states in terms of which we expand the time-dependent wavefunction satisfying the Schrödinger equation which includes the interaction with the time-dependent laser field represented by a realistic pulse shape. Recently published results[1, 2] include ATI and photoelectron angular distributions in He which showed very small correlation effects as evaluated through a comparison with frozen core or single-active-electron calculations which are conveniently performed using the same technique.

In the second stage, the method was extended to the case of ionization above several thresholds so that the ion may be left in one of several possible ionic states, with branching ratios which in perturbation theory are determined by the number and the frequency of the photons absorbed, and are independent of the intensity. This problem involves several open channels with the well-known difficulties even in single-photon absorption. In our approach, as in any approach involving discretized basis sets, we had to handle an obstacle arising from the fact that the different continua, corresponding to the various thresholds, are discretized so that the degeneracy in the continuum that leads to different ionic states is practically lost, when the L^2-basis is constructed through a fixed boundary condition, namely that the wavefunction vanishes at the end of the box.

Even with that restriction, we were able, through a renormalization and averaging technique, to circumvent that difficulty and to obtain photoelectron energy spectra[3], including ATI showing the branching of the signal above the various thresholds in atomic Mg which was employed as a test case to illustrate our quantitative results. One example of those results illustrating the effect of intensity on branching ratios in the ATI spectrum is shown in Fig. 1.

Through the averaging procedure, we lose, however, the angular information necessary for the calculation of photoelectron angular distributions. In a further development[4], we solved that problem through a major extension of the technique which amounts to a novel

method for solving the time-dependent Schrödinger equation in the presence of multiple open continua. By relaxing the boundary condition at the end of the box, the problem is turned into an eigenvalue problem. Without going into technical details, it will suffice to mention here that the technique enables us to obtain sufficiently high density of states to calculate all features of the problem, including photoelectron anular distributions, one example of which is shown in Fig. 2. A comparison of the refinement obtained in the photoelectron energy spectra with that of the averaging techique is shown in Fig. 1.

In the third major extention, we have been able to develop a method for the time-dependent nonperturbative solution of the two-electron Schrödinger equation including double ionization. The use of the free-boundary condition approach was critical in implementing this generalization. First, we calculated in He single-photon two-electron ejection in perturbation theory, with results in good ageement with experiment and the most recent theory by Pont and Shakeshaft[5]. We have now begun obtaining nonperturbative results of single and double ionization in He for photon frequencies ranging from 15 eV to 5 eV. Details of the techniques and results will be presented.

Finally, we present a number of results[6, 7, 8] illustrating the application and usefulness of the B-splines discretized basis technique to the calculation of nonlinear susceptibilities for photons of XUV frequencies where the transitions are deep into the continuum posing thus special difficulties due to the multiple poles in the trasition matrix elements.

References

[1] Jian Zhang and P. Lambropoulos, J. Phys. B**28**, L101 (1995).

[2] Jian Zhang and P. Lambropoulos, J. of Nonlinear Opt. & Materials **4**, 633 (1995).

[3] Jian Zhang and P. Lambropoulos, Phys. Rev. Lett., **77**, 2186 (1996).

[4] Jian Zhang and P. Lambropoulos, "Free boundary condition method for calculating the multichannel continua wavefunction in a finite space: Application to time-dependent calculation of photoelectron spectra in Mg", (submitted to Euro. Phys. Lett.).

[5] M. Pont and R Shakeshaft, J. Phys. B**28**, L571 (1995).

[6] S.J. van Enk, Jian Zhang and P. Lambropoulos, J. Phys. B**28**, 3453 (1995).

[7] S.J. van Enk, Jian Zhang and P. Lambropoulos, Z. Phys. D**37**, 211 (1996).

[8] E.E. Fill, S.J. van Enk, J. Zhang and P. Lambropoulos, Phys. Rev. A, (in press).

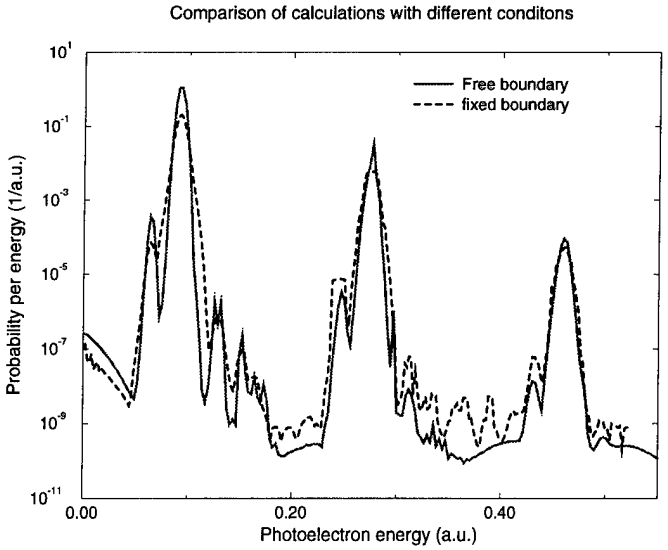

Figure 1: Comparison of calculations with different boundary conditions. $I = 10^{12} W/cm^2$, $\hbar\omega = 5$ eV.

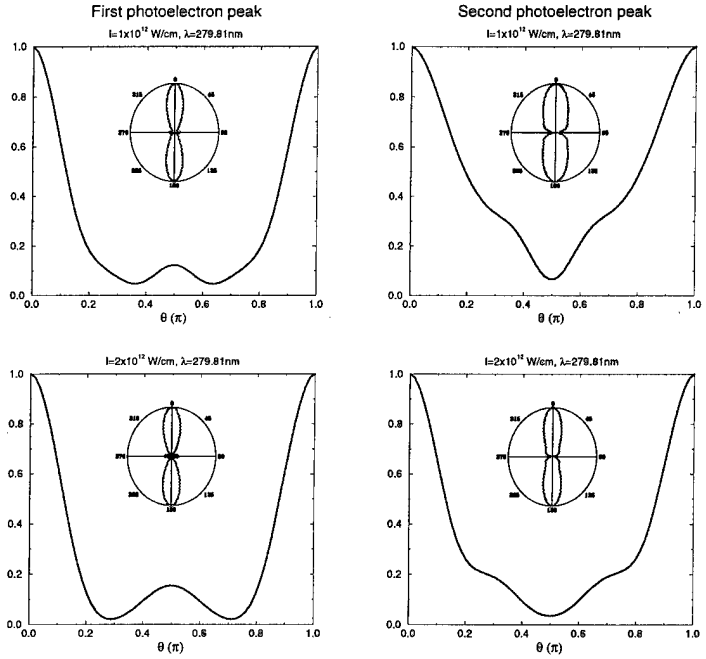

Figure 2: Polar and linear plots of photoelectron angular distributions at two energies, and at two laser intensities. Upper figures, $I = 10^{12} W/cm^2$; lower figures, $I = 2 \times 10^{12} W/cm^2$.

Photoelectron Spetrometry of XUV Multiphoton processes in Helium

A. Bouhal[1], P. Breger[2], P. Agostini[2]
R. Constantinescu[3], H. G. Muller[3], L. F. DiMauro[4]
G. Hamoniaux[1], A. Mysyrowicz[1], A. Antonetti[1]

([1]) Laboratoire d'Optique appliquée, ENSTA-Ecole-Polytechnique, 91125 Palaiseau, France
([2]) Service des Photons, Atomes et Molécules,CE de Saclay, 91191 Gif Sur Yvette, France
([3]) FOM-AMOLF 407 Kruislaan 1098 SJ Amsterdam , Netherlands
([4]) Chemistry Department , Brookhaven National Lab POB 500 Upton NY 11973

High-order harmonic generation by means of high-energy, femtosecond laser pulse has proved to be a convenient way to generating coherent radiation in the extreme-ultraviolet (XUV) spectral regions. Recent experiments [1,2] show that harmonic duration is much shorter than the pump one while divergence measurements show that the harmonic beam should be focussable to a fairly small spotsize and reach intensities high enough for nonlinear interactions. In this contribution we report the first electron energy spectrum(*) resulting from non-resonant multiphoton transitions induced in the XUV domain using harmonics produced in xenon by the 120 fs, 10 mJ Ti:sapphire laser at the Palaiseau facility. An annular beam geometry[3] is used to separate the fundamental from the harmonics which are focussed in a magnetic bottle electron spectrometer filled with 10^{-2} torr of helium by a (W-Re)-coated spherical mirror (R=70mm). The intensity of the pump laser is adjusted to .9 mJ for a cutoff at harmonics 15. Consequently, no one-photon ionization of helium is observed. Photoelectrons are detected only when the XUV radiation reflected by the mirror is focussed in the sensitivity zone of the magnetic bottle (Fig.1). This behavior is the signature of a strong intensity dependence of the ionization process and rules out one-photon processes.

A typical electron energy spectrum is displayed in Fig.2. The low energy electron peak result from a total absorbed energy of about 25 eV and most likely correspond to two-photon processes adding up to16 fundamental photons (h13+h3, h11+h5, h9+h7). The shape of this peak is affected by the drop of the spectrometer transmission for energies below 1 eV. The much smaller part around 28-29 eV probably results from processes adding up to 18 fundamental photons involving h15+h3, h13+h5, h11+h7, h9+h9. The absence of a "17-photon" peak would then result from the odd parity of the harmonics and too low an intensity to induce three-photon processes. Work is in progress to interpret the detail of the structure of these peaks.

References :

[1] C. Glover et al, Phys. Rev. Lett. 76, 2468 (1996)
[2] A. Bouhal et al, to appear in JOSA B (1997)
[3] J. Peatross et al, Opt. Lett. 19, No. 13 (1994).

(*) Two-photon XUV processes detected through ion charge spectrometry aree reported in this Workshop by the Ohio group.

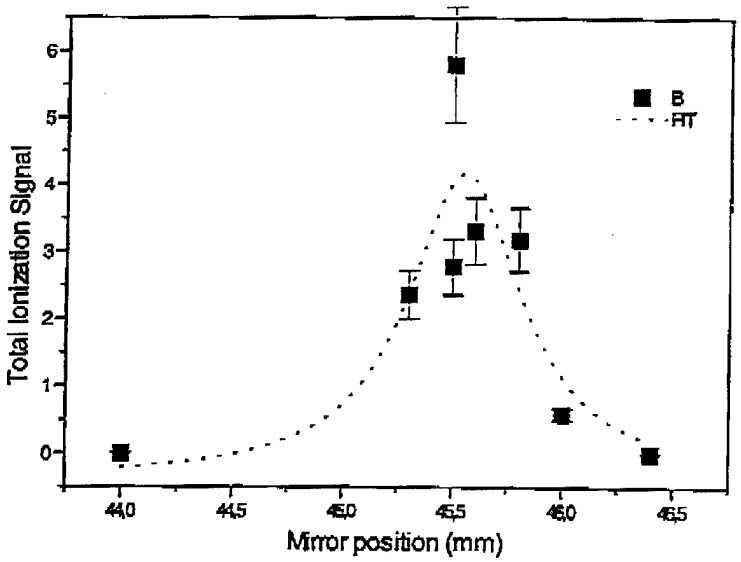

Fig. 1 Total Ionization signal vs focus position. The lorentzian fit has FWHM of 1 mm corresponding to the sensitivity zone of the magnetic bottle spectrometer.

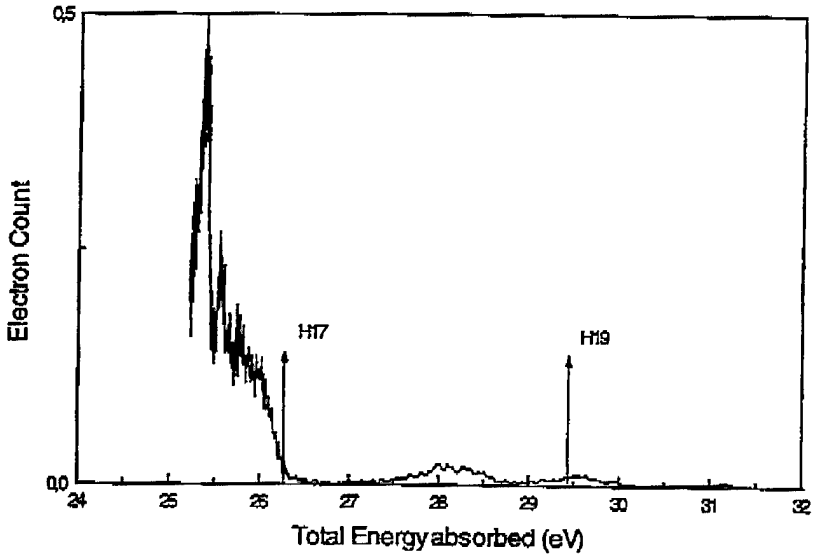

Fig. 2 Electron energy spectrum from two-photon ionization of helium by harmonics 3-15 of a Ti:sapphire laser with an energy of .9 mJ. The arrows show the positions of one-photon ionization peaks by harmonics 17 and 19. Theses peak appear only at higher pump energy.

LASER-ASSISTED MULTICOLOR PHOTOIONIZATION OF ATOMS WITH HIGHER HARMONICS

Alfred Maquet, Richard Taïeb and Valérie Véniard

Laboratoire de Chimie Physique - Matière et Rayonement, Université Pierre et Marie Curie, 11 Rue Pierre et Marie Curie, 75231 Paris Cedex 05, France.

e-mail: vv@ccr.jussieu.fr; Phone: 33-1 44 27 66 31 ; Fax: 33-1 44 27 66 31

We discuss, via a numerical calculation, the main properties of atomic photoelectron spectra, as they would be obtained by using a radiation pulse containing higher harmonics together with the laser which has been used to generate them. We address more precisely the physically relevant situation in which the harmonics have much weaker intensities than the one of the laser. In such multicolor photoionization processes, the atom can simultaneously absorb harmonic UV photons and exchange, i.e. absorb and/or emit (via stimulated emission) laser IR photons. An interesting outcome of our study is to show that such new effects should be observable with currently developed harmonic sources.

We have simulated the photoelectron spectra by numerically solving the time-dependent Schrödinger equation (TDSE) for a real (3-D) hydrogen atom in the presence of the radiation pulse. The photoelectron spectra are obtained from a spectral analysis of the atomic wave function after the end of the pulse.

Our results show that, when the frequency of the harmonics is larger than the ionization potential of the atom, everything else being kept fixed, the magnitudes of the photoelectron peaks are strongly dependent on the difference of phase between successive harmonics. This strong dependence results from interference effects taking place between competing quantum paths leading to a given final state. It shows that a detailed study of multicolor photoionization spectra, involving high harmonics and the laser field which has been used to generate them, can provide interesting information on the phase differences between successive harmonics [1].

On the other hand, for lower harmonics frequency (below threshold) two-color experiments can lead interesting informations concerning the dynamics of some resonant ionization processes ("pump-probe" simulations). New results concerning 1-D (Soft-Coulomb

potential) and 3-D atoms will be presented.

[1] V. Véniard, R. Taïeb and A. Maquet, Phys. Rev. Lett. **74**, 4161 (1995); V. Véniard, R. Taïeb and A. Maquet, Phys. Rev. A **54**, 721 (1996).

Generation and Stimulated Amplification of High Energy Photon Bursts at Gas Ionization by Few-Optical-Cycle Laser Pulses

A.V. Kim, M.D.Chernobrovtseva, D.V. Kartashov, and A.M. Sergeev

Institute of Applied Physics, Russian Academy of Sciences,
46 Uljanov St., Nizhny Novgorod 603600, Russia
phone: (+7-8312) 384-553; fax: (+7-8312) 363-792
e-mail: kim@ufp.appl.sci-nnov.ru

The application of laser pulses with supershort duration of the order of 10 fs has recently been proposed [1,2] for enhancement of high order harmonic emission and subfemtosecond pulse production in the soft X-ray range. Such short driving pulses contain only a small number of optical cycles and therefore high energy photon bursts are generated due to atom ionization at rapidly increasing field amplitudes. It is obvious that the efficiency of this process becomes dependent on the concrete field distribution over the pulse or, in the other words, on the absolute phase of the optical field.

The original idea of an enhancement of energetic x-ray burst production with a decrease of the pulse duration consists in the following. At a sharply increasing laser field amplitude, atoms may be ionized with high probability (or the main part of the electron Ψ-function may be detached from the intraatomic potential) for a fraction of an optical cycle when the field strength passes the ionization threshold value. For the subsequent laser period the electron wave packet including almost all particles will be accelerated by the laser field and may collide with the parent ion core at a velocity higher than that for the case of slowly varying field amplitude.

The efficiency of this mechanism may be easily illustrated by considering the classical picture of the relevant trajectories of freed electrons that are responsible for the high energy photon emission. Let us assume that the leading front of the pulse is characterized by the exponential growth of the field amplitude with an increment β measured in the laser field frequencies. We will be interested in the phase φ_{col} and the energy U_{col} of return collisions of classical electrons with parent ions depending on the electron release phase φ. In the case $\beta=0$, considering the one-dimensional electron trajectory, precisely half of the electrons will collide with ions at least once. These are the electrons released from intraatomic potential during quarters of the field cycles after achieving the local maximum values. The electrons released within quarters of the increasing field cycles do not return to parent ions at all. The picture changes for $\beta>0$. It is seen in Fig.1a that with increasing β the boundary of the "non-return phase" shifts to the negative domain, i.e. the electrons released before the field maxima may participate in the bremsstrahlung. In this case the maximum of the return collision energy (Fig.1b) broadens and shifts from $\approx 18°$ at $\beta=0$ to the earlier phases, so that it arrives at $\varphi=0$ when $\beta\approx 0.2$. In general, this fact indicates an improved conditions for the soft X-ray burst generation and an increase in the maximum energy of emitted photons. However, it is clear that the process of soft X-ray burst generation is rather sensitive to a specific temporal profile of the pulse and one can imagine a situation when the non-return effect of the most released electrons will lead to a dramatic reduction of the bremsstrahlung efficiency.

This can happen for example if the field passes the range of strengths that are critical for the atom decay in the growing phase but close to the pulse center when the amplitude reaches the maximum. Then a freed electron bunch is mainly generated for $\varphi<0$, while the value β is close to 0. It is interesting to note that if the non-return condition is fulfilled near the axis of

the 3d pulse cross-section, at the periphery, vice versa, the excitation of short wavelength bursts does occur, since electrons are released for lower field envelopes near the field maximum $\varphi=0$. This may cause hollow distributions in the spatial domain where subfemtosecond pulses are generated.

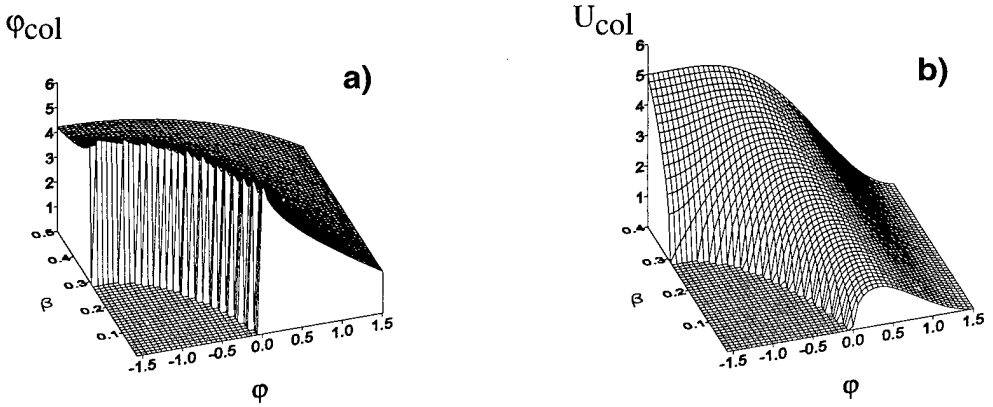

Fig.1 The phase φ_{col} (a) and the energy U_{col} (b) of electron return collisions with parent atoms versus the phase of electron production φ and the rate β of the field amplitude increase.

From the above simple consideration we conclude that the high energy photon burst emission may be controlled by shaping the driving laser pulse. A next question that arises is how collective processes in the ionized gas affect the characteristics of the burst. To investigate this problem quantitatively we have employed a 1+1 simulation model developed in our previous work [3] to consider the self-consistent dynamics of linearly polarized electromagnetic wave propagating in a gas of single-type atoms. The set of equations are the Maxwell equations for a field in the medium written in the simplest form of a one-dimensional scalar wave equation (z-direction along propagation path) and the Schroedinger equation with the intraatomic potential V(x) (x-direction along electric field) for the single electron Ψ-function . We have chosen the potential in the form of $V(x)=(1+x^2)^{-0.5}$ with a binding energy of 0.67 a.u. and considered laser-gas interaction for the few-optical-cycle pulses.

Fig. 2 shows the time dependence of the driving field that has the Gaussian envelope with carrier frequency of 0.2 a.u. and the response function, $R(t)=\int|\Psi|^2\frac{\partial V}{\partial x}dx$, for the field amplitude of 2.1 a.u. Since the R function is responsible for the high-energy photon emission due to the electron-core interaction, we see that it is possible to ionize atom almost completely for one half period. During this time interval the electromagnetic radiation emitted by atoms mainly consists of comparatively low frequency components (as follows from the curve for the response function) and is produced at electron tunneling [4] through the barrier formed by the atomic potential and the driving field. For the subsequent half-period, the electron wave packet is free (R~0), and then, returning back and colliding with parent ion (t ~ 125), it generates radiation with higher frequencies. As it is seen in Fig. 3, where the frequency spectrum of

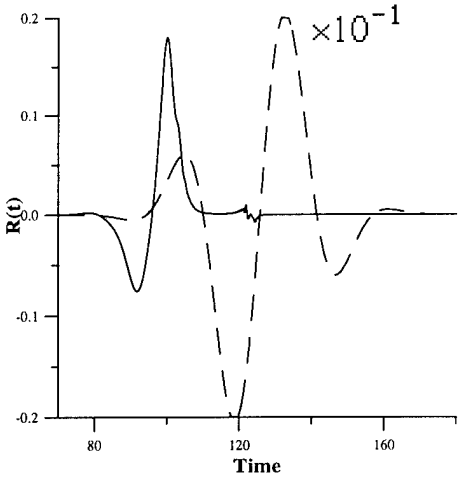

Fig.2. The time dependence of the driving field (dotted line) and the response function R caused by electron-core interaction (solid line).

electric field is shown at various distances of pulse propagation, the plateau region is extended over the harmonic order up to n~80-90. We also see that spectral intensities in several frequency domains have different dependencies on the propagation distance. In Fig. 4, we present the value of energy contained in definite intervals of spectrum versus the propagation path. The main feature of these functions is that they grow exponentially at the initial stage (small z), i.e. high frequency signal is exponentially amplified. This is a manifestation of the effect of stimulated emission at freed electron interaction with parent ion in the presence of super-strong laser field. A detailed analysis of this phenomenon will be done in the report. Here we only note that the saturation effect in the amplification of the stimulated emission is mainly caused by wave dispersion in the emerging plasma and it is more essential at higher frequencies (see Fig. 3 and 4).

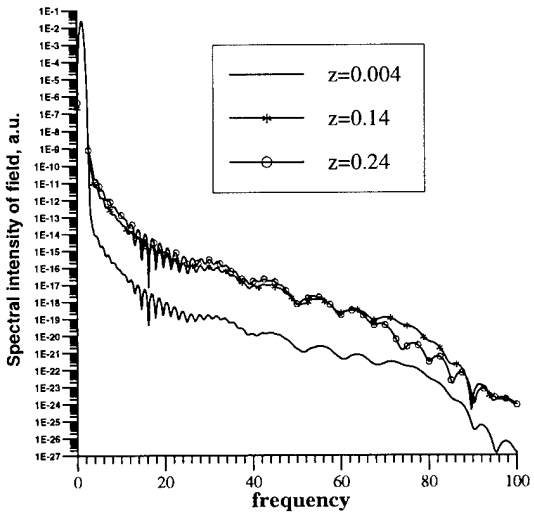

Fig.3. Field spectrum at the various propagation distances.

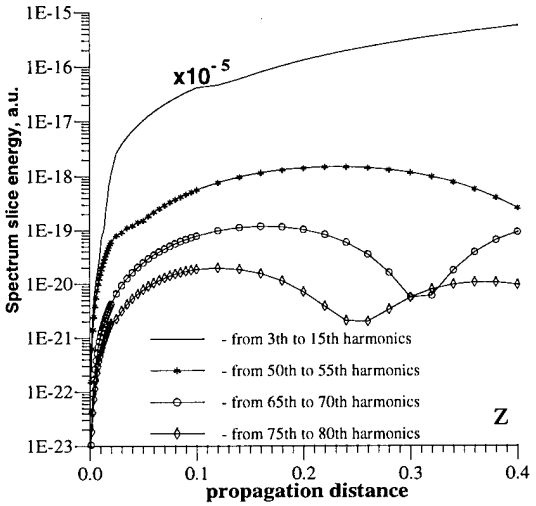

Fig.4. Energy of high-frequency components integrated over definite spectral intervals versus the propagation distance.

References

1. J.Zhou, J.Peatross, M.M.Murname et al., Phys.Rev.Lett. **76**, 752 (1996).
2. A.M.Sergeev, A.V.Kim, and E.V.Vanin, in "Generation, Amplification, and Measurements of Ultrashort Laser Pulses" Proc. SPIE, **2701**, 416, (1996).
3. E.V.Vanin, A.V.Kim, M.C.Downer, and A.M.Sergeev, JETP Lett. **58**, 900 (1993).
4. M.I.Dyakonov and I.V.Gornyi, Phys.Rev. Lett. **76**, 3542 (1996).

Electron dynamics in the strong field limit of photoionization

B. Sheehy†, B. Walker†, R. Lafon†, M. Widmer†, A. Gambhir†, L.F. DiMauro†, P. Agostini‡, and K.C. Kulander•

† Brookhaven National Laboratory, Dept. of Chemistry, Upton, NY, 11973, US

‡ Service des Photons, Atomes et Molecules, Centre d'Etudes de Saclay, 91191 Gif Sur Yvette, France

• TAMP Group, Lawrence Livermore National Laboratory, Livermore, CA 94551, US

The behavior of atoms in strong fields has been the subject of many investigations, both experimental and theoretical. Previously, the majority of experimental studies have been confined to the multi-photon ionization or mixed regimes while few experiments have been done in the tunneling regime[1,2]. The data we will present is the first to examine the photoionization process over the intensity range from multiphoton ionization to well within the tunneling regime. We have taken photoelectron energy spectra, ion yield curves, and angular distributions of helium and neon over a wide range of intensities using a titanium sapphire laser operating at 1 kHz , 780 nm, and a pulse width of ~120 fs, focused into an UHV chamber with f/4 optics, allowing maximum intensities of 20 PW/cm^2. The large dynamic range allowed by the kilohertz repetition rate makes it possible for a quantitative comparison between experiment and theory. Helium and neon were chosen for the study since previous investigations have established that ionization occurs in the tunneling regime [3]. Our investigations show that while the rescattering model [4,5] describes the one electron dynamics *quantitatively*, the extension of the rescattering model to inelastic rescattering as a mechanism for creating higher charge states fails to provide even a qualitative description.

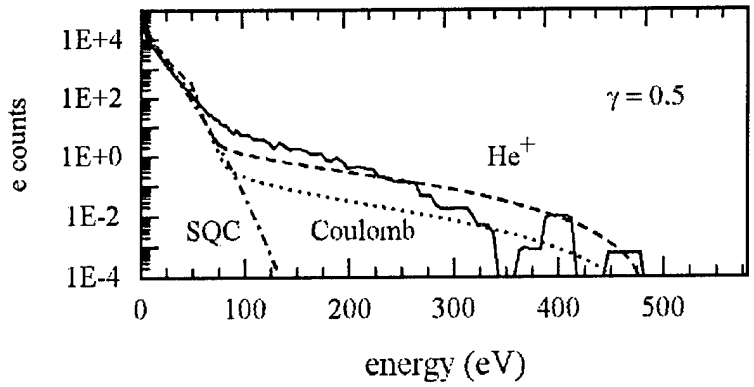

Figure 1: *Total He photoelectron distributions for 780 nm at* $8 \times 10^{14}\ W/cm^2$

Figure 1 shows a photoelectron energy spectrum of helium taken in the tunneling regime, (solid line). The photoelectron spectrum consists of a low energy peak followed by a high energy plateau several orders of magnitude lower. The low energy peak can best be understood by looking at a simple quasiclassical model, (SQC) [1], where only the interaction of the electron with the time varying laser field is considered. Figure 1 makes it clear that the SQC model alone is insufficient to explain the observed photoelectron energy spectrum. The maximum energy a photoelectron can have in this model is $2U_P$, (in atomic units $U_P=I/4\omega^2$). We find that the observed photoelectron energy spectra can be *quantitatively* described by a complete rescattering model. In the rescattering model electrons tunnel into the continuum, as in the SQC model, but unlike the SQC model the electron wave packet may return, via acceleration in the laser field, to rescatter off the core. In this model the high energy electrons can extend out to 8-10 U_P as can be seen in Fig. 1. This model shows good agreement with the measured photoelectron energy spectrum, however to achieve this agreement it is insufficient to consider the scattering potential as a simple Coulomb potential, but is necessary to consider also the short range part of the potential. Figure 1 shows the calculated spectrum with, (dashed line), and without, (dotted line), the short range potential.

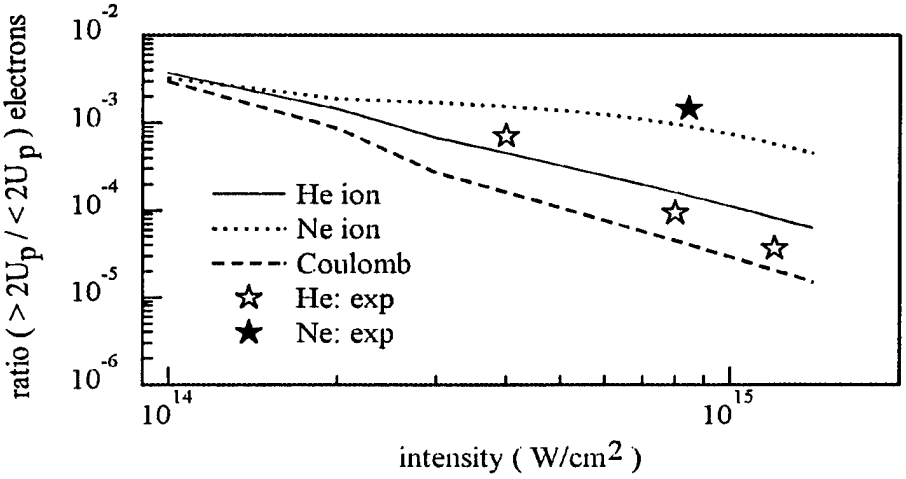

Figure 2: *Experimental and calculated ratio of the total number of electrons with energies $>2U_P$ over those with $<2U_P$.*

Figure 2 shows the compiled experimental, (filled stars Ne data, unfilled are He), and calculated ratios of electrons with energies $>2U_P$ to those with energies $<2U_P$ for helium, (solid line), and neon, (dotted line) and the pure Coulombic, (dashed line), scattering potential calculation. Coulomb scattering underestimates the observed ratios, while the calculations including the short range physics result in excellent agreement.

One may be tempted to extend the rescattering model to inelastic rescattering events where the returning electron scatters inelastically from the core with enough energy to liberate another electron. This model predicts a threshold intensity where the intensity is not sufficient to impart enough energy to the first electron to free a second. There is no indication of this threshold in our data.

The ratio between the second and first charge states were measured. Figure 3 shows the measured ion ratio curves for helium and neon, at 780 nm. Also shown are the ion ratios, as calculated by our rescattering model. The inelastic rescattering model underestimates the ratio by nearly an order of magnitude since, using the initial wave packet size and spreading established by the elastic rescattering model, the cross-section for the e-2e process is too low. The difference between the calculated He, (solid line), and Ne, (dashed line), curves is due to the difference in their short range potential. This difference is not reflected in our data, (filled circles are our helium data, unfilled are neon), strongly indicating that another process is responsible for the double ionization. Ratio curves for helium were also taken with 390 nm excitation, this data also shows inconsistency with the e-2e model.

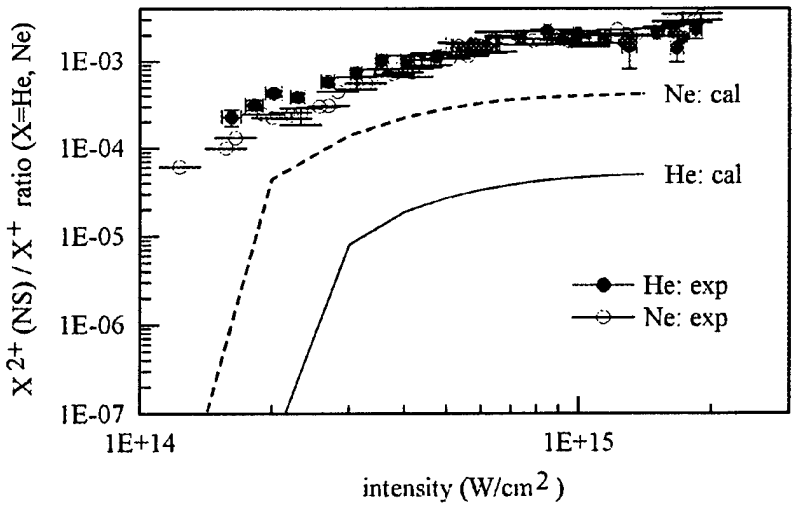

Figure 3: *Experimental and calculated ratio of nonsequential double ionization to single ionization for helium at 780 nm*

In conclusion we will show that the rescattering model explains observed one electron dynamics quantitatively. Furthermore, we will demonstrate the necessity of including the short range potential in the calculations, and the sensitivity to initial wave packet width. We will also show that the inelastic rescattering fails to even show qualitative resemblance to the observed double ionization rate, indicating that some process other than the e-2e inelastic rescattering is responsible for the observed double ionization. This work constitutes the first quantitative analysis and comprehensive experimental survey of the strong field rescattering of electrons.

[1] Corkum P B, Burnett N H and Brunel F, 1989 *Phys. Rev. Lett.*, **62**, 1259-1262
[2] Mohideen U, Sher M H, Tom H W K, Aumiller G D, Wood II O R, Freeman R R, Bokor J and Bucksbaum P H, 1993, *Phys. Rev. Lett.*, **71**, 509-512
[3] Walker B, Sheehy B, DiMauro L F, Agostini P, Schafer K J and Kulander K C,1994, *Phys. Rev. Lett.*,**73**, 1227-1230
[4] Schafer K J, Yang B, DiMauro L F, and Kulander K C, 1993, *Phys. Rev. Lett.*, **70**, 1599-1602
[5] Corkum P B, 1993, *Phys. Rev. Lett.*, **71**, 1994-1997

MOLECULAR HYDROGEN IN AN INTENSE LIGHT FIELD

J. Ludwig, H. Rottke, W.Sandner
Max-Born-Institut, Rudower Chaussee 6, D-12474 Berlin, Germany

The dissociation and ionization mechanisms of molecules and molecular ions in a high intensity non-perturbative optical radiation field has attracted much interest experimentally as well as theoretically ([1,2] and refs. cited there). Especially investigations on molecular hydrogen have revealed many new molecule specific high field phenomena originating in the coupled electronic and nuclear degrees of freedom. Zaviyev et al. and Yang et al. found mechanisms like bond-softening dissociation, above threshold dissociation, or multiphoton dissociation to be active in the hydrogen molecular ion [3,4,5]. Also an indication of light-induced vibrational structure in H_2^+ and D_2^+ was detected [6]. At the high intensities reached in a focused laser beam finally the molecular ion may become ionized resulting in Coulomb explosion of the remaining bare nuclei. Hints pointing to this mechanism to be active have been found in H^+ and D^+ kinetic energy distributions [2,6].

In our experiments at excitation wavelengths 1053 nm and 527 nm we use sub-picosecond laser pulses in an intensity range up to $5x10^{14}$ Watt/cm^2 to investigate the ionization and dissociation mechanisms of $X^1\Sigma_g^+$ ground state molecular hydrogen in a strong optical radiation field and their dependence on wavelength. This extends previous experiments at or close to these wavelengths done with laser pulses having a pulse width longer than ~50 psec [3-5]. Our shorter pulse width allows us to look into processes at a much higher intensity level because of a higher saturation fluence for all processes. The laser radiation we use for these experiments is generated by a Ti:Sapphire oscillator emitting at 1053 nm. After chirped pulse amplification and recompression the pulses have ~0.7 psec pulse width and reach a focused peak intensity of ~$2x10^{14}$ Watt/cm^2 in the interaction region with the hydrogen molecules. Pulses at 527 nm are generated by frequency doubling. In the focused 527 nm beam we reach an intensity of ~$5x10^{14}$ Watt/cm^2. For the experiments on $B^1\Sigma_u^+$ H_2 molecules either 1064 nm Nd:YAG laser pulses with ~5 nsec pulse duration or 100 fsec Ti:Sapphire pulses at 790 nm are used. Single (v = 3,J) ro-vibrational levels of the $B^1\Sigma_u^+$ electronically excited state are prepared by 1-photon absorption of narrow bandwidth tunable VUV radiation at 106 nm. In these experiments the IR laser intensity is kept below approximatly 10^{13} W/cm^2 to discriminate against ground state multiphoton excitation of the molecule.

At 527 nm the dependence of the total yield of molecular and atomic ions and therefore also of the dissocition fraction $X^+/(X^+ + X_2^+)$ (X = H,D) on the light pulse intensity we measure does not show a significant isotope effect. In contrast at 1053 nm we observe a very strong isotope effect in the dissociation fraction. For D_2 it rises much faster with increasing intensity than for H_2 [7]. An isotope effect can only arise for a process which is not purely electronic in nature but is influenced by nuclear dynamics.

The photoelectron kinetic energy distributions at 527 nm excitation wavelength show besides above threshold ionization (ATI) structure a pronounced resonance substructure up to $1x10^{14}$ Watt/cm^2 laser pulse peak intensity [7]. Since we are working in the 'short' pulse excitation regime this means that 7-photon resonant ionization via AC-Stark shifted excited states is the dominating ionization pathway. We are able to identify the resonant states as excited molecular hydrogen states with principal quantum numbers n = 4,5,6 having Rydberg character. Above $1x10^{14}$ Watt/cm^2 laser pulse peak intensity the photoelectron spectra loose the resonance substructure. A broad nearly

structureless spectrum appears. In an intermediate intensity regime two local electron yield enhancements may have their origin in multiphoton ionization of H(1s)/D(1s) atoms formed in a dissociation process. The photoelectron spectra we measure do not show a significant isotope effect meaning that they are determined by the electronic structure of the molecules alone. The 1053 nm spectra show some structure (ATI, resonances) at intensities I below $8x10^{13}$ W/cm^2, at higher intensities a broad hump develops which extends out to ~30 eV at the highest intensity used. This may indicate a transition to tunnel ionization which is expected to occur near $8x10^{13}$ W/cm^2.

The photoion kinetic energy distributions show a similar overall dependence on the laser pulse peak intensity, irrespective of the isotopomere and laser wavelength used [8]. At low intensity a low kinetic energy peak at $E_{kin} \sim 0.32$ eV with a very small, wavelength and isotopomere dependent, intrinsic width (~30 meV (D_2, 527 nm), ~70 meV (H_2, 527 nm), ~70 meV (D_2, 1053 nm), ~150 meV (H_2, 1053 nm)) dominates the spectrum. At 527 nm this peak is expected to originate in bond-softening dissociation of H_2^+/D_2^+ [3,4] while at 1053 nm above threshold dissociation is suspected as its origin [5]. The small intrinsic width indicates that only very few vibrational states take part in these processes.

At high light intensity ($I > 2x10^{14}$ W/cm^2 (527 nm), $I > 1.2x10^{14}$ W/cm^2 (1053 nm)) only one broad yield maximum remains near $E_{kin} \sim 1.6$ eV. For H_2 and D_2 at 1053 nm this ion yield maximum shifts slightly to higher kinetic energies and develops a shoulder on the high energy side with rising light peak intensity. This broad yield maximum may be interpreted as Coulomb explosion dissociation after enhanced tunnel or above barrier ionization of H_2^+/D_2^+ [9] at internuclear distances near R = 8.5 a.u.. The calculated starting intensity for above barrier ionization reaches a minimum at R = 7 a.u., thus supporting this interpretation. The dependence of the dissociation ratio at 1053 nm on the isotopomere and the shifting Coulomb explosion peak in the photoion spectrum seem to indicate that at this wavelength the molecular ion passes only once through the critical region of internuclear distances where it is ionized preferentially. Contrary at 527 nm a Coulomb explosion peak which does not change shape and position with rising light peak intensity may indicate that the molecular ion is ionized from a stabilized state near the critical internuclear distance where the photoionization rate is maximum.

First experiments were done to investigate the $B^1\Sigma_u^+$ state in an intense near infrared (IR) light field. Excitation to the $B^1\Sigma_u^+(v = 3,J)$ rotational levels in intense 1064 nm Nd:YAG laser pulses which have approximatly the same pulse duration as the VUV pulses allows to study linewidths and shapes of individual rotational lines of the $B^1\Sigma_u^+ - X^1\Sigma_g^+$ (3,0) band. An intensity dependent line broadening by decay of the excited states and by the AC-Stark effect in the strong IR laser field is found and analysed. The total H_2^+ and H^+ ion yields measured give rise to dissociation fractions which saturate as a function of the IR light intensity at different levels depending on the $B^1\Sigma_u^+(v = 3,J)$ rotational state. H^+ photoion kinetic energy distributions taken for IR laser intensities up to about 10^{12} W/cm^2 show a single narrow peak located at ~0.3 eV kinetic energy. The shape and width of this peak do not depend on the specific $B^1\Sigma_u^+(v = 3,J)$ rotational state and on light intensity up to 10^{12} W/cm^2. There are two possible lowest order pathways which both may contribute to this peak, either 6-photon ionization of H_2 from $B^1\Sigma_u^+(v = 3,J)$ or 3-photon dissociation of H_2 to H(1s) + H(2l) with subsequent 3-photon photoionization of the excited dissociation product H(2l). Both processes result in ions with similar kinetic energies which we cannot resolve with the presently poor energy resolution of our experimental setup.

[1] K. Codling and L. J. Frasinski, J. Phys. B 26, 783 (1993)
[2] A. Giusti Suzor, F. H. Mies, L. F. DiMauro, E. Charron, and B. Yang, J. Phys. B, 28 (1995)
[3] A. Zavriyev, P. H. Bucksbaum, H. G. Muller, and D. W. Schumacher, Phys. Rev. A 42, 5500 (1990)
[4] B. Yang, M. Saeed, L. F. DiMauro, A. Zavriyev, and P. H. Bucksbaum, Phys. Rev. A 44, R1458 (1991)
[5] B. Yang and L. F. DiMauro, Laser Physics 3, 398 (1993)
[6] A. Zavriyev, P. H. Bucksbaum, J. Squier, and F. Saline, Phys. Rev. Lett. 70, 1077 (1993)
[7] H. Rottke, J. Ludwig, and W. Sandner, Phys. Rev. A, 54, 2224 (1996)
[8] J. Ludwig, H. Rottke, and W. Sandner, Phys. Rev. A, submitted
[9] J. H. Posthumus, L. J. Frasinski, A. J. Giles, and K. Codling, J. Phys. B 28, L349 (1995); T. Seideman, M. Yu. Ivanov, and P. B. Corkum, Phys. Rev. Lett. 75, 2819 (1995); T. Zuo and A. D. Bandrauk, Phys. Rev. A 52, R2511 (1995)

Saturday, March 22, 1997

Wakefields

SaA 8:30am – 10:15am
Zia A

Henry Kapteyn, *Presider*
University of Michigan

Time and space resolved density development of a laser-produced plasma waveguide

T. R. Clark, S. P. Nikitin, and H. M. Milchberg
Institute for Physical Science and Technology
University of Maryland, College Park, MD 20742
Tele: (301) 405 - 4869
Fax: (301) 314 - 9363
tclark@delphi.umd.edu
milch@ipst.umd.edu

The recently developed plasma waveguide has achieved one of the major goals in intense laser-matter interaction physics, that of a large intensity - interaction length product.[1] Applications such as highly nonperturbative nonlinear optics and high harmonics generation[2], soft x-ray laser development[3], and laser-driven electron accelerators[4] would benefit from a large laser-plasma interaction length. Important to all these applications is knowledge of the time and space dependent electron density profile forming the waveguide. We present interferometer measurements of the density development of a laser produced plasma waveguide during its initial formation as well as its later evolution during which a second pulse has been guided over many Rayleigh lengths.

The time and space-resolved density profiles of this experiment are determined using a folded wave interferometer in a pump-probe configuration. The pump pulse (1.064μm, 100ps width, up to 500mJ) from a Nd:YAG regenerative/power amplifier system generates the plasma waveguide at the ~1 cm long focus of a 35° base angle axicon, with intensities of ~5 x 10^{13} W/cm^2. A synchronous probe pulse (0.532μm, 70ps width, ~100μJ, ~1cm diameter) with an adjustable delay (-1 to 11ns) is directed transversely through the plasma waveguide. The probe beam picks up a phase shift as a function of vertical position in the plasma, whose overall diameter is no greater than ~200μm for the delays used here. Most of the probe beam is not phase shifted and can be used as a phase reference in the interferometer, which consists of an optical quality BK7 glass wedge, a matched two lens imaging system, and a microscope objective producing a net magnification of 23X.

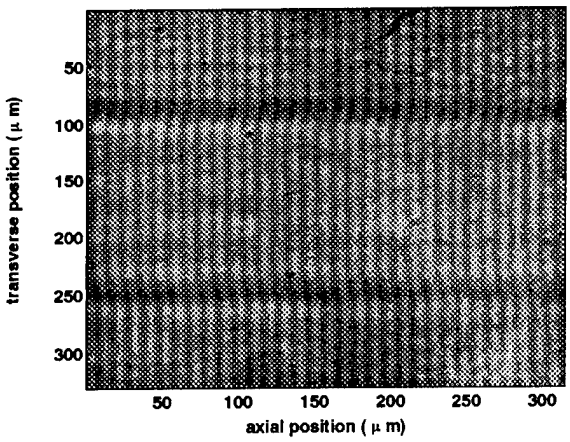

Figure 1: Interferogram data using 532 nm probe at a delay of 5 ns showing the central 300 μm of a waveguide formed in a 230/20 torr Ar/N_2O gas mixture.

The high degree of axial and radial symmetry of the waveguides produced is evident in the sample interferogram of figure 1. The top and bottom regions of the image show the portions of the probe without phase disturbance

by the plasma, with a fringe pattern due to the wedge alone. The phase shift imposed

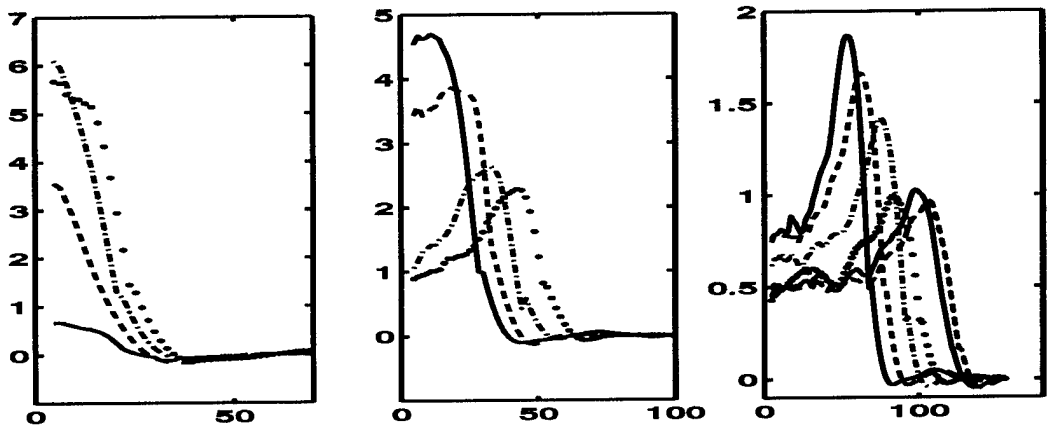

Figure 2: Density (10^{19} cm^{-3}) vs. Radius (μm): Electron density profiles obtained from Abel inverting phase data for 230/20 torr Ar/N_2O gas mixture. (a) - t=-80 s, -- t=-10 ps, -· t=50 ps, ·· t=180 ps (b) - t=0.3 ns, -- t=0.5 ns, -· t=1.2 ns, ·· t=2.0 ns (c) - t=3.2 ns, -- t=4.0 ns, -· t=5.7 ns, ·· t=8.1 ns, - t=9.7 ns, -- t=11.0 ns.

as a function of vertical distance x in the plasma is given by $\Phi(x) = k_0 \int_{s_1(x)}^{s_2(x)} n(s,x)ds$

where $k_0=2\pi/\lambda$ is the vacuum wavenumber of the probe, $s_1(x)$ and $s_2(x)$ are the plasma entrance and exit positions of the horizontal chord through x, and $n^2 = 1 - \frac{\omega_p^2}{\omega^2}$ gives the index of refraction n, where ω_p is the plasma frequency, and ω is the probe frequency. The phase is extracted from the interferograms using fast fourier transform techniques.[5] Obtaining the electron density is then reduced to the well known Abel problem for a cylindrically symmetric object from which chordally integrated information is known.[6] Figure 2 shows the electron density development for a plasma produced in a background gas mixture of 230 torr Ar and 20 torr N_2O. The experimental uncertainty is due mostly to the calibration of the magnification of our lens system and is measured to be ~4%. The data confirms the general features of channel formation predicted by our calculations and suggested by our guiding experiments.[17] Figure 2a shows a peak density $N_e \approx 6 \times 10^{19}$ cm^{-3}, corresponding to an average argon ionization level of $Z \approx 6$ estimated from the measured fill pressure. The appearance of this level of ionization in Ar, and also $Z \approx 5$-6 in N_2O plasma is consistent with our observed strong spectroscopic appearance of the O^{5+} 3d-2p 173Å line. The onset of shock development and the on-axis electron density minimum is seen in figure 2b. Note the density minimum develops within approximately 1 ns, consistent with earlier experiments showing leaky guiding at this delay.[7] The sequence in figure 3c shows the slowing of the expansion and flattening of the central density.

Measurements of the shock position vs. time have shown that after an initial rapid expansion and cooling period (T_e dropping from ~100 eV to ~20 eV within ~400

ps), the shock expands with an $\sim t^{1/2}$ dependence in good agreement with the expression for self-similar expansion of a cylindrical blast wave[8], where expansion is due to pressure work alone. The initial thermal energy per unit length driving this phase of the expansion is measured to be around 1% of pump energy for various initial conditions, which is significantly lower than would be expected from our measured pump absorption fractions of ~10 - 15%. This indicates a rapid cooling has already taken place at earlier times, within a few hundred picoseconds of the pump pulse.

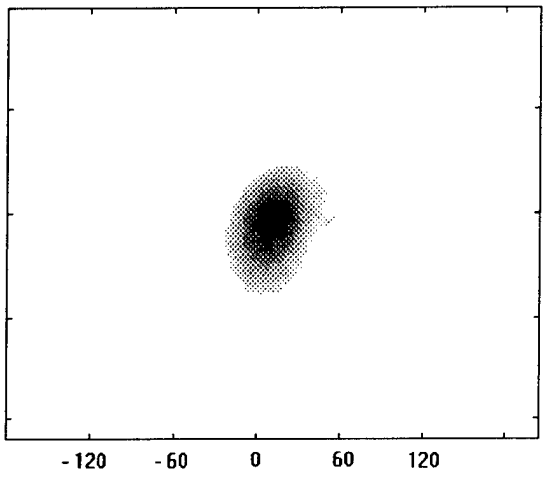

Figure 3: Output mode of an 80 fs pulse from a CPA Ti:Sapphire laser system guided by a plasma waveguide formed in 100 torr N_2O. The spot size is measured to be 50μm FWHM.

A sub-100 fs CPA Ti:Sapphire laser system has recently been synchronized with the plasma waveguide producing Nd:YAG laser system described above. Figure 3 shows the output mode of a guided 80 fs pulse imaged onto a CCD camera. Plasma density profiles of the end of the waveguide have also been measured using interferometry methods. These measurements are of importance to the actual coupling of a pulse to the waveguide.

The results presented here demonstrate the ability of a single shot interferometer to extract high resolution density profiles for the relatively smaller phase shifts of gas target laser plasmas. They verify many of the previously assumed or inferred parameters of the plasma waveguide, including the channel formation dynamics and evolution, the approximate ionization level, the uniformity along the axis, and the electron density structure near the input/output coupling region at the end of the waveguide.

---

[1] H. M. Milchberg, T. R. Clark, C. G. Durfee III, and T. M. Antonsen, Phys. Plasmas **3**, 2149 (1996).
[2] J. Krause, K. Schafer and K. Kulander, Phys. Rev. Lett. **68**, 3535 (1992); H. M. Milchberg, C. G. Durfee III, and T. J. McIlrath, Phys. Rev. Lett. **75**, 2494 (1995).
[3] H. M. Milchberg, C. G. Durfee III, and J. Lynch, J. Opt. Soc. Am. B **12**, 731 (1995).
[4] T. Tajima and J. M. Dawson, Phys. Rev. Lett. **43**, 267 (1979); P. Sprangle, E. Esarey, A. Ting, and G. Joyce, Appl. Phys. Lett. **53**, 2146 (1988).
[5] M. Takeda, H. Ina, S. Kobayashi, J. Opt. Soc. Am. B **72**, 156 (1981).
[6] I. H. Hutchinson, *Principles of plasma diagnostics* (Cambridge University Press, Cambridge, 1987).
[7] C. G. Durfee III, J. Lynch, and H. M. Milchberg, Opt. Lett. **19**, 1937 (1994).
[8] Y. A. Zeldovich and Y. P. Raizer, *Physics of Shock Waves and High-Temperature Hydrodynamic Phenomena*, (Academic Press, New York, 1966).

Relativistically Self-Guided Laser-Wakefield Acceleration

R. Wagner, S.-Y. Chen, A. Maksimchuk, D. Umstadter
Center for Ultrafast Optical Science,
University of Michigan, Ann Arbor, MI 48109
(313) 764-2284, (313) 763-4876 (fax), dpu@umich.edu

Due to recent advances in laser technology, there is much current interest in the interactions of high-intensity and ultrashort-duration laser pulses with plasmas. Applications include advanced fusion energy, x-ray lasers, and ultrahigh-gradient electron accelerators. In the latter case, the field gradient of a laser-driven plasma wave has recently been demonstrated to exceed that of an RF linac by four orders-of-magnitude ($E \geq 200$ GV/m) and has been used to accelerate electrons with over 1-nC of charge per bunch in a low-emittance beam (1 mm-mrad) [1]. However, in the absense of some form of light guiding, the acceleration distance is limited by diffraction to the Rayleigh range. We report experimental results that demonstrate for the first time that relativistic self-guiding can significantly extend the distance over which electrons can be accelerated by a laser wakefield.

When a laser propagates through a plasma, the index of refraction, $n = (1-\omega_p^2/\omega_o^2)^{1/2}$, depends on the laser frequency, ω_o, and the plasma frequency, ω_p. For low laser power, the index is essentially constant; however, for higher laser power, the index varies with the radius, since the laser intensity varies with radius and the plasma frequency changes with the relativistic mass factor. The plasma can then act as a positive lens, relativistically self-focusing and, under certain conditions, guiding the laser pulse. This effect has been shown to have a power threshold given by $P_c = 16.5(\omega_o^2/\omega_p^2)$ [GW]. These transverse effects can also lead to focusing and defocusing of different sections of the laser pulse [2], temporally modulating the laser pulse and driving an electrostatic wakefield that propagates with the laser pulse at at nearly the speed of light, which can trap and accelerate hot electrons.

In our experiment, laser-wakefield acceleration of a space-charge-limited low-emittance beam of MeV electrons (1 nC charge), and self-modulation of the laser light are both observed to appear at P_c, the critical power threshold [1]. A similar correlation was found in the 1960's between the onset of conventional molecular Raman scattering and the threshold for self-focusing due to the nonlinear atomic susceptibility. Furthermore, sidescattering indicates that the laser was guided by a relativistically self-focused channel, which extended a distance equal to four times the Rayleigh range (limited only by the length of the gas jet). Self-guiding was correlated with higher electron energy and lower electron beam emittance.

In this experiment, we utilized a hybrid Ti:sapphire-Nd:glass laser system based on chirped-pulse-amplification that produces 3 J, 400 fs pulses at 1.053 μm. The 43 mm diameter beam was focused with an f/4 off-axis parabolic mirror to $r_o = 8.5$ μm ($1/e^2$), corresponding to vacuum intensities exceeding 4×10^{18} W/cm^2. This pulse was focused onto a supersonic helium gas jet with a sharp gradient (250 μm) and a long flat-topped interaction region (750 μm). The maximum density varies linearly with backing pressure up to the maximum backing pressure of 1000 PSI, and an underdense plasma at 3.6×10^{19} cm^{-3} is formed by the foot of the laser pulse tunnel-ionizing the gas. This plasma density corresponds to a critical power of $P_c = 470$ GW. The sharp gradient and long interaction region are found to be essential for producing an electron beam and for self-guiding to occur.

The existence of a large amplitude plasma wave was inferred by observing a highly modulated forward Raman scattered spectrum with up to the 4th anti-Stokes side-band visible [1]. The onset of the Raman scattering occurred at $0.5P_c$ [1] which is consistent with theoretical onset of 3D Raman scattering [2]. The absolute plasma wave amplitude was measured using a collinear collective Thomson scattering probe that was split off from the main pulse after the compressor stage. This

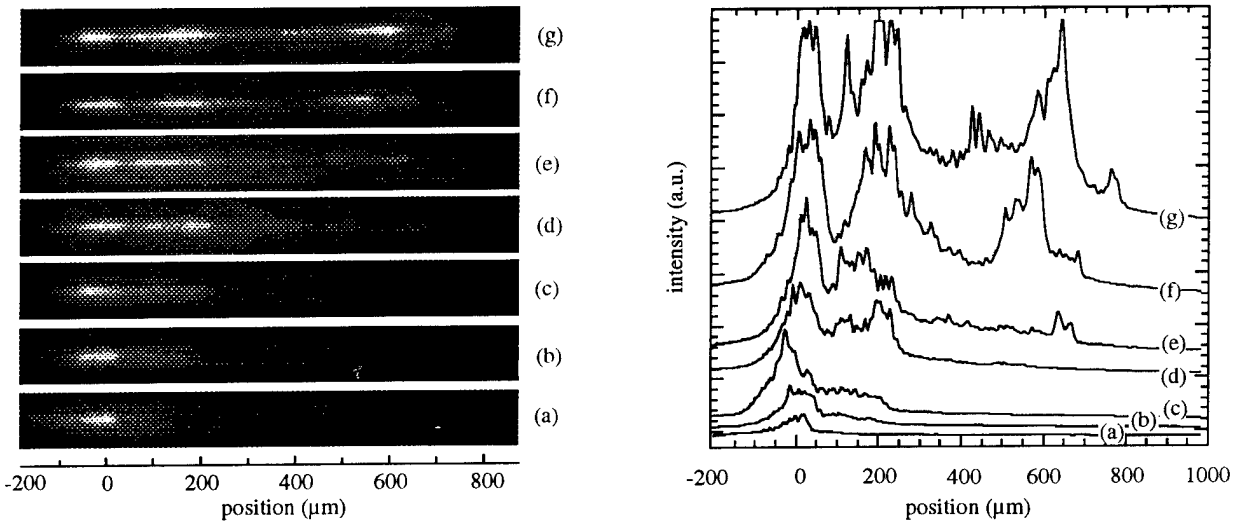

Figure 1: On-axis images (left) and corresponding lineouts (right) of sidescattered light at various laser powers and a fixed initial electron density of 3.6×10^{19} cm^{-3}. The various images and lineouts represent laser powers of P/P_c = (a) 1.6, (b) 2.6, (c) 3.9, (d) 5.5, (e) 7.2, (f) 8.4, and (g) 9.1. Note: the curves have been displaced vertically for ease of viewing.

pulse was frequency-doubled by a type I KDP crystal and then recombined with the main pulse. By measuring the spectrum of the scattered probe light, we found [3] that the plasma wave lasts for approximately 1.5 ps (FWHM), and the spatial averaged peak plasma wave amplitude varies from $\delta n_e/n_e = 0.1 - 0.4$ at laser powers of 2-3 TW.

In order to diagnose the spatial extent of the plasma, a sidescattering imaging system consisting of relay optics, various filters, and a 12-bit CCD with a spatial resolution of 15 μm was utilized. We were able to resolve the growth of the plasma channel as a function of both laser power and plasma density. Fig. 1 shows the sidescattered intensity distribution as a function of laser power, and the plasma channel clearly extends as the laser power increases. In the lower power cases ($< 2.6P_c$), the channel length is only $\sim$ 125 μm, which is smaller than the confocal parameter ($2Z_R$) of 430 μm. As the laser power increases for a fixed gas density, the channel length first jumps to 250 μm at $3.9P_c$ and then reaches 750 μm at $7.2P_c$. The maximum channel length was observed to be 850 μm at $9.1P_c$. Note this is limited by the interaction length of the gas jet. At $5.5P_c$, the sidescattered image formed has two distinct foci, and when the power exceeds $7.2P_c$, multiple foci or a channel are observed, depending on shot-to-shot fluctuations and the gas jet position. A similar channel extension occurs if the gas density is varied at fixed laser power. For a 3.9 TW laser pulse, the channel extends to 250 μm at 400 PSI backing pressure (1.4×10^{19} cm^{-3}, $3.2P_c$) and 750 μm at 800 PSI (2.9×10^{19} cm^{-3}, $7.0P_c$). The consistent behavior at specific values of P_c for varying laser power or plasma density indicates that the channeling mechanism is relativistic self-focusing.

The total number of accelerated electrons was measured using both a Faraday cup and a plastic scintillator coupled to a photomultiplier tube, and the results were found to be consistent with each other. There is a sharp threshold for electron production at $\sim 1.5P_c$, and the total number of electrons increases exponentially and finally saturates beyond $4P_c$ [1]. At $6P_c$, 6×10^9 accelerated electrons were measured coming out of the plasma in a beam. The electron energy spectrum (see Fig. 2) was measured using a 60° sector dipole magnet by imaging a LANEX scintillating screen with a CCD camera. By using aluminum absorbers, we determined that 50% of the electrons

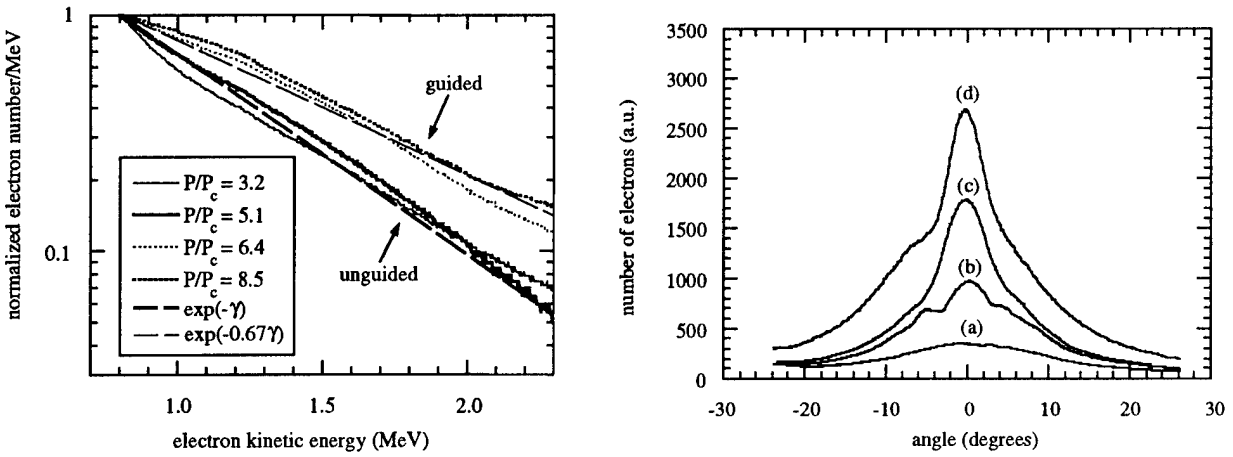

Figure 2: Normalized electron kinetic energy spectrum as a function of laser power at fixed electron density. (left) Electron beam divergence as a function of laser power. (right)

detected have energy greater than 1 MeV which corresponds to 0.5 mJ of energy being transferred to the electron beam. The normalized distribution is found to have a functional form of $\exp(-\alpha\gamma)$ where α is a fitting parameter. In the low power case ($< 6P_c$, no channeling), the normalized distribution follows $\exp(-\gamma)$, and when the laser power increases ($> 6P_c$, with channeling), the electron energy distribution discretely jumps to follow $\exp(-0.67\gamma)$. Even though the plasma wave amplitude increases as the laser power increases, the distribution only dramatically changes when self-guiding occurs.

The electron beam profile was measured using a LANEX scintillating screen imaged by a CCD camera [1]. The LANEX is placed behind an aluminum sheet which blocks the laser light, so only electrons greater than 100 keV can be imaged. Analysis of the electron spectrum indicates that the bulk of the electrons that create an image on the screen are in the 100 keV to 3 MeV range. We have found, using aluminum absorbers, that the electron divergence does not depend on electron energy in this range. At low power ($< 5P_c$), the electron beam has a Gaussian-like profile with a 10° radius at half-maximum (see Fig. 2). As the laser power increases and the plasma channel length increases to ~ 250 μm , a second peak seems to grow out of the low-power profile. Ultimately at the highest laser powers and longest channel lengths, the divergence decreases to 5°, and the profile becomes more Lorentzian-like. The electron beam divergence should decrease as the energy of the electrons increase since space charge will be less and the relative transverse momentum decreases due to the longer accelerating length.

References

[1] D. Umstadter, S.-Y. Chen, A. Maksimchuk, G. Mourou, and R. Wagner, Science **273**, 472 (1996).

[2] P. Sprangle *et al.*, Phys. Rev. Lett. **69**, 2200 (1992); T. M. Antonsen and P. Mora, Phys. Rev. Lett. **69**, 2204 (1992); N. E. Andreev *et al.*, JETP Lett., **55**, 571 (1992).

[3] S. P. Le Blanc, M. C. Downer, R. Wagner, S.-Y. Chen, A. Maksimchuk, G. Mourou and D. Umstadter, Phys. Rev. Lett. (to be published, 1996).

Temporal characterization of plasma wakefields driven by intense femtosecond laser pulses

S. P. Le Blanc, M. C. Downer, T. Tajima
Department of Physics, The University of Texas at Austin, Austin, Tx 78712
email: spl@physics.utexas.edu, phone: 512-471-7251, fax: 512-471-9637

C. W. Siders
Los Alamos National Laboratory

R. Wagner, S.-Y. Chen, A. Maksimchuk, G. Mourou, D. Umstadter
Center for Ultrafast Optical Science, University of Michigan, Ann Arbor, MI 48109

Because electrostatic fields in a plasma wave ($E \geq 100$ GV/m) can exceed by three orders of magnitude those in conventional RF linacs, plasma based accelerators can potentially offer a compact method for accelerating high energy electrons. Of the several methods for driving large amplitude plasma waves, the laser wakefield accelerator (LWFA) and its variant, the self-modulated LWFA, have recently received considerable attention because of the reduction in size of the terawatt class laser systems needed to drive the wakefield [1]. In this paper, we demonstrate all optical techniques based on frequency domain interferometry [2] and forward, collective Thomson scattering [3] for temporal characterization of the plasma wakefield. The ability to measure the plasma wake temporal structure is of fundamental importance for a number of issues, including: wakefield generation by optimized pulse trains, the design of particle injectors synchronized to the wakefield on a femtosecond time scale, and the growth dynamics of plasma wave instabilities.

In the standard LWFA, the amplitude $\alpha = \delta n_e/n_e$ of the plasma wave can be resonantly excited by the ponderomotive force of an intense laser pulse if the laser pulse duration is approximately half of the plasma wave period $\tau_p = 2\pi/\omega_p$, where $\omega_p = \sqrt{4\pi e^2 n_e/m_e}$ is the electron plasma frequency and n_e is the plasma density. To diagnose the resonantly driven wakefield by frequency domain interferometry, a Ti:Sapphire laser system based on chirped pulse amplification and capable of delivering 20 mJ, 100 fs, laser pulses at 30 Hz and $\lambda = 0.8\mu$m was used to generate orthogonally polarized pump and probe pulses for the experiment. Probe pulses produced from a Michelson interferometer propagated in front of and behind the pump pulse and the delay of the pump pulse was varied relative to the two probe pulses. The probe pulse sequence produces a frequency domain interferogram whose phase shifts, relative to a reference frequency domain interferogram, due to the plasma wakefield oscillations. For a peak pump pulse intensity of 2×10^{17} W/cm^2 in 4.8 (2.7) Torr helium, Fig. 1 shows the measured phase shifts extracted from the interferograms oscillating with a period of $220 \pm 25 fs$ ($270 \pm 10 fs$) and an amplitude of 0.007 rad (0.005 rad). Under these conditions, we detect wakefield oscillations 3-5 (4-5) cycles behind the pump pulse. From the amplitude of the phase modulation in Fig. 1, we determine that the amplitude of the wakefield oscillation is at least $\alpha = 0.8$. The peak longitudinal electric field is estimated as ~ 10 GV/m.

To help explain the details of the experimental results, numerical simulations were performed with a two-dimensional, fully relativistic, cold fluid model. In this model, a Gaussian shaped laser pulse propagates through a preformed plasma where the plasma wavelength λ_p is approximately equal to the Rayleigh range of the focused laser pulse. The simulations indicate the excitation of nonlinear plasma waves near the focus with significant density peaking and a peak $\delta n_e/n_e \sim 5$. This amplitude is much larger than a simple one dimensional estimation of the laser plasma interaction due to the fact that the radial component of the ponderomotive force is order ten times larger than the axial component. The simulations also confirm the existence of wakefield oscillations for at least five cycles after the pump pulse.

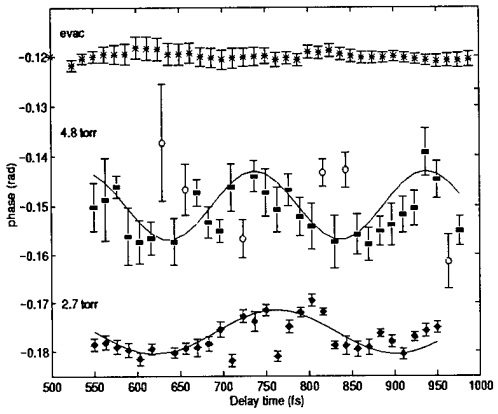

Fig. 1. Measured wakefield oscillations in helium. For the 4.8 Torr data, the two probe pulses are separated by 2.2 ps about the pump, while in the 2.7 Torr data (offset from zero and shifted by -400 fs) the probes trail the pump with 415 fs separation. For the 4.8 (2.7) Torr data, 10 (9) mJ of energy was focused with an e^{-1} radius of 3.6 (5.0) μm. The solid lines show the calculated phase shift due to the wakefield oscillations, while the top line of data shows the noise level for a scan in an evacuated chamber.

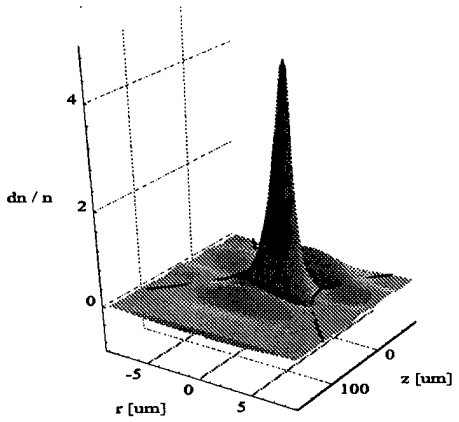

Fig. 2. Two dimensional (r, z) numerical simulation of wakefield oscillations $\delta n_e/n_e$ corresponding to $E = 10$ mJ, 3.6μm spot radius, $\tau = 100$ fs, $n_e = 3 \times 10^{17}\text{cm}^{-3}$. The figure shows the electron density oscillations within the confocal parameter of the tightly focused beam and in the moving frame of the pump pulse (centered at $z = 111\mu$m and moving in the positive z direction, but not shown). The heavy line represents the e^{-1} contour of the laser focus.

For the self-modulated LWFA, the plasma density is chosen to be much larger than for the standard LWFA so that the forward Raman scattering (FRS) instability can grow. Since the maximum longitudinal electric field E scales as $E \propto \alpha\sqrt{n_e}$, the self-modulated wakefield can produce a much larger accelerating field than the standard LWFA. In a separate set of experiments experiments, a hybrid Ti:Sapphire - Nd:Glass laser system capable of delivering 3 J, 400 fs laser pulses was used to drive the self modulated LWFA. The laser was focused onto a supersonic helium gas jet whose neutral density varied linearly with backing pressure. To probe the lifetime of the plasma wave, a small portion (20%) of the infrared laser pulse was split off, frequency doubled in a 4 mm Type I KDP crystal, and then made to co-propagate with the infrared pump pulse. Forward scattered light from the probe pulse was collected on axis, passed through a polarizer to suppress scattered pump light, and measured with a prism spectrometer. When the peak power of the IR pump pulse (P $\geq$ 1 TW) is near the critical power for relativistic self-focusing $P_c = 17(\omega_o^2/\omega_p^2)$ GW, the forward scattered light from the pump pulse shows the appearance of three anti-Stokes Raman shifted side bands separated by the plasma frequency ($\omega_p \sim 3\times 10^{14}$ s^{-1}). Under these conditions(I $\sim 10^{18}$ W/cm^2), a collimated beam of 2 MeV electrons with a transverse emittance of 1 mm mrad is emitted in the laser propagation direction [4].

When the green probe pulse propagates through the plasma, collective Thomson scattering from the relativistic plasma wave causes multiple side bands to appear in the spectrum of the forward scattered probe light. For P = 3 TW and a backing pressure of 100 psi, Fig. 2a shows the appearance of first and second order Thomson scattered satellites which are separated by the plasma frequency $\omega_p = 2.7 \times 10^{14}$ s^{-1}. The amplitude of the plasma wave determined from both the absolute ($\alpha = 0.08$) and relative scattering efficiency ($\alpha = 0.1$) of the first order Thomson side bands are in reasonable agreement. From the second order satellites, the amplitude of the second

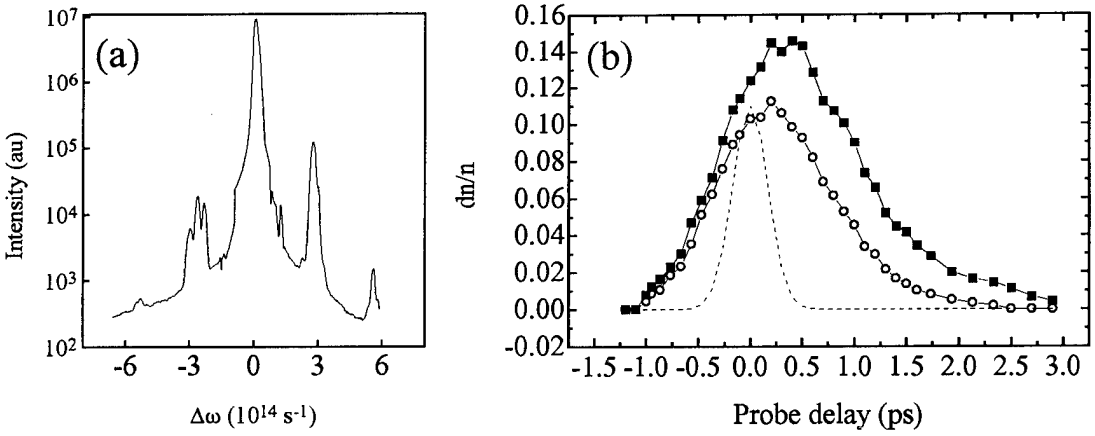

Figure 1: a) Spectrum of the Thomson scattered probe light for a helium backing pressure of 100 psi, P_{pump}= 3 TW, and Δt=0. b) Amplitude of the plasma wave determined from the scattering efficiency of the Stokes (filled squares) and anti-Stokes (open circles) satellites as a function of delay for a helium backing pressure of 180 psi. The dotted line indicates the 1.5 TW, 400 fs pump pulse.

harmonic of the plasma wave is $\delta n_2/n$=0.01.

By measuring Thomson scattering from the probe pulse as a function of the delay between the pump and probe, the temporal envelope of the wakefield oscillations can be recorded. Fig. 2b shows the plasma wave amplitude as function of the probe delay time for a helium backing pressure of 180 psi. The plasma wave is measured to have a peak amplitude $\alpha = 0.1$, which corresponds to a maximum longitudinal field of $E = 56$ GV/m for a cold, nonrelativistic fluid. Under the current tight focusing conditions, the maximum radial electric field is $E_r = 2E_z/k_p r_o = 0.2E_z$. Fig. 2b shows that the wakefield amplitude maximizes at the end of the pump pulse ($\Delta t = 300 \pm 100 fs$) and lasts for approximately 2 ps longer. Note that the probe pulse duration ($\sim$ 300 fs) is much longer than the plasma period (τ_p=21 fs for $n_e = 3 \times 10^{19}$ cm^{-3}) in the present experiment. Therefore, we do not resolve individual wakefield oscillations as was the case with the previous experiments using frequency domain interferometry [2].

The measured exponential rise time (4.0 ps^{-1}) of the self-modulated wakefield is in agreement with that expected from the growth of the FRS instability. The onset of FRS is coincident the development of an ionization-induced blueshifted spectral wing on the probe pulse, suggesting that the FRS is seeded by a ionization front noise source [5]. The decay of the wakefield is caused by the conversion of collective plasma wave energy into particle energy. Since the total energy of the accelerated electron beam is approximately equal to the energy in the plasma wave, the measured exponential decay of the wakefield (1.9 ps^{-1}) is consistent with nonlinear Landau damping of trapped electrons or beam loading of the plasma wave.

References

1. For a recent review see E. Esarey *et al.*, IEEE. Trans. on Plasma Sci. **24**, 252 (1996).
2. C. W. Siders *et al.*, Phys. Rev. Lett. **76**, 3570 (1996); J. R. Marques *et al.*, ibid., 3566 (1996).
3. S. P. LeBlanc *et al.*, submitted to Phys. Rev. Lett. ; C. I. Moore *et al.*, Bull. Am. Phys. Soc. **40**, 1797 (1995).
4. D. Umstadter *et al.*, Science **273**, 472 (1996).
5. C. D. Decker *et al.*, Phys. Plasmas **3**, 1360 (1996).

Research in Laser Acceleration at LLNL

C.A. Back[1], H.A. Baldis[1], T.E. Cowan[1]*, R.R. Freeman[1], A. Friedman[1], D.P. Grote[1], C.A. Hagmann[1], F. Hartemann[2], J.P. Heritage[2], C.J. Jackson[2], A.K. Kerman[4], B. Kolner[2], W.L. Kruer[1], A.B. Langdon[1], G. Le Sage[2,3], N.C. Luhmann[1], M.J. Mugge[1], M.D. Perry[1], T.W. Phillips[1], W.M. Sharp[1], A.L. Troha[2], K. van Bibber[1], W.E. White[1], S.C. Wilks[1], J.G. Woodworth[1]

Laser acceleration holds out the prospect of very high gradient machines. High energy physics will ultimately need such a technological leap to keep energy-frontier research ($E >> 1$ TeV) within the realm of practicality. Compact high-brightness GeV-sources would have broad applicability in science, industry and defense. Both vacuum- and plasma-based concepts for laser acceleration promise gradients of $G > 1$ GeV/meter, which has already been borne out experimentally in the latter case. However, there is no idea at present how to build a real accelerator based on any such scheme (i.e. a design which is stageable to high energies, producing a monochromatic, high current, low-emittance beam).

An effort has begun at Lawrence Livermore National Laboratory to examine the issues of practical laser-driven acceleration of electrons. Initially the program will emphasize basic science, but evolve towards identification and development of one or more concepts most promising with regards to scalability, and result in systems studies and key demonstrations. Discussed briefly below are our plans for initial experiments, and the advanced accelerator facility to be built up at the LLNL electron linac.

Experiments in 1997 will be carried out at the Ultra-Short Pulse (USP) laser facility on laser-electron interactions in a vacuum. These include non-linear Compton scattering and ponderomotive acceleration, utilizing the USP laser and free-space electrons from a low-energy gun (~20 keV). The Compton scattering experiment should observe the fragmentation of the Compton scattering peak into a spectrum (or broad envelope) as the laser strength parameter, a_0 is increased. The heart of the USP facility is a 10 TW Ti:Sapphire laser (>1J, 100 fs) with a well-characterized Gaussian beam. Also planned are the first survey experiments of energetic electron production from gas jet and solid targets using the recently commissioned 1.25 PW laser (600J, 400 fs). Measurements of the electron spectrum in the forward direction could see electrons in the several hundred MeV range.

In the longer term, we will establish a test-bed for laser acceleration at the existing 100 MeV electron linac on site. Presently under construction are both an X-band RF photocathode gun (8.56 GHz) for the linac injector (UC Davis), and a glass-pumped 100 TW Ti:Sapphire laser (5J, 50 fs). The experimental program will be oriented towards measurements of channel formation, optical propagation and acceleration in plasma channels, as well as testing of free-wave concepts. There will be an active theory and modeling effort in parallel with the experimental activities. A specific intent in setting up the facility is to create the opportunities for collaborative work with other laboratories and universities in laser acceleration.

1. *Lawrence Livermore National Laboratory, Livermore, CA 94550*
2. *University of California, Davis, CA 95616*
3. *University of California, Los Angeles, CA 90024*
4. *Massachusetts Institute of Technology, Cambridge, MA 02139*
* Telephone: 510-422-9678

Lasers I

SaB 10:45am – 12:15pm
Zia A

Catherine LeBlanc, *Presider*
ENSTA, France

Ultrahigh Peak Power Lasers in the 10-fs Regime

C. P. J. Barty (a), T. Guo (b), C. LeBlanc (d), F. Raksi (b),C. Rose-Petruck (b), J. Squier (c), B. Walker (b),K. R. Wilson (b), V. V. Yakovlev (b), K. Yamakawa (e)

(a) Institute for Nonlinear Science, (b) Department of Chemistry and Biochemistry, (c) Department of Electrical and Computer Engineering, University of California, San Diego,Urey Hall Addition 3050 G, La Jolla, CA 92093-0339 Phone: (619)-534-2417 Fax: (619)-534-7654

(d) ENSTA-LOA,Batterie de l'Yvette, 91120 Palaisea, France

(e) Japan Atomic Energy Research Institute,Tokai-mura, Naka-gun, Ibaraki 319-11, Japan

We review the evolution of chirped pulse amplification into the 10-fs regime. This evolution has been made possible by the advent of ultrabroadband amplification media such as Ti:sapphire, the development of sub-10-fs laser Kerr-lens-modelocked oscillators [1, 2] to provide stable and reliable seed pulses for amplification and the implementation of new technologies and strategies to minimize or circumvent gain narrowing and higher order phase distortions during amplification. As an example, a three stage, multi-output, laser system, at the University of California at San Diego will be described. This system is designed to produce > 1-J pulses of ~15-fs duration at a 10-Hz repetition. After two stages of amplification, 18-fs, 4-TW pulses have been produced at a repetition rate of 50 Hz and an average power > 4 W.[3] To our knowledge, these are the shortest duration terawatt pulses yet produced by a chirped pulse amplification system. Pulses at this level have been used at UCSD to produce ultrafast x-rays (both broadband and K_α radiation) for use in ultrafast diffraction studies of molecular dissociation, ultrafast near edge absorption studies of molecular dynamics, and time-gated x-ray mammography and angiography. Full system amplification at a 10 Hz repetition rate to energies of approximately 2 J before compression has also been demonstrated and transform limited pulses of ~20 fs have been measured. These pulses will be used for investigations of high field phenomena in the highly relativistic regime (i.e. at intensities > 10^{20} W/cm^2), charged particle acceleration relevant to laser driven nuclear fusion and hard x-ray lasers. Further optimization of both intermediate and full level amplified outputs which to date have been limited to amplified bandwidths of ~ 70 nm is currently underway and should result in compressed pulse durations of <15-fs and peak powers of > 70 TW.

Efficiency and fidelity in ultrashort pulse, chirped pulse amplification are limited primarily by two concerns: 1) control of higher order phase distortion and 2) gain narrowing during amplification. We have addressed these problems with an optimized, quintic-phase-limited expander and compressor[4] design and with regenerative pulse shaping[5].

Our present expansion and compression system utilizes a cylindrical mirror based pulse expander. This expander is capable of introducing high order phase distortions on the amplified pulse which exactly cancel the 2nd, 3rd and 4th order phase distortions introduced by over a meter of dispersive material in the amplification chain and by the pulse compressor. As a result, the entire system is capable of expanding a 100-nm bandwidth seed pulse by >100,000 times and recompressing it with less than 1 fs of pulse delay across the entire bandwidth. In typical operation, a 9 fs seed pulse is stretched to ~950 ps before amplification. To our knowledge this expansion ratio is the largest used in any CPA system. By stretching to 950 ps, we are able to operate the amplifiers at nearly 4 times the saturation fluence of Ti:sapphire without encountering intensity dependent damage of the dielectric coatings in

the amplification chain. As a result, it is possible to reach record levels of efficiency with respect to extraction of the stored energy in our amplifiers, nearly 50% of absorbed pump light can be converted into 800 nm radiation or >90% of the theoretical limit. Presently new expander designs are being developed which either increase the bandwidth over which phase compensation is possible, simplify construction and/or increase efficiency.

Regenerative pulse shaping is used to control gain narrowing during amplification.[5] In this technique a spectral filter is placed inside of a regenerative amplifier to compensate for gain narrowing on each round trip of the cavity. In order to achieve the largest amplified bandwidth, the filter must produce a transmission which is the inverse of the single pass gain profile. For Ti:sapphire, this requires a large filter bandwidth (~100 nm) and modulation depth (>40%). Several novel filter designs have been investigated and the relative merits of each will be discussed. Using a thin film polarizer etalon at anti-resonance[6], we have produced pulses with >100 nm FWHM of amplified bandwidth, pulses of ~20 nm bandwidth but electronically tunable over the same range, and two color 10 nm FWHM amplified pulses with separations approaching 100 nm. This latter mode of operation is ideal for generation of high energy infrared radiation via difference frequency mixing or for the study of beat wave plasma interactions.

A schematic of the UCSD laser system is shown in Figure 1. Depending upon the state of a 10-Hz repetition electro-optic switch after the second stage of amplification, the output is sent either to final 2-pass amplifier which is pumped by a custom built 4-J, frequency-doubled, 10-Hz Nd:YAG laser or to a separate compressor. Both compressor chains may be operated simultaneously. Both compressors operate with the final pass under vacuum in order to avoid self phase modulated beam distortions introduced by propagation through the atmosphere or vacuum windows. It should be noted that only the final grating in each compressor is under vacuum. This greatly simplifies the construction of the vacuum arrangement while introducing small but correctable phase distortions on the compressed pulse. A full suite of diagnostics is employed in the amplification chain, including stage by stage monitoring of pulse spectrum, profile and energy. The final compressed pulse durations are measured with noncolinear single-shot second-order autocorrelation, single-shot, second-harmonic FROG, single shot STRUT and high dynamic range scanning second-order autocorrelation. The near and far field pulse profiles of the amplified pulses are measured with CCD cameras and equivalent plane imaging. In addition an ion spectrometer has been constructed to monitor the state of field induced ionization achieved for a single rare gas atom placed in the focus of the final output. From knowledge of the maximum ion state, the intensity at focus is directly calculable.

Ultrashort duration amplification in Ti:sapphire promises to open a new era of high repetition rate, ultrahigh peak power applications. The techniques and considerations described in this presentation are applicable to both higher power and higher repetition rate systems. Extensions to petawatt powers and kHz repetition rates are possible and will also be outlined.

References:

1. J. Zhou, G. Taft, C.-P. Huang, M. M. Murnane and H. C. Kapteyn, Opt. Lett., **19**, 1149-1151, 1994.

2. L. Xu, C. Spielmann, F. Krausz and R. Szipöcs, Opt. Lett., **21**, 1259-1261, 1996.

3. C. P. J. Barty, T. Guo, C. Le Blanc, F. Raksi, C. Rose-Petruck, J. Squier, K. R. Wilson, V. V. Yakovlev and K. Yamakawa, Opt. Lett., **21**, 668-670, 1996.

4. B. E. Lemoff and C. P. J. Barty, Opt. Lett., **18**, 1651-1653, 1993.

5. C. P. J. Barty, G. Korn, F. Raksi, C. Rose-Petruck, J. Squier, A.-C. Tien, K. R. Wilson, V. V. Yakovlev and K. Yamakawa, Opt. Lett., **21**, 219-221, 1996.

6. K. Yamakawa, T. Guo, G. Korn, C. Le Blanc, F. Raksi, C. G. Rose-Petruck, J. A. Squier, V. V. Yakovlev and C. P. J. Barty, in *Generation, Amplification, and Measurement of Ultrashort Laser Pulses III*, W. E. White and D. H. Reitze; ed., SPIE, 2701, 198-208, San Jose, CA, 1996.

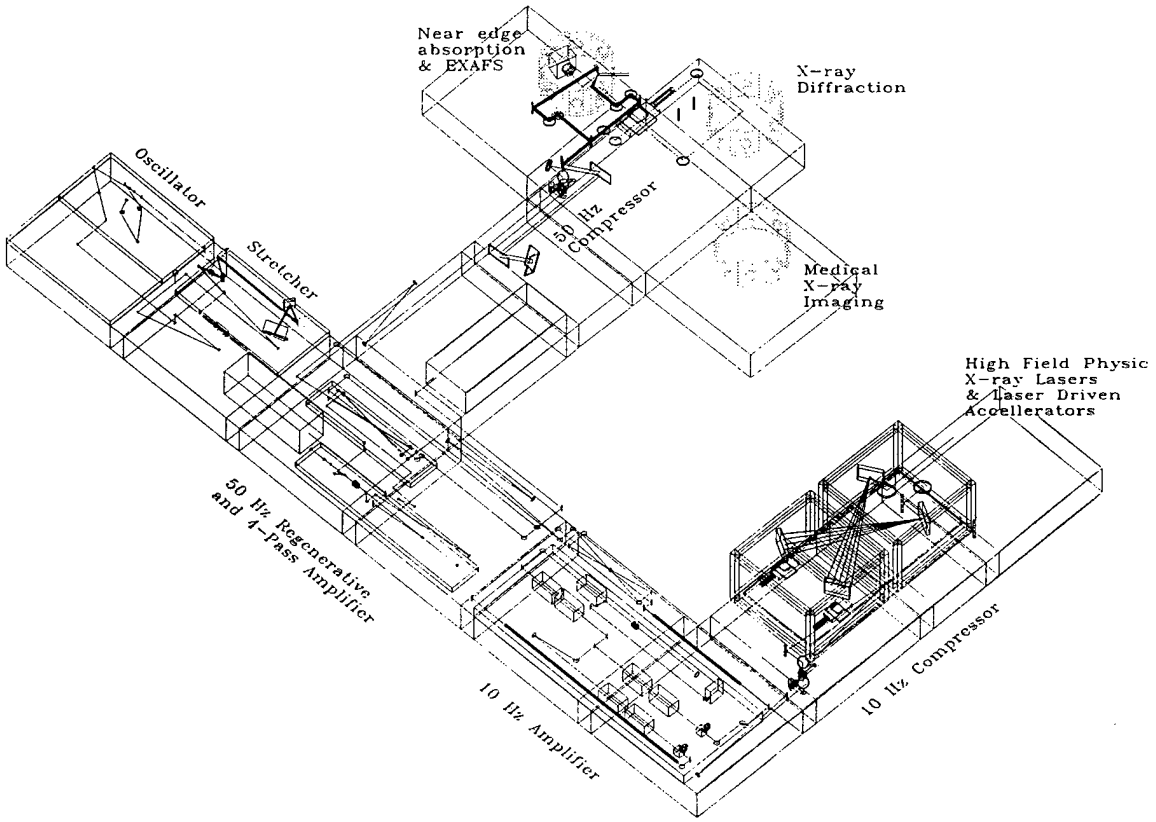

Figure 1. Schematic of the UCSD, 10-Hz and 50-Hz, multiterawatt amplification system.

Scaling of Nd:Glass pumped Ti:Sapphire Chirped Pulse Amplification (CPA) systems to 100 TW and beyond.

W. E. White, D. F. Price, J. Bonlie, F. G. Patterson, and R. E. Stewart
Lawrence Livermore National Laboratory,
P.O. Box 808, L-251, Livermore CA 94550
white24@llnl.gov

We have been working on the development of high energy, ultrashort pulse laser systems based on Chirped Pulse Amplification (CPA) in Ti:Sapphire pumped by Nd:YAG and Nd:Glass. These systems begin with the now standard "front end" consisting of a mode-locked Ti:Sapphire oscillator followed by a pulse stretcher, and a regenerative amplifier pumped by a commercially available frequency doubled Nd:YAG. The resulting mJ level pulses are then amplified to several hundred mJ in Ti:Sapphire amplifiers that are also pumped by commercially available Nd:YAG lasers. At this point the pulses can be compressed to the multi-TW level. Systems of this type have become fairly common and even commercially available. However, the pump energy needed to further amplify to energies of several Joules, or even >10 J is beyond what is currently available as a standard commercial product.

Our solution to this problem is to use frequency doubled, flashlamp pumped, Nd:Glass lasers as pump sources for large Ti:Sapphire amplifiers. Glass lasers have been used for many years and the technology needed to produce tens and even hundreds of Joules of pump energy in a smooth spatial profile is very available and well understood. For this talk, we present results of our first glass

pumped Ti:Sapphire amplifier. This system is capable of producing 100 fs pulses with energy in excess of 1J. The high spatial quality of this system is evident in the focal spot images which indicate near diffraction limited performance yielding peak intensities if $>5x10^{19}$ W/cm^2.

We will also discuss the present limitations in scaling of this type of system to higher energies. This will include a report on our progress in producing <100 fs pulses energies in excess of 10J.

This work was performed under the auspices of the U.S. Department of Energy by Lawrence Livermore National Laboratory under contract No. W-7405-Eng-48.

Amplitude and phase characterization of 10 fs pulses generated by hollow-core fiber pulse compression

Charles G. Durfee III, Sterling Backus, Henry C. Kapteyn, Margaret Murnane

Center for Ultrafast Optical Science, University of Michigan
2200 Bonisteel Blvd., 1006/IST, Ann Arbor, MI 48109-2099
phone: 313-763-0566, *email:* charlesd@eecs.umich.edu

For many nonlinear optics and high-field experiments, including high-order harmonic generation, X-ray lasers and particle acceleration, energetic pulses on the order of 10 fs and shorter would result in the observation of completely new phenomena. For example, calculations suggest that high-order harmonic generation with a 5 fs pulse would result in soft x-ray pulse with a duration on the order of 100 attoseconds. While 10 fs pulses are readily available at low energy (nJ) directly from Kerr-lens mode-locked laser oscillators, gain narrowing and high-order phase compensation have limited the pulse duration from ultra-short pulse laser amplifiers to about 20 fs. The route we are pursuing toward the goal of energetic sub-10 fs pulses is to compress amplified 20 fs pulses after self-phase modulation in a noble-gas-filled hollow-core dielectric waveguide, first used by Nisoli *et al* [1] for much longer input pulses. Along with the development of this technique, we have adapted the transient-grating frequency-resolved optical gating (TG-FROG) technique [2] for ultrashort, wide bandwidth pulse characterization. Since the guided pulse spectrum is broadened under the simultaneous action of several linear and nonlinear processes, including self-phase modulation, linear dispersion and self-steepening, the use of the FROG technique provides information necessary for optimal compression. Perhaps more important is that such coherent detection dramatically broadens the scope of experiments and applications using these pulses. For example, full characterization of amplitude and phase is crucial for control of the complex field profile.

In the experimental arrangement, pulses from a kilohertz multipass Ti:sapphire amplifier were focused at the entrance of a capillary tube held in a gas cell that could be evacuated or filled with pressures up to 15 atmospheres. For optimum matching of the gaussian beam to the lowest order mode of the waveguide, the input beam must be focused to a $1/e^2$ radius of $w_0 \approx 0.69\ a$, where a is the radius of the capillary tube [3]. With proper mode matching the calculated transmission was expected to be 90% for the borosilicate glass capillary tube used here (a = 150 μm, length = 1.2 m). The measured transmission of the capillary in air at low power was 55%. Transmission values closer to the calculated values are expected with fused silica capillaries. The light emerging from the waveguide was recollimated with a curved mirror and directed into either a prism pair compressor (60° apex angle, BK-7) or a grating (600 lines/mm) compressor constructed in a geometry similar to an all-reflective stretcher. The compressed pulse was analyzed using the TG-FROG apparatus.

In the TG-FROG technique, three replicas of the input pulse are directed parallel to each other, and focused together with a mirror into a fused silica substrate. The beam geometry results in a third-order nonlinear interaction that is phase matched, independent of wavelength. Two of the input beams arrive simultaneously and their interference

pattern writes a diffraction grating in the substrate that serves as the temporal gate. The third, probe pulse arrives with variable delay and scatters from this grating. After the substrate, only the signal beam is passed through and iris. To reduce the time blurring that would result from the finite beam size in the substrate, an image of the interaction region is relayed with magnification to the entrance of a spectrometer. The spectrum is recorded as delay of the probe pulse is varied, yielding a spectrogram which is then deconvolved to yield the complex field profile. The third-order of the non-linearity allows unambiguous interpretation of the direction of time, as well as the sign of any residual chirp. Background-free measurements are such as this are essential in determining the true baseline of the waveform and in measuring contrast ratio.

In early results from our lab presented here, we have compressed 160 μJ, 25 fs input pulses to 11 fs (see Fig. 1a). This pulse has a clean rising edge that is especially critical for high-field experiments. For this measurement, the grating compressor was used; note that the residual phase (Fig. 1b) is dominated by third-order dispersion that should be eliminated with the use of both the prisms and gratings. As expected, compression with the prism pair alone resulted in very strong third-order spectral distortion. In other measurements, we have also measured shorter pulses (10 fs) that have a higher pedestal. For the fiber tested here, some of the self-phase modulated light at high input intensity is coupled into higher-order spatial modes. This issue will be addressed by using fibers that more effectively attenuate these modes.

While we expect to achieve even higher compression ratios in the very near future, what distinguishes this work is that we are able to completely characterize the complex field both before and after compression. This allows direct measurement of the nonlinear processes present in the hollow-core fiber and, most importantly, to determine the parameters for optimum pulse compression. Interferometric autocorrelation, the traditional approach for measurement of such wide-bandwidth ultrashort pulses, does not have a background-free signal, and simply does not yield enough information to even give a proper pulse duration measurement since a pulse shape must be assumed. The present results are the shortest waveforms characterized using the FROG technique.

References

1. M. Nisoli, S. De Silvestri and O. Svelto, Appl. Phys. Lett. 68, 2793 (1996).
2. J. Sweetzer, D. Fittinghoff, R. Trebino, Conference on Lasers and Electrooptics, Vol. 9, 1996 OSA Technical Digest Series (Optical Society of America, Washington, D.C., 1996), pp.223-224.
3. E. A. J. Marcatili and R. A. Schmeltzer, Bell Syst. Tech. J. **43,** 1783 (1964).

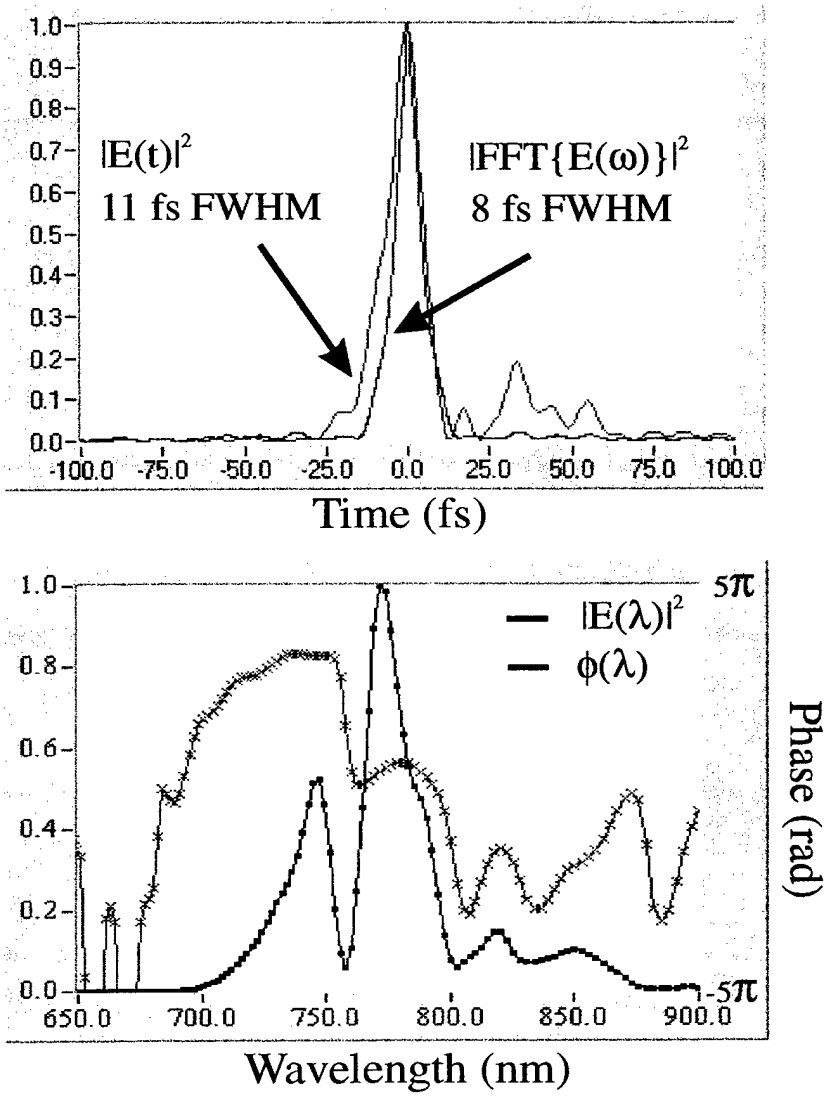

Figure 1. a) Intensity profile obtained by using a grating pair to compress the output of a 300 μm inner diameter fiber filled with 1 atm argon; also shown is the Fourier transform of the spectrum, assuming constant spectral phase. b) Spectral intensity and phase of experimental field shown in (a).

Multi-pulse Interferometric Frequency Resolved Optical Gating: Real-time Phase-sensitive Imaging of Ultrafast Dynamics

C. W. Siders and A. J. Taylor

Materials Science and Technology Division
Los Alamos National Laboratory
Los Alamos, New Mexico 87545
505/665-5847 (Office) 505/665-4292 (FAX)

M. C. Downer

Department of Physics
The University of Texas at Austin
Austin, Texas 78712

Recent advances in ultrafast laser technology and measurement techniques have pushed optical communication rates beyond a Terabit per second [1] and moved high-speed opto-electronics into the Terahertz domain [2]. Similar advances in high-field laser-matter interactions promise compact table-top sources of tunable short-pulse VUV- and X-radiation with brightness comparable to large electron storage ring facilities [3]. Also of great interest to the high energy and particle accelerator communities, large-amplitude relativistic Langmuir waves excited by super-strong ultrafast laser pulses in plasmas may lead to both "compact" (kilometer) TeV scale accelerator facilities and small laboratory/medical facility table-top electron accelerators with GeV beam energies [4]. Continued advancement in our understanding of the underlying fundamental physics in these fields depends critically on the successful development, refinement, and application of sensitive optical diagnostics with femtosecond temporal resolution. As the dominant interaction between a probe laser pulse $E(t)$ and these materials is a shift in optical phase, $E(t) \rightarrow E(t)e^{i\phi(t)}$, where $\phi(t) = (n(t)\omega z/c)$ and $n(t)$ is the refractive index, optical diagnostics designed to directly measure the phase change $\phi(t)$ have shown the most promise. The inter-related techniques of spectral blueshifting [5], longitudinal (i.e. frequency domain) interferometry (LI) [6], and frequency resolved optical gating (FROG) [7] have been successfully used by many researchers to extract from spectral power density measurements sensitive details of ultrafast time-domain phase shifts. The first two of these techniques, being linear optical effects, have been shown to be powerful tools for measuring DC and slowly varying time-domain phase shifts with extremely high sensitivity (one part in 3000 of a fringe) over a temporal span of many pulse-widths about the peak of the pulse. On the other hand, the optically nonlinear FROG, which accurately recovers detailed variations in temporal phase about the intense portions of the pulse but is largely insensitive to DC and slowly varying terms, acts as a complementary diagnostic for highly structured phase shifts, such as those in ionization fronts. We have developed a new marriage of standard FROG with multi-pulse longitudinal interferometry, termed Multi-pulse Interferometric FROG, or MI-FROG, which promises to become a powerful real-time diagnostic of ultrafast dynamics: a femtosecond phase-sensitive oscilloscope if you will.

Though the general case can be easily considered [8], for brevity, let us examine here the measured quantity in polarization-gate FROG (the "FROG trace", [7]),

$$I_{\mathrm{FROG}}(\tau,\omega) = \left| \int_{-\infty}^{\infty} E(t)\, |E_{\mathrm{gate}}(t-\tau)|^2\, e^{i\omega t} dt \right|^2 \tag{1}$$

which is a two-dimensional (τ,ω) spectrogram of the probe field $E(t)$, in the idealized situation when the gate pulse is much shorter than $E(t)$. We depart from the usual FROG apparatus and assume that, as in LI [6], both $E(t)$ and $E_{\mathrm{gate}}(t)$ are two-pulse assemblies, e.g. $E(t) = E_0(t)e^{i\phi(t)} + E_0(t-\Delta)$ and $E_{\mathrm{gate}}(t) = \delta(t) + \delta(t-\Delta)$, where $\phi(t)$ is a relative time-domain phase difference impressed between the two pulses in $E(t)$. The multi-pulse assemblies $E(t)$ and $E_{\mathrm{gate}}(t)$ are obtained from a single input pulse and, since the simultaneous gating and frequency dispersion yields a differential phase shift, the gate pulse could be modified using nonlinear pulse compression techniques while the probe pulse can be broadened from an initially short pulse by linear dispersion or spectral narrowing. That is to say, the individual sub-pulses within each of $E(t)$ and $E_{\mathrm{gate}}(t)$ maintain their phase coherence. Substituting $E(t)$ and $E_{\mathrm{gate}}(t)$ into Eq. 1, we have (neglecting normalization)

$$I_{\mathrm{MI-FROG}}(\tau,\omega) = |E_0(\tau-\Delta)|^2 + |E_0(\tau+\Delta)|^2 + 2\,|E_0(\tau)|^2\,[1+\cos(\omega\Delta+\phi(\tau))]\,, \tag{2}$$

where numerous temporally separated cross terms (e.g. $E_0(\tau)E_0^*(\tau-\Delta)e^{i\phi(\tau)}$) have been dropped. An illustrative plot of Equation 1, with $\phi(\tau)$ proportional to a short collinearly propagating pump pulse, is

presented in Figure 1. The two side-features, given by $|E_0(\tau \pm \Delta)|^2$, are the normal single-pulse FROG traces of the leading and trailing pulses individually. In addition, the central feature, $2\,|E_0(\tau)|^2\,[1+\cos(\omega\Delta)]$, is formed by the interference of the two complex-valued FROG fields ($E_{\rm sig}(\tau,\omega)$ in the traditional notation of [3]). For a non-zero $\phi(\tau)$, the time-resolved frequency-domain fringe pattern deforms from the null-phase condition of perfectly straight frequency-domain fringes to directly follow $\phi(\tau)$, as shown in Figure 1.

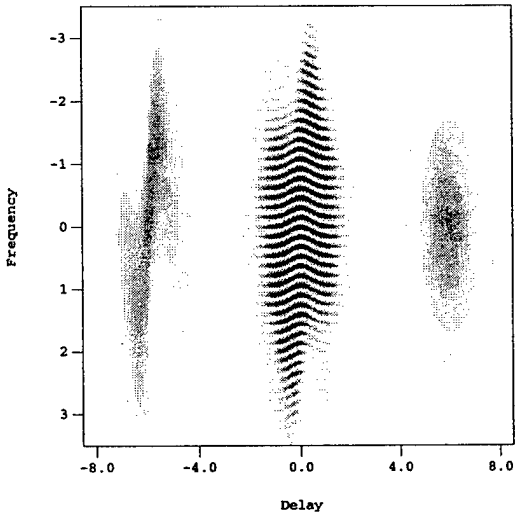

Figure 1: Illustrative calculation of MI-FROG trace. Time is in units of pump pulse widths with the probe two units wide, the gate 0.33 units wide, and $\Delta = 6$.

The unique abilities of MI-FROG center around its inherently differential nature: ultrafast changes in the time-domain phase of a laser pulse are measured, unlike standard FROG, to all orders while shot-to-shot fluctuations in the pulse structure are discriminated against. Additionally, a time-domain phase shift $\phi(t)$ can be measured, unlike longitudinal interferometry, *in a single shot* over a time-scale much longer than the pump pulse which induces it. The real-time nature of MI-FROG allows immediate and direct observation of pump-pulse time scale dynamics *without* computational analysis, a significant advantage over traditional single-pulse FROG. Finally, iterative computational techniques similar to those used in standard FROG [9] can elucidate femtosecond time-scale detail from the MI-FROG trace. In fact, it is possible to recover the time-domain intensity and phase of not only the two pulses which make up $E(t)$, but, in the case of SHG MI-FROG, the gate pulse as well (in PG MI-FROG only $|E_{\rm gate}(t)|^2$ is recovered). That is to say, with MI-FROG, the intensity and phase of *three* pulses can be measured in a single shot.

A real-time "phase-scope" of this kind would, of course, be useful in mapping numerous ultrafast processes or effects and, clearly, the rapid, real-time, direct viewing of temporal phase could be of important use in the optimization, adaptive feedback, and control of future processes based upon coherent-control of molecular wavepackets, laser-driven plasma-based accelerators, or ionization-front based sources of tunable radiation. Among those processes being presently studied at LANL are high-field atomic and molecular ionization fronts, laser driven wakefields in plasmas, and ultrafast electro-optic dynamics in technologically relevant materials. In addition, MI-FROG can be of great utility in measuring both fast (fs) or slow time-scale (ps) changes in refractive index caused by atomic or molecular response, respectively, to a copropagating pump pulse in optical media. The former is also a particularly simple demonstration of this new technique.

A standard chirped pulse amplified laser system was used to provide 1 mJ, 100 fs, pulses at a kHz rate. Twenty percent of this pulse was used to generate, in a standard Michelson interferometer, the multi-pulse probe and gate sequences. The remainder of the 802 nm pulse was frequency doubled in a 300 μm BBO crystal and dispersively broadened to provide a 30 μJ, $\sim$ 300 fs pump pulse at 401 nm. After dumping the residual IR, the UV pump and IR probes, all of the same linear polarization, were collinearly focused in a 10 cm focal length unit-magnification telescope. Temporal overlap of the pump with the trailing probe pulse was established using sum frequency generation in a 500 μm KDP crystal. The gate pulses traveled a separate path to a modified FROG apparatus while the probes were dichroically separated from the pump and entered the same FROG apparatus. A 500 μm fused silica plate, thinner than the 650 μm walkoff length, was translated longitudinally near the focus to induce an adjustable amount of cross-phase modulation (XPM) [10]. By blocking individual arms in the Michelson, single-pulse FROG traces of the leading or trailing pulse could be measured in addition to the MI-FROG trace. Three sets of FROG/MI-FROG traces are shown in Figure 2: one each for 0 fs, and $\pm$50 fs delay between the pump and trailing probe pulse. As expected, the FROG traces of the leading pulse did not differ from the unpumped traces (not shown). The single-pulse FROG traces of the trailing pulse do, though, show the characteristic frequency blue/red shift for the delayed cases and a symmetric broadening for the overlapped case, with shifts of $\pm$2.5 nm. Note that when the probe rides on the leading/trailing edge of the pump (right/left-most column), the probe is red/blue-shifted, as expected from the $n_2 I(t)$ nature of the XPM. The MI-FROG traces, all of which have straight fringe patterns with the pump blocked (not shown), display in these instances a characteristic fringe tilt, indicative of the

clean blue/red shift seen in the FROG trace, while the overlapped case evidences a downward curvature. That is to say, the fringe pattern follows the time-domain phase shift $\phi(t) = n_2 I(t)\omega z/c$. Indeed, the $\sim \pi/2$ per 200 fs phase ramp in the ± 50 fs delay cases corresponds to a shift of $\Delta\lambda = \frac{\lambda^2}{2\pi c}\frac{\pi/2}{200\text{fs}} = 2.7$ nm, in excellent agreement with the single-pulse FROG traces.

In summary, MI-FROG, being a rapid, real-time, direct-reading "oscilloscope" of ultrafast phase shifts, promises to be a powerful new tool for ultrafast science. In addition, iterative phase recovery techniques allow the unprecedented recovery, with femtosecond accuracy, of the intensity and phase of three laser pulses in a single-shot.

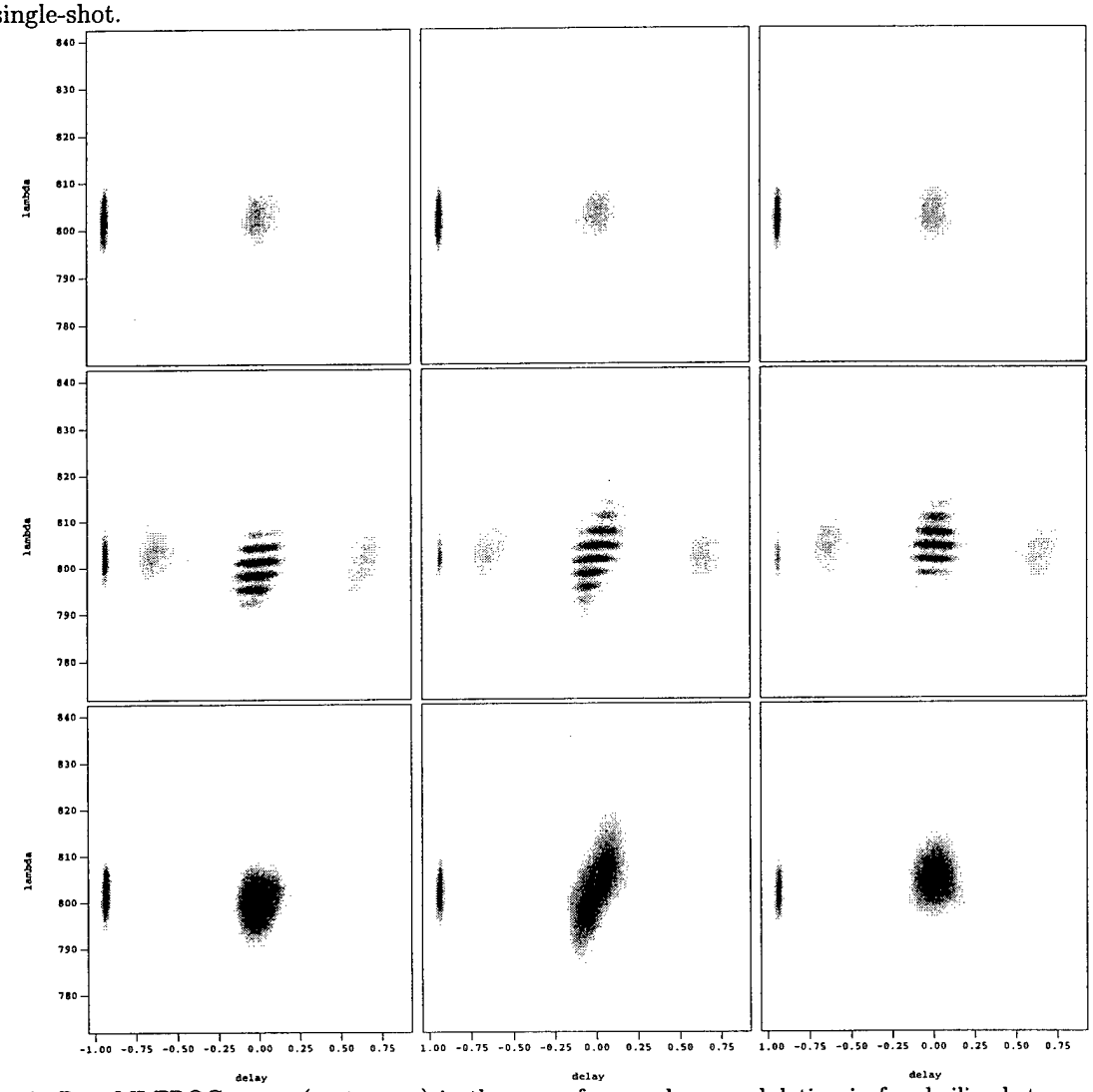

Figure 2: Raw MI-FROG traces (center row) in the case of cross-phase modulation in fused silica between a long 400 nm pump pulse and shorter 800 nm probe for -50 fs (left column), 0 fs (center column), and +50 fs (right column) pump-probe delay. The y-axis is in nm, the x in ps. Upper and lower rows are the individual single-pulse FROG traces for the leading or trailing probe pulse respectively. The feature displayed at -1.0 ps and 802 nm is the power spectrum of the input pulse, measured in the same spectrometer independently from and simultaneously with the FROG/MI-FROG traces, and is used in the interative phase recovery analysis.

References

[1] A. Chraplyvy, et al., *Opt. Fiber Comm. '96,* San Jose.
[2] D. Grischkowsky, et al., *JOSA B* **7**, 2006 (1990).
[3] C.W. Siders, et al., *JOSA B* **13**, 330 (1996).
[4] T. Tajima, et al., *PRL* **43**, 267 (1979).
[5] Wm.M. Wood, et al., *PRL* **67**, 3523 (1991).
[6] C.W. Siders, et al., *PRL* **76**, 3570 (1996).
[7] D.J. Kane, et al., *Opt. Lett.* **18**, 823 (1993).
[8] C.W. Siders, et al., *Opt. Lett.,* (in prep.).
[9] K. DeLong, et al., *Opt. Lett.* **12**, 2463 (1995).
[10] R. Alfano, et al., *Opt. Lett.* **11**, 626 (1986).

Generation of tunable femtosecond VUV pulses around 100nm by resonant and near resonant four-wave difference frequency mixing

G. Korn, O. Kittelmann, J. Ringling, A. Nazarkin*, I. V. Hertel

Max-Born-Institut für Nichtlineare Optik und Kurzzeitspektroskopie im Forschungsverbund Berlin e. V., Rudower Chaussee 6, D-12474 Berlin, Germany.

Tel.: +49-30-6392 1273

Fax.: +49-30-6392 1289

Time resolved spectroscopic investigations of ultrafast processes at surfaces or in gaseous media, e. g. photodissociation and fragmentation of molecules and clusters[1,2] require femtosecond pulses tunable in the vacuum ultraviolet (VUV) spectral range. Clusters show for instance a very strong dependence of the absorption peak on the their size. The region between 100nm-150nm is of special interest for small clusters. Single photon ionization will be possible for photons of this energy range.

We report on the generation of femtosecond VUV radiation tunable between 102-124 nm by two photon resonant (Krypton $\left[4p^5\,6p(3/2)_2\right]$) and near resonant (Argon $\left[3p^5\,4p(1/2)_2\right]$) Four-wave difference-frequency mixing (FWDFM) of intense ultrashort ArF pulses and tunable synchronized femtosecond output pulses (signal and idler) of an optical parametric generator.

As the "master laser" we employed a home made Ti:Sapphire oscillator/amplifier system providing 8 mJ, 80 fs (0.1 TW) output (fundamental) pulses at a wavelength tunable around 774 nm with 10 Hz repetition rate.

Quadrupling one part (2 mJ) of the intense Ti:Sapphire fundamental output in a cascaded second order sum-frequency mixing scheme $\left(\omega \rightarrow 2\omega(\omega+\omega) \rightarrow 3\omega(2\omega+\omega) \rightarrow 4\omega(3\omega+\omega)\right)$ employing three β barium borate (BBO) crystals[3] provides nearly 10 μJ, 150 fs seed pulses at 193 nm. Subsequent amplification of these pulses in a commercial ArF gain modul (EMG 150 MSC) in a double pass configuration resulted in ≈1.5 mJ, 250 fs pulses[4] which serve as pump pulses (ω_P) in the FWDFM scheme.

A second part of the femtosecond fundamental radiation is frequency doubled in a BBO crystal resulting in 0.5 mJ pulses at 387 nm which were used to pump a travelling wave optical parametric system consisting of an optical parametric generator and a parametric amplifier arranged in a configuration similar to Ref. 10. The pump pulse (ω_P) and the tunable injection pulse (ω_I) are combined and focused into the gas cell . The maximum focused intensity in the cell is 10 TW/cm^2.

A selection of the spectra of the generated VUV radiation is shown in Fig. 1. It should be noted that the radiation in the spectral range from 112-124 nm has been generated by mixing the pump radiation with the tunable signal radiation in Argon whereas the radiation in the range below 110 nm results from mixing with the idler in krypton. Besides the mixing with the OPA radiation strong fs radiation can be generated by using the harmonics the fundamental (774nm), 2nd and 3d harmonic of the " master laser ".

A detailed theoretical and experimental investigation of the difference between two-photon resonant and nonresonant excitation has been performed.

We report a direct experimental observation of the coherent dynamics of an atomic two-photon excitation process using time resolved four-wave difference-frequency mixing ($\omega_s = 2\omega_p \pm \omega_i$) with femtosecond UV- and VUV-pulses[5]. Keeping the injected pulses (ω_i) significantly shorter than the pump pulses (ω_p) we were able to resolve Rabi oscillations and subsequent relaxation of the excitation at the probe difference- frequency (ω_s). The results are of great importance for the understanding of coherent phenomena underlying the femtosecond VUV-pulse generation and further optimization of this process.

We will show that fs-pulse four-wave frequency mixing makes it possible to study the coherent dynamics of a quantum transition in an intense resonant field. With this technique, the two-photon resonant response of atomic Ar and Kr excited by an intense VUV pulse with duration short compared to the polarization relaxation time was investigated. The presented results are the first direct observation of the coherence induced by a two-photon excitation of an atomic medium by femtosecond VUV pulses. The measured difference-frequency signal probes the squared amplitude of the off-diagonal matrix element of the transition. Such information about

the dynamics of quantum transitions is of prime importance for controlling and optimizing such processes as two-photon resonant frequency conversion and harmonic generation, as well as time-resolved studies of Rydberg states in atoms and molecules.

References

/1/ R. E. Walkup, J. A. Misewich, J. H. Glownia, and P. P. Sorokin, J. Chem. Phys. **94**, 3389 (1991).

/2/ Th. Freudenberg, W. Radloff, H.-H. Ritze, V. Stert, F. Noack, and I. V. Hertel, Chem. Phys. Letters 258, 507 (1996)

/3/ J. Ringling, O. Kittelmann, F. Noack, G. Korn, and J. Squier, Opt. Lett. **18**, 2035 (1993).

/4/ J. Ringling, O. Kittelmann, F. Noack, U. Stamm, J. Kleinschmidt, and F. Voss, Opt. Lett. **19**, 1639 (1994).

/5/ O. Kittelmann, J. Ringling, G. Korn, A. Nazarkin, I.V. Hertel Phys. Rev. Letters **76,** 2682 (1996)

Figure caption

Fig. 1 Tuning curve showing the relative VUV energy values as a function of the generated VUV wavelength(open squares, Ar; filled squares, Kr) and inset selected number of spectra of the generated femtosecond tunable VUV-radiation (102 - 124 nm) and spectra of the radiation at 129 nm and 155 nm generated by mixing ω_p with fixed frequencies (2ω, 3ω). Note the break on the X-axis to show the whole spectral range while keeping a reliable resolution of the spectra.

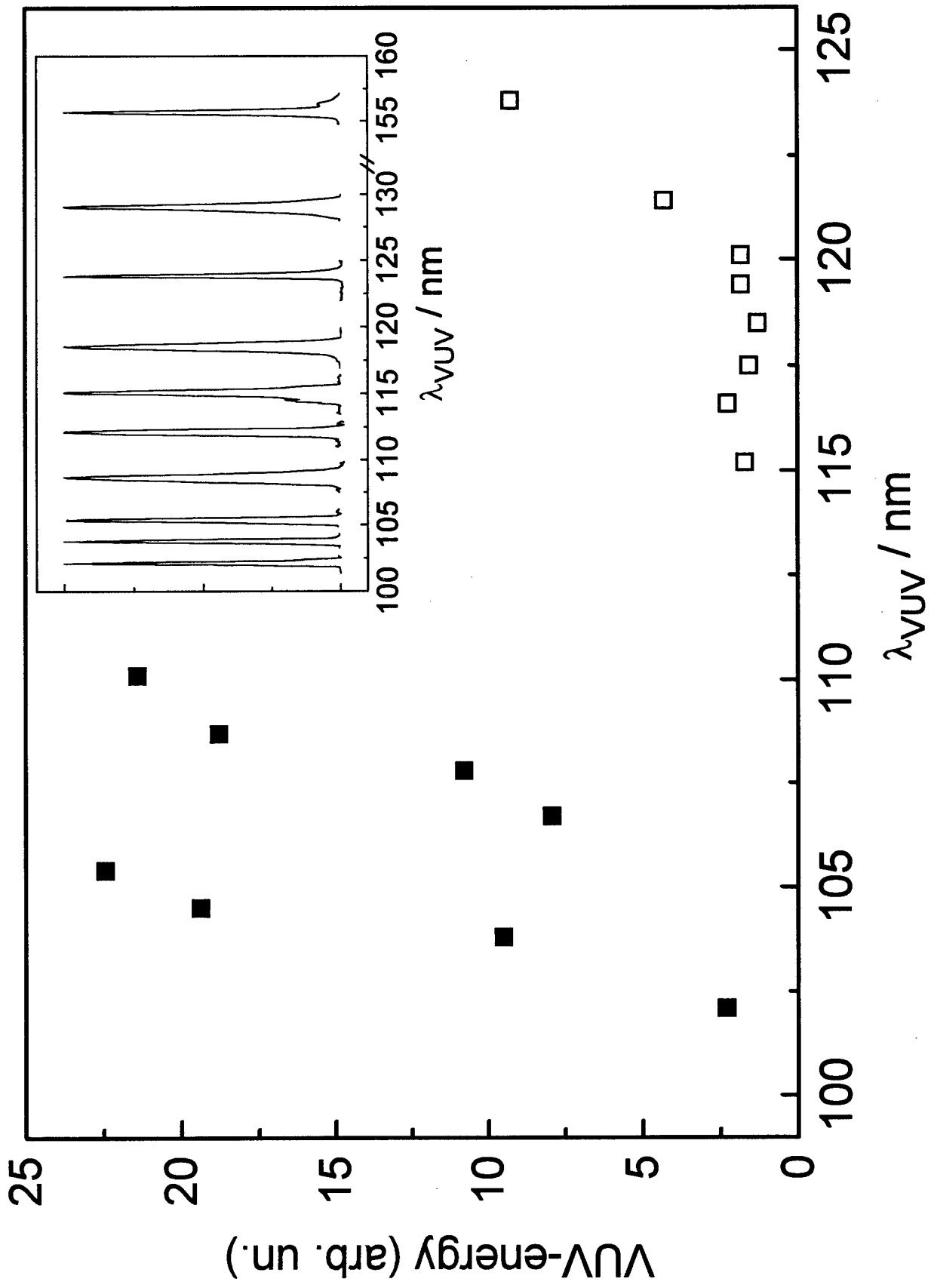
VUV-energy (arb. un.)
0
5
10
15
20
25
100
105
110
115
120
125
λVUV / nm
100
105
110
115
120
125
130
155
160
λVUV / nm

Lasers II

SaC 2:00pm – 3:30pm
Zia A

A. Taylor, *Presider*
Los Alamos National Laboratory

DESIGN AND PERFORMANCE OF THE PETAWATT LASER SYSTEM

M. D. Perry, D.M. Pennington, B. C. Stuart, R. Boyd, J. A. Britten, C. G. Brown,

S. Herman, J. L. Miller, H. Nguyen, B. Shore, G. Tietbohl, V. Yanovsky

Laser Program, Lawrence Livermore National Laboratory,

PO Box 808, L-439, Livermore, CA 94550

Telephone: (510) 423-4915 Telefax: (510) 422-5537

e-mail: perry10@llnl.gov

We recently demonstrated the production of over a petawatt of peak power in the Nova/Petawatt Laser Facility, generating >500 J in 430 fs. The Petawatt Laser Project was initiated to develop the capability to test the fast ignitor concept[1] for inertial confinement fusion (ICF), and to provide a unique capability in high energy density physics. The laser was designed to produce near kJ pulses with a pulse duration adjustable between 0.5 and 100 ps and a focused irradiance in excess of 10^{21} W/cm^2 .

The laser system begins with a Ti:sapphire chirped pulse amplification system operating at 1054 nm. The pulse is stretched to ~ 3 ns and is amplified up to 50 mJ in the titanium-sapphire section with minimal bandwidth narrowing. Further amplification in mixed phosphate glass rod amplifiers produces a spectrally-shaped 12 J pulse. This pulse is further amplified up to the near kilojoule level by a series of disk amplifiers. Near diffraction-limited beam quality is achieved by utilizing only the central 80% of the disk amplifiers and the use of adaptive (deformable) optics to correct any residual thermal or pump induced aberrations. Following amplification, the chirped nanosecond pulse is compressed to 480 fsec by a pair of large aperture diffraction gratings arranged in a single pass geometry. Pulse compression occurs in vacuum with a compressor throughput of 84%. Currently, this system is limited to 600 J pulses in a 46-cm beam. Expansion of the beam to 58 cm with the installation of 94-cm gratings will enable 1 kJ operation.

---

[1] M. Tabak, et. al., Phys. Rev. Lett. (1994)

Target experiments with petawatt pulses will be possible either integrated with the Nova 10 beam target chamber for fast ignition experiments, or as a stand alone system in an independent chamber. Focusing the beam onto a target is accomplished using an on axis parabolic mirror. The focal spot is diagnosed with an optical imaging system, as well as an axial x-ray imaging camera. Since debris from target experiments would put the parabola at risk, a secondary "plasma" mirror is used in conjunction with the parabola to focus the beam on target. For irradiances > 10^{14} W/cm^2, short pulse radiation creates a critical density plasma on the surface of a dielectric substrate, with a demonstrated reflectivity > 90%.[2] For incident pulses on the order of 500 fs, the plasma has insufficient time to undergo hydrodynamic expansion, producing a density scale length less than the incident wavelength. This novel targeting system will enable the production of ultrahigh contrast pulses, with an easily variiable effective focal length by changing the curvature of the secondary mirror.

Figure Caption

Figure 1: a) Far-field distribution of the beam from the front-end of the Petawatt laser after reflecting from a polished SiO_2 surface. The central spot is diffraction-limited.
b) Same as fig 1a but after reflecting from the plasma mirror at 90% reflectivity.

This work was performed under the auspices of the U.S. Department of Energy by the Lawrence Livermore National Laboratory under Contract No. W-7405-ENG-48

[2] M. Perry, et. al., submitted to (1995)

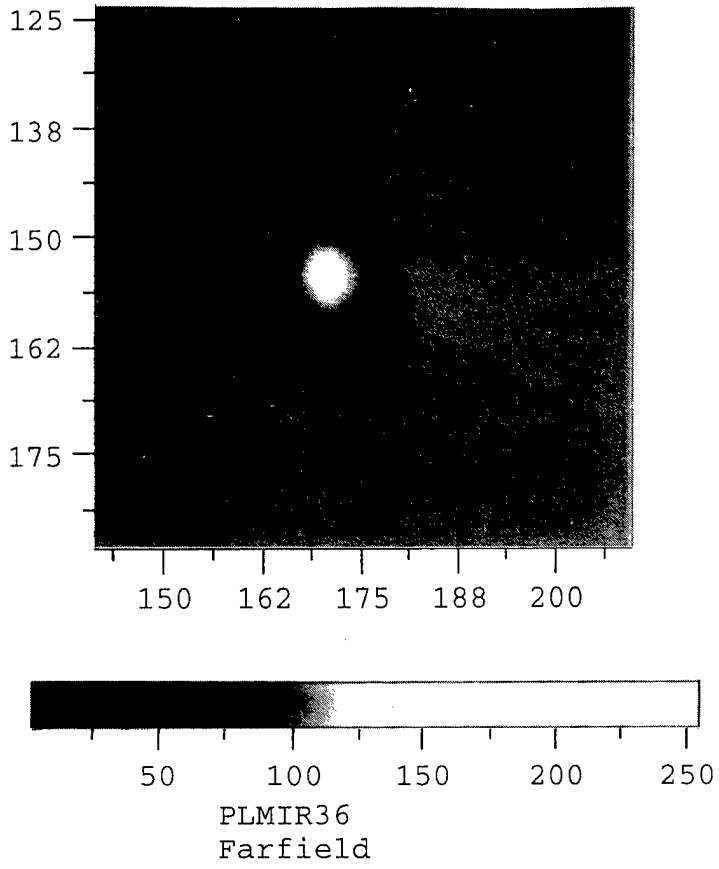
125
138
150
162
175
150
162
175
188
200
50
100
150
200
250
PLMIR36
Farfield

a)

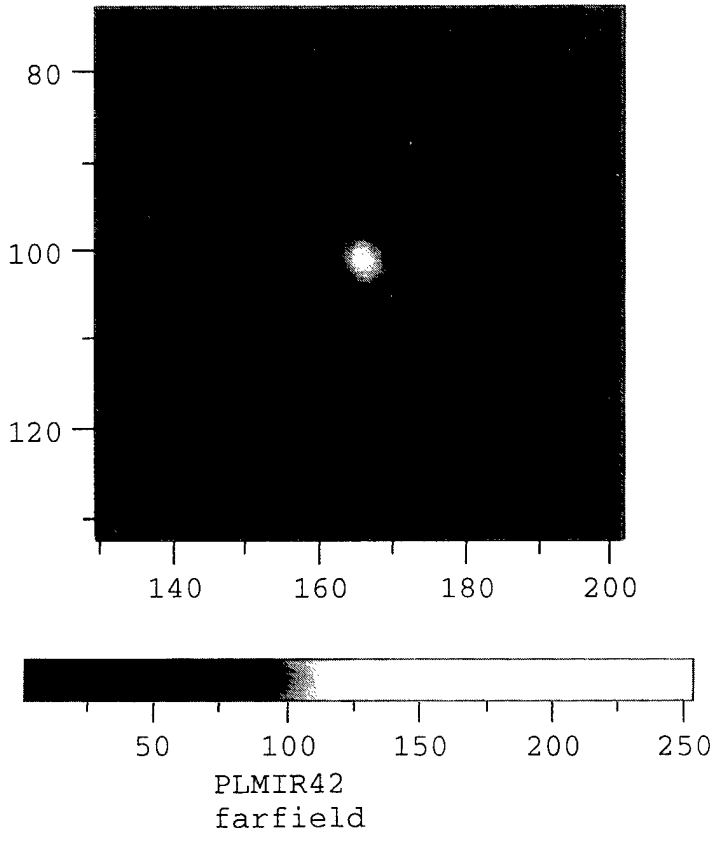
80
100
120
140
160
180
200
50
100
150
200
250
PLMIR42
farfield

b)

Ultrahigh Peak Power Lasers Present and Future

Gerard Mourou
University of Michigan

We have seen over the past few years an explosion in laser peak power. Today the lasers have peak power of TW and average power of few watts with focused intensity well in the exawatt/cm^2 range. We will describe the next generation of CPA lasers that will take us into the yottawatt/cm^2 range with kW average power.

Generation of 30 TW femtosecond pulses at 10 Hz in a Ti:Sapphire laser chain

A. Antonetti, F. Blasco, J.P. Chambaret, G. Chériaux, G. Darpentigny,
G. Hamoniaux, C. Le Blanc, P. Rousseau, and F. Salin

Laboratoire d'Optique Appliquée,
ENSTA-Ecole Polytechnique, CNRS URA 1406,
Chemin de la Hunière, 91761 Palaiseau Cedex, France.

The technique of chirped pulse amplification has sucessfully been applied to the amplification of sub-50fs pulses from Ti:sapphire oscillators and energies approaching 125 mJ have been achieved [1,2]. Although these pulses have very high peak power they are useful to solid-state target experiment only if they are free of any prepulse or wings below an intensity of 10^{11} W/cm^2 . We describe here a Ti:sapphire amplifier producing 30 TW pulses at 10 Hz which has been designed to produce pedestal free pulses. To reduce any prepulse, we designed the amplifier with broad transmission bandwidth, minimum material path length, high gain, and an aberration free system for stretching and recompressing the pulses [3].

We generated femtosecond pulses in a 10-50 fs Ti-Sapphire oscillator, using a 4.5 mm long, highly doped Ti:Sapphire crystal. We use a new aberration-free stretcher compressor system that is able to stretch and recompress 25 fs pulses with a peak to background contrast greater than 10^6 [3]. The spectral acceptance of our design is 100 nm. In order to limit spectral clipping, which introduces prepulses, we chose to amplify 25 fs.

The pulses are first amplified in a 8-pass reflective multipass amplifier using 2 mirrors with two different radius of curvature in a confocal arrangement (see figure 1). This amplifier includes a 1cm long Ti:Sapphire crystal pumped by 80 mJ from a Nd:YAG laser. The 0.7 nJ stretched pulse is amplified up to 5 mJ, with a good spatial profile. The high gain (>10), and low losses per pass leads to a reduction in the effect of the gain narrowing.

Pulses are then amplified in a 5-pass power amplifier. A 1 cm^3 crystal is pumped on both sides by 1 Joule of 532nm light. We obtain an output energy of 300 mJ . After spatial filtering the pulses are injected in a four-pass amplifier pumped by 4 Joules of 532nm from a Nd:Yag laser working at 10 Hz. After four passes the output energy is 1.6 Joules while the beam profile keeps its quasi-Gaussian shape. As predicted by our numerical model, the pulse spectrum shifts toward the infrared during amplification. By choosing the right input pulse wavelength we have been able to produce 40 nm spectra at the 1.6 J level.

The pulse then enters a large vacuum chamber (2 meters in diameter) which includes the compressor. We measure the pulse duration using a scaning autocorrelator. The shortest pulses we measured were around 27 fs (fig.2). The compressor efficiency is around 50 % leading to pulses over 30 TW.

The compressor vacuum chamber is coupled to the experiment chambers through a 100 μm thick window. In a first try to characterize the source we focused the 30 TW pulses on a hyper-sonic Argon jet using an off-axis parabola. We measured a 6μm diameter spot size leading to intensities above $6x10^{19}$ W/cm^2. At that intensity we observed clear indications of relativistic self-focusing in the gas.

[1] C. P. J. Barty, C. L. Gordon III, and B. E. Lemoff. Opt. Let., Vol. 19, No. 18, p. 1442, 1994.
[2] J. Zhou C. P Huang, C. Shi, M. Murnane, and C. Kapteyn, Opt. Let Vol 19 No. 2,p. 126, 1994.
[3] G. Chériaux, P. Rousseau, F. salin, J. P. Chambaret, B. Walker and L. Dimauro, Opt Lett. **6**, p. 414, 1996.

Figure captions

Figure 1: Experimental setup of the amplifier system. PC = Pockel Cell.
Figure 2: Measured autocorrelation using a scaning autocorrelator, (FWHM = 27fs).

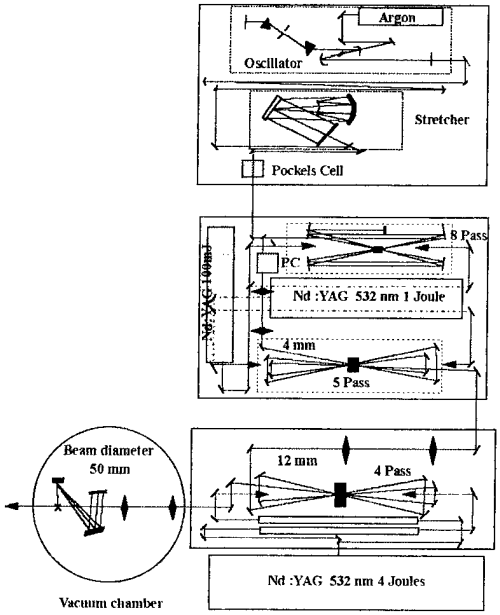

Figure 1

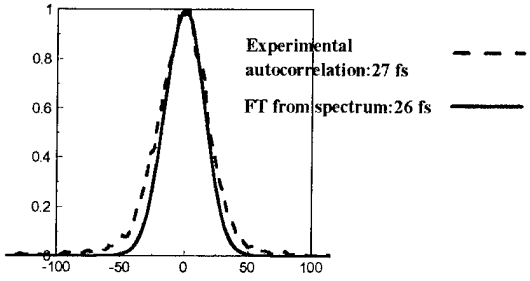

Figure 2

Applications of High Field and Short Wavelength Sources VII
Technical Program Committee

Chairs

Louis DiMauro, *Brookhaven National Laboratory, U.S.A.*
Margaret Murnane, *University of Michigan, U.S.A.*
Anne L'Huillier (European Cochair), *Lund Institute of Technology, Sweden*

Committee Members

Pierre Agostini, *Centre d'Etudes de Saclay, France*
Jean-Patrick Connerade, *Imperial College of Science and Technology, U.K.*
Paul Corkum, *National Research Council, Canada*
L. DaSilva, *Lawrence Livermore National Laboratory, U.S.A.*
David Ederer, *Tulane University, U.S.A.*
Eckhart Foerster, *Max-Planck-Gellschaft, Germany*
Richard Freeman, *Lawrence Livermore National Laboratory, U.S.A.*
George Gibson, *University of Connecticut, U.S.A.*
Chris Jacobson, *SUNY Stony Brook, U.S.A.*
Henry Kapteyn, *University of Michigan, U.S.A.*
Yoshiaki Kato, *Osaka University, Japan*
Vladimir Krainov, *Moscow Institute of Physics and Technology, Russia*
Kenneth Kulander, *Lawrence Livermore National Laboratory, U.S.A.*
Peter Lambropoulos, *Max Planck Institute for Quantenoptik, Germany*
James Long, *Naval Research Laboratory, U.S.A.*
Thomas McIlrath, *University of Maryland, U.S.A.*
Howard Milchberg, *University of Maryland, U.S.A.*
Gerard Mourou, *University of Michigan, U.S.A.*
Harm Muller, *FOM Institute for Atomic and Molecular Physics, The Netherlands*
Wolfgang Sandner, *Max Born Institute, Germany*
Sune Svanberg, *Lund Institute for Technology, Sweden*
Gregory Tallents, *University of Essex, U.K.*
Michael White, *Brookhaven National Laboratory, U.S.A.*